

- *J. T. Henderson, *President*
- Yasujiro Niwa, *Vice-President*
- *W. R. G. Baker, *Treasurer*
- *Haraden Pratt, *Secretary*
- *D. G. Fink, *Editor*
- *J. D. Ryder, *Senior Past President*
- *A. V. Loughren, *Junior Past President*

1957

- J. G. Brainerd (R3)
- J. F. Byrne
- J. J. Gershon (R5)
- A. N. Goldsmith
- A. W. Graf
- W. R. Hewlett
- R. L. McFarlan (R1)
- *Ernst Weber
- C. F. Wolcott (R7)

1957-1958

- H. R. Hegbar (R4)
- E. W. Herold
- K. V. Newton (R6)
- A. B. Oxley (R8)
- F. A. Polkinghorn (R2)
- J. R. Whinnery

1957-1959

- D. E. Noble
- Samuel Seely

*Members of Executive Committee

George W. Bailey,
Executive Secretary

- Evelyn Benson, *Assistant to the Executive Secretary*
- John B. Buckley, *Chief Accountant*
- Laurence G. Cumming, *Technical Secretary*
- Emily Sirjane, *Office Manager*

EDITORIAL DEPARTMENT

- Alfred N. Goldsmith, *Editor Emeritus*
- D. G. Fink, *Editor*
- E. K. Gannett, *Managing Editor*
- Helene Frischauer, *Associate Editor*

ADVERTISING DEPARTMENT

- William C. Copp, *Advertising Manager*
- Lillian Petranek, *Assistant Advertising Manager*

EDITORIAL BOARD

- D. G. Fink, *Chairman*
- E. W. Herold, *Vice-Chairman*
- E. K. Gannett
- Ferdinand Hamburger, Jr.
- T. A. Hunter
- A. V. Loughren
- W. N. Tuttle

Authors are requested to submit three copies of manuscripts and illustrations to the Editorial Department, Institute of Radio Engineers, 1 East 79 St., New York 21, N. Y.

Responsibility for the contents of papers published in the PROCEEDINGS OF THE IRE rests upon the authors. Statements made in papers are not binding on the IRE or its members.



Change of address (with 15 days advance notice) and letters regarding subscriptions and payments should be mailed to the Secretary of the IRE, 1 East 79 Street, New York 21, N. Y.

All rights of publication, including foreign language translations are reserved by the IRE. Abstracts of papers with mention of their source may be printed. Requests for republication should be addressed to The Institute of Radio Engineers.

PROCEEDINGS OF THE IRE®

Published Monthly by

The Institute of Radio Engineers, Inc.

VOLUME 45

August, 1957

NUMBER 8

CONTENTS

Samuel Seely, Director, 1957-1959.....	1056
Poles and Zeros	<i>The Editor</i> 1057
Scanning the Issue	<i>The Managing Editor</i> 1058
6169. Ultrasonics in Medicine and Dentistry.....	<i>Walter Welkowitz</i> 1059
6170. Ion Oscillations in Electron Beam Tubes; Ion Motion and Energy Transfer.....	<i>Robert L. Jepsen</i> 1069
6171. Multihole Ferrite Core Configurations and Applications.....	<i>H. W. Abbott and J. J. Suran</i> 1081
6172. Polarization Reversal and Switching in Guanidinium Aluminum Sulfate Hexahydrate Single Crystals.....	<i>Harry H. Wieder</i> 1094
6173. Straight-Field Permanent Magnets of Minimum Weight for TWT Focusing—Design and Graphic Aids in Design.....	<i>Myron S. Glass</i> 1100
6174. Some New Circuits for High-Power Traveling-Wave Tubes.....	<i>M. Chodorow and R. A. Craig</i> 1106
6175. Correction to "Space-Charge Waves Along Magnetically-Focused Electron Beams".....	<i>Johannes Labus</i> 1118
6176. On Multimode Oscillators with Constant Time Delay.....	<i>Viktor Met</i> 1119
6177. A Reactance Theorem for Antennas.....	<i>Curt A. Levis</i> 1128
6178. Heat Loss in Grooved Metallic Surface.....	<i>Enrique A. Marcatili</i> 1134
6179. IRE Standards on Letter Symbols and Mathematical Signs, 1948 (Reprinted 1957).....	1140
Correspondence:	
6180. The Use of Speech Clipping in Single-Sideband Communications Systems.....	<i>Leonard R. Kahn</i> 1148
6181. Fast Switching by Use of Avalanche Phenomena in Junction Diodes.....	<i>B. Salzberg and E. W. Sard</i> 1149
6182. Differentiating Devices.....	<i>Herbert B. Voelcker, Jr.</i> 1151
Contributors	1151
IRE News and Radio Notes	1153
Calendar of Coming Events and Authors' Deadlines.....	1153
Professional Group News.....	1155
1957 Western Electronic Show and Convention.....	1156
Books:	
6183. "An Introduction to Cybernetics," by W. R. Ashby.....	<i>Reviewed by W. A. Rosenblith</i> 1161
6184. "Elektronische Rechenmaschinen und Informationsverarbeitung," ed. by A. Walther.....	<i>Reviewed by Werner Buchholz</i> 1161
6185. "Theorie und Technik der Pulsmodulation," by E. Hölzler and H. Holzwarth.....	<i>Reviewed by W. H. von Aulock</i> 1162
6186. "Transistor Engineering Reference Handbook," by H. E. Marrows.....	<i>Reviewed by A. P. Stern</i> 1162
6187. Abstracts of IRE TRANSACTIONS.....	1163
6188. Abstracts and References.....	1170

ADVERTISING SECTION

Meetings with Exhibits.....	6A	Notes.....	46A	Section Meetings.....	90A
News—New Products.....	28A	Professional Group Meetings.....	50A	Positions Open.....	124A
IRE People.....	34A	Membership.....	70A	Positions Wanted.....	134A
Industrial Engineering.....				Advertising Index.....	189A



THE COVER—An over-all view is shown of a transportable ultrasonic instrument for human neurosurgery, just being completed at the Bioacoustics Laboratory of the University of Illinois. The inset shows a close-up of the four-beam ultrasonic irradiator at the top, a pan which will contain a degassed saline solution, and a head holder supporting a human skull immediately below the pan. The ultrasonic waves are transmitted to the brain through a hole in the skull by means of the saline in the pan. The position of the skull opening shown here will be that used in the first human ultrasonic neurosurgery operations for the relief of tremor. A review of this and other applications of ultrasonics in medicine starts on page 1059 of this issue.

Photo—Bioacoustics Laboratory, University of Illinois



Samuel Seely

DIRECTOR, 1957-1959

Samuel Seely was born in New York City on May 7, 1909. He received the E.E. degree from the Polytechnic Institute of Brooklyn in 1931, the M.S. degree from Stevens Institute of Technology in 1932, and the Ph.D. degree in physics from Columbia University in 1936.

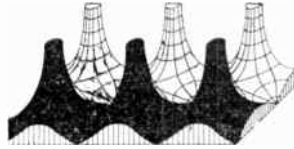
From 1936 until 1941 he was a member of the electrical engineering staff of the City College of New York. During the war he was a staff member of the M.I.T. Radiation Laboratory and served as group leader and project engineer working on radar and the supersonic radar trainer. He was leader of the Australian Group of the Radiation Laboratory at the Radiophysics Laboratory in Sydney, N. S. W. He received the Army-Navy Certificate of Appreciation in 1947 for his radar work. From 1946 to 1947 he was associate professor of electronics at the Naval Postgraduate School, and then joined the staff of Syracuse University's electrical engineering department as professor. He became chairman of the department in 1951, a post

he retained until 1956, when he left to become professor and head of the electrical engineering department at the Case Institute of Technology.

Dr. Seely is the author of four books in the electronics field, and one in the networks field, and has done research in diamagnetism, nuclear physics, physical electronics, antenna theory, and electronic circuits. He holds membership in Tau Beta Pi, Sigma Xi, and Eta Kappa Nu. He is a Fellow of the American Physical Society, and a member of AIEE and ASEE.

He has participated in a number of IRE activities, serving successively as Secretary-Treasurer, Vice-Chairman, and Chairman of the Syracuse Section; as a member of the Papers Review Committee since 1946, and present chairman of the IRE Education Committee, as a member of the IRE Policy Advisory Committee, and the AIEE-IRE Joint Committee on Student Activities. He became an Associate in 1939, a Senior Member in 1945, and was elected a Fellow in 1955.

Poles and Zeros



New Groups. We are happy to welcome two new IRE Professional Groups whose constitutions were approved earlier this year: the Group on Education and the Group on Engineering Writing and Speech. With these additions, the PG roster now stands at 26. Their formation is worthy of special note because these new Groups, together with the Group on Engineering Management, which was formed in 1951, constitute a subroster of three whose fields of interest are very broad and by no means unique to the IRE. In fact, the techniques and objectives of education, management, and communication by the written and spoken word transcend science and engineering and extend into virtually every field of organized endeavor.

It is not surprising, therefore, that the wisdom of organizing IRE activities in these fields has been questioned both inside and outside of the Institute circle. There are well-established societies devoted exclusively to engineering education, to industrial management, and to technical writing. By exercising what option does IRE establish groups in these already pre-empted fields?

This question has been pondered by those who petitioned for the new Groups, and by the Executive Committee in passing on the petitions. There are two answers. First, the purpose of these groups is *not* competition with existing bodies. Quite the opposite. Accreditation of sister societies in these fields under the PG Affiliate Plan is proceeding rapidly. Through these and other cooperative measures, it is the plan of the new IRE Groups to aid existing activities in their fields and it is their hope that they can be particularly effective within the profession of electronics.

Secondly, in electronics and the allied arts, there are particular and special problems in education (see *P and Z* last month), in management (see any issue of PGEM TRANSACTIONS), and publications and conferences which deserve the organized attention of IRE members. In other societies, these questions often have, and deserve, lower priority. The Group petitioners see jobs to do, many that are peculiar to conditions and motivations in our profession, and they feel that in organizing for these jobs they will help rather than hinder the over-all activity in their respective fields.

Calendar. Few literary frustrations compare with that suffered by an author who, having thought out his paper and prepared the abstract, finds that he has missed the final date for submitting same to the pro-

gram committee. Since such tardiness is often associated with technical brilliance, or at least with a high level of other productive activity, we suspect that many good papers are lost down this road and we have set up a small countermeasure. Since the June issue, the Calendar of Coming Events, which is printed each month in the News Section, has contained the dates for submitting abstracts for all meetings on which we have information. Potential authors are therefore urged to consult the Calendar, and Program Chairmen are particularly requested to send their closing dates to the Managing Editor immediately after they are established.

In time, after the word gets around on this system, we hope that closing dates will be published in plenty of time for all meetings, and we suppose that lack of such publication will be *prima facie* evidence that the program committee got started too late or was otherwise not on the job. We admit this is not much of a threat, since we never heard of a program committee that would accept reappointment, let alone seek it. But, having once been trapped into the job, committee members do value the widest possible choice of abstracts in selecting the program, and prompt publication of the closing dates would appear to be strictly nondeleterious. So, send the dates. We'll publish them in the first available issue following receipt and thereafter until the closing date is passed.

Mileposts. During the month of May, IRE membership passed the 60,000 mark, with 60,030 names on the roster at the end of the month. The increase in membership in twelve months was 20 per cent, up from 15 per cent the previous year. It seems fair to conclude, from the increasing rate of growth, that the IRE program of conferences, publications, and PG activities is attracting many recruits and holding the interest of the old timers.

Since last February, there have been more Professional Group memberships (currently over 63,000) than there are IRE members, but almost half of the IRE members belong to no Group. This conundrum is explained by the fact that the average (or should it be "median") member of a professional group belongs to two groups at once. With 26 groups to choose from there's plenty of room for growth in this department. Group membership is open to all IRE members, and through the affiliate plan, to members of many other professional societies. Headquarters will send full information on request.—D.G.F.

Scanning the Issue

Ultrasonics in Medicine and Dentistry (Welkowitz, p. 1059)—When various parts of the human body are subjected to sound waves at frequencies of about one megacycle or higher, a number of interesting and medically useful effects may be observed. The reflection and absorption characteristics of tissue, together with the thermal and mechanical effects produced by the sound energy, can be utilized to visualize soft tissues that are transparent to X rays, detect tumors, drill teeth, perform brain surgery and, in the field of bacteriology, to sterilize foods and pasteurize milk. These and other important applications of ultrasonics have for the most part been developed just within the last eight years; many of them are still in the laboratory stage. Nevertheless, as will be seen from this review paper, they already show great promise as important tools in medicine and biology.

Ion Oscillations in Electron Beam Tubes: Ion Motion and Energy Transfer (Jepsen, p. 1069)—Many types of vacuum tubes are affected, usually adversely, by positive ions which become trapped in the electron beam region. Although the effects of ion trapping have been described in many articles, the mechanism by which it occurs has eluded experimenters. Particularly baffling is the fact that under seemingly similar circumstances, in one case there are no apparent undesirable effects, while in another case ion oscillations occur giving rise to instabilities and distortions in the output wave. In this paper the author develops a plausible picture of ion motion and energy transfer in microwave tubes by which he explains this misbehavior. Moreover, in analyzing the conditions under which ion oscillations are sustained, it is shown that a new type of negative beam loaded oscillator, called a "nonotron," appears possible.

Multihole Ferrite Core Configurations and Applications (Abbott and Suran, p. 1081)—This paper reports further work on the transfluxor, a multihole ferrite disk recently developed as a switching element for control and computer type circuitry. As is elaborated on in this paper the multihole geometry of this device provides the circuit designer with an intriguing new component that can perform some very novel and complex gating and memory functions. As a case in point, a six-hole transfluxor is described which will perform complex logical functions that would require as many as twelve transistors.

Polarization Reversal and Switching in Guanidium Aluminum Sulfate Hexahydrate Single Crystals (Wieder, p. 1094)—The foregoing rather imposing title refers to a recently discovered ferroelectric sulfate, nicknamed GASH, which like its better known ferroelectric cousin, barium titanate, has been advanced by many as a possible new computer switching and memory device. The author delves into the switching properties of GASH, carefully comparing them with those of barium titanate. The result is a timely and much-needed statement of the limitations and capabilities of both materials, indicating that for the present GASH must be limited to low-speed (less than 1 kc) switching applications.

Straight-Field Permanent Magnets of Minimum Weight for TWT Focusing—Design and Graphic Aids (Glass, p. 1100)—This paper fills an outstanding need for information on the design of lighter weight focusing magnets for traveling-wave tubes. Its importance derives from the fact that a major problem in the use of traveling-wave tubes in systems has been the cumbersome electromagnets. Periodic focusing, although it reduces magnet weight, is nevertheless difficult to apply in

many practical cases. Straight-field focusing, because of its simplicity and convenience, is more attractive, provided the size and weight of the magnets are acceptable. This can now be quickly calculated by the excellent design charts and procedures presented here.

Some New Circuits for High-Power Traveling-Wave Tubes (Chodorow and Craig, p. 1106)—Two basic types of slow-wave structures have received considerable attention as interaction circuits for traveling-wave tubes: the helix and the periodically-loaded waveguide. When it comes to high-power applications the helix takes a back seat to the loaded waveguide because of its limited heat dissipation capabilities. The loaded waveguide, on the other hand, tends to have narrow bandwidth properties because of the resonances of the obstacles used to load the guide. This paper describes a new class of broad-band slow-wave structures, consisting of sets of coupled cavities, which mark important progress in providing microwave tubes with greater bandwidths at megawatt power levels.

On Multimode Oscillators with Constant Time Delay (Met, p. 1119)—An investigation is made of the stability of oscillators that can operate in two or more stable modes and that include substantial time delay in their feedback paths. Special emphasis is paid to narrow-band systems with a small number of modes, and to high switching speed from one mode to another. The actual system considered is a recirculating frequency memory device and the details come out in a form which will not only be of particular interest to people interested in such systems, but to a broader group of engineers interested in the basic theory of oscillators.

A Reactance Theorem for Antennas (Levis, p. 1128)—From Maxwell's equations a rigorous formula is developed for the frequency derivative of the reactance or susceptance of an antenna, containing terms relating the expression to the polarization properties of the far field of the antenna and the electromagnetic energy stored in its near field. In effect, this theoretical study sets down relationships, previously known intuitively, in a precise form that furnishes valuable additional insight into antenna resonance phenomena.

Heat Loss in Grooved Metallic Surface (Marcatili, p. 1134)—An approximate solution is presented to the interesting problem of calculating the conduction current losses in grooved metallic waveguide walls, a matter of interest both to groups solving boundary value problems and to those interested in transmission line problems. Although of primary application in the microwave field, this method of computing losses in irregular surfaces may be of interest in lower frequency regions as well, for instance in computing surface wave propagation over a rough sea.

IRE Standards on Letter Symbols and Mathematical Signs (p. 1140)—In 1948 the IRE published a Standard covering abbreviations, graphical symbols, letter symbols, and mathematical signs. The abbreviations and graphical symbols portions of that Standard were later superseded by new Standards issued in 1951 and 1954, respectively. The Standard printed in this issue is a reprint of the remaining portions of the 1948 Standard, now out of print. It provides a valuable guide to the notational use of subscripts, superscripts, bold face, and italics, and identifies nearly 200 letter symbols and mathematical signs common to the radio engineering literature.

Ultrasonics in Medicine and Dentistry*

WALTER WELKOWITZ†, MEMBER, IRE

Summary—In recent years, there has been much research on the applications of ultrasonic techniques to medicine. This paper discusses some of the projects being carried out in the fields of diagnosis, therapy, dentistry, and bacteriology. The diagnostic investigations presented include brain tumor detection, soft tissue visualization, and analysis of cancers for malignancy. The therapy studies include tissue diathermy, brain surgery, and tumor inhibition. Drilling of teeth is the application discussed in dentistry. In all cases, an attempt is made to elucidate the mechanisms pertinent to the applications.

INTRODUCTION

AN acoustical instrument, the stethoscope, was one of the earliest physical instruments utilized in medical diagnosis. Since the work by Laennec over one hundred years ago, this instrument has been in constant use by physicians in diagnosing cardiac disorders.

More recently, there has been a great expansion in the application of acoustic devices to medicine. This has come about through the extensive development of both electronic and acoustic instruments for industrial applications. In these more recent applications, use is made not only of the measurement of sounds generated in the body, but, in addition, waves generated outside the body are introduced into it and use is made of the acoustic impedance and absorption of the tissue plus the thermal and mechanical destructive effects that are sometimes a concomitant of sound propagation.

Since the mechanical properties of tissue are different from the electrical ones, acoustic examination will at times show up variations in tissue that are not seen with X-ray examination. In addition, because of the ease of focusing sound waves in the millimeter wavelength range, it is sometimes possible to produce, by the use of ultrasound, localized lesions that are difficult to obtain by any other means.

DIAGNOSTIC APPLICATIONS OF ULTRASOUND

As an extension of the stethoscope procedure, Walker, Thurston, and Kirby¹ worked out a percussion system to detect gallstones which utilizes a microphone and amplifier system to pick up the sounds of a tapped gallstone.

At the present time, most diagnostic systems which are being studied utilize either the transmission properties of the body tissues or their reflective properties.

The principles of these systems can best be understood with reference to Fig. 1. In Fig. 1(a) a simplified

sound transmission diagnostic system is diagrammed. A sound source (which can be a piezoelectric crystal appropriately driven) is pressed against the tissue on the left. A sound receiver (which can be an identical unit) picks up the transmitted sound on the right. If there is an abnormal object present in the tissue, and if this object has an acoustic absorption coefficient that is much different from the normal tissue, then a change will be observed in the received sound. A sound reflection diagnostic system is diagrammed in Fig. 1(b).

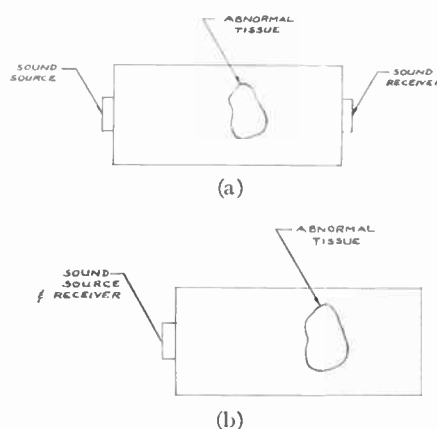


Fig. 1—(a) Transmission system. (b) Reflection system.

Under normal conditions, a pulse of sound is sent out from the transducer. This sound pulse is reflected from the back face of the tissue and the echo is picked up by the transducer. A suitable display system shows the reflected pulse appearing some time after the transmitted pulse. If some abnormal tissue is present in the transmission path, and if the acoustic impedance of this tissue is different from that of the normal tissue, then there will be some energy reflected when the pulse of sound arrives at the interface between the normal and abnormal tissue. From the geometry of the system, this abnormal echo would appear on the time display between the transmitted pulse and the echo from the back face of the tissue.

Reflection Measurements

A number of medical experiments can be presented to exemplify the diagnostic methods. One set of these experiments is the detection of gallstones in tissue as carried out by Ludwig and Struthers.² The reflection method of diagnosis was investigated using a Sperry Reflectoscope. Since this method involves the presence of an

* Original manuscript received by the IRE, January 22, 1957; revised manuscript received, May 24, 1957.

† Gulton Industries, Inc., Metuchen, N. J.

¹ Walker, Thurston, and Kirby, *Electronics*, vol. 22, p. 92; 1949.

² Ludwig and Struthers, Naval Medical Res. Inst. Project NM004001, Rep. No. 4; 1949.

impedance mismatch between the normal tissue and the gallstone, the authors made an extensive study of acoustic impedances of normal tissue and gallstone. Their results are summarized in Table I, below. These

TABLE I
CHARACTERISTIC ACOUSTIC IMPEDANCE OF TISSUE AND GALLSTONE

Material	Density (ρ) gm/cm ³	Velocity (c) cm/second	Impedance (Z) gm/cm ² / second
Water	1.00	1.50×10^5	1.50×10^5
Tissue (range)	1.06	1.54×10^5 (1.49 to 1.61×10^5)	1.6×10^5 (1.5 to 1.7×10^5)
Gallstone slabs			
1. (almost pure cholesterol)	1.067	2.19×10^5	2.3×10^5
2. (mostly pigment)	1.069	1.78×10^5	1.9×10^5
3. (pigment-calcium)	1.013	2.04×10^5	2.0×10^5
4. (mixed cholesterol center lamellae of pigment+cholesterol)	0.936	1.87×10^5	1.7×10^5
5. (mostly cholesterol)	0.900	1.40×10^5	1.3×10^5
Series of gallstones	0.82 to 1.10	1.40×10^5 to 2.30×10^5	1.15×10^5 to 2.42×10^5

measurements indicate that for most gallstones there is an appreciable difference in impedance between the gallstone and normal tissue. Calculations based on the assumption of plane interfaces indicate that between 0.1 and 4.0 per cent of the incident energy would be reflected in most cases. Since the Reflectoscope is capable of satisfactory operation with 0.1 per cent of the energy reflected, most gallstones should be detected by this method. Measurements and analyses were also carried out to determine the optimum frequency of operation. This decision involves a compromise between the particle size resolution and the depth of penetration. With instruments of the power output of the Reflectoscope, frequencies between 1.0 and 2.5 mc were found to be optimum. Final experiments were carried out with gallstones implanted in the back muscles and gall bladder of a dog. These gallstones ranged in size between 0.5 and 1.0 cm and were detected with little difficulty.

Another diagnostic problem being investigated using reflection methods is the study of tumor detection carried out by Wild and his associates at the University of Minnesota.³ In this case, $\frac{1}{2}$ -microsecond pulses of 15-mc sound are projected into the tissue and the resultant echoes are recorded. Gross structural interfaces, such as between muscle and fat, are readily detected at this high-ultrasonic frequency. Anisotropy of tissue is demonstrated with this device. As is evident in Fig. 2, the pattern of echoes from a piece of beef is much different when the sound is projected along the fibers than when

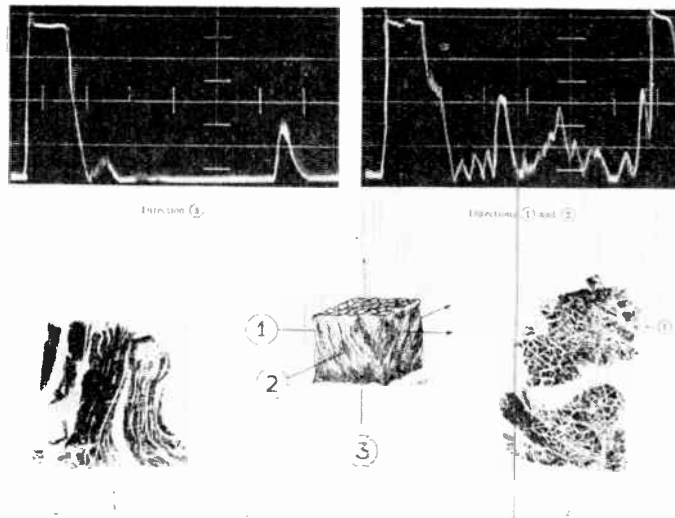


Fig. 2—Anisotropy of tissues. The known orientation of muscle bundles in beef steak is demonstrated. Few echoes are produced when sound beam is parallel to the muscle fibers, 3. Many echoes are produced when the sound beam is directed across the fibers 1 and 2. Longitudinal and cross sections of the material are shown; magnified slightly.

it is projected transverse to the fibers. The application to tumor detection is well illustrated by Fig. 3. The transducer and holder are shown in the upper right. The water column is used to introduce an acoustic time delay so that echoes from regions near the surface of the tissue can be detected without being hidden by the transmitting pulse. The method used to survey a brain with the skull removed is shown in the upper left. The differences in the echo patterns between normal and tumor regions are shown in the lower pictures. The presence of the tumor appears to produce many more echoes than does the normal tissue. This is similar to what was produced by highly anisotropic tissue. The method, therefore, seems to be a measure of the anisotropy of the tissue. The authors³ have attempted to quantize the method by measuring the area under the echogram. They claim to have found a significant difference between tumor relative to control echogram areas for benign and malignant tumors.

A group under the direction of Dr. Howry at the University of Colorado at Denver is also working on the problem of soft tissue visualization by utilizing reflection techniques. Their approach includes a mechanical scan and an intensity^{4,5} modulation scheme by which three-dimensional portrayals can be obtained. Some early results obtained in picturing the cross section of an arm are shown in Fig. 4. The resolution obtainable is shown by the scan of a wire box in Fig. 5. The difficulties in the system are inherent in geometric optics. A glance at Fig. 6, in which a sound wave impinges on a curved surface, demonstrates the problem. No amount of rotation on the part of the trans-

³ J. J. Wild and J. M. Reid, "The effects of biological tissues on 15 mc pulsed ultrasound," *J. Acoust. Soc. Amer.*, vol. 25, pp. 270-280; March, 1953.

⁴ Howry, Stott, and Bliss, *Cancer*, vol. 7, p. 354; 1954.

⁵ Howry and Bliss, *J. Lab. and Clinical Med.*, vol. 40, p. 579; 1952.

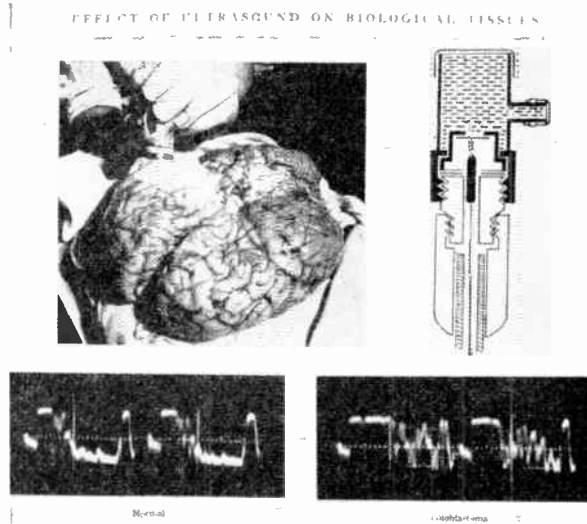


Fig. 3—Cancer of the brain. Top left, two echograms of normal brain tissue approximately 1.4-cm thick. Top right, two echograms of a piece of malignant tumor arising from the same brain. The tumor was reduced to half-thickness. Two pairs of echograms recorded with the echoscope (midright) on the whole brain (mid-left) are shown at the bottom. Normal echograms (bottom left) were taken from the opposite lobe of the brain from that occupied by the tumor. The greater number of echoes coming from the tumor can be seen in the echograms (bottom right).

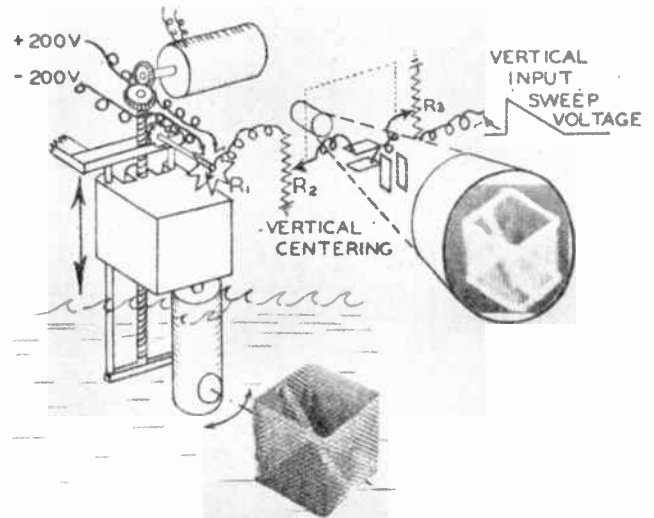


Fig. 5—Variable projection, three dimensional somagraphy.

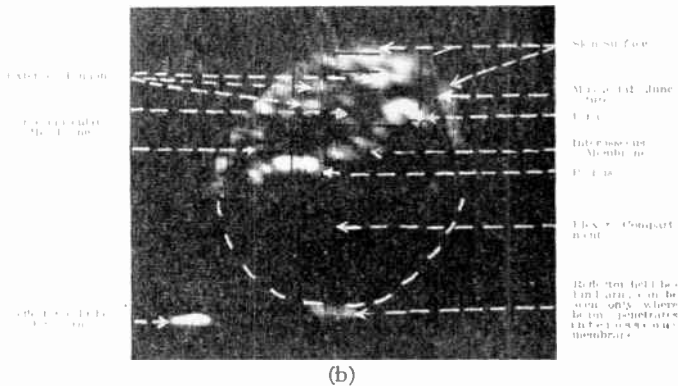
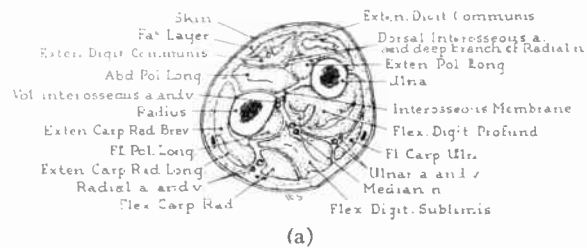


Fig. 4—(a) Transverse section through midforearm. (b) Somagram of extensor compartment of midforearm.

ducer will cause echoes to return to it from most of the curve.

The partial successes of these endeavors have encouraged work of this sort all over the world. In Japan, some very interesting work under the direction of Dr. Kikuchi⁶ has been carried out on diagnoses of brain tumors utilizing a reflection-type ultrasonic system.

⁶ Kikuchi, Uchida, Tanaka, and Wagai, *Proc. Second Internat. Cong. of Acoustics*; 1956.

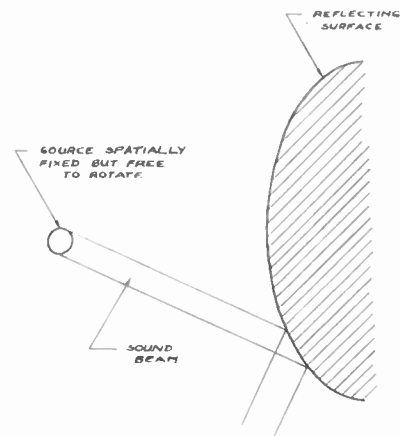


Fig. 6.

Kikuchi was able to obtain echoes through the skull which may be useful in diagnosing physical brain disorders by utilizing barium titanate transducers. Echoes were obtained from the brain tumor, from the ventricle walls, and from the opposite side of the brain.

Transmission Measurements

In addition to utilizing reflection-type measurements for diagnosis, there have been a number of attempts at diagnosis by means of transmission measurements. One of the most extensive projects of this sort was the work on outlining cerebral ventricles and the detection of brain tumors with ultrasound. In this case, the study was carried out without removal of any part of the skull. This procedure was first investigated in Austria by Dr. Dussik.⁷ An extensive continuation of this study was recently carried out in this country by a group at the Acoustics Laboratory at M.I.T.⁸ A schematic of one of the systems used by the group at M.I.T. is shown in

⁷ Dussik, Dussik, and Wyt, *Wiener Med. Wchnscho*, vol. 97, p. 425; 1947.

⁸ T. F. Hueter and R. Bolt, *J. Acoust. Soc. Amer.*, vol. 23, p. 160; 1951.

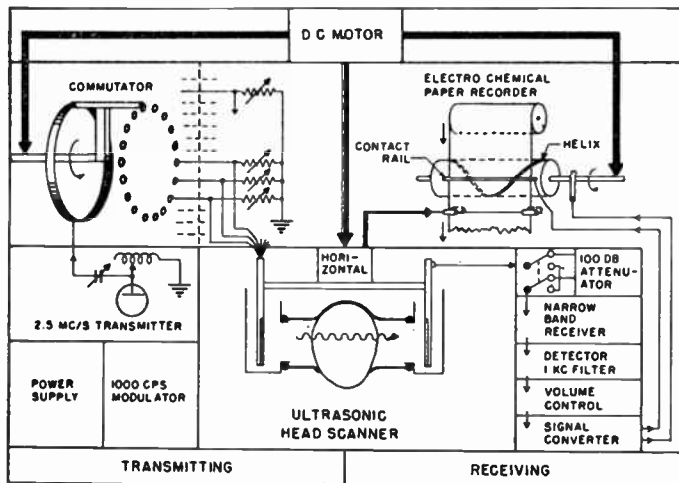


Fig. 7—Schematic representation of apparatus used to make ultrasonogram.

Fig. 7. A 20-element transducer strip was used to scan in the vertical direction to get a picture of a large area. The mosaic strip was moved in the horizontal direction to obtain a picture of the whole head. The expected method of recognizing tumors or other distortions in the brain was to observe abnormalities in the shape of the ventricles—fluid-filled cavities—in the head. The presence of a growth in the brain will often distort the shape of these cavities. It was hoped that the ventricles would show up readily in the ultrasonogram, since the brain matter has an attenuation of 1.5 db/cm at 1.0-mc sound frequency, while the liquid in the ventricles has an attenuation of only about 0.01 db/cm in this frequency range.⁹ The difficulties that were encountered in using this transmission system demonstrate some of the problems that are encountered in using ultrasonic diagnostic systems to examine complex humans. The acoustic absorption of the skull is about 17 times that of the brain tissue. Thus at 1 mc, a thickness variation of 1 mm produces the same change in signal intensity as a variation of 1.7 cm in the ventricle path length. Thus, the “noise” produced by skull thickness variation may readily override any signal variations produced by distorted ventricles. This is the case at present, and even attempts at reducing the “noise” by compensation schemes which take advantage of differences in attenuation—frequency characteristics of bone and soft tissue—have not been very successful when tried clinically. Thus, what theoretically seems like a straightforward application of ultrasound in medicine may, in practice, be beset by many difficulties because of the complex structure of the body.

Another approach in which an attempt is made to utilize the transmission method is represented by the work of Suckling and MacLean¹⁰ at the New York

⁹ Ballentine, Hueter, and Bolt, *J. Acoust. Soc. Amer.*, vol. 26, p. 581; 1954.

¹⁰ Suckling and MacLean, *J. Acoust. Soc. Amer.*, vol. 27, p. 297; 1955.

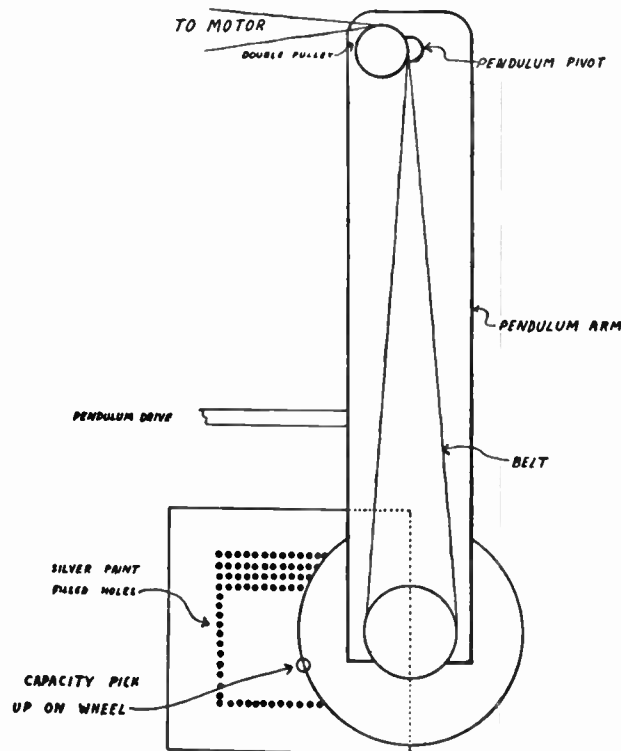


Fig. 8—Pendulum and rotary scan system allowing capacity pickup to cover whole area of crystals. Position indicator and capacity slip rings not shown.



Fig. 9—See text.

State Medical School. In this case, quartz plates are used as the ultrasonic transmission and receiving transducers. The receiving quartz is mechanically scanned with a small capacitive probe and the output is displayed on an oscilloscope synchronized with the scan. A diagram of the system is shown in Fig. 8. An acoustic picture of a cardboard mask as observed with this system is shown in Fig. 9.

In order to improve on the mechanical scan feature of Suckling's device use can be made of an electronic-acoustic converter electron beam tube described by

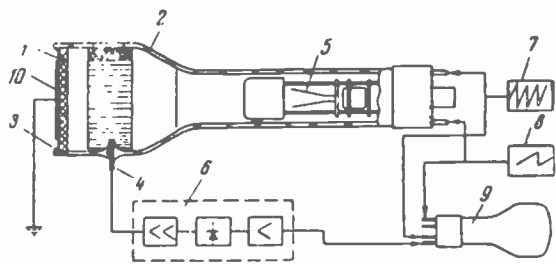


Fig. 10—Connection diagram of electronic-acoustic converter.

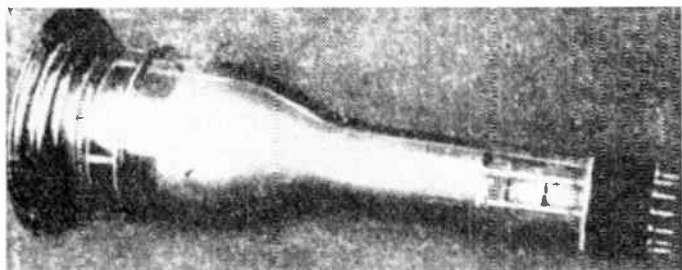


Fig. 11—External view of converter.

Oshchepkov¹¹ and his co-workers. A diagram of this tube is shown in Fig. 10. A picture of the tube is given in Fig. 11. This tube utilizes a piezoelectric barium titanate ceramic front face and a scanning electron beam. The signal is picked up as variation in the stream of secondary electrons going to the collector. When a sound wave impinges on the front face of the tube, varying voltages are produced which modify the condition of secondary electron production and therefore provide an amplitude modulated signal in the output. Tubes of this type are also under development in this country at Gulton Industries, Inc.¹²

THERAPEUTIC APPLICATIONS OF ULTRASOUND

In considering therapeutic applications of ultrasound, one finds that there has been extensive clinical work performed both in this country and in Europe.¹³⁻¹⁵

Thus, work has been carried out in the treatment of neuritis, bursitis, osteoarthritis, and many other ailments with sound. In many of these clinical investigations, inadequate controls make it difficult to evaluate the effectiveness of the treatment and furthermore, because of the nature of clinical work, it is difficult to distinguish the mechanism or sometimes even the tissue affected. Before discussing some of the therapeutic potentialities, it seems reasonable to discuss the possible mechanisms by which ultrasound can do its work and some of the results of investigations carried out on specific tissues.

¹¹ Oschepkov, Rozenberg, and Semennikow, *Akusticheskii Zhurnal*, vol. 1, pp. 348-351; 1955.

¹² Gulton Industries, Inc., private communication.

¹³ "Der Ultraschall in der Medizin," S. Hirzel, Zürich, Switzerland; 1949.

¹⁴ *Nuevo Cimento*, suppl. vol. VII, ser. IX, Rome, Italy; 1950.

¹⁵ "Proceedings of Conferences on Ultrasonic Therapy," *Amer. J. Phys. Med.*; 1953, 1954, 1955, and 1956.

Mechanisms

The mechanisms by which sound effects tissue can be grouped under the general classifications of heating, cavitation, chemical effects, and direct mechanical forces. Heating effects are secondary phenomena which result from the fact that some tissues have high acoustic absorption coefficients, that is to say, a large fraction of the mechanical energy in the sound wave is converted into heat. Any beneficial results that are then produced are similar to benefits obtained by applying heat from a thermal source. The probability of introducing the heat into a desired internal location is better with the sound, though, than with many other heat sources. Cavitation effects can often be produced when the peak pressure amplitude of the sinusoidal sound wave is greater than 1 atmosphere. The local tension forces that are then produced in the tissue may cause the growth of bubbles containing gases or vapors. After a certain amount of growth, these bubbles tend to collapse rapidly with the production of high local forces and high local temperatures. These secondary forces and temperatures produce some of the observed tissue alterations or destructions. Aside from these secondary mechanisms, there can be direct effects produced by forces that are inherent in the mechanical nature of the sound wave. Such forces are the direct pressure stresses that can be varying at the rate of millions of cycles per second, oscillating viscous forces resulting from the complex semiliquid nature of the tissue medium, and unidirectional forces which arise from the nature of the sound field. An example of these is radiation pressure. Forces due to the sound field which manifest themselves on the molecular level may produce effects which are observable as chemical changes in the irradiated material. If we classify mechanisms on the basis of gross observations, we should then include these chemical mechanisms. It should be kept in mind, though, that the sound waves are mechanical waves and that, therefore, all the mechanisms are basically mechanical in nature. Some clear cut results of sound irradiations, and the classification of the observations with respect to the mechanisms discussed can best be presented by analyzing some of the work carried out on specific tissues.

Tissue Irradiations

Studies by Herrick and associates¹⁶ at the Mayo Clinic and Fry and associates¹⁷ at the University of Illinois, demonstrate the high acoustic absorption in bone. The temperature increase recorded in the femur bone of a dog by the group at Mayo is shown in Fig. 12 for continuous and pulsed ultrasound. The total output of the transducer used in these studies was 10 watts at a

¹⁶ J. R. Herrick, *J. Acoust. Soc. Amer.*, vol. 25, p. 12; 1953.

¹⁷ W. J. Fry, V. J. Wulff, D. Tucker, and F. J. Fry, "Physical factors involved in ultrasonically induced changes in living systems: I. Identification of non-temperature effects," *J. Acoust. Soc. Amer.*, vol. 22, pp. 867-876; November, 1950.

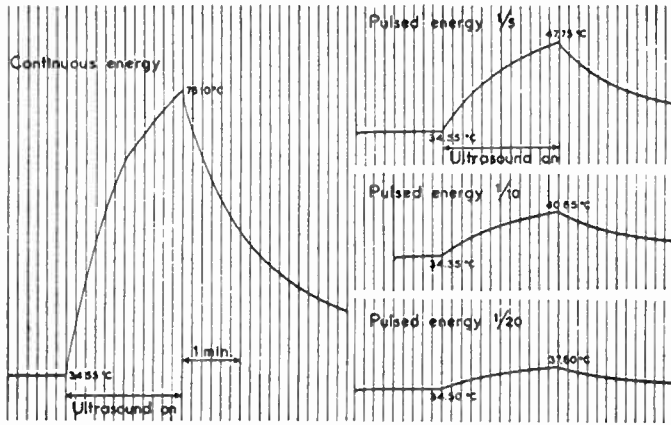


Fig. 12—Changes in temperature in the femur of the dog when ultrasound is generated continuously (left) and when ultrasound is pulsed (right). Stationary application, 10 watts.

frequency of about 800 kc. As is apparent from Fig. 12, a continuous two-minute irradiation at this comparatively low sound power raised the temperature of the bone more than 30°C. If the temperature increase can readily be controlled, diathermy applications are suggested. The temperature changes produced in various frog tissues by pulsed ultrasound, as measured by Fry, are shown in Fig. 13. In this case, a peak sound intensity of 35 watts/cm² was used. At this relatively high intensity, the temperature of the bone was increasing at the rate of 55°C per second of irradiation.

In nerve tissue, ultrasonic irradiation studies have been carried out which indicate both thermal and non-thermal effects on the physiology of the nerve. The group at Mayo studied the suppression of the propagated action potential (the electrical pulse) in a bull frog's sciatic nerve. They found that at the relatively low ultrasonic intensity used, suppression was accomplished only when the temperature of the nerve was raised by the sound to a level which would cause suppression of the propagated action potential if the temperature increases were otherwise produced. Fry's group found that when sonic irradiation was directed at the lumbar enlargement region of a frog's spinal cord, paralysis was obtained under conditions that precluded temperature effects or cavitation effects.¹⁸ This is best shown in Fig. 14, which represents the results obtained on frogs irradiated at 1 atmosphere and at 13 atmospheres of static pressure at an initial temperature of 1°C. It can be observed from Fig. 14 that even with 13 atmospheres of static pressure applied (enough to completely suppress cavitation), the quantitative results were very similar to those obtained at atmospheric pressure. Both sets of results were obtained under temperature conditions such that with the sound on, the temperatures produced in the spinal cord were not sufficient to cause damage. In some recent work by Fry and Dunn,¹⁹ similar irradiations

¹⁸ W. J. Fry, *J. Acoust. Soc. Amer.*, vol. 25, p. 1; 1953.

¹⁹ W. J. Fry, and F. Dunn, "Ultrasonic irradiation of the central nervous system at high sound levels," *J. Acoust. Soc. Amer.*, vol. 28, pp. 129-131; January, 1956.

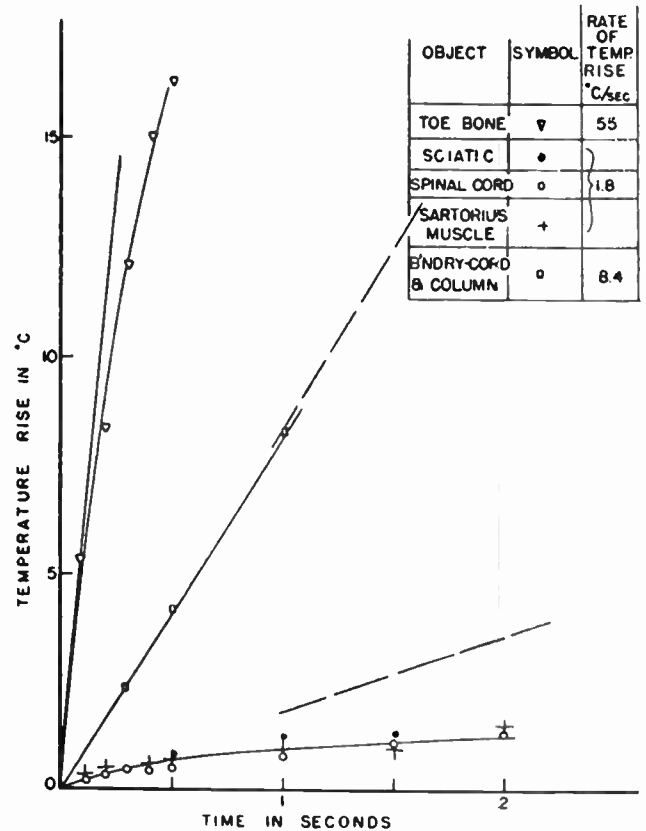


Fig. 13—Temperature rise as a function of time in various tissues under ultrasonic irradiation at a frequency of 980 kc and an intensity ~35 w/cm².

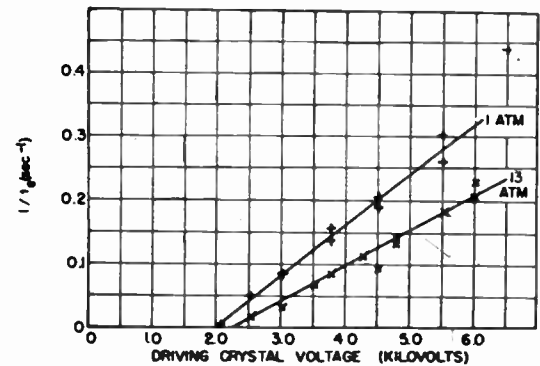


Fig. 14—Relations between driving crystal voltage, which is proportional to acoustic pressure amplitude, and reciprocal of the "minimum time for paralysis" frogs cooled to 1°C and under hydrostatic pressures of one and thirteen atmospheres.

were carried out on mouse spinal cords in an attempt to elucidate a mechanism. Again the results preclude the possibilities of their being only a heating mechanism.

A situation similar to that in the work on nerve tissue exists in studies of muscle tissue. Under certain ultrasonic irradiation conditions effects are produced which are undoubtedly thermally caused, while under other experimental conditions nonthermal effects have been observed. Gersten²⁰ has irradiated frog muscle with

²⁰ J. W. Gersten, *Archives of Phys. Med. and Rehabil.*, vol. 34, p. 675; 1953.

sound at a frequency of 1 mc and of average sound intensities of 0.75 watt/cm² and 3 watts/cm². Changes observed, such as changes in isometric tension, at the lower intensity are completely attributable to the increase in temperature produced by the sound. At the higher intensity level, though, some changes produced, such as changes in injury potential level, were apparently different from effects produced by temperature alone. Welkowitz²¹ irradiated isolated frog muscles under conditions such that the resultant temperature rise in the muscle was not great enough to produce thermal effects, and he studied the changes produced in the propagated action potential. A sound frequency of 1 mc and intensities of the order of 100 watts/cm² were used. Fig. 15 shows the effect produced on the amplitude of the action potential. The propagated action potential was permanently blocked. In Fig. 16, a dosage curve obtained in these studies is shown. It is obviously similar in form to the dosage curves obtained by Fry in the frog spinal cord paralysis experiments. This similarity suggests that perhaps under these nonthermal and non-cavitation situations, the observed effects were produced by similar mechanical mechanisms.

Before terminating the discussion of irradiation of specific tissues, mention should be made of some studies carried out on the irradiation of tumor and cancer tissue. Studies carried out at the Mayo Clinic indicated that under their experimental conditions, little inhibition of tumor growth was observed except when the tumor was burned by the ultrasound. Newcomer, at the University of Connecticut,²² indicated that he obtained regression in tumors implanted in mice when these were irradiated at sound intensities above 20 watts/cm². It would appear that this is a fruitful field for further inquiry.

A major problem often arises in the analyses and comparisons of the different studies. This is the very limited and often inaccurate description of the exact physical experimental conditions. It is apparent that there is a great need in this field for more accurate ultrasonic measurements. These must include measurements of the field configuration, and measurements of intensity at various points in the field. An indication is needed of whether the field is a traveling-wave field or a standing wave field or a combination of the two. A knowledge of the medium of irradiation, the geometry of the irradiated object, some measurement of temperatures generated in the irradiated tissue, and an indication of viscosity and gas content of the medium and irradiated object are also desirable. The latter could be replaced by mentioning that the experiments were carried out under a high enough static pressure to preclude the possibility of cavitation damage. Some indications of the field configurations that have been used are

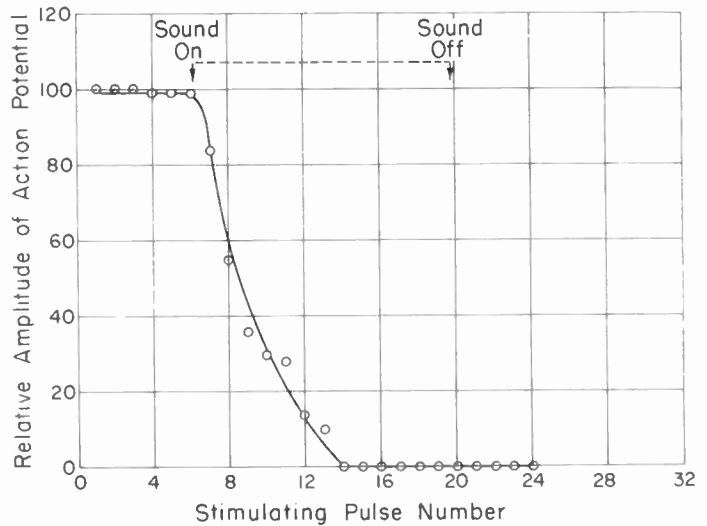


Fig. 15.

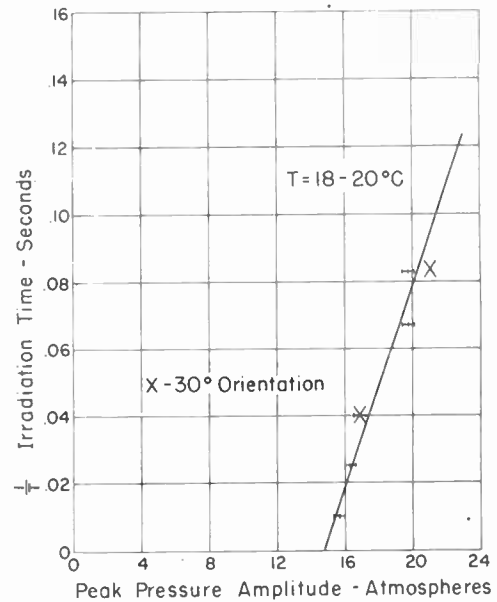


Fig. 16.

shown in Figs. 17 and 18 (next page). Fig. 17 illustrates the field pattern obtained from a 1-inch X-cut round 1-mc quartz crystal radiating into water. The zero distance was about six inches from the crystal. The beam pattern obtained at the focus of a quartz crystal with a polystyrene lens in front of it is shown in Fig. 18. It is apparent that this focused beam is only half as wide at the half-power points as was the first beam described. Even sharper focusing has been obtained by using other focusing methods and the influences of these different sized beams will vary when used on bulk tissue.

Brain Surgery with Ultrasound

Ever since it became apparent that ultrasound could damage tissue, attempts have been made to perform brain surgery by producing lesions in the brain sonically. Much of the early work, exemplified by the experiments

²¹ W. Welkowitz and W. J. Fry, "Effects of high intensity sound on electrical conduction in muscle," *J. Cell. Comp. Physiol.*, vol. 48; December, 1956.

²² E. H. Newcomer, "Effects of ultrasound on living cell structure," 1954 IRE CONVENTION RECORD, pt. 6, pp. 107-108.

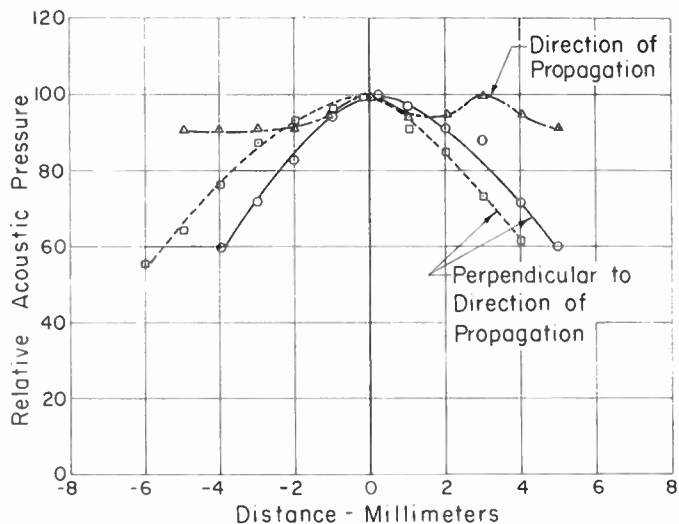


Fig. 17.

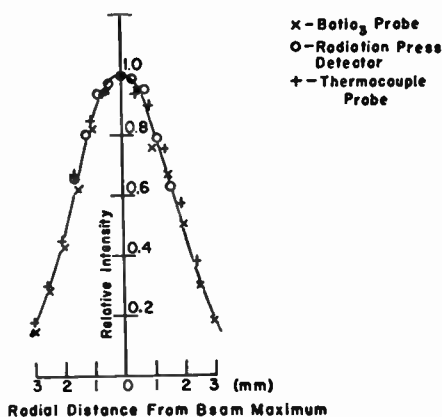


Fig. 18—Comparison of beam patterns taken with 1) thermocouple probe and 2) BaTiO₃ radiation pressure detector.

of Lynn and associates,²³ was carried out by irradiation through the skin and skull with both focused and unfocused sound beams. Recent investigations²⁴ indicate that more consistency can be obtained if the skin and skull bone in the path of the sound beam are removed. In addition to the variability problem, it has been pointed out by Fry²⁵ that bone is highly absorbing at the ultrasonic frequencies used, and that the bone therefore must be removed to prevent overheating and to introduce most of the sound in the beam into the brain.

Lindstrom and his group at the University of Pittsburgh carried out some irradiations on both animals and humans. The work on animals was carried out to study the path of the sound beam through the brain and to see what effects were obtainable. The irradiations were carried out with sound frequencies of 1 mc. The only intensity measurements that were made were average

²³ Lynn, Zwemer, Chick, and Miller, *J. Gen. Physiol.*, vol. 26, p. 179; 1942.

²⁴ P. A. Lindstrom, *AMA Archives of Neurology and Psychiatry*, vol. 72, p. 399; 1954.

²⁵ Fry, Mosberg, Barnard, and Fry, *J. Neurosurgery*, vol. 11, p. 471; 1954.

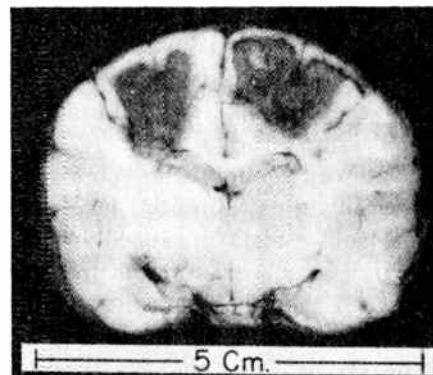


Fig. 19—Excessive ultrasonic necroses which extended along the boundary between cortex and white matter in a dog brain. A non-focused beam of 7 watts per square centimeter at 1000 kc was used. A dural flap was turned at the right side of the picture. On the opposite side the same irradiation was given through the intact dura.

values over the entire beam. Sound levels of 2 watts/cm² average were too low to produce histological brain lesions. With 5–7 watts/cm² and a two-minute exposure, definite tissue damage was obtained. Resultant damage could be controlled so that ranges from relatively minor effects to complete necrosis in a restricted area could be obtained. The type of destruction that was observed in a dog's brain is shown in Fig. 19. Lindstrom's animal studies indicated that the white matter in the brain was affected more than the cortical gray matter. The clinical studies carried out irradiation through an opening in the skull with average sound intensities of 7 watts/cm² and 12 watts/cm² showed definite symptomatic improvement and pain relief in most of the patients. Lobotomy irradiations were attempted, and besides the symptomatic improvements, the absence of secondary phenomena such as mental deterioration, hemorrhages, and convulsions makes the method appear very promising.

Fry and his associates have been studying the production of localized lesions in brains of animals using focused sound beams. Two types of focusing sound transducers are being used. In one, the sound is focused by means of a polystyrene lens in front of a quartz crystal. Four such focused beams are then crossed to yield a small spot of very high intensity. This system is diagrammed in Fig. 20. Another type of focusing system described by Barone²⁶ is illustrated in Fig. 21. In this system, the sound emanating from the crystal is reflected from the cone onto the parabola and then focused. Sound beams obtained by this method have been almost as sharply focused as those produced by Fry's four-beam apparatus. The following is a description of the irradiation procedure used by Fry. A section of the skull of the animal is removed. The head of the animal is fixed in a stereotaxic apparatus. The motion of the irradiator is determined with respect to the calibrations of the stereotaxic machine. The precise localization of the focused beam with respect to mapped

²⁶ A. Barone, *Acustica*, vol. 2, p. 221; 1952.

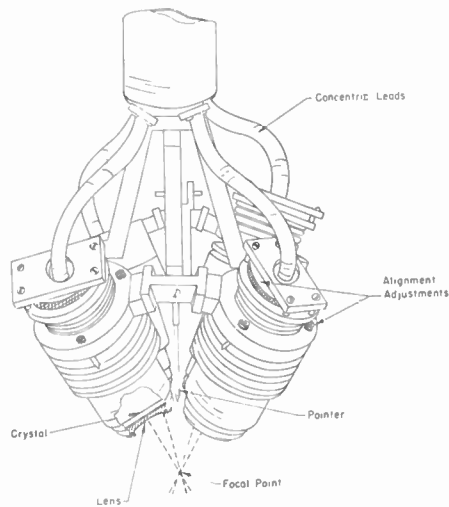


Fig. 20—Schematic diagram of multibeam irradiator.



Fig. 22—Transverse section of brain of cat no. 101 in a plane of irradiation. Left internal capsule was irradiated at 210 watts/cm² for 4.0 seconds. Three days postoperative. Weil stain.

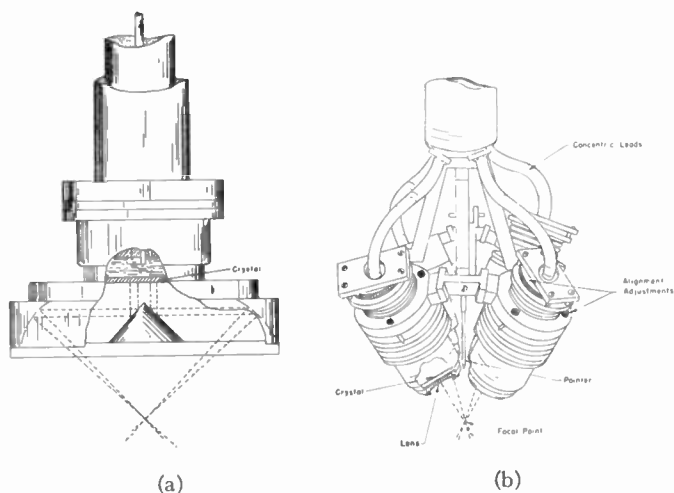


Fig. 21—(a) The parabolic acoustic transducer which produces a focused beam. (b) The multiple beam acoustic transducer consists of four separate focusing elements. The focused beams from all the elements intersect in a common region.



Fig. 23—Partial view of the irradiation room showing control panels, irradiator, and head holder.

brain locations is then known. A lesion is produced by laying down a pattern of spots spaced half a millimeter between centers. The frequency of the sound used is 1 mc. The pulse time for each shot of sound is in the range from 0.5 to 10 seconds. The intensities that are used range from 50 watts/cm² to 1000 watts/cm². The results obtained by irradiation of the internal capsule region of the brain of a cat is shown in Fig. 22. The lesion produced in the internal capsule shows up readily in comparison to the unirradiated (control) side of the brain. Some of the advantages of using focused ultrasound in brain surgery have been outlined by Fry to be 1) no disturbance of the brain tissue except in the focal region, 2) no cutting of any brain tissue, 3) opening of the dura unnecessary, and 4) no disturbance to blood vessels.

A picture of a typical operating room with a brain surgery apparatus located at the University of Illinois is shown in Fig. 23.

A program parallel to the one being carried out at Illinois is going on at Massachusetts General Hospital.²⁷ Again focused irradiators are being utilized to produce lesions in cat brains with skull sections removed. The results appear to be similar insofar as the production of localized brain lesions is concerned.

BACTERIOLOGICAL APPLICATIONS OF ULTRASOUND

Thus far, we have discussed mechanisms of ultrasonic effects in biology mainly in terms of thermal effects or the suppression of possible thermal and cavitation effects. There are many useful biological ultrasonic effects which depend upon cavitation as a mechanism. Most of these involve effects on cells or chemicals in liquid solutions. Ultrasonic waves have been used to kill or disintegrate protozoa, yeast, algae, and bacteria. Also, they were used to destroy the infectivity of viruses such as cowpox and staphylococcus-bacteriophage.²⁸

²⁷ T. F. Hueter, H. T. Ballantine, Jr., and W. C. Cotter, "Production of lesions in the central nervous system with focused ultrasound: a study of dosage factors," *J. Acoust. Soc. Amer.*, vol. 28, pp. 192-201; March, 1956.

²⁸ A. Weissler, "Sonochemistry: the production of chemical changes with sound waves," *J. Acoust. Soc. Amer.*, vol. 25, pp. 651-657; July, 1953.

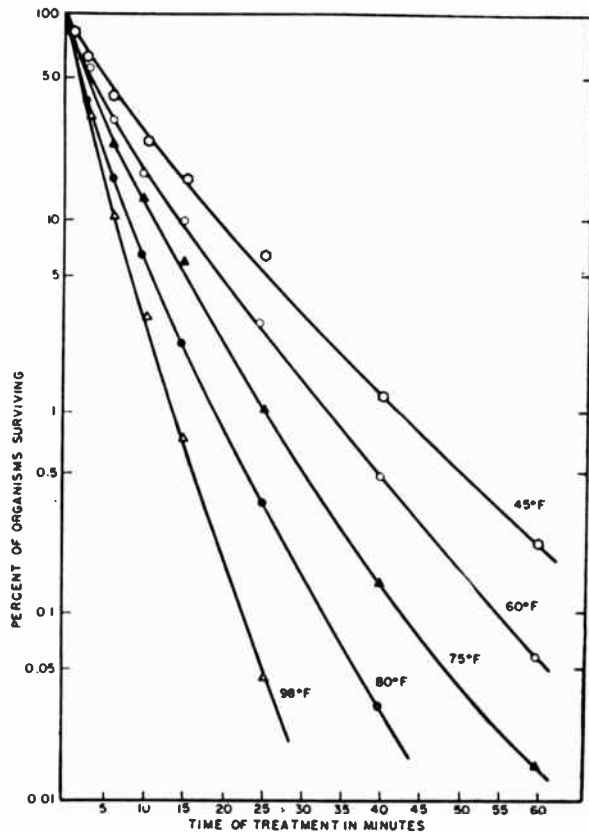


Fig. 24—Relation of environmental temperature to the survival by *E. Coli* of ultrasonic vibrations.

The destructive effect of ultrasonically induced cavitation on bacteria is demonstrated by some of the work of Horton.²⁹ Fig. 24 illustrates the per cent survival of *E. Coli* bacteria irradiated in water for various lengths of time and at different environmental temperatures. It is apparent from Fig. 24 that the rate of kill is higher at higher temperatures. Horton explains this as an effect whereby the higher temperatures facilitate cavitation in the water.

The possible applications of ultrasonic bacteriocidal action to milk "pasteurization" are apparent, but much work must still be carried out to study the killing of bacteria in milk and to investigate the effects of the ultrasonic irradiation on the milk flavor. Similarly, it is possible that sound or a combination of ultrasound and heat can be used in other food sterilization procedures, but again much work needs to be done to study the killing process and possible side effects.

ULTRASONIC DENTISTRY

In the continuous search for improved dental techniques, the application of the industrial method of ultrasonic drilling to dental work has gained great impetus in recent years. Since the early work by Oman³⁰ at Columbia Presbyterian Hospital, the field has spread to

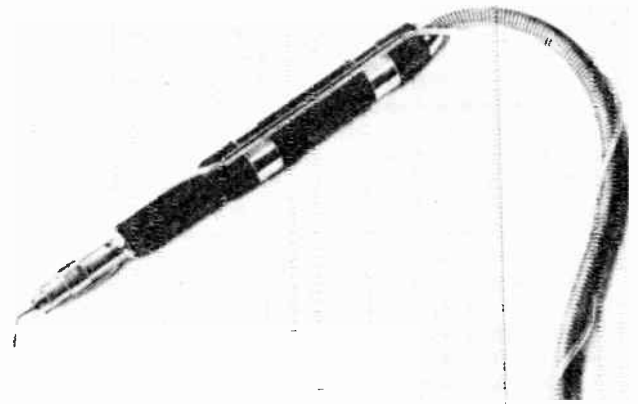


Fig. 25—Ultrasonic dental drill.

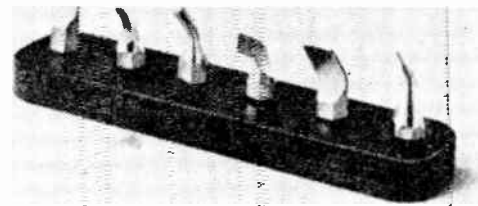


Fig. 26—Tools for use with ultrasonic dental drill.

the point where dentists all over the country are utilizing these methods.³¹

The ultrasonic dental drill utilizes an ultrasonically vibrating rod with a linear reciprocating motion of an excursion of about 0.0014 inch. An abrasive (aluminum oxide) is circulated between the tool and the tooth. The movement of the tool in the abrasive slurry causes the abrasive to cut into the tooth. An ultrasonic frequency of 30,000 cycles per second is utilized and the speed at which the tooth is cut is comparable to a bur wheel or a diamond wheel drill. The impact velocity of the cutting edge or particle is small compared to rotary drills. For example, using a bur drill, this velocity is about 100 feet/minute, using a diamond wheel it is about 1200 feet/minute, but with an ultrasonic tool it is only 0.2 foot/minute. The resultant smaller impact force (and consequent smaller removal of material per impact) is compensated for by the fact that the number of impacts per second is very large. With an eight-tooth bur wheel at 6000 rpm, there are 800 impacts per second. Using a diamond wheel with a customary distribution of diamond particles on the wheel and a speed of 9000 rpm, this figure is about 300,000 impacts per second. With the customary distribution of abrasive and a 1/16-inch square tool operating at 30 kc, the comparable figure for the ultrasonic drill is greater than 3,000,000 impacts per second. The ultrasonic tool operates by having large numbers of small force impacts per second.

A photograph of an ultrasonic dental drill is shown in Fig. 25 with Fig. 26 illustrating the variety of tools that can be used with it.

²⁹ J. P. Horton, *J. Acoust. Soc. Amer.*, vol. 25, p. 480; 1953.

³⁰ Oman and Appelbaum, *New York State Dental J.*, vol. 20, p. 256; 1954.

³¹ L. Balamuth, "Technical aspects of the cavitation ultrasonic process in dentistry," 1955 IRE CONVENTION RECORD, pt. 9, pp. 89-97.

It should be pointed out that the desirability of ultrasonic dentistry is still a controversial subject. While Oman and his associates have obtained very satisfactory results, other investigators at the Bethesda General Medical Research Institute and the University of Minnesota have raised objections to the method. Some of these objections are based upon the aforementioned concomitant production of heating by the absorption of the sound waves in the tooth materials.

CONCLUSION

In the course of this paper, we have touched on a variety of the applications of ultrasonics to medicine and biology. Many of these are still in the laboratory

stage although they already show great promise, but some of these applications have been rapidly pushed to clinical practice. Ultrasonic dental drills and ultrasonic therapy machines are already in the offices of many dentists and medical practitioners, while even the complex brain surgery apparatus is ready for hospital use.

It should be pointed out as a general criticism of the field that until recently careful measurements of the physical properties of the acoustic parameters have not always been made. This has led to a certain amount of uncertainty in the explanations of experiments. As applications are pursued using higher and higher sound intensities, it will become increasingly necessary that accurate measurements be made so that this new tool, ultrasonics, can be safely applied in medicine.

Ion Oscillations in Electron Beam Tubes; Ion Motion and Energy Transfer*

ROBERT L. JEPSEN†, ASSOCIATE MEMBER, IRE

Summary—This paper refers briefly to some of the deleterious effects that often arise when positive ions are trapped in electron beams. Calculations aimed at establishing a useful picture of ion oscillations in gridded drift tubes are presented, and a plausible physical picture of some possible ion motions is obtained. In consequence of these motions, the electric field inside the drift tube undergoes one or more space reversals. When a beam of fast electrons traverses such a region, beam loading may be negative; this is calculated in some detail, both for ions and for a simple LC circuit. Thus a mechanism for energy transfer from the electron beam to the oscillating ions has now been found. The question of whether or not this energy is sufficient to sustain oscillations is examined in a preliminary way. The importance of secondary electrons in some cases is discussed. Comparison between experiment and theory shows that a good qualitative understanding now exists of such observed phenomena as continuous oscillations. The occurrence, however, of fluctuating ion oscillations is not predicted by the present theory.

I. INTRODUCTION

OPERATION and performance of many vacuum tubes is affected, usually deleteriously, by the presence of positive ions in the electron beam region. In some cases, ions are trapped intentionally to achieve focusing by neutralizing space charge forces in the electron beam. In other cases, ions are trapped incidentally by virtue of geometry and voltages, as dictated by such other considerations as the need for using grids

for rf reasons. In still other cases, ion accumulation may occur because of a high rate of ion production relative to the available drainage paths (pressure-sensitive ion trapping). Gridded drift tubes constitute one of the more important kinds of ion traps in microwave tubes, and will be considered in some detail in this paper.^{1,2}

Experimental observations on many of the effects due to positive ions trapped in electron beams have been described elsewhere.³⁻¹⁰ Under certain circumstances, no discernible undesirable effects occur. Under seemingly similar circumstances, continuous ion oscillations

¹ L. M. Field, K. Spangenberg, and R. Helm, "Control of electron beam dispersion at high vacuum by ions," *Elec. Commun.*, vol. 24, pp. 108-121; March, 1947.

² K. G. Hernqvist, "Space-charge and ion-trapping effects in tetrodes," *Proc. IRE*, vol. 39, pp. 1541-1547; December, 1951.

³ J. R. Pierce, "Possible fluctuations in electron streams due to ions," *J. Appl. Phys.*, vol. 19, pp. 231-236; March, 1948.

⁴ E. G. Linder and K. G. Hernqvist, "Space-charge effects in electron beams and their reduction by positive ion trapping," *J. Appl. Phys.*, vol. 21, pp. 1088-1097; November, 1950.

⁵ T. Moreno, "Some Anomalous Modulation Effects in Reflex Klystrons," Tenth IRE Electron Tube Conference, Ottawa, Can., June, 1952.

⁶ R. L. Jepsen, "Some Beam Instabilities in Klystrons," Tenth IRE Electron Tube Conference, Ottawa, Can.; June, 1952.

⁷ W. E. Waters, Jr., "Observations on ion oscillations in a cylindrical-beam tetrode under hard vacuum conditions," *IRE TRANS.*, vol. ED-1, pp. 216-220; December, 1954.

⁸ K. G. Hernqvist, "Plasma ion oscillations in electron beams," *J. Appl. Phys.*, vol. 26, pp. 544-548; May, 1955.

⁹ C. C. Cutler, "Spurious modulation of electron beams," *Proc. IRE*, vol. 44, pp. 61-64; January, 1956.

¹⁰ T. Moreno, "Spurious modulation of electron beams," *Proc. IRE*, vol. 44, p. 693; May, 1956.

* Original manuscript received by the IRE, February 1, 1957; revised manuscript received, May 20, 1957.

† Varian Associates, Palo Alto, Calif.

may exist, typically in the frequency range 0.5–10 mc. Again under similar conditions, fluctuating ion oscillations occur; the fluctuations are usually of modified sawtooth shape with repetition frequencies in the range 0.1 cps to 50 kc. Other undesirable effects arise if a modulation frequency at or near the ion oscillation frequency is applied to the tube.

In the present paper, we shall not attempt to explain all of the observed phenomena. Rather, an effort will be made to understand some of the simpler observations. In particular we will try to see why it is that either a state of no ion oscillation at all or a state of continuous ion oscillation can occur under rather seemingly similar conditions.

Some years ago Pierce³ found that wave amplification can exist in an electron beam traversing a region neutralized by positive ions. This wave travels with the velocity of the electron beam. The frequencies amplified are those at and below the ion plasma frequency, with the maximum amplification occurring at the ion plasma frequency. It has been proposed that the mechanism for the occurrence of ion oscillations is that of amplification near the ion plasma frequency with feedback between entrance and exit of the electron beam being provided by slow speed secondary electrons moving in the backward direction.

For this mechanism to work, there must be a total phase delay of $2n\pi$ radians around the oscillating loop. For an ion oscillation frequency of 1 mc, for example, the minimum time delay allowable around the loop is 10^{-6} sec. In a 300-volt beam 100 cm long, transit time for primary electrons would be 10^{-7} sec. Thus most of the time delay must come from slow speed secondaries. Three-volt secondaries would be required for a transit time of 10^{-6} sec. Since 3-volt secondaries are often relatively abundant, the above mechanism for oscillations is fairly plausible in long electron beams.

We observe, however, that ion oscillations are not restricted to long electron beams. They often occur in ion traps which are substantially less than 1 cm in length. For the mechanism just described to operate successfully in such cases, the returning secondaries must have energies of less than a millivolt. While it may not be impossible that a sufficient number of such secondaries exist, it does strain our intuition to the point that we seek alternative explanations.

II. CALCULATIONS AND DISCUSSIONS

A. Initial Assumptions

In the treatment that follows we shall assume that:

- 1) The ions have no dc velocity.
- 2) The ions are singly-ionized molecules having the same mass.
- 3) Complete dc space charge neutralization exists.
- 4) No static electric fields exist.

- 5) The ac electric field is conservative, whence $E = -\nabla V$.
- 6) There is no focusing magnetic field.
- 7) Magnetic forces are unimportant.
- 8) Effects due to thermal motions can be neglected.
- 9) A linearized treatment is adequate (*i.e.*, neglect second-order ac quantities).
- 10) DC static quantities have no space variations, except at well-defined boundaries.
- 11) Metal boundaries have infinite conductivity.
- 12) Losses of ions at boundaries can be neglected.

In addition to the divergence equation, our basic equations include also the separate continuity and force equations for positive ions and electrons or negative particles.

As a matter of notation we write various quantities as $\vec{A} = \vec{A}_0 + \vec{A}$, where \vec{A}_0 is the static (dc) part of \vec{A} and \vec{A} is the ac part. We use subscripts i , e , and $-$ respectively for ions, electrons, and negative particles. Unit vectors are \hat{x} , \hat{y} , and \hat{z} . MKS units are used unless otherwise stated.

B. Negative Particles with Zero DC Velocity

In the interest of acquiring a feeling for some of the simpler ion motions that can occur in small, enclosed regions, let us consider the case of negative particles (charge $-e$, mass m_-) neutralized by positive ions (charge e , mass m_+). Let both sets of particles have zero dc velocity. The case of *heavy* negative particles without dc velocity is of interest because the resultant ion motion is very nearly the same as when the negative space charge arises from a beam of fast electrons.

Our basic equations may be written

$$\vec{E} = -\nabla V \quad (1)$$

$$\nabla \cdot \vec{E} = \frac{1}{\epsilon_0} (\tilde{\rho}_+ + \tilde{\rho}_-) \quad (\text{divergence equation}) \quad (2)$$

$$\rho_0 \nabla \cdot \vec{v}_+ + \frac{\partial \tilde{\rho}_+}{\partial t} = 0 \quad (\text{ion continuity equation}) \quad (3)$$

$$-\rho_0 \nabla \cdot \vec{v}_- + \frac{\partial \tilde{\rho}_-}{\partial t} = 0 \quad (\text{negative particle continuity equation}) \quad (4)$$

$$\frac{\partial \vec{v}_+}{\partial t} = -\frac{e}{m_+} \vec{E} \quad (\text{ion force equation}) \quad (5)$$

$$\frac{\partial \vec{v}_-}{\partial t} = -\frac{e}{m_-} \vec{E} \quad (\text{negative particle force equation}). \quad (6)$$

Upon taking the divergence of the force equations and the partial time derivative of the continuity equations, and eliminating $(\partial/\partial t)\nabla \cdot \vec{v}$, we obtain two equations,

$$\frac{1}{\rho_0} \frac{\partial^2 \tilde{\rho}_i}{\partial t^2} = - \frac{e}{m_i} \nabla \cdot \vec{E} \text{ for the ions,}$$

and

$$\frac{1}{\rho_0} \frac{\partial^2 \tilde{\rho}_-}{\partial t^2} = - \frac{e}{m_-} \nabla \cdot \vec{E} \text{ for the negative particles.}$$

Now add these equations and substitute for $\nabla \cdot \vec{E}$ from the divergence equation. Assume that $\tilde{\rho}_i$ and $\tilde{\rho}_-$ have the same time dependence, *i.e.*, that $\tilde{\rho}_i = \vec{\rho}_i(\vec{r})\rho(t)$ and $\tilde{\rho}_- = \vec{\rho}_-(\vec{r})\rho(t)$. Assume also that $\rho_i(\vec{r}) + \rho_-(\vec{r}) \neq 0$. Use

$$\omega_i^2 \equiv \frac{\rho_0}{\epsilon_0} \frac{e}{m_i} \quad \text{and} \quad \omega_-^2 \equiv \frac{\rho_0}{\epsilon_0} \frac{e}{m_-}.$$

Then

$$\frac{d^2 \rho(t)}{dt^2} + (\omega_i^2 + \omega_-^2)\rho(t) = 0.$$

Thus $\tilde{\rho}_i$ and $\tilde{\rho}_-$ have solutions of the form

$$\tilde{\rho}_i = \vec{\rho}_i(\vec{r}) \begin{vmatrix} \sin \omega t \\ \cos \omega t \end{vmatrix} \tag{7}$$

$$\tilde{\rho}_- = \vec{\rho}_-(\vec{r}) \begin{vmatrix} \sin \omega t \\ \cos \omega t \end{vmatrix} \tag{8}$$

where

$$\omega = \sqrt{\omega_i^2 + \omega_-^2} = \omega_i \sqrt{1 + \frac{m_i}{m_-}}. \tag{9}$$

From this we see that ω , the natural angular frequency of the system, is independent of the spatial variations or wavelengths of the ac charge densities, velocities, electric field, and voltage. Thus there is no dispersion. Oscillations, if they are to occur at all, must occur at angular frequency ω . Phase velocity of these plasma waves can have any value from zero to infinity, or many values at once. For $m_- \rightarrow \infty$, $\omega \rightarrow \omega_i$, the ion plasma angular frequency. For $m_- \gg m_i$, ω is slightly greater than ω_i .

$$\omega = \omega_i \sqrt{1 + \frac{m_i}{m_-}} \simeq \omega_i \left(1 + \frac{1}{2} \frac{m_i}{m_-} \right). \tag{10}$$

The chief motion will be that of the ions, with the heavy negative particles moving only slightly.

Now let us examine some of the ion motions that could exist. For simplicity assume the negative particles have infinite mass. Suppose all particles are initially at rest and uniformly distributed. Then the electric field is zero, and no ion motion occurs. Suppose now the ions are displaced by some means in such a way that the electric field has a spatial variation. In regions where ions are concentrated, resulting space charge forces will act to disperse them; where ions are scarce, space charge

forces due to the negative particles will attract them. Now let the ions be released at $t=0$. They will oscillate sinusoidally in time at the ion plasma frequency $\omega_i/2\pi$ about their initially undisplaced positions. Throughout the medium all the ions will move in unison in "jelly-like" fashion. At certain times ($\omega_i t = 0, \pi, 2\pi, \dots$) they are all at rest, having reached their extreme positions. At certain other times ($\omega_i t = \pi/2, 3\pi/2, \dots$) they are passing through their initially undisplaced positions; at these times the particles are uniformly distributed, so that the space charge forces are zero, but the magnitudes of the ac velocities have their maxima at these times, so the oscillations continue.

Metallic boundaries strongly influence the allowed ion motions. Consider a volume of plasma bounded by conducting surfaces. Let the dimensions of this volume be small compared with a free-space wavelength of an electromagnetic wave of angular frequency ω , *i.e.*, let the small, enclosed region be "cut off" to ordinary electromagnetic waves of this frequency. Then we can plausibly require that the ac potential of the bounding surface be zero. Space charge fields arising from ion oscillations can still exist in such a volume. The allowed spatial distributions, however, are significantly restricted.

As a particularly simple example, consider a rectangular metallic box of linear dimensions a , b , and c , as shown in Fig. 1. Let the box be filled with plasma.

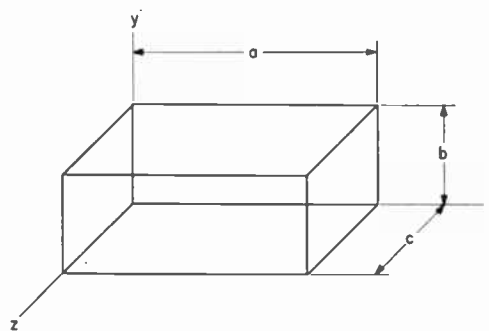


Fig. 1—Rectangular metallic box enclosing plasma.

A simple nontrivial potential variation that can exist in the box is

$$\vec{V} = V_1 \sin \beta_x x \sin \beta_y y \sin \beta_z z \cos \omega t. \tag{11}$$

For \vec{V} to be zero at the boundaries with $V_1 \neq 0$, we need

$$\beta_x = \frac{n_x \pi}{a}, \quad \beta_y = \frac{n_y \pi}{b}, \quad \beta_z = \frac{n_z \pi}{c} \tag{12}$$

where n_x , n_y , and n_z are integers 1, 2, 3, \dots .

The simplest spatial distribution is that for the lowest mode of the system, which exists when $n_x = n_y = n_z = 1$. By superposition of modes, an arbitrary spatial distribution for \vec{V} which vanishes at the boundary can be built up.

For the case where \vec{V} has the particularly simple form of (11), \vec{v}_i and $\tilde{\rho}_i$ are given by:

$$\left. \begin{aligned} \tilde{v}_{ix} &= -\frac{e}{m_i \omega} \beta_x V_1 \cos \beta_x x \sin \beta_y y \sin \beta_z z \sin \omega t \\ \tilde{v}_{iy} &= -\frac{e}{m_i \omega} \beta_y V_1 \sin \beta_x x \cos \beta_y y \sin \beta_z z \sin \omega t \\ \tilde{v}_{iz} &= -\frac{e}{m_i \omega} \beta_z V_1 \sin \beta_x x \sin \beta_y y \cos \beta_z z \sin \omega t \end{aligned} \right\} \quad (13)$$

$$\tilde{\rho}_i = \rho_0 \frac{e}{m_i \omega^2} (\beta_x^2 + \beta_y^2 + \beta_z^2) V_1 \sin \beta_x x \sin \beta_y y \cdot \sin \beta_z z \cos \omega t. \quad (14)$$

In Fig. 2 we plot ion positions and velocities, and the resulting equipotentials, at four different times for the lowest mode in a rectangular box. This is an interpretation of (11), (12), and (13) with $n_x = n_y = n_z = 1$ and $y = b/2$. From Fig. 2 we can acquire a feeling for the sorts of ion motions that can occur. In Fig. 3 we plot equipotentials for four of the lowest modes in a rectangular box.

It is, perhaps, useful to observe that for the lowest mode the motion of the ions is a sort of "pulsation"—alternate "expansion" and "contraction," *i.e.*, ions near the center remain at rest while those near the walls move in unison, first toward the center, then toward the walls, and then back toward the center again. We expect closely related kinds of motion to occur in volumes of rather arbitrary shape.

C. Fast Electrons Traversing an Ion Trap

In this case we make the further approximations that $\partial \tilde{v}_e / \partial t$ and $\partial \tilde{\rho}_e / \partial t$ are negligible in the electron force and continuity equations. This is equivalent to saying that during the transit of the electrons through the ion trap, the fields, etc., have changed in time by a negligible amount. We also take $\vec{v}_0 = v_0 \hat{z}$. Our starting equations thus become:

$$\vec{E} = -\nabla \tilde{V} \quad (1)$$

$$\nabla \cdot \vec{E} = \frac{1}{\epsilon_0} (\tilde{\rho}_i + \tilde{\rho}_e) \quad (\text{divergence equation}) \quad (15)$$

$$\rho_0 \nabla \cdot \vec{v}_i + \frac{\partial \tilde{\rho}_i}{\partial t} = 0 \quad (\text{ion continuity equation}) \quad (3)$$

$$-\rho_0 \nabla \cdot \vec{v}_e + v_0 \frac{\partial \tilde{\rho}_e}{\partial z} = 0 \quad (\text{electron continuity equation}) \quad (16)$$

$$\frac{\partial \tilde{v}_i}{\partial t} = -\frac{e}{m_i} \vec{E} \quad (\text{ion force equation}) \quad (5)$$

$$v_0 \frac{\partial \tilde{v}_e}{\partial z} = -\frac{e}{m_e} \vec{E} \quad (\text{electron force equation}). \quad (17)$$

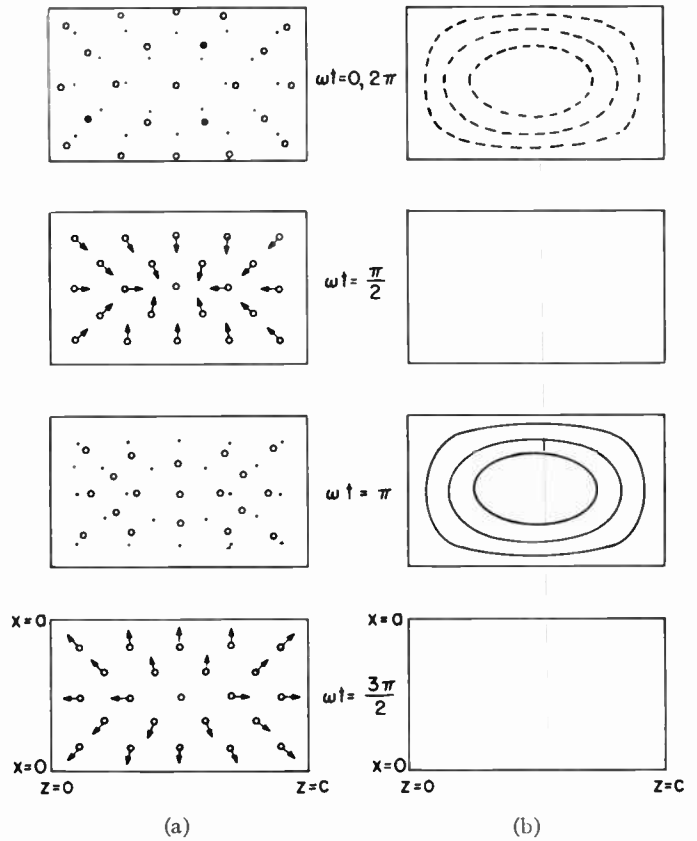


Fig. 2—Ion positions and velocities, and the resulting equipotentials in a rectangular box. (a) Ion positions and velocities; (b) equipotentials.

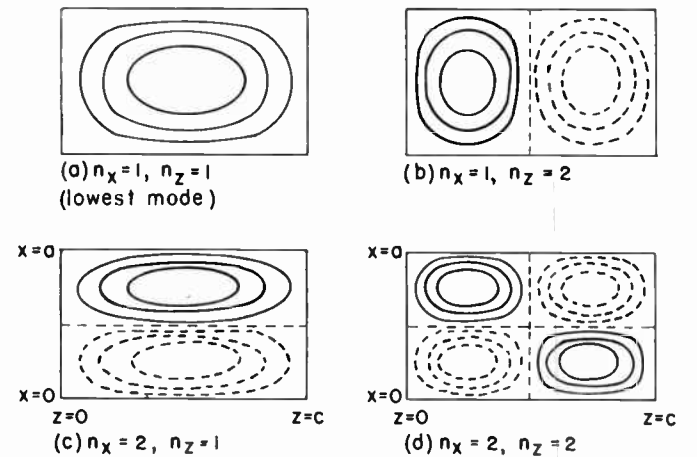


Fig. 3—Equipotentials for some of the lower modes of ion oscillation with a rectangular box.

Let the ion trap be a cylinder (not necessarily circular) whose axis is parallel with the z axis, bounded at $z = 0$ and $z = l$ by idealized grids which are also conducting planes, and bounded elsewhere by metal walls. Assume that the beam and ions fill the drift tube. Choose a coordinate system (ξ, η, z) . Let \vec{V} be of the form

$$\vec{V} = V' \sin \beta_z z \cos \omega t,$$

where

$$\beta_z = \frac{n\pi}{l} \quad \text{and} \quad V' = V'(\xi, \eta). \quad (18)$$

This restriction on β_z ensures that \tilde{V} will vanish at $z=0$ and $z=l$. V' is a function of ξ and η only, and not of z . A further requirement is that V' shall vanish on the remaining boundaries of the ion trap.

With this assumed form for \tilde{V} , we obtain at once for \vec{E} , using

$$\nabla \equiv \nabla_{\perp} + \frac{\partial}{\partial z} \hat{z},$$

$$\vec{E} = - [(\nabla_{\perp} V') \sin \beta_z z + \beta_z V' \cos \beta_z z] \cos \omega t. \quad (19)$$

From the force equations we then obtain \vec{v}_i and \vec{v}_e , and from the continuity equations $\tilde{\rho}_i$ and $\tilde{\rho}_e$:

$$\vec{v}_i = - \frac{e}{m_i \omega} [(\nabla_{\perp} V') \sin \beta_z z + \beta_z V' \cos \beta_z z] \sin \omega t \quad (20)$$

$$\tilde{\rho}_i = - \rho_0 \frac{e}{m_i \omega^2} [\nabla_{\perp}^2 V' - \beta_z^2 V'] \sin \beta_z z \cos \omega t \quad (21)$$

$$\vec{v}_e = - \frac{e}{m_e \beta_z v_0} [(\nabla_{\perp} V') \cos \beta_z z - \beta_z V' \sin \beta_z z] \cos \omega t \quad (22)$$

$$\tilde{\rho}_e = - \rho_0 \frac{e}{m_e \beta_z^2 v_0^2} [\nabla_{\perp}^2 V' - \beta_z^2 V'] \sin \beta_z z \cos \omega t. \quad (23)$$

Satisfaction of the divergence equation yields the dispersion relation:

$$\left(\frac{\omega_i}{\omega}\right)^2 + \left(\frac{\omega_e}{\beta_z v_0}\right)^2 = 1, \quad \text{where} \quad \omega_e^2 \equiv \frac{\rho_0}{\epsilon_0} \frac{e}{m_e}.$$

This is readily solved for ω as a function of β_z .

$$\omega = \omega_i \left[1 - \left(\frac{\omega_e}{\beta_z v_0}\right)^2 \right]^{-1/2} \quad (24)$$

For $\beta_z v_0$ large, $\omega \simeq \omega_i$, so $\beta_z \simeq (\omega_i/v_p)$ (v_p is the phase velocity of the wave). Using $(\omega_e/\omega_i)^2 = m_i/m_e$, we obtain approximately

$$\omega \simeq \omega_i \left[1 + \frac{1}{2} \frac{m_i}{\left(\frac{v_0}{v_p}\right)^2 m_e} \right]. \quad (25)$$

In the case of heavy negative particles with zero dc velocity (treated in the last section) we found that

$$\omega \simeq \omega_i \left[1 + \frac{1}{2} \frac{m_i}{m_-} \right]. \quad (10)$$

Thus, so far as the natural frequency of oscillation is concerned, the result is virtually the same for particles of mass

$$m_- = \left(\frac{v_0}{v_p}\right)^2 m_e \quad (26)$$

at rest as for electrons moving at velocity v_0 in a standing wave field of phase velocity v_p . In other words, the "effective rest mass" of equivalent negative particles is given by (26).

Examination of the relevant equations shows that most other features of the ion motion are also essentially the same whether the negative space charge arises from fast electrons or from heavy negative particles at rest. Thus we can use much of the picture obtained in the last section regarding allowable ion motions.

One difference between these two cases is the absence of dispersion in the first and its presence in the second. With the heavy negative particles, ω was independent of the β 's. Thus different modes (different values of the β 's) having the same frequency could be superposed to obtain a variety of spatial distributions. With fast electrons, however, ω depends on β_z . Thus modes of differing β_z will have different frequencies, so that a variety of axial spatial distributions cannot be built up by superposition. On the other hand, ω is independent of the spatial variation in directions transverse to the axis. Thus for a rectangular box, ω depends only on β_z , and not at all on β_x and β_y . Modes of the same β_z , but differing β_x and β_y , can therefore be superposed to build up a variety of transverse spatial variations. \rightarrow

We note, incidentally, from (22) that $\vec{v}_{e\perp} \neq 0$ at $z=0$. This implies that the electron beam must be premodulated, *i.e.*, that the entering electron beam must have on it an appropriate transverse velocity modulation. If the beam is not premodulated, then, according to our equations, \vec{V} must be zero, and no oscillations can occur at all. Strictly speaking, this is true, but it is simply a result of the approximations used. In order to impose the boundary condition $\vec{v}_{e\perp} = 0$ at $z=0$, it would be necessary to do a more exact calculation. Examination of (19) through (23) shows, however, that for $\beta_z v_0$ large compared with ω_e , the ac electron charge density is small relative to the ac ion charge density. Thus the potential distribution is governed almost entirely by oscillation of the ions. Small discrepancies in calculating the behavior of the electrons would not be expected to seriously impair the validity of conclusions based on this simplified model. We, therefore, consider the requirement for premodulation of the electron beam to be more apparent than real.

D. Transfer of Energy from an Electron Beam to Oscillating Ions

Let us now consider an ion plasma region of indefinite transverse extent bounded by short-circuited grids at $z=0$ and $z=l$, as in Fig. 4. Restrict the problem to one dimension by allowing only z variations in the quantities of interest. Let the electron transit time through the ion plasma region be short in comparison with an rf cycle.

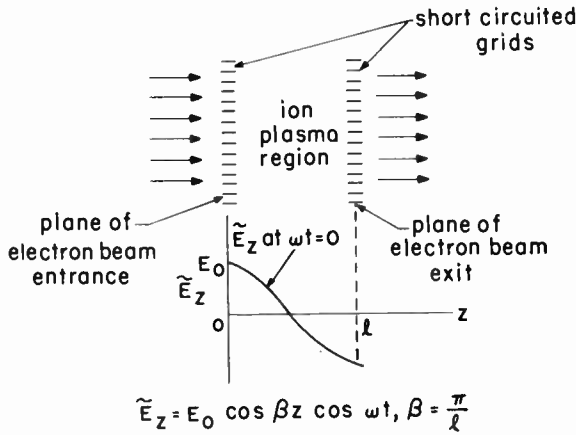


Fig. 4—Electric field distribution due to ions oscillating between short-circuited grids (lowest mode).

whence the force equation is solved to yield

$$v = v_0 \left[1 - 2\alpha\beta_e \int_0^z \cos \beta u \cos \omega t(u) du \right]^{1/2}, \quad (34)$$

where

$$\alpha \equiv \frac{e}{m_e} \frac{E_0}{\omega v_0} \quad \text{and} \quad \beta_e \equiv \frac{\omega}{v_0}.$$

Integral equations for τ and v in terms of t_0 and z are readily obtained by combining (31), (32), and (34). We choose, however, to employ the following method of successive approximation for calculating τ and v . As n th approximations, use

$$v_n = v_0 \left[1 - 2\alpha\beta_e \int_0^z \cos \beta u \cos (\phi_0 + \omega\tau_n) du \right]^{1/2} \quad (35)$$

$$\tau_n = \int_0^z \frac{du}{v_{n-1}}. \quad (36)$$

It turns out that we can expand v_n and τ_n as power series in (β_e/β) , and that the valid degree of the series is the same as the order of the approximation. We employ the standard trigonometric expansion for $\cos (\phi_0 + \omega\tau_n)$, and, since $\omega\tau_n$ is a small quantity, we can use the usual power series expansions for $\sin \omega\tau_n$ and $\cos \omega\tau_n$. We also employ binomial series expansions as required.

We obtain

$$\begin{aligned} \omega\tau_1 &= \left(\frac{\beta_e}{\beta}\right) \beta z \\ \omega\tau_2 &= \left(\frac{\beta_e}{\beta}\right) \beta z + \left(\frac{\beta_e}{\beta}\right)^2 \alpha \cos \phi_0 (1 - \cos \beta z) \\ \omega\tau_3 &= \left(\frac{\beta_e}{\beta}\right) \beta z + \left(\frac{\beta_e}{\beta}\right)^2 \alpha \cos \phi_0 (1 - \cos \beta z) \\ &\quad + \left(\frac{\beta_e}{\beta}\right)^3 \cdot \left[\alpha \sin \phi_0 (\beta z - 2 \sin \beta z + \beta z \cos \beta z) \right. \\ &\quad \left. + \frac{3\alpha^2}{8} \cos^2 \phi_0 (2\beta z - \sin 2\beta z) \right] \end{aligned} \quad (37)$$

$$\begin{aligned} v_1 &= v_0 \left[1 - \left(\frac{\beta_e}{\beta}\right) \alpha \cos \phi_0 \sin \beta z \right] \\ v_2 &= v_0 \left[1 - \left(\frac{\beta_e}{\beta}\right) \alpha \cos \phi_0 \sin \beta z \right. \\ &\quad \left. - \left(\frac{\beta_e}{\beta}\right)^2 \left\{ \alpha \sin \phi_0 (1 - \cos \beta z - \beta z \sin \beta z) \right. \right. \\ &\quad \left. \left. + \frac{\alpha^2}{2} \cos^2 \phi_0 \sin^2 \beta z \right\} \right]. \end{aligned} \quad (38)$$

We can now compute $\cos \omega t$. To obtain a nonzero result we must use the third approximation for τ . This yields

From (19) the electric field for this case would be given by

$$\tilde{E}_z = E_0 \cos \beta z \cos \omega t. \quad (27)$$

One method of obtaining energy transfer is to calculate the work done on an average electron through

$$\overline{W}_e = \int_0^z \overline{F} du. \quad (28)$$

The averaging is done over all entrance times t_0 or entrance phases $\phi_0 \equiv \omega t_0$. Thus

$$\overline{F} = -e\overline{\tilde{E}_z} = -eE_0 \overline{\cos \beta z \cos \omega t} \quad (29)$$

and

$$\overline{\cos \omega t} = \frac{1}{2\pi} \int_0^{2\pi} \cos (\phi_0 + \omega\tau) d\phi_0 \quad (30)$$

where

$$t = t_0 + \tau. \quad (31)$$

The transit time τ from the entrance plane to a point z is

$$\tau = \int_0^z \frac{du}{v}. \quad (32)$$

Electron velocity v is related to position (z or u) through the force equation:

$$\frac{dv}{dt} = -\frac{e}{m_e} E_0 \cos \beta z \cos \omega t. \quad (33)$$

We wish to obtain v in terms of entrance time t_0 and position z , and with no explicit dependence on t . To do this we use (31) and express τ in terms of t_0 and z . For no explicit dependence of v on t , we can use

$$\frac{dv}{dt} = v \frac{dv}{dz},$$

$$\frac{1}{2\pi} \int_0^{2\pi} \cos(\phi_0 + \omega\tau_3) d\phi_0 = -\left(\frac{\beta_e}{\beta}\right)^3 \alpha(\beta z - \sin \beta z). \quad (39)$$

Combining (28), (29), and (39), and substituting for α , we obtain for the energy transferred to an average electron

$$\overline{W}_e = \frac{e^2 E_0^2 \beta_e^3}{m_e \omega v_0 \beta^4} F(\beta z) \quad (40)$$

where

$$F(\beta z) \equiv [\beta z \sin \beta z - \frac{1}{2} \sin^2 \beta z - (1 - \cos \beta z)] \quad (41)$$

$F(\beta z)$ is plotted vs βz in Fig. 5.

When $F(\beta z) > 0$, $\overline{W}_e > 0$, and energy flows from the field to the electrons; when $F(\beta z) < 0$, energy flows to the field from the electrons. If we follow an average electron along the beam from $z=0$, the direction of energy flow is from the field to the beam until shortly after the first space reversal of electric field is passed (E_z changes sign at $\beta z = \pi/2$); then the direction of energy flow reverses. At $\beta z = \pi$, which is the plane of electron exit for the lowest mode, $F(\pi) = -2$. $F(\beta z)$ oscillates with larger and larger amplitude as βz is increased. Despite this, $F(n\pi) = -2$ for n odd ($\beta z = \pi, 3\pi, 5\pi, \dots$), while for n even, $F(n\pi) = 0$.

It is of interest to see what fraction of the beam energy is transferred from the field to the electron beam. This is just \overline{W}_e/W_0 , where W_0 is the dc energy of an electron. It is also convenient to make use of some additional notation. Using

$$E_0 \equiv -\beta V_1, \quad W_0 \equiv eV_0 = \frac{1}{2} m v_0^2,$$

$$\beta = \frac{n\pi}{l}, \quad \beta_e \equiv \frac{\omega}{v_0},$$

and $\phi \equiv \omega l/v_0$ (total electron transit angle through the ion trap), we obtain

$$\left. \frac{\overline{W}_e}{W_0} \right|_{z=l} = \frac{F(n\pi)}{2(n\pi)^2} \left(\frac{V_1}{V_0}\right)^2 \phi^2. \quad (42)$$

For $n=1$ (the lowest mode), $F(\pi) = -2$, and

$$\left. \frac{\overline{W}_e}{W_0} \right|_{z=l} = -\frac{1}{\pi^2} \left(\frac{V_1}{V_0}\right)^2 \phi^2. \quad (43)$$

Because of $1/n^2$ dependence, energy transfer from the electrons to the oscillating ions is greater if n is small; this favors excitation of low n -number modes.

We can define a beam-loading conductance G_b such that the beam-loading power is

$$P_b = \frac{1}{2} G_b V_1^2 = I_0 V_0 \left. \frac{\overline{W}_e}{W_0} \right|_{z=l}.$$

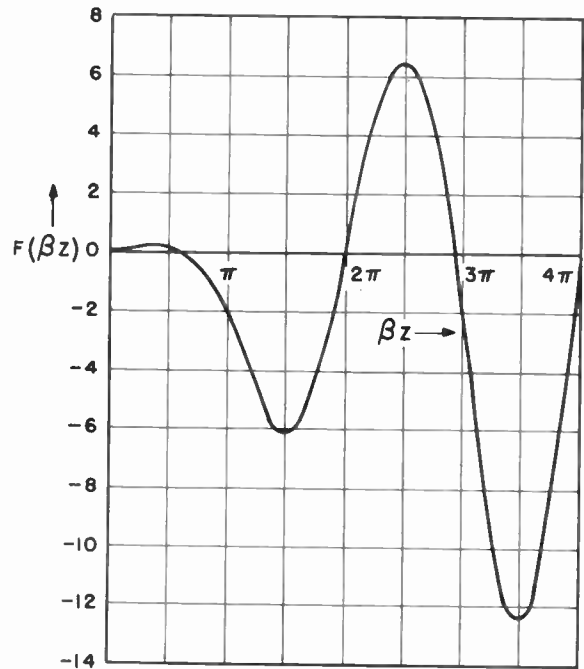
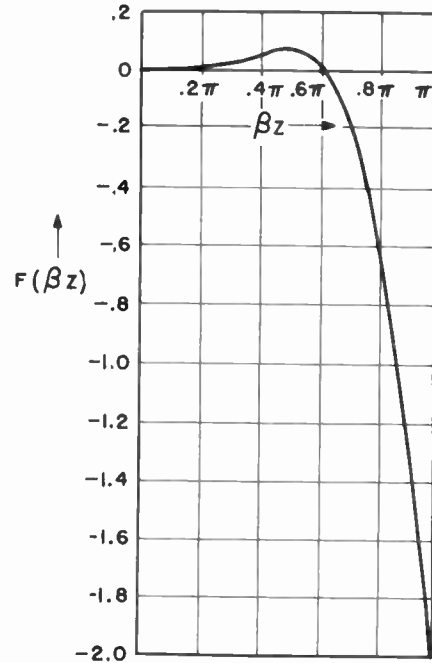


Fig. 5—Plots of $F(\beta z)$ vs βz where $F(\beta z) \equiv [\beta z \sin \beta z - 1/2 \sin^2 \beta z - (1 - \cos \beta z)]$.

Thus defined,

$$G_b \Big|_{n=1} = -\frac{2}{\pi^2} \frac{I_0}{V_0} \phi^2. \quad (44)$$

We have thus found that negative beam loading arises for modes of odd n number from the passage of an electron beam through an ion trap. Whether or not the energy that can be transferred in this way is sufficient to sustain ion oscillations is discussed in Part F.

E. Space Reversal of Electric Field and Negative Beam Loading

A possible objection to the calculation of Part D is the following: To obtain a nonzero result for the beam loading, electron velocities must be calculated to third order in electron transit angle. It is conceivable that if a completely self-consistent calculation were done in which ion motion and resulting electric fields were also calculated to higher order, the beam loading might turn out to be positive rather than negative.

While it is true that more accurate calculations will give results that differ from those obtained under the present approximations, we expect the differences to be detailed rather than fundamental. The gross behavior of the ions should be in accord with the present picture. A basic consequence of this sort of ion motion is that the ac electric field in the ion trap undergoes one or more *space reversals*.

We believe that the occurrence of negative beam loading is a consequence of the *space reversal* of the electric field, and is little affected by other details of its space variation, whence a more precise calculation would still allow negative beam loading to be predicted. This view is supported by the result obtained in the present section. Here we calculate beam loading for the case of a simple, passive LC circuit employed in place of the ions; the elements are so disposed that a space reversal occurs in the electric field, and the electron transit time is taken to be short in comparison with an rf cycle.

The present beam-loading calculation is done for the case of an electron beam traversing a two-region rf gap, as shown in Fig. 6. The entrance and exit grids are tied together, and remain at anode potential. The intermediate grid can vary up and down in potential, either by being driven from an external voltage source or by being part of an oscillating resonant circuit. One simple LC circuit which would allow selfexcited sinusoidal oscillations to occur in the event of negative beam loading is shown in Fig. 7.

As usual, the analysis is small signal and one dimensional. Space charge effects are neglected and velocity spread in the beam is ignored. Idealized grids are assumed (no beam interception, no secondary electrons). No positive ions are present. The electric field is given by

$$\left. \begin{aligned} \tilde{E}_z &= E_0 \cos \omega t \text{ in region 1, and} \\ \tilde{E}_z &= -E_0 \cos \omega t \text{ in region 2} \end{aligned} \right\} \quad (45)$$

Details of the beam loading calculation are given in the Appendix.

In region 1, the energy transferred to an average electron when it has reached a transit angle θ is, in units of its dc energy,

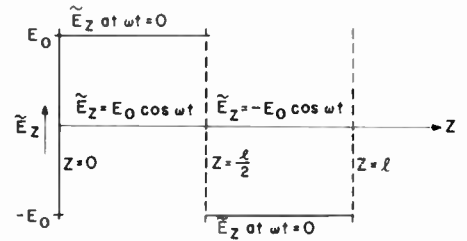
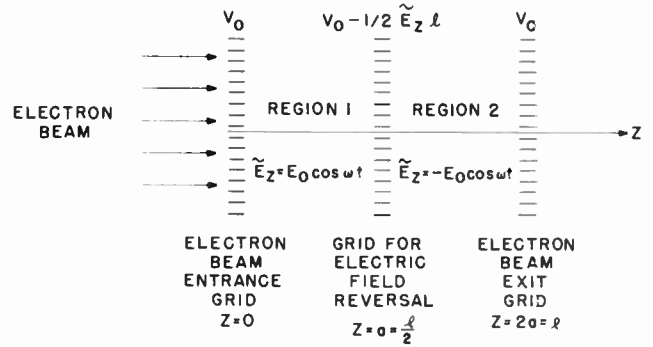


Fig. 6—Two-region rf gap, showing electric field distribution.

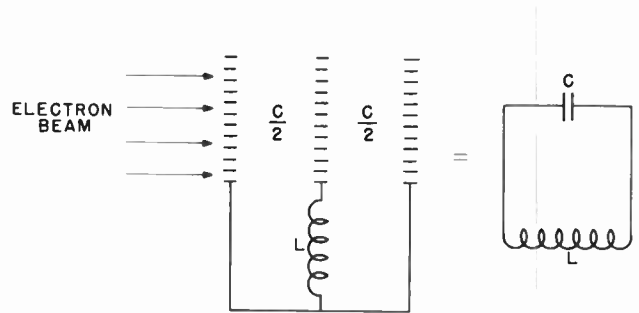


Fig. 7—Simple LC circuit for self-excited oscillations.

$$\frac{\bar{W}_{e1}}{W_0} = \frac{1}{192} \left(\frac{V}{V_0} \right)^2 \theta_i^2 \left(2 \frac{\theta}{\theta_i} \right)^4, \quad 0 \leq \theta \leq \frac{\theta_i}{2} \quad (46)$$

In region 2, the corresponding expression for net energy transferred to an average electron is

$$\frac{\bar{W}_{e2}}{W_0} = \frac{1}{192} \left(\frac{V}{V_0} \right)^2 \theta_i^2 F \left(\frac{\theta}{\theta_i} \right), \quad \frac{\theta_i}{2} \leq \theta \leq \theta_i \quad (47)$$

$F(\theta/\theta_i)$ is given by

$$F \left(\frac{\theta}{\theta_i} \right) = 4 \left[1 - 4 \left(\frac{\theta}{\theta_i} \right) + 12 \left(\frac{\theta}{\theta_i} \right)^2 - 16 \left(\frac{\theta}{\theta_i} \right)^3 + 4 \left(\frac{\theta}{\theta_i} \right)^4 \right] \quad (48)$$

In Fig. 8 we plot

$$\left(2 \frac{\theta}{\theta_i} \right)^4 \text{ vs } \left(\frac{\theta}{\theta_i} \right) \text{ for } 0 \leq \theta \leq \frac{\theta_i}{2},$$

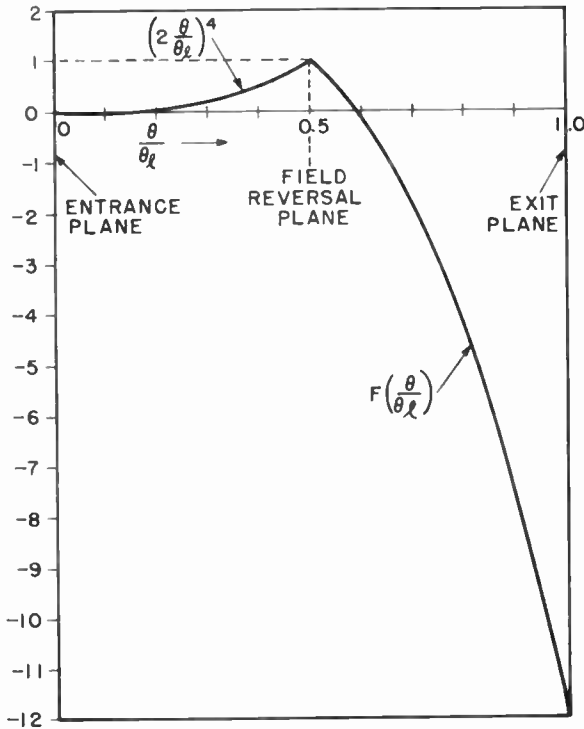


Fig. 8—Plots of

$$2 \left(\frac{\theta}{\theta_l} \right)^4 \text{ and } F \left(\frac{\theta}{\theta_l} \right) \text{ vs } \frac{\theta}{\theta_l},$$

where

$$F \left(\frac{\theta}{\theta_l} \right) = 4 \left[1 - 4 \left(\frac{\theta}{\theta_l} \right) + 12 \left(\frac{\theta}{\theta_l} \right)^2 - 16 \left(\frac{\theta}{\theta_l} \right)^3 + 4 \left(\frac{\theta}{\theta_l} \right)^4 \right].$$

and

$$F \left(\frac{\theta}{\theta_l} \right) \text{ vs } \left(\frac{\theta}{\theta_l} \right) \text{ for } \frac{\theta_l}{2} \leq \theta \leq \theta_l.$$

Examination of the curves or equations reveals that the energy transfer rises from zero, and is positive, as the electrons move from $Z=0$ to $Z=l/2$. At $Z=l/2$, a space reversal in the electric field occurs. From that point on the net energy transferred falls,¹¹ becoming zero near $Z=0.6l$, and being negative from there on. At $Z=l$ the net energy transferred is 12 times as great, in magnitude, as at $Z=l/2$.

We can convert our expressions for energy transfer into beam loading conductances. For any single-region rf gap of total transit angle ϕ ($\phi \ll 2\pi$), we obtain, using (46) when $\theta = \phi = \theta_l/2$,

$$\left. \frac{\overline{W}_{e1}}{W_0} \right|_{\text{total}} = \frac{1}{48} \left(\frac{V}{V_0} \right)^2 \phi^2. \tag{49}$$

¹¹ When the beam is in the first region, its interaction with the electric field gives rise to positive beam loading in the usual fashion. Then when this partially bunched beam encounters an electric field of opposite sign, the energy, rather plausibly, begins to flow from the beam to the circuit.

Defining beam-loading conductance in the usual way, we obtain for single-region rf gaps

$$G_{b1} = \frac{1}{24} \frac{I_0}{V_0} \phi^2 \tag{50}$$

For any two-region (equal regions) rf gap of total transit angle ϕ ($\phi \ll 2\pi$), we obtain, using (47) and (48) when $\theta = \phi = \theta_l$,

$$\left. \frac{\overline{W}_{e2}}{W_0} \right|_{\text{total}} = - \frac{1}{16} \left(\frac{V}{V_0} \right) \phi^2. \tag{51}$$

The corresponding beam-loading conductance is negative, and is given by

$$G_{b2} = - \frac{1}{8} \frac{I_0}{V_0} \phi^2. \tag{52}$$

Thus we conclude that a space reversal in the ac electric field can give rise to negative beam loading, even for small transit angles. One consequence of this is that the validity of the negative beam loading result obtained in Part D for the oscillating ions is strengthened. Another consequence is that a new type of oscillator appears to be possible, for which the name "nonotron"^{15,16} has been suggested.

F. Sustaining of Ion Oscillations by Negative Beam Loading

For short ion traps, fast electrons, and typical frequencies of ion oscillation, the electron transit angle, ϕ , is very small. Hence, the amount of energy transferred from the electron beam to the oscillating ions is small. The sufficiency of this energy for sustaining ion oscillations is thus in doubt.

While it is true that the energy available from negative beam loading is small, the energy stored in the oscillations is also small. To judge the adequacy of the available energy requires knowledge of the energy losses. No attempt is made here to estimate these. Instead we calculate a "minimum Q " for the oscillating ions. This is the lowest natural Q for which ion oscillations can be excited by a given negative beam loading

¹² J. R. Pierce and W. G. Shepherd, "Reflex oscillators," *Bell. Syst. Tech. J.*, vol. 26, pp. 671; July, 1947.

¹³ D. R. Hamilton, J. K. Knipp, and J. B. H. Kuper, "Klystrons and Microwave Triodes," McGraw-Hill Book Co., New York, N. Y., p. 45; 1948.

¹⁴ This is positive, as it should be, and agrees with the expressions of Pierce and Knipp (footnotes 12 and 13) in the limit of small transit angles. Even for $\phi = 2$ radians, G_{b1} exceeds that predicted by the more exact theory by less than 25 per cent. Thus, despite the fact that this analysis has been restricted to small transit angles, we can have reasonable confidence in its validity even for transit angles up to 1 radian or so.

¹⁵ Hamilton, *et al.*, *op. cit.*, p. 30.

¹⁶ The nonotron resembles the monotron (footnote 15) somewhat. In a sense, the negative beam loading of a monotron arises when a *time reversal* of the ac electric field occurs during the electron's transit through the gap. In the nonotron the negative beam loading occurs because of a *space reversal* of the ac electric field.

conductance. If the natural Q is greater than Q_{\min} , oscillations will be sustained; if the natural Q is less than Q_{\min} , oscillations will not build up.

Our minimum Q is defined as

$$Q_{\min} \equiv 2\pi \frac{\text{energy stored}}{\text{energy available per cycle}}. \quad (53)$$

From (20), the velocity of an ion is

$$\bar{v}_i = -\frac{e}{m_i \omega} \beta V_1 \cos \beta z \sin \omega t. \quad (54)$$

The kinetic energy is just $\frac{1}{2} m \bar{v}_i^2$. Averaging over-all z positions, the maximum value of the kinetic energy, and hence the value of energy stored, for an average ion is

(energy stored per average ion)

$$= \frac{(n\pi)^2}{8} e V_0 \left(\frac{m_e}{m_i} \right) \left(\frac{V_1}{V_0} \right)^2 \frac{1}{\phi^2}. \quad (55)$$

If N is the number of electrons traversing the ion trap in one second, then the number of electrons, and hence ions, in the trap is just $N(l/v_0) = N(\phi/\omega)$. Energy stored is thus

$$(\text{energy stored}) = \frac{(n\pi)^2}{8} e V_0 \frac{N}{\omega} \left(\frac{m_e}{m_i} \right) \left(\frac{V_1}{V_0} \right)^2 \frac{1}{\phi}. \quad (56)$$

The number of electrons passing through the ion trap in one cycle is $2\pi N/\omega$. Using (42) with n odd,

$$(\text{energy available per cycle}) = \frac{N\pi}{\omega} \frac{2eV_0}{(n\pi)^2} \left(\frac{V_1}{V_0} \right)^2 \phi^2. \quad (57)$$

Thus our minimum Q becomes

$$Q_{\min} = \frac{(n\pi)^4}{8} \frac{m_e}{m_i} \frac{1}{\phi^3} \quad (\text{for } n \text{ odd}). \quad (58)$$

Let us compute the minimum Q for a particular case. Choose $m_i = 5.5 \times 10^4 m_e$ (mass number 30 for the ions), $\omega/2\pi = 1$ mc, $l = 1$ cm, and $V_0 = 300$ volts; then $\phi \simeq 6.1 \times 10^{-3}$ radians. For $n = 1$ (the lowest mode), $Q_{\min} \simeq 980$, while for $n = 3$ (the next lowest mode for which negative beam loading is predicted), $Q_{\min} \simeq 80,000$.

From this calculation we see that, although the energy available from negative beam loading is very small, the energy of ion oscillation is also very small. Further, it is not hard to believe that the natural Q 's of ion plasmas found in typical ion traps are of the order of 10^3 , or perhaps even greater. Thus it appears plausible that negative beam loading is an entirely adequate source of energy to allow ion oscillations to be sustained, at least in some cases. It also appears that the n^4 behavior of Q_{\min} strongly favors excitation of low n -number modes.

G. Possible Importance of Secondary Electrons

In the treatments thus far of ion motion and energy transfer, we have assumed that all of the electrons present have the same dc velocity. In actual gridded drift tubes, however, slow speed secondary electrons from the grids may be present in significant numbers. One effect of the secondaries would be to increase the total amount of negative space charge present in the drift tube, which in turn would increase the number of ions trapped. The dispersion relation would also be modified. Of perhaps greater importance is the role of secondary electrons in the energy transfer process.

In (58) for Q_{\min} we note the inverse cube dependence on transit angle. Three-volt secondaries, for example, have a transit angle 10 times that of 300-volt primary beam electrons. Thus a given number of slow speed secondaries is enormously more effective in supplying energy to the oscillating ions than the same number of primary beam electrons.

For some ion traps sufficient energy to sustain ion oscillations may be obtainable from the primary beam electrons alone. For others the presence of some minimum number of secondary electrons may be necessary. Thus we might expect to see no ion oscillations at all in certain cases, even though ions are trapped. Then a slight increase in the number of secondary electrons present could cause "starting current" to be exceeded, whence oscillations would occur. This is consistent with certain of the experimental observations.

III. CONCLUSION

Subject to a number of simplifying assumptions, we have calculated some of the allowed positive ion motions inside ion traps bounded by conducting walls. The analysis is restricted to systems in which the electron transit times through the ion trap are short compared with an oscillation period, and also in which the dimensions of the ion trap are small enough that it is well below cutoff for the ion oscillation frequencies. It turns out that the ion motions are nearly the same when the negative space charge arises from a beam of fast electrons as when it arises from heavy negative particles of mass $m_- = (v_0/v_p)^2 m_e$. Figs. 2 and 3 exhibit some representative ion motions and equipotentials.

The ion motions give rise to space charge electric fields inside the ion trap. In a one-dimensional problem, the electric field varies as $\cos \pi z/l \cos \omega t$ for the lowest mode. This means that most of the electrons encounter a space reversal in electric field during their traversal of the ion trap. It turns out that this space reversal causes the beam loading to be negative, even for small transit angles. This means that energy is transferred from the electron beam to the rf electric field in the ion trap. For small transit angles, this energy transfer is very small. But the energy of ion oscillation is also very small. It

appears quite plausible that in many cases negative beam loading is sufficient to sustain ion oscillations.

Because of the strong dependence of negative beam loading on transit angle, slow speed secondary electrons are much more effective in supplying energy than are the primary electrons in typical beams. Thus in some cases secondaries may be of crucial importance in determining whether or not ion oscillations can exist. With too few secondaries, the negative beam loading would be too small, and oscillations could not be sustained. With some larger number of secondaries, starting current for oscillations would be exceeded, and oscillations would occur.

It is observed experimentally that in many cases ions can be trapped without oscillations occurring. Yet under seemingly identical conditions, ion oscillations, either continuous or fluctuating, may exist. A transition from the nonoscillating to the oscillating state often takes place after a tube has been operated for a number of hours. We speculate that this transition is associated with an increase in the secondary emission ratio of grids and other surfaces in the neighborhood of the ion trap.

If the ions are not oscillating initially, a slight amount of externally supplied energy may permit oscillations to occur. We believe that this is closely associated with induced effects, such as "ringing" and "modulation hop," observed in some reflex klystrons.

As has been mentioned in the Introduction, ion oscillations are often modified by low-frequency fluctuations. The present theory does not appear to give much insight into this aspect of the problem. This is not surprising, since our theory is small signal, and we would expect the fluctuation mechanism to depend on large signal effects.

On the basis of the foregoing we can understand, at least qualitatively, the occurrence or nonoccurrence of continuous ion oscillations. Obviously the calculations could be refined and extended in a number of ways. For one thing, losses could be examined. This would permit an estimate of starting current to be made. And further effort can be made to understand the low-frequency fluctuations.

We find also that negative beam loading can occur with a simple LC circuit, even for short transit angles, provided the electron beam traverses a two-region rf gap in which there is a space reversal of the electric field. Thus a new type of oscillator is possible, for which the name "nonotron" has been suggested.

APPENDIX

Consider a beam of electrons of velocity v_0 entering the two-region rf gap of Fig. 6. Let the electric field \tilde{E}_z be given by (45).

As a matter of notation, we use unprimed quantities in region 1 and primed quantities in region 2. Let

$$v_a \equiv v \Big|_{z=a}, \quad \alpha \equiv \frac{e}{m_e} \frac{E_0}{\omega v_0}, \quad \phi_0 \equiv \omega t_0, \quad \tau \equiv t - t_0,$$

and

$$\theta \equiv \frac{\omega Z}{v_0}.$$

Integration of the force equation gives

$$v = v_0 - \frac{e}{m_e} \frac{E_0}{\omega} (\sin \omega t - \sin \omega t_0) \text{ in region 1 and } \tag{59}$$

$$v' = v_a + \frac{e}{m_e} \frac{E_0}{\omega} (\sin \omega t - \sin \omega t_a) \text{ in region 2. } \tag{60}$$

We now proceed to calculate energy transfer in region 1 for the case where the time of electron transit through the region is much less than a period of the oscillation. To use the method employed here, we need to obtain v as a function of Z rather than as a function of t . This velocity will depend also on the entrance time t_0 ; hence we will need to average over all entrance times to obtain the energy transferred to an average electron. The time of transit from entrance to Z is τ , and is given by

$$\tau = \int_0^Z \frac{du}{v}. \tag{61}$$

Since we are unable to solve directly for τ as a function of Z , or conversely, we employ a method of successive approximation. Let the n th approximations for τ and v be given by

$$\tau_n \equiv \int_0^Z \frac{du}{v_{n-1}} \text{ and } \tag{62}$$

$$v_n \equiv v_0 [1 - \alpha \sin(\phi_0 + \omega \tau_n) + \alpha \sin \phi_0]. \tag{63}$$

It turns out that we can expand v_n and τ_n as power series in θ , and that the valid degree of the series is the same as the order of the approximation. We employ the standard trigonometric expansions, and, since $\omega \tau_n$ is a small quantity, we can employ the usual power series expansions for $\sin \omega \tau_n$ and $\cos \omega \tau_n$. We also make use of the binomial series expansion as required.

We obtain

$$\omega \tau_1 = \theta$$

$$\omega \tau_2 = \theta + \frac{\alpha}{2} \cos \phi_0 \theta^2$$

$$\omega \tau_3 = \theta + \frac{\alpha}{2} \cos \phi_0 \theta^2 - \left(\frac{\alpha}{6} \sin \phi_0 - \frac{\alpha^2}{2} \cos^2 \phi_0 \right) \theta^3 \tag{64}$$

$$v_1 = v_0 (1 - \alpha \cos \phi_0 \theta)$$

$$v_2 = v_0 \left[1 - \alpha \cos \phi_0 \theta + \left(\frac{\alpha}{2} \sin \phi_0 - \frac{\alpha^2}{2} \cos^2 \phi_0 \right) \theta^2 \right]. \quad (65)$$

The work done on an average electron is

$$\overline{W}_{e1} = \int_0^Z \overline{F} du \quad (66)$$

where

$$\overline{F} = -eE_0 \overline{\cos \omega t} = -\frac{eE_0}{2\pi} \int_0^{2\pi} \cos(\phi_0 + \omega\tau) d\phi_0. \quad (67)$$

Using the third approximation for $\omega\tau$, we find that

$$\overline{\cos(\phi_0 + \omega\tau_3)} = -\frac{\alpha}{6} \theta^3. \quad (68)$$

Using

$$W_0 \equiv \frac{1}{2} m_e v_0^2, \quad \alpha \equiv \frac{e E_0}{m_e \omega v_0} = -\frac{V}{V_0} \frac{1}{\theta_l}, \quad \text{and } \theta_l \equiv \theta \Big|_{z=l},$$

we obtain an expression for energy transferred to an average electron in units of its dc energy:

$$\frac{\overline{W}_{e1}}{W_0} = \frac{\alpha^2}{12} \theta^4 = \frac{1}{192} \left(\frac{V}{V_0} \right)^2 \theta_l^2 \left(2 \frac{\theta}{\theta_l} \right)^4. \quad (69)$$

The calculation of energy transfer for region 2 proceeds in a parallel fashion to that of region 1, but is more complicated. As n th approximations for τ' and v' we use

$$\tau_n' \equiv \int_a^Z \frac{du}{v_{n-1}'} \quad (70)$$

$$\begin{aligned} v_n' &\equiv v_{an} + v_0 \alpha \sin \omega t - v_0 \alpha \sin \omega t_{an} \\ &= v_{an} - v_0 \alpha \sin \omega t_{an} (1 - \cos \omega \tau_n') \\ &\quad + v_0 \alpha \cos \omega t_{an} \sin \omega \tau_n' \end{aligned} \quad (71)$$

where

$$\begin{aligned} l &\equiv l_{an} + \tau_n' \\ l_{an} &\equiv l_0 + \tau_{an} \\ \tau_{an} &\equiv \tau_n \Big|_{z=a} \\ v_{an} &\equiv v_n \Big|_{z=a}. \end{aligned}$$

Also let

$$\begin{aligned} \theta_a &\equiv \frac{\omega a}{v_0} \\ \theta' &\equiv \theta - \theta_a. \end{aligned}$$

Eventually we obtain the following:

$$\omega \tau_1' = \theta' \quad (72)$$

$$\omega \tau_2' = \theta' + \alpha \cos \phi_0 \theta_a \theta' - \frac{\alpha}{2} \cos \phi_0 \theta'^2 \quad (73)$$

$$\omega \tau_3' = \theta' + \alpha \cos \phi_0 \theta_a \theta' - \frac{\alpha}{2} \cos \phi_0 \theta'^2$$

$$\begin{aligned} & - \left(\frac{\alpha}{2} \sin \phi_0 - \frac{3\alpha^2}{2} \cos^2 \phi_0 \right) \theta_a^2 \theta' \\ & + \left(\frac{\alpha}{2} \sin \phi_0 - \frac{3\alpha^2}{2} \cos^2 \phi_0 \right) \theta_a \theta'^2 \\ & + \left(\frac{\alpha}{6} \sin \phi_0 + \frac{\alpha^2}{2} \cos^2 \phi_0 \right) \theta'^3 \end{aligned} \quad (74)$$

$$\begin{aligned} v_1' &= v_0 [1 - \alpha \cos \phi_0 \theta_a + \alpha \cos \phi_0 \theta'] \\ v_2' &= v_0 [1 - \alpha \cos \phi_0 \theta_a + \alpha \cos \phi_0 \theta' \\ & + \left(\frac{\alpha}{2} \sin \phi_0 - \frac{\alpha^2}{2} \cos^2 \phi_0 \right) \theta_a^2 \\ & - (\alpha \sin \phi_0 - \alpha^2 \cos^2 \phi_0) \theta_a \theta' \\ & - \left(\frac{\alpha}{2} \sin \phi_0 + \frac{\alpha^2}{2} \cos^2 \phi_0 \right) \theta'^2]. \end{aligned} \quad (75)$$

The energy transfer in region 2 only is given by

$$\overline{W}_{e2}' = \int_a^Z \overline{F}' du \quad (76)$$

where

$$\overline{F}' = eE_0 \overline{\cos \omega t} = \frac{eE_0}{2\pi} \int_0^{2\pi} \cos \omega t d\phi_0. \quad (77)$$

Using the third approximation for $\omega\tau'$, we obtain

$$\frac{\overline{W}_{e2}'}{W_0} = -\frac{\alpha^2}{12} [4\theta_a^3 \theta' + 6\theta_a^2 \theta'^2 + 4\theta_a \theta'^3 - \theta'^4]. \quad (78)$$

This holds for region 2 only.

The energy transferred to an average electron upon entrance to region 2, from (69) evaluated at $Z=a$ (or $\theta=\theta_a$), is

$$\frac{\overline{W}_{e1}}{W_0} \Big|_{z=a} = \frac{\alpha^2}{12} \theta_a^4 = \frac{1}{48} \left(\frac{V}{V_0} \right)^2 \theta_a^2. \quad (79)$$

Thus the net energy transfer per average electron in region 2 is

$$\frac{\overline{W}_{e2}}{W_0} = \frac{\overline{W}_{e1}}{W_0} \Big|_{z=a} + \frac{\overline{W}_{e2}'}{W_0} = \frac{1}{192} \left(\frac{V}{V_0} \right)^2 \theta_l^2 F \left(\frac{\theta}{\theta_l} \right), \quad (80)$$

where

$$\begin{aligned} F \left(\frac{\theta}{\theta_l} \right) &\equiv 4 \left[1 - 4 \left(\frac{\theta}{\theta_l} \right) + 12 \left(\frac{\theta}{\theta_l} \right)^2 \right. \\ &\quad \left. - 16 \left(\frac{\theta}{\theta_l} \right)^3 + 4 \left(\frac{\theta}{\theta_l} \right)^4 \right]. \end{aligned} \quad (81)$$

ACKNOWLEDGMENT

It is a pleasure to acknowledge the assistance of stimulating discussions with B. Beaver, M. Muller, R. Varian, and C. Ward regarding formulations of the problem and validity of the results.

Multihole Ferrite Core Configurations and Applications*

H. W. ABBOTT† AND J. J. SURAN‡, SENIOR MEMBER, IRE

Summary—Combined gating and memory functions may be performed by the use of multihole ferrite cores called transfluxors. By proper topological design, transfluxors may be made noncritical to control pulse amplitude. In addition, by use of novel compensation and ac driving techniques, the transfluxor may be operated noncritically over an ambient temperature range from -50°C to $+200^{\circ}\text{C}$. By making full use of multiple path geometries single multihole disks referred to as logicors have been designed to perform such complex logical operations as sequential pulse gating, odd parity checking, binary half adding, selective channeling, etc. One such logicor may replace as many as twelve switching devices in a logical circuit.

INTRODUCTION

THE USE of single-hole ferrite cores as switching elements in control and computer type circuitry is well known.¹ Recent investigations in the electronic field have resulted in the development of a new ferrite component which consists of a single ferrite disk containing two or more apertures. By virtue of the multihole geometry, several distinct flux paths are obtained in a single device. Control of the saturation states in each flux path makes it possible to control an ac output signal with pulses applied to trigger terminals. Consequently, a two-hole disk, which has been named the transfluxor, may be used to gate an ac signal on or off by the application of suitable control pulses.^{2,3} In its elemental form, therefore, the transfluxor is a magnetic switching device which may be "read" continuously by an ac signal.

This report describes some aspects of the development of transfluxors which permits them to be applied to practical control circuitry and to logical networks. The advantages of transfluxors over single cores are enumerated and some of the problems inherent in the elemental devices are discussed. An advanced design utilizing a four-hole topology is then described. By use of a unique driving technique it is shown that four-hole transfluxors may be operated in switching applications over an ambient temperature range extending from -50°C to $+180^{\circ}\text{C}$ without benefit of temperature-compensation circuitry.

An outgrowth of the transfluxor study has been the development of multihole cores which may be used to perform complex logical operations. For example, six-hole cores, called logicors, are described which perform

complex logical functions such as digital half-adding and odd-parity checking. One such logicor may replace as many as twelve transistors in a logical circuit. The same six-hole topology is used for various logic functions and only winding configuration changes are required to change the logicor operation.

TWO-HOLE TRANSFLUXORS

A two-hole transfluxor which may be used to switch an ac signal on and off by control pulses is illustrated in Fig. 1. When the saturation flux states in legs 1 and 2

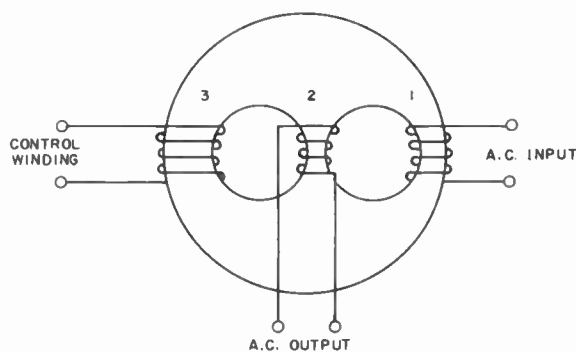


Fig. 1—Two-hole transfluxor.

are of the same sign, the transfluxor is blocked and ideally no ac signal transfer can occur between legs 1 and 2. However, if a pulse of sufficient energy is applied to the control winding so that the saturation flux state of leg 2 is reversed without the flux state of leg 1 being altered, the transfluxor is unblocked. In the unblocked condition, flux changes in the closed magnetic path 1-2 may occur and hence an ac signal is readily transferred from input to output terminals. The magnetic hysteresis characteristics of the two-hole transfluxor, as seen from the control winding, are illustrated in Fig. 2. If the control winding has N_3 turns, the control pulse must satisfy the following conditions in order to block the transfluxor:

$$|I_p| > |I_{C3-1}| \quad (1)$$

$$|E_p T_p| > |2(\phi_{S3-2} + \phi_{S3-1})N_3| \quad (2)$$

In (1) and (2), the subscript p denotes the control pulse parameters, I_{C3-1} is the current required to establish the coercive mmf in the closed magnetic path 3-1, ϕ_{S3-2} denotes the saturation flux corresponding to the magnetic path 3-2, and E and T are the voltage and pulse width requirements, respectively, of the control signal. (Note that if ϕ is expressed in webers, the dimension of ET is volt-seconds.)

* Original manuscript received by the IRE, February 14, 1957.

† Electronics Lab., General Electric Co., Syracuse, N. Y.

¹ S. Guterman, R. Kodis, and S. Ruhman, "Logical and control functions performed with magnetic cores," *PROC. IRE*, vol. 43, pp. 291-298; March, 1955.

² J. A. Rajchman and A. W. Lo, "The transfluxor—a magnetic gate with stored variable setting," *RCA Rev.*, vol. XVI, pp. 303-311; June, 1955.

³ J. A. Rajchman and A. W. Lo, "The transfluxor," *PROC. IRE*, vol. 44, pp. 321-332; March, 1956.

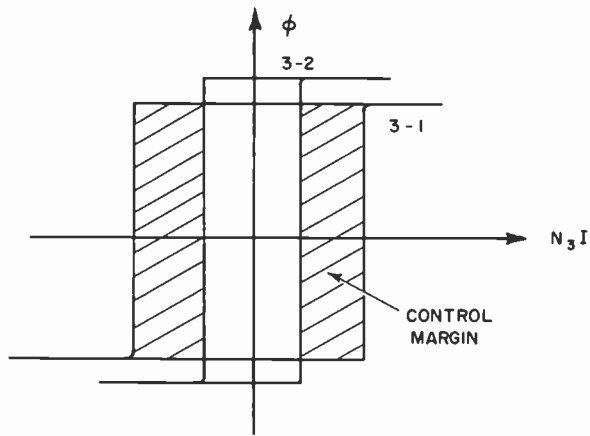


Fig. 2—Magnetic control characteristics.

In order to unblock the transfluxor, the control pulse must establish an mmf which falls within the control margin illustrated in Fig. 2, *i.e.*,

$$|I_{C3-1}| > |I_p| > |I_{C3-2}|. \quad (3)$$

The volt-second requirement of the unblocking pulse is fulfilled by (2) or is sufficient if given by

$$|E_p T_p| > |2\phi_{S3-2} N_3|. \quad (4)$$

A consequence of (3) is that the control pulse must be limited in amplitude when it is desired to unblock the transfluxor; for, if the pulse amplitude is too large, the saturation fluxes of *both* legs 2 and 1 may be reversed and the transfluxor will be carried from one blocked state to another.

Magnetic hysteresis characteristics having the same form as those illustrated in Fig. 2 may be obtained when leg 1 is used as the reference. The requirements imposed upon the ac signal input are

$$|I_{C1-3}| > |I_m| > |I_{C1-2}| \quad (5)$$

$$f_m > \frac{|E_m|}{|N_1 \phi_{S1-2}|} \quad (6)$$

where I_m is the peak magnitude of the ac current, I_{C1-2} is the magnitude of current which will establish the coercive mmf for the closed path 1-2, f_m is the frequency of the ac signal, E_m is the peak magnitude of the ac voltage, ϕ_{S1-2} is the saturation flux corresponding to the path 1-2, and N_1 is the number of turns around leg 1. Eq. (5) indicates that the signal current must be large enough to insure flux changes in the magnetic path 1-2, but must be small enough to prevent substantial flux changes in the path 1-3. The inequality given by (6) is established by the requirement that the ac signal should not exceed the volt-second limit which would cause complete reversal of the saturation flux states in the path 1-2.

The saturation flux values and the coercive magnetomotive force values of the transfluxor are determined by the geometry of the core. Thus, if the ferrite material from which the transfluxor is fabricated has a saturation

flux density given by B_s (webers/ m^2 in the mks system), the saturation flux, ϕ_s , for any leg, i , is

$$\phi_{Si} = B_s A_i \quad (7)$$

where A_i is the smallest cross-sectional area of the leg i . Similarly, if the ferrite material has a coercive field intensity given by H_c (amp-turns/m in the mks system), the coercive mmf value for any closed path $i-j$ is

$$N_i I_{Ci-j} = H_c l_{i-j} \quad (8)$$

where N_i is the number of turns around the leg i , l_{i-j} is the mean circumference of the path $i-j$ and I_{Ci-j} is the corresponding coercive current required to establish the coercive mmf for the path $i-j$.

If it is desired to maximize the control margin of the transfluxor illustrated in Fig. 1, the magnetic path 3-1 should be much longer than the path 3-2. However, in order to provide the greatest tolerance for the ac input signal, the path 1-3 should be much longer than the path 1-2. These two conditions are incompatible with one another and hence, the topological dimensioning of the transfluxor must represent a compromise between control and ac signal requirements.

The over-all size of the transfluxor is governed by practical considerations relating to its fabrication as well as by the control pulse repetition rate and the ac signal frequency which is intended as the controlled signal. Eq. (6) determines the condition which must be met if the half-cycle energy of the signal is to be limited to a value which will not reverse the flux states in the magnetic path between signal primary and secondary windings. It is apparent that for low-signal frequencies ϕ_s must be large, a condition which from (7) implies a large cross-sectional area in legs 1 and 2. In order to maintain as large an incremental inductance ($d\phi/di$) as possible, the ratio of leg width to mean circumferential path diameter should be as small as practicable.⁴ Consequently, low-frequency signals require thick disks, in order to maintain reasonable control characteristics and still obtain the required flux saturation level.

The power requirements of both the control and ac signals are determined by the areas of the requisite $\phi-NI$ curves and by the driving frequency. Thus, the magnetizing power loss P in the core is given by

$$P = \frac{Vf}{4\pi} \oint B dH \quad (9)$$

where V is the material volume, f is the signal frequency, and the circular integral represents the area enclosed by the hysteresis curve. In most cases where ferrite disk construction is used, eddy current losses may be neglected due to the high resistance of the material.

A unique feature of the transfluxor illustrated in Fig. 1 is that a combined gating and memory function

⁴ R. W. Roberts and R. Van Nice, "Influence of ID-OD ratio on magnetic properties of toroidal cores," *Elec. Eng.*, vol. 74, pp. 910-914; October, 1955.

is performed in a single device. The same functions may be realized by a conventional saturable reactor core in combination with a dc control circuit of the bistable type, as illustrated in Fig. 3. An example of the circuit simplifications which are afforded by the transfluxor is illustrated by the three-stage digital-analog converter of Fig. 4. In the circuit of Fig. 4, the control terminals of the transfluxors are energized by binary code pulses so that the presence of a pulse unblocks the particular device to which it is applied. The ac output windings of each device are connected in series so that the output voltage is the sum of the individual transfluxor secondary voltages. If the number of primary turns are the same for each stage but if the secondary turns are doubled with each succeeding stage, binary conversion may be obtained. Once a code has been applied to the control terminals the analog output signal will persist even when the binary code pulses are no longer present. In order to change the "word" stored in the converter, the transfluxors must be reset by blocking pulses prior to the entry of the new word. The relative simplicity of the transfluxor converter circuit illustrates the advantages of having a single device which combines both gating and memory operations.

In practical applications, the elemental two-hole transfluxor exhibits several operational difficulties. The first such difficulty pertains to the amplitude constraints imposed upon the control pulses (3). The magnitude of the control margin itself is not critical; but, due to the decrease of coercivity with increasing temperature, the *relative* magnitudes of control pulse and control margin become critical for ambient temperature variations in the order of ± 30 degrees C.⁵ Therefore, for applications of the transfluxor in environments where the temperature may vary over more than 50°C compensation techniques which adjust the control pulse amplitude as a function of temperature are required.

A second difficulty of the elemental transfluxor arises from the amplitude constraints imposed upon the ac signal (5). If the ac signal is made too large, the core may be inadvertently unblocked by a cumulative addition of flux changes around the path 1-3. Consequently, the change of magnetic coercivity with temperature requires a compensatory control of the ac signal amplitude. When the transfluxor is blocked, the peak current amplitude of the ac must not exceed the coercive current of the path 1-3 and yet, when the transfluxor is unblocked, the volt-second characteristic of the ac must be sufficient to induce a secondary voltage.

A method for obtaining a suitable ac source impedance in view of the current constraints imposed by the coercive characteristics of the core is a serious driving problem of elemental transfluxor circuits. When the transfluxor is blocked, the ac input impedance is very low and current limiting is required; thus, a current

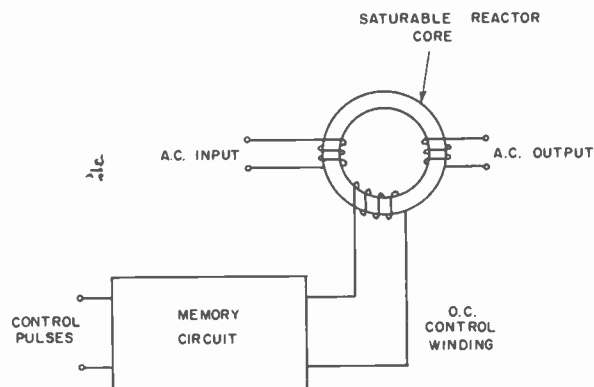


Fig. 3—Functional equivalent of transfluxor.

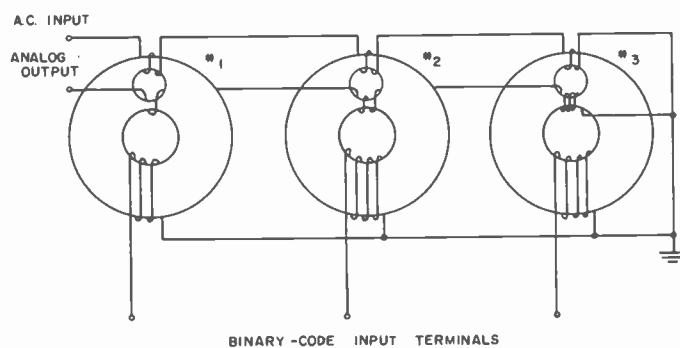


Fig. 4—Transfluxor digital-analog converter.

source is desirable. However, when the transfluxor is unblocked, the ac impedance varies from a low to a high value as the operating point varies about the $\phi-NI$ characteristic and hence, for linear voltage transfer between primary and secondary, a voltage source is desirable. Thus, the driving problem presents another difficulty in the practical utilization of transfluxors.

Other difficulties are introduced by the departure of the ferrite material from ideal squareness. For example, the fact that the slope of the $\phi-NI$ characteristics is not zero in the saturation states of the core results in an induced voltage between primary and secondary when the transfluxor is blocked. Consequently, the signal ratio for the unblocked-blocked conditions is finite and depends somewhat upon the amplitude of the input ac signal. In addition, this ratio is temperature sensitive.⁵ The fact that the slope of the $\phi-NI$ characteristic is less than infinite in the transitional state of the core results in a dependency of the unblock-block ac signal ratio upon the amplitude of the control pulses.⁵

The practical difficulties relating to the circuit utilization of two-hole transfluxors required further development of the device. A result of this development effort has been the design of four-hole transfluxors which eliminate some of the serious problems inherent in the two-hole geometry. The new device is described below.

FOUR-HOLE TRANSFLUXORS

Fig. 5 illustrates an experimental design of a four-hole transfluxor. The addition of the two auxiliary holes in-

⁵ H. W. Abbott and J. J. Suran, "Temperature characteristics of the transfluxor," IRE TRANS., vol. ED-4, pp. 113-119; April, 1957.

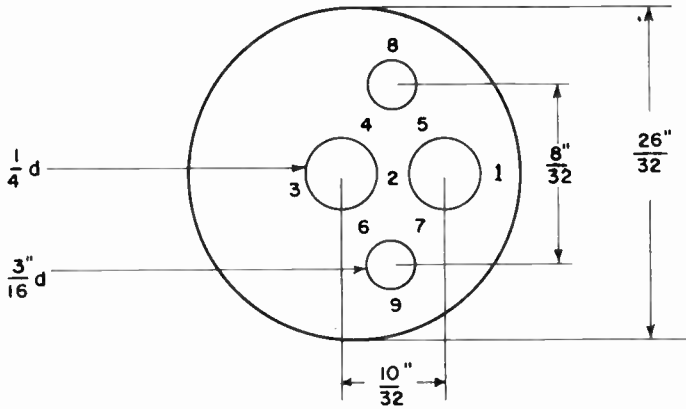


Fig. 5—Experimental four-hole transfluxor.

roduces six more legs, which are numbered 4, 5, 6, 7, 8, and 9. This device may be used in the conventional manner by placing a control winding on leg 3 and using legs 1 and 2 as ac signal windings. The advantage of having two extra holes in the core under these circumstances is due to the fact that when closed path 3-4-2-6-3 saturates, any further changes in flux are forced into the circumferential path 3-8-1-9-3. This results from making the cross-sectional area of legs 4 and 6 equal to (or only slightly larger than) the area of leg 2. A consequence of this operation is that the magnetic path involved in the saturation of leg 1 is made considerably longer than the path involved in the saturation of leg 2 and hence, the control margin of the transfluxor is significantly increased over the margin which would be obtained from a comparable two-hole device. In the experimental transfluxor illustrated in Fig. 5, the control margin was increased by 50 per cent with the addition of the two-auxiliary holes.

A method for electrically utilizing the additional holes in the four-hole transfluxor is illustrated in Fig. 6(a). By using separate block and unblock windings in the configuration shown, the control margin is made practically infinite. The flux states for the blocked and unblocked conditions of the transfluxor are illustrated in Fig. 7. The core is blocked by saturating the parallel flux paths 3-4-2-6-3 and 3-8-1-9-3 from the control leg 3. If the ac signal is introduced in a primary winding around leg 1 and is constrained in current amplitude so that the signal can induce flux changes only in the magnetic path 1-5-2-7-1, it is apparent that the transfluxor is blocked when the flux saturation states in legs 1 and 2 are of the same polarity. Thus, *any* amplitude of control pulse applied to blocking terminals will block the transfluxor, if the following requirements are satisfied.

$$|I_p| > |I_{C_{3-8-1}}| \tag{10}$$

$$|E_p T_p| > |2(\phi_{S_{3-4-2}} + \phi_{S_{3-8-1}})N_3| \tag{11}$$

In (10) and (11), the subscripts 3-8-1 refer to the closed magnetic path 3-8-1-9-3 and the subscripts 3-4-2 refer to the closed magnetic path 3-4-2-6-3.

The transfluxor of Fig. 6 is unblocked by introducing a control signal at the unblock terminals. The latter

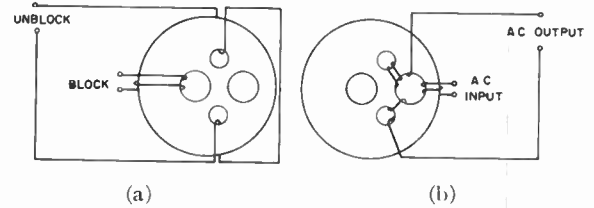


Fig. 6—Winding configurations: (a) control windings and (b) signal windings.

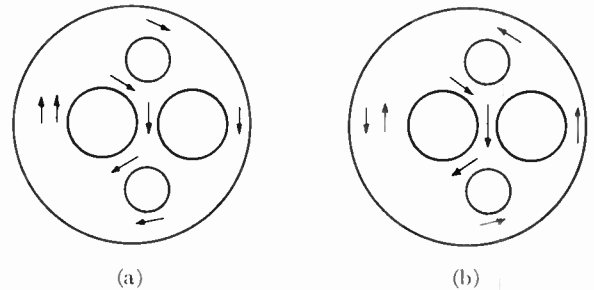


Fig. 7—Flux directions for four-hole transfluxor: (a) blocked condition and (b) unblocked condition.

consist of windings around legs 8 and 9 which are series connected so that the flux induced in leg 9 is in the same rotational direction as the flux induced in leg 8. As illustrated by the flux-state diagrams of Fig. 7, flux changes induced by the unblock signal can occur only in the periphery path, *i.e.*, in the closed path 3-8-1-9-3. If the unblocking pulse satisfies the requirements

$$|I_p| > |I_{C_{3-8-1}}| \tag{12}$$

$$|E_p T_p| > |2\phi_{S_{3-8-1}}N_3| \tag{13}$$

the saturation state of the flux in leg 1 will be reversed from the original blocked state and the ac induction path given by 1-5-2-7-1 is unblocked.

From (10) and (13) it is observed that, if both the blocking and unblocking pulses satisfy the *minimum* energy requirements for flux reversal in the requisite magnetic paths, the transfluxor will operate satisfactorily. Any control-signal having at *least* the *minimum* current amplitude and the *minimum* volt-second requirement will trigger the transfluxor "on" or "off" and hence, the control signal level is no longer critical. Furthermore, the transfluxor of Fig. 6 has separate blocking and unblocking windings which allow the circuit designer to block and unblock the device with a control pulse of either polarity depending upon the sense of the windings around the control legs.

Fig. 6(b) illustrates a method for utilizing two of the extra legs of the four-hole transfluxor by winding the ac secondary around legs 5 and 7 instead of around leg 2 or leg 1. This technique isolates the ac output from the magnetic paths associated with the control signals and, consequently, the control signals are not transmitted to the output terminals when the core is blocked or unblocked.

A principal feature of the four-hole transfluxor is that it can be blocked and unblocked with control pulses of arbitrarily large magnitude, providing that they are

above the coercive requirements of the magnetic paths. Thus, for all practical purposes, the control margin of the device has been made infinite in comparison with the finite margin of two-hole transfluxors. This feature helps considerably in extending the practical operating range of transfluxors. In particular, as is shown below, a major temperature problem of the transfluxor is overcome by the four-hole topology.

DRIVING AND COMPENSATION TECHNIQUES

A serious problem in the operation of transfluxors is the possibility of unblocking the device with the ac signal. For example, in the two-hole device of Fig. 1, it is apparent that if the coercive mmf of the periphery path 1-3 is exceeded by the ac input signal, flux changes may occur in leg 3 due to the ac signal impressed in leg 1. Any flux change in leg 3 must be accompanied by equal flux changes in leg 1. Hence, if the flux in path 1-3 changes during one half of the ac signal period, an equal flux change will occur in the path 1-2 upon the reversal of the ac amplitude. Cumulative unblocking of the transfluxor may thus occur.

In order to prevent accidental unblocking, it is desirable to use a current source for the ac input drive. The peak current delivered by this source should not exceed the coercive current of the path 1-3 in the transfluxor of Fig. 1 but must be greater than the coercive value of the path 1-2. This condition is given by (5). In addition, in order to prevent saturation effects which may cause I_{c1-3} to be exceeded, the frequency of the ac drive signal must be maintained above a minimum value as given by (6).

The disadvantages imposed by these requirements are summarized below.

1) The necessity for a current-source as the ac input leads to considerable signal waveform distortion as a result of the nonlinearity of the ϕ - NI characteristic. In fact, for an ideally square-loop core material, the induced waveform in the ac output winding would be of pulse form for a sine-wave input current.

2) Due to changes in the coercive mmf requirements of the various transfluxor paths as a consequence of temperature variations, the peak value of the ac input current must be varied in a compensating manner if wide ambient temperature variations are anticipated.

3) The volt-second limitation imposed upon the ac input signal (6) limits the magnitude of the induced output signal below the value theoretically possible and hence, power transfer efficiency is sacrificed.

4) The effective ac input impedance varies considerably between the blocked and unblocked states of the transfluxor and this leads to severe driving source requirements when it is desired to drive several devices from a single ac source.

A method for driving transfluxors in order to elimi-

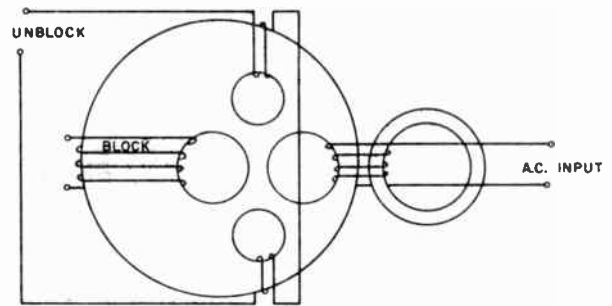


Fig. 8—Transfluxor core-driving circuit.

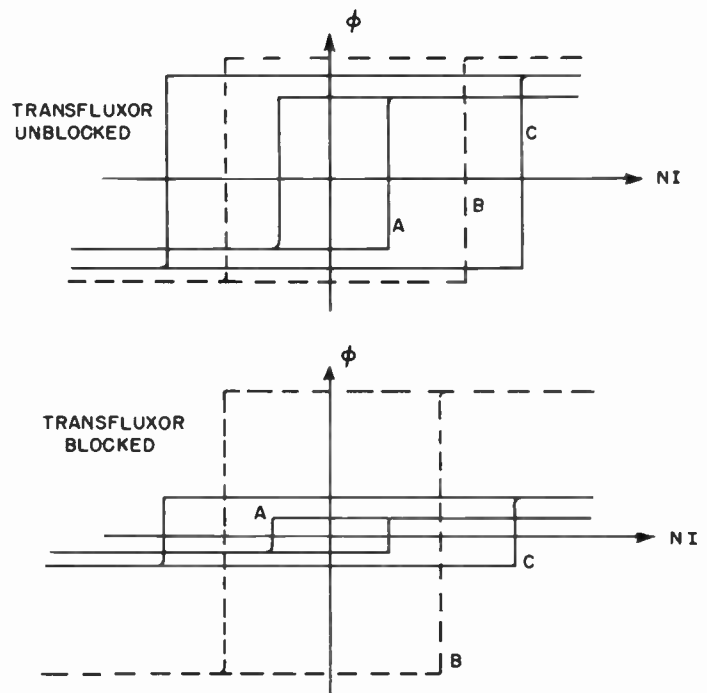
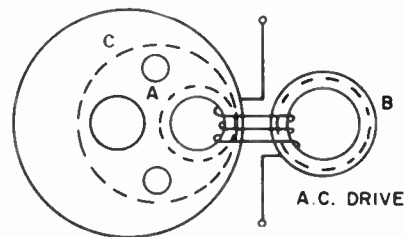


Fig. 9—Hysteresis curves from ac driving terminals.

nate the current-source problems described above is illustrated in Fig. 8. A single-hole core is wound in parallel with the ac input leg of the transfluxor. By proper design of the single-hole core, which will be referred to as the driver-core, a voltage source may be used as the ac input-signal generator.

The design requirements of the driver core are illustrated in Fig. 9. Denoting the closed magnetic paths of the transfluxor as referred to the ac input leg by the subscripts A and C , where A is the desired signal path and C is the peripheral path, and denoting the closed path of the driver core by the subscript B , the coercive requirement of the driver core is given by

$$(NI)_{CA} < (NI)_{CB} < (NI)_{CC}. \quad (14)$$

Eq. (14) states that the coercive mmf of the driver core should have a magnitude which lies between the coercive requirements of transfluxor paths *A* and *C*. Thus, the effective length of the flux path of the driver core is greater than l_A but less than l_C of the transfluxor, if both the transfluxor and driver core are fabricated from the same material and if the turns linking both are the same.

The requirements imposed upon the ac signal source are

$$|I_m| > |I_{CB}| \quad (15)$$

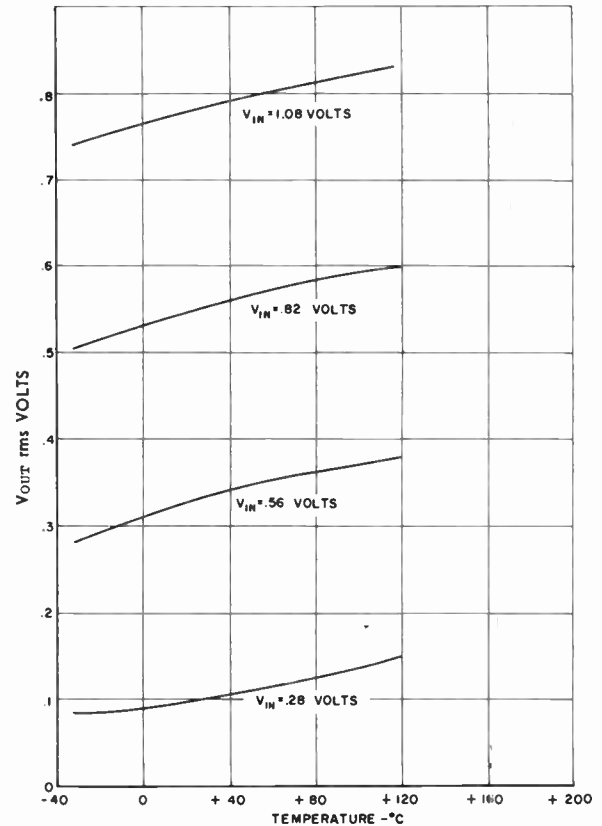
$$f_m > \frac{|E_m|}{|N_1\phi_{sB}|} \quad (16)$$

where I_{CB} is the current required for reaching the coercive mmf of the driver core and ϕ_{sB} is the saturation flux density of the driver core. It is noted from (15) and (16) that the ac signal requirements are now *independent* of the transfluxor.

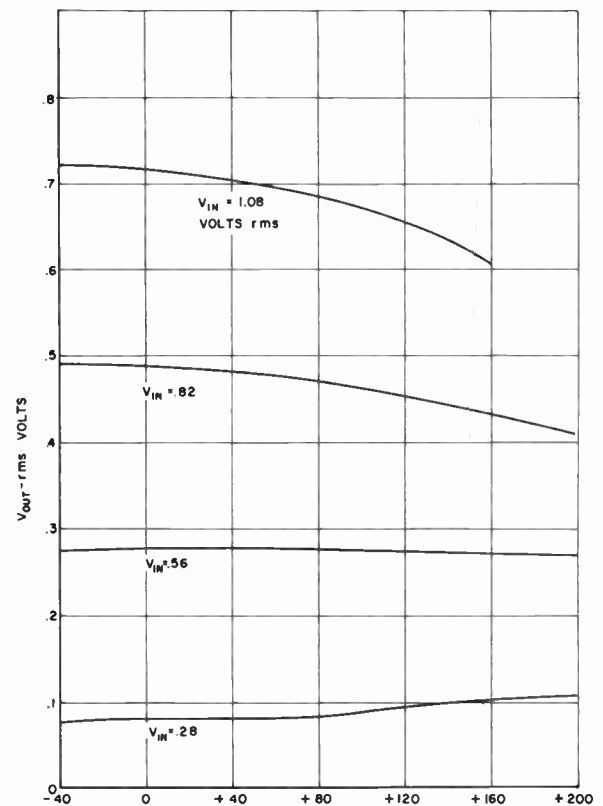
By requiring that the ac signal should never fully reverse the saturation state of the driver core, as given by (16), the peak value of ac magnetizing current supplied to the transfluxor can never exceed the coercive current of the driver core. As a consequence of (14), therefore, the transfluxor can never be unblocked by the ac signal. Furthermore, if the transfluxor and driver core are made from the same ferrite materials, the temperature effects upon the magnetic properties of both will be the same and automatic temperature compensation will occur.

An additional advantage of the driver-core input technique is that the transfluxor is driven from a voltage source and hence, a more sinusoidal waveform is induced in the ac output winding. Since current is no longer limited by the generator, the ac output winding may be more heavily loaded. When the transfluxor is blocked, the impedance of the ac driving terminals remains substantially the same as when the transfluxor is unblocked, since the ϕ - NI excursion is now controlled by the driver core. Hence, all of the disadvantages of an ac current source are overcome by using the driving core technique illustrated in Fig. 8, while all the advantages associated with the use of a current source are maintained.

Fig. 10 shows experimental curves of ac output voltage as a function of temperature when the transfluxor is driven from: a) a current source and b) a core driver in series with a voltage source. The input voltage to the transfluxor is plotted as a parameter and is varied in amplitude from 0.25 to 1.0 volt rms at a constant frequency of 20 kc. The experimental transfluxor has the dimensions illustrated in Fig. 5 and the driver core has an outside diameter of $\frac{3}{8}$ inch and an inside diameter of $\frac{1}{4}$ inch. As is apparent from the curves of Fig. 10, the output voltage is very nearly constant over a wide temperature range when the transfluxor is driven from the



(a)



(b)

Fig. 10—(a) V_{out} vs temperature for current source and various input voltages and (b) V_{out} vs temperature for core driver and various input voltages.

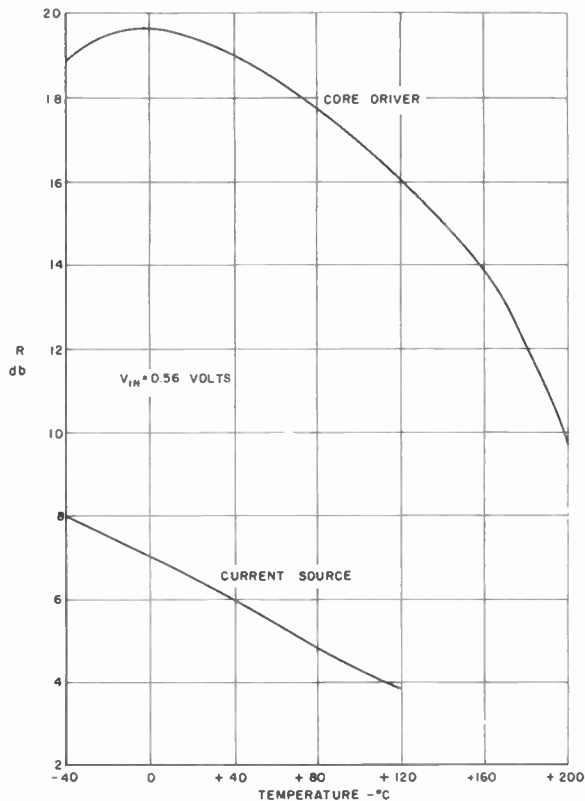


Fig. 11—Ratio vs temperature for constant current and core drive.

driver core, while the output voltage varies considerably when the transfluxor is driven from a current source. The change in ac output voltage when a current source is used is due to the variation of the coercive mmf of the transfluxor with ambient temperature variations.

Fig. 11 illustrates the ac output voltage unblock-to-block ratio, R , of the transfluxor, as a function of temperature, when a current generator and when a driver core in combination with a voltage source are used, respectively, at the ac signal input. It is seen that the use of a driver core materially increases the unblock-to-block ratio. A consequence of this improved ratio is that the transfluxor can be operated over a significantly greater temperature range than would be possible if a current-source drive were used.

The fact that ferrite core materials depart from ideal squareness in the saturated regions of the $B-H$ characteristics results in ac signal unblock-to-block ratios which are finite. This is due to the fact that flux changes are induced in the magnetic ac signal path by the ac input signal when the transfluxor is blocked. A method for compensating the transfluxor against flux changes in the blocked state is illustrated in Fig. 12. The ac output is wound around legs 2 and 3 so that flux changes in leg 3 induce a signal in the output winding which bucks the signal induced by flux changes in leg 2. When the transfluxor is unblocked, the compensation winding around leg 3 has virtually no effect on the ac output, since most of the flux changes occur in legs 1 and 2. The ratio of turns around leg 3 to the number of turns around leg 2

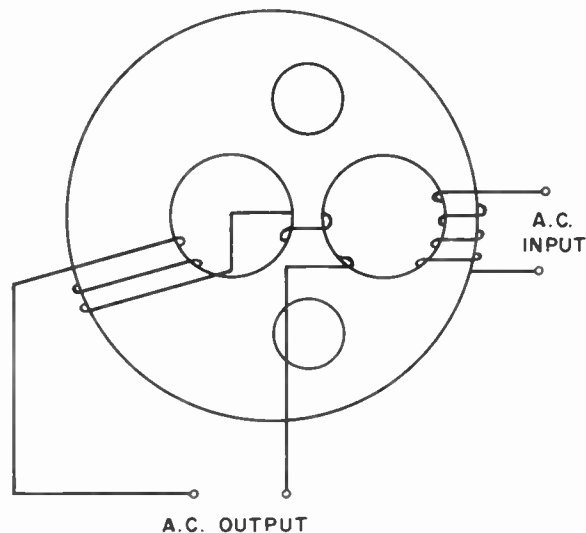


Fig. 12—Ratio compensation for transfluxors.

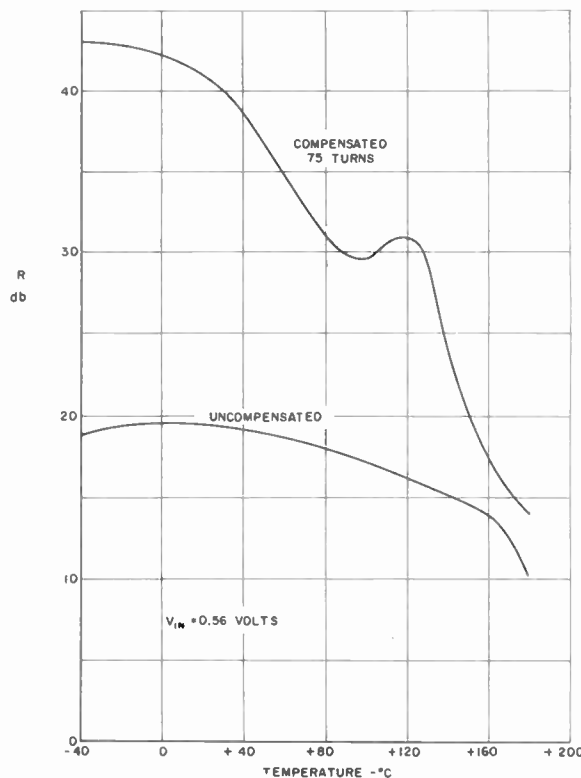


Fig. 13—Ratio vs temperature with core drive compensated and uncompensated.

for optimum compensation at room temperature is approximately proportional to the ratio of the length of the flux paths 1-3 and 1-2 for the experimental results shown.

Fig. 13 illustrates the variation of unblock-to-block ac signal ratio R as a function of temperature for an experimental transfluxor before and after ratio compensation is applied. Fig. 14 illustrates the unblock-to-block signal ratio as a function of temperature for varying compensation ratios. It is apparent from the experimental curves of Fig. 14 that the unblock-block ratio may be optimized for different temperatures by variation of

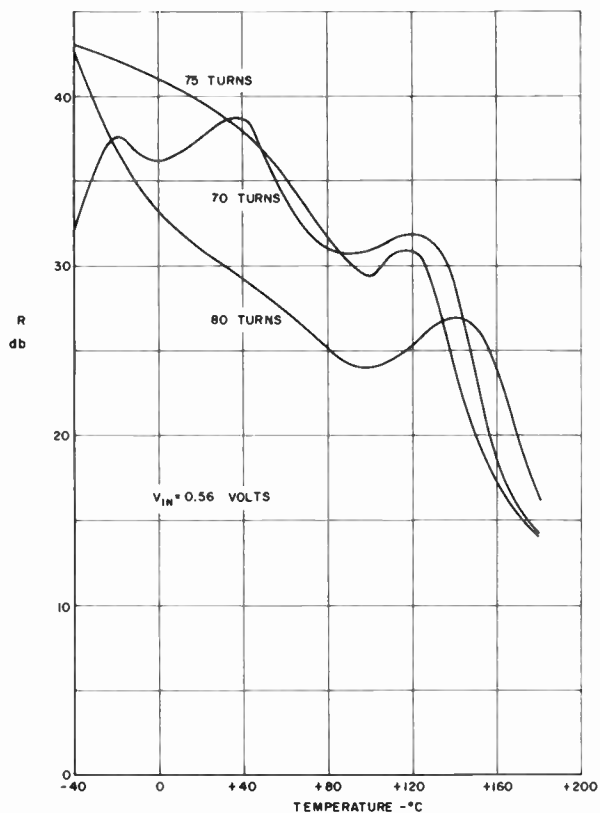


Fig. 14—Ratio vs temperature for core drive, fixed input, for varying compensation.

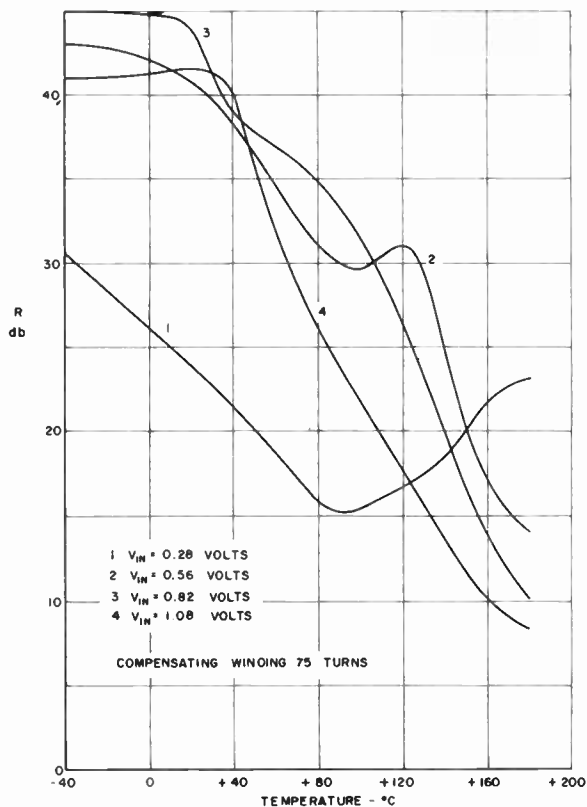


Fig. 15—Ratio vs temperature for fixed compensation, varying drive.

the compensation turns ratio. Fig. 15 illustrates a family of experimental curves for a ratio-compensated transfluxor when the ac input signal magnitude is varied. The optimizing effects of both the core driver and ratio compensation are evident when the curves of Fig. 15 are compared to those of Fig. 11. By utilizing both driving and ratio compensation techniques, the transfluxor may be operated over an ambient temperature range from -50°C to $+180^{\circ}\text{C}$ with an ac signal unblock-to-block ratio of at least 25 db.

MULTIHOLE LOGICORS

Since the elemental transfluxor is basically an on-off switching device, it is possible to build complex logic circuits utilizing several transfluxors. However, in many applications it may be desirable to take advantage of the multihole topology of transfluxors in order to perform more complex logic operations with a single device. For example, an "or" circuit may be built by adding an additional winding to the control leg. Such an "or" configuration is illustrated in Fig. 16. The ac signal windings around legs 1 and 2 are not shown. The "or" circuit of Fig. 16 performs a logical operation given in Boolean notation by

$$AB^1 + A^1B + AB = e_0 \tag{17a}$$

$$A^1B^1 = e_0^1. \tag{17b}$$

In (17a) and (17b), A denotes the presence of an unblocking pulse at the A terminal in Fig. 16 and A^1 denotes the absence of an unblocking pulse at the A terminal. The presence of an ac output signal is denoted by e_0 and the absence of an ac output signal is denoted by e_0^1 . Thus, after the transfluxor has been blocked, the application of unblocking pulses to either A or B terminals, or to both, will unblock the transfluxor and will cause an ac output signal to be induced in the output winding around leg 2. The output will persist until the transfluxor is reset by a blocking pulse.

The transfluxor configuration of Fig. 16 may be used to detect pulse coincidences at the terminals A and B , if the individual pulse currents are limited to the values given by

$$\frac{1}{2} |I_{C1-8-3-9}| < |I_A| < |I_{C1-8-3-9}| \tag{18a}$$

$$\frac{1}{2} |I_{C1-8-3-9}| < |I_B| < |I_{C1-8-3-9}|. \tag{18b}$$

Thus, the current magnitude of each pulse is insufficient by itself to exceed the coercive requirement of the peripheral flux path 1-8-3-9-1, but the sum of the currents at A and B , if coincident, will be sufficient to unblock the transfluxor. Memory is associated with the operation, since an ac output will appear after a pulse coincidence has occurred and the ac output will remain until the transfluxor has been reset by a blocking pulse.

Time sequence operations may also be performed with single multihole cores by utilizing a configuration of the

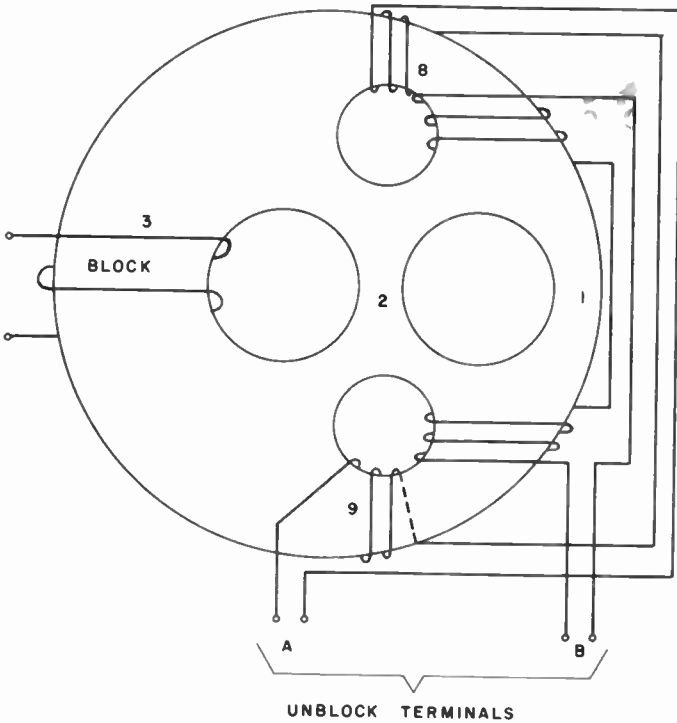


Fig. 16—Transfluxor "or" circuit.

type illustrated in Fig. 17.³ An ac output will appear only if both terminals *A* and *B* are pulsed in the time sequence *A - B*. The core is reset by applying a blocking pulse to the winding around leg 4 so that legs 1, 2, and 3 are saturated in the same direction. An unblocking pulse applied to the *A* terminal in Fig. 17 will cause a reversal in the flux saturation state of leg 3; but, if the current in the *A* winding is properly limited, the *A* pulse will not affect the flux saturation states in legs 2 and 1. If the pulse current magnitude in the *B* winding is limited so that a pulse at *B* has sufficient mmf to reverse the flux saturation state only in the closed path 2-3-2, it is evident that a pulse at *B* can unblock the transfluxor *only after* a pulse at *A* has been applied. An ac output signal, e_o , will result only when the pulses applied to terminals *A* and *B* are in the proper time sequence.

A three-hole core which may be used as an "exclusive or" gate is illustrated in Fig. 18. The logical operation of the "exclusive or" circuit is given by the following Boolean equations

$$AB^1 + A^1B = e_o \quad (19a)$$

$$A^1B^1 + AB = e_o^1. \quad (19b)$$

In the core of Fig. 18, the internal legs 1 and 2 are referred to as the "control legs." A pulse applied to the reset winding will saturate the control legs simultaneously in counter-rotational directions. Thus, after resetting, the ac input signal, e_i , cannot induce flux changes in the closed magnetic path 1-2-1 and hence, no ac output signal appears. However, a pulse applied to

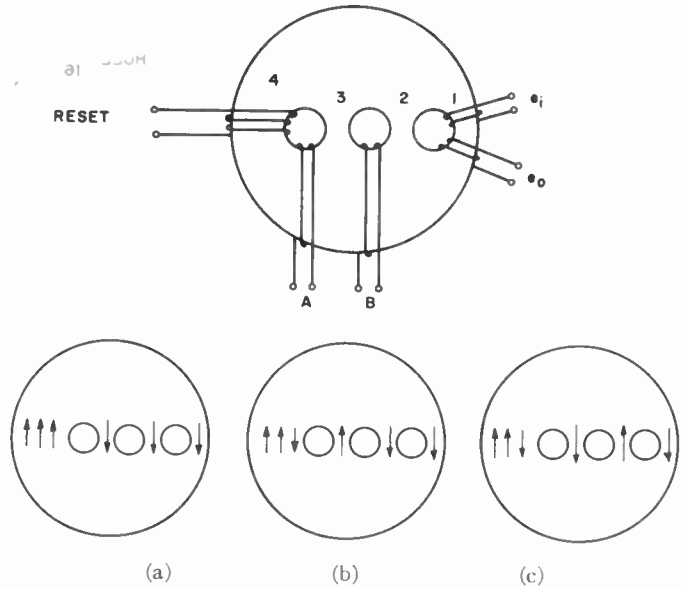


Fig. 17—Logicor sequential gate circuit: (a) after reset; (b) after *A*, and (c) after *B*.

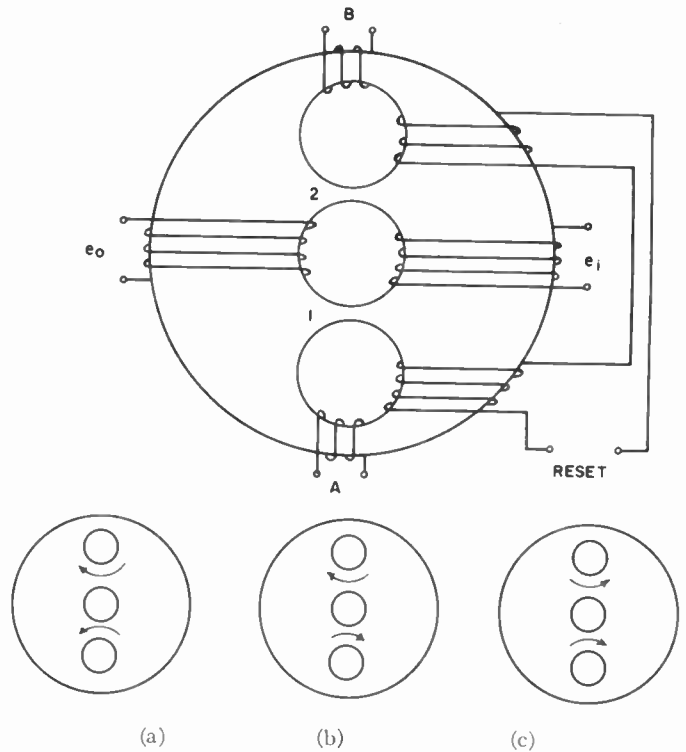


Fig. 18—Logicor "exclusive or" circuit: (a) after reset, (b) after *A*, and (c) after *A* and *B*.

either *A* or *B* terminals will reverse the flux saturation state in either control leg 1 *or* control leg 2, thus, unblocking the ac signal path and permitting an ac output signal to appear. For proper operation, the current magnitudes of the pulses applied to the *A* or *B* windings must be limited so that the coercive mmf associated with the closed circumferential paths around only the outer holes is exceeded whenever control pulses are ap-

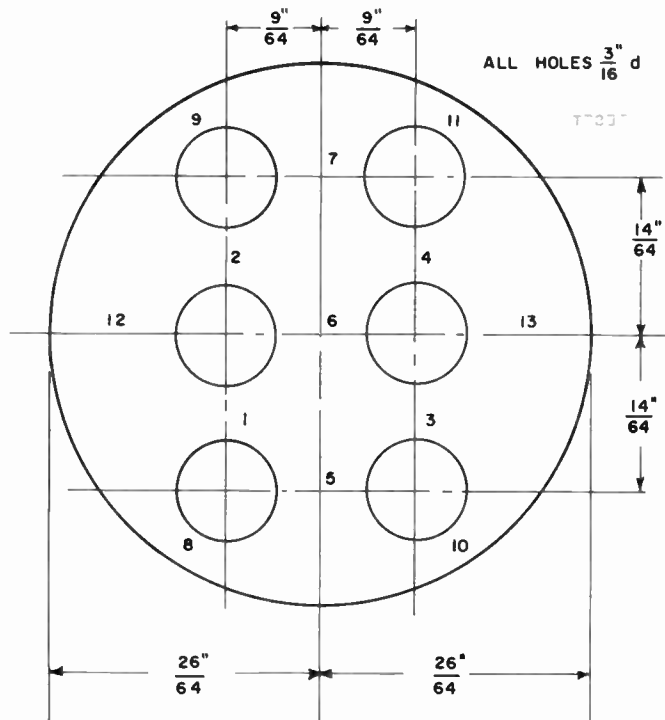
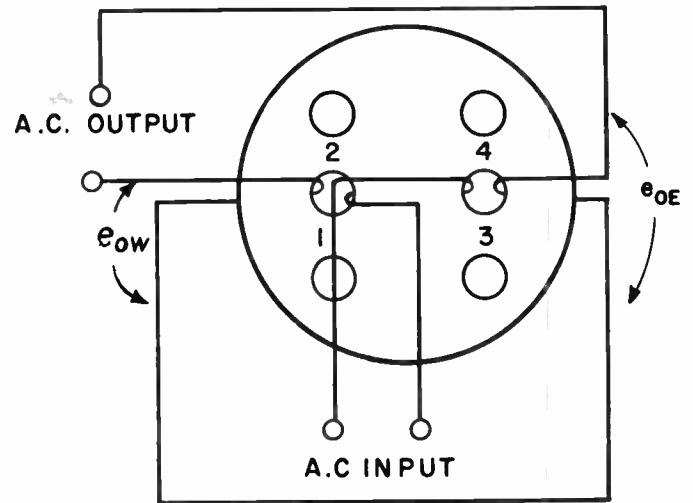


Fig. 19—Experimental six-hole logicor.

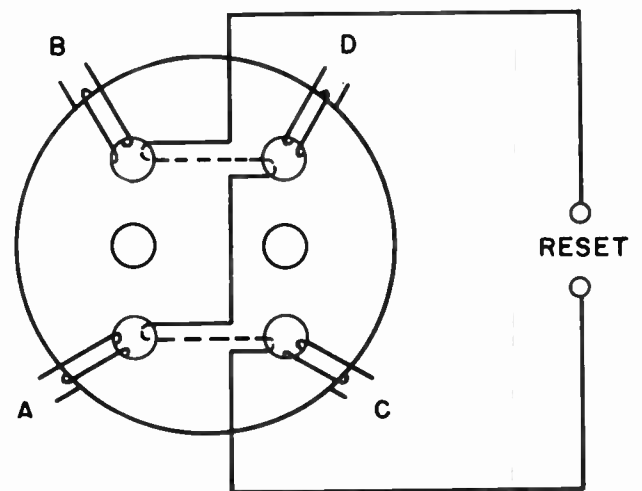
plied. When pulses are applied at *both A and B*, the saturation flux states in *both* the control legs are reversed and hence, the core remains blocked. Cores which are able to perform multiple logical operations of the “exclusive or” type will be referred to as “logicors.”

It is noted that the “exclusive or” circuit of Fig. 18 may also be used as a two-terminal odd-parity checker. An odd-parity checker is a logical configuration which is used to discriminate between an even and odd coincidence of pulses applied simultaneously to a set of input terminals.

It is possible to design a four-terminal odd-parity checker by utilizing a six-hole core topology of the type illustrated in Fig. 19. The dimensions shown are those used in an experimental logicor which was operated up to a pulse repetition rate of 20 kc and with an ac signal frequency of 60 kc. The winding configurations for the quadripole odd-parity checking logicor are illustrated in Fig. 20. The ac signal input consists of a winding around the middle leg, *i.e.*, around leg 6 (see Fig. 19). Two ac output windings around legs 12 and 13 are connected in a series-bucking combination so that the ac signal induced by flux changes in the closed path 6-2-12-1-6 cancels the ac signal induced by flux changes in the path 6-4-13-3-6. Consequently, an ac output will occur only when one side of the logicor is unblocked. The reset winding configuration is illustrated in Fig. 20(b). Reset windings around legs 5 and 7 are connected in series so that a reset pulse sets the flux saturation states in legs 1 and 4 in counter-rotational directions to the flux states in legs 2 and 3. An example of the flux states in legs 1, 2, 3, and 4, which are called the “control legs,” after the



(a)



(b)

Fig. 20—Logicor four-terminal odd-parity checker: (a) ac signal windings for six-hole logicor and (b) reset and logical configuration for odd-parity checking.

logicor is reset is illustrated in Fig. 21(a). The windings comprising the logical configuration of the quadripole odd-parity checker are lettered *A*, *B*, *C*, and *D* in Fig. 20(b). A pulse applied to winding *A* must be current limited so that the resultant mmf in winding *A* can reverse the flux state only in control leg 1. Fig. 21(b) illustrates the change in the control-leg flux saturation states after *A* terminal has been pulsed. For this condition, the left side of the logicor has been unblocked so that an ac signal output, e_{ow} , is generated. Since the right side of the logicor is blocked, the total ac signal output of the logicor is just equal to e_{ow} . However, if both *A* and *C* terminals are pulsed, the flux saturation states in both control legs 1 and 3 are reversed and, consequently, both sides of the logicor are simultaneously unblocked. Signals are then induced in both outputs; but, due to the series-bucking connection of the output windings, the net ac output is zero. Similar consideration of all possible flux states in the control legs of

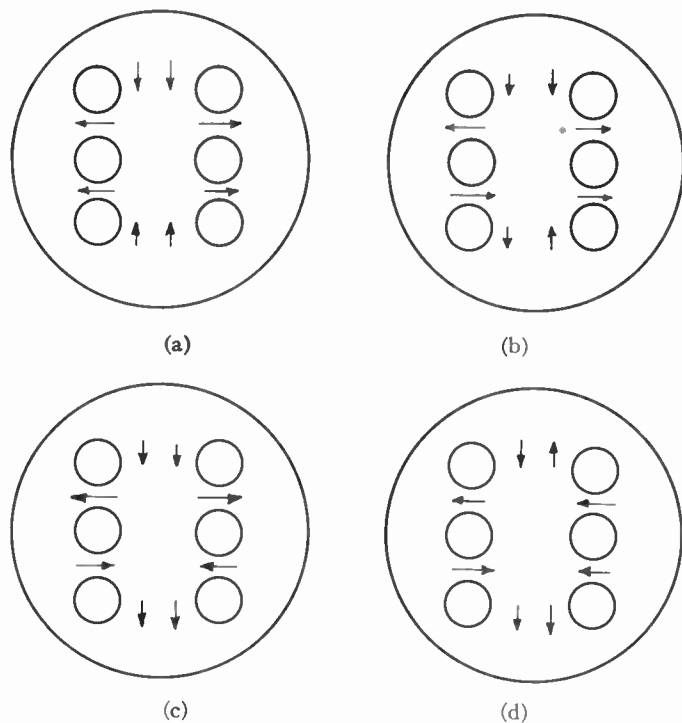


Fig. 21—Illustration of flux states for odd-parity checker: (a) after resetting; (b) after *A* pulse; (c) after *A* and *C* pulses, and (d) after *A*, *C*, and *D* pulses.

the odd parity-check logicor shows that an ac signal output occurs only when an odd number of the control windings are excited.

Fig. 22 illustrates a functional block diagram of the elemental logical requirements for a four-terminal input odd-parity checking circuit. A total of nine “or,” “and,” and “inhibit” circuits are required for the logical operation which a single logicor of the type shown in Fig. 20 can perform. It is evident from Fig. 22 that the odd-parity function may be synthesized by interconnecting three “exclusive or” circuits. Comparison of the six-hole logicor of Fig. 19 with the three-hole device of Fig. 18 shows that the former combines two “exclusive or” configurations in a single disk. The third “exclusive or” function required for the parity checking operation is provided by a unique interconnection of the two ac output windings. Thus, the operation of the six-hole logicor odd-parity checker may be summarized in Boolean form by the following set of equations.

$$AB + A^1B^1 = e_{0w}^1 \tag{20a}$$

$$AB^1 + A^1B = e_{0w} \tag{20b}$$

$$CD + C^1D^1 = e_{0e}^1 \tag{21a}$$

$$CD^1 + C^1D = e_{0e} \tag{21b}$$

$$e_{0w}e_{0e} + e_{0w}^1e_{0e}^1 = e_0^1 \tag{22a}$$

$$e_{0w}e_{0e}^1 + e_{0w}^1e_{0e} = e_0 \tag{22b}$$

Eqs. (20) and (21) specify the requirements for ac output signals from the left and right sides of the logicor, re-

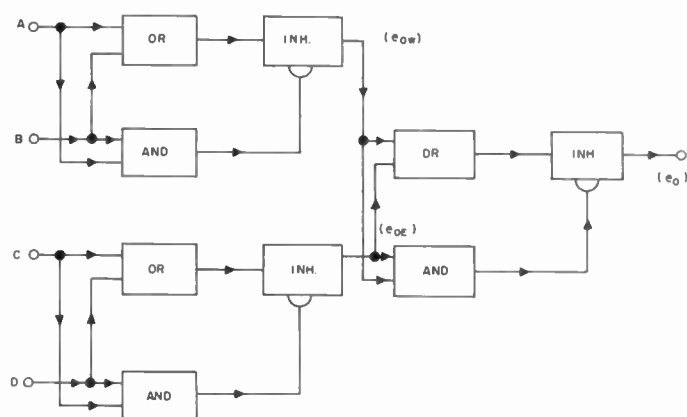


Fig. 22—Logical block diagram for quadrupole-input odd-parity checker.

spectively. The effect of the series-bucking connection of the two output windings is then formulated by (22a) and (22b). Substituting (20) and (21) into (22) gives the final result of the odd-parity operation in Boolean form.

$$AB^1C^1D^1 + A^1BC^1D^1 + A^1B^1CD^1 + A^1B^1C^1D + A^1BCD + AB^1CD + ABC^1D + ABCD^1 = e_0 \tag{23a}$$

$$ABCD + A^1B^1C^1D^1 + ABC^1D^1 + A^1BCD^1 + A^1B^1CD + A^1BC^1D + AB^1CD^1 + AB^1C^1D = e_0^1 \tag{23b}$$

It should be noted that, in addition to performing the complex logical operations given by (23), the logicor has inherent memory, since the ac output signal persists until the logicor is blocked by the reset pulse.

The same six-hole topology used for the quadrupole odd-parity checker may be employed in a logical configuration which is capable of binary half-adding operations. A binary half-adder may be functionally represented by the block diagram illustrated in Fig. 23 (next page). The circuit has two inputs, *A* and *B*, and two outputs *e*_{0e} and *e*_{0w}. In Boolean form, the circuit requirements are given by

$$AB = e_{0w}e_{0e}^1 \tag{24a}$$

$$AB^1 + A^1B = e_{0w}^1e_{0e} \tag{24b}$$

$$A^1B^1 = e_{0w}^1e_{0e}^1 \tag{24c}$$

Thus, a pulse coincidence at *A* and *B* will cause an output at *e*_{0w}, while a pulse at either *A* or *B* will cause an output at *e*_{0e}. The complete configuration for a half-adder logicor is illustrated in Fig. 24. Both the ac input and reset windings for the half-adder are wound in the same manner as the corresponding terminals of the odd-parity checker. However, in the half-adder configuration, the ac output windings are separate; in addition, there are only two logic-input windings which control the flux saturation states in legs 2, 3, and 4. Winding *A* connects legs 9 and 10 in series. However, the *A* winding spans leg 10 with twice as many turns as leg 9 so that a pulse input at *A* will generate sufficient mmf in the closed path 10-3-5-10 to reverse the flux saturation state in leg 3, but the mmf generated in the closed path 9-2-7-

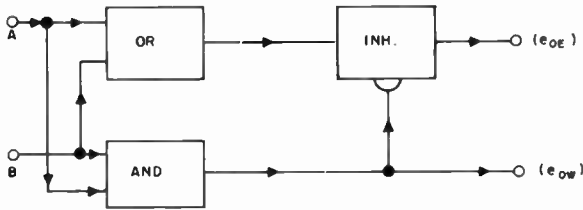


Fig. 23—Functional representation of half-adder.

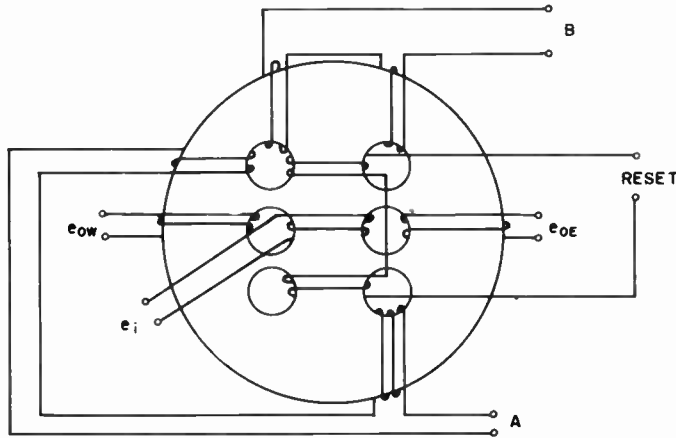


Fig. 24—Logisor half-adder configuration.

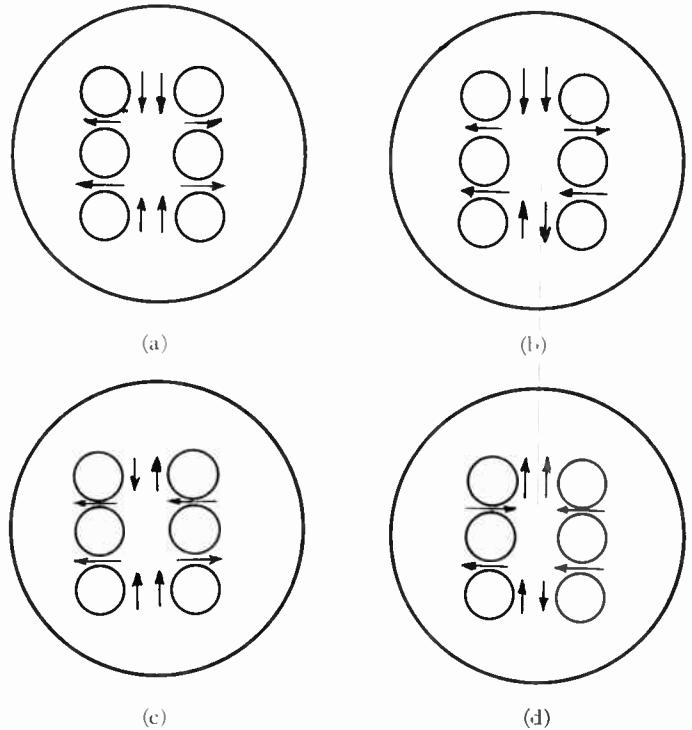


Fig. 25—Illustration of flux states in control legs for binary half-adder; (a) after resetting; (b) AB' ; (c) $A'B$ (preceded by reset), and (d) AB coincidence.

9 will be insufficient to reverse the flux saturation state in leg 2. Similarly, the B winding spans leg 11 with twice as many turns as leg 9 so that a pulse at B will reverse the flux saturation state in leg 4 but not in leg 2. Thus, either a pulse at A or B will unblock the right side of the logisor but will leave the left side of the logisor blocked, resulting in a signal output only at e_{oe} . Coincident pulses at both A and B will generate additive mmf's in leg 9 with the result that the flux saturation states in control legs 2, 3, and 4 will be reversed. The net result of a pulse coincidence is to unblock the left side but to reblock the right side of the logisor and thus cause an ac output signal to appear at e_{ow} but not at e_{oe} . The possible flux combinations of the half-adder, as described above, are illustrated in Fig. 25.

Another application of six-hole logisors to complex logical circuits is found in the area of selective channeling or selective calling. For example, it is possible to wire a single six-hole device so that an ac signal output occurs only after a desired one of four possible binary codes is applied to the two input terminals. A selective logisor which responds only to an "11" code is illustrated in Fig. 26(a). The ac signal windings and the reset winding for this logisor are wound in the same manner as for the odd-parity checker shown in Fig. 20. In Boolean form, the "11" logisor performs the following operations.

$$AB = e_o \quad (25a)$$

$$AB^1 + A^1B + A^1B^1 = e_o^1. \quad (25b)$$

To realize the functions given by (25a) and (25b), the A terminal is wound around legs 8 and 10 so that a pulse applied to the A winding will reverse the flux saturation

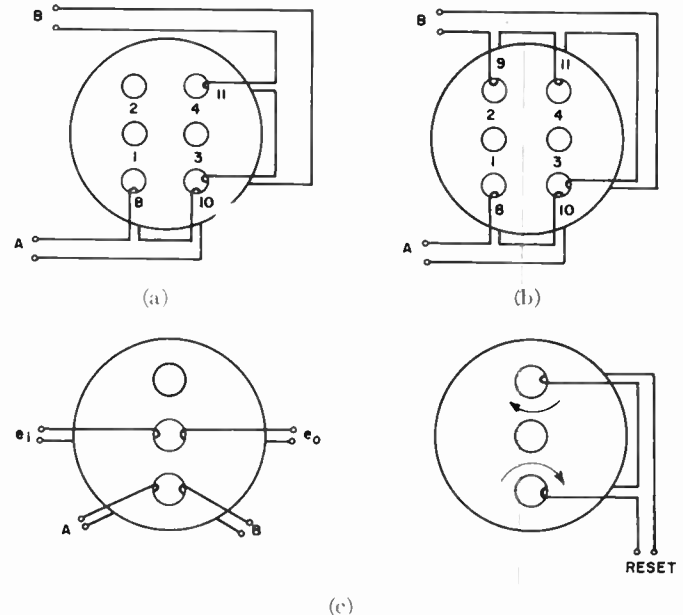


Fig. 26—Binary selection logisors: (a) "11" logisor; (b) "01" or "10" logisor, and (c) "00" logisor.

states of control legs 1 and 3. In addition, the B terminal spans legs 10 and 11 so that a pulse applied at B will reverse the flux saturation states (in reference to the reset states) in control legs 3 and 4. Consequently, a pulse at only A will unblock both sides of the logisor; but, since the two ac output windings are connected in a series-bucking arrangement, the net ac output is ideally zero. Furthermore, a pulse at only B will not affect the left side of the logisor but will reblock the right side so that

the net result is again zero ac output signal. However, if both A and B are activated (in any time sequence), the left side of the logicor is unblocked, but the right side remains blocked. This results in an ac output signal.

The control winding configuration for a "10" or "01" selective logicor is illustrated in Fig. 26(b). " A " terminal spans legs 8 and 10 so that a pulse applied to A will reverse the flux saturation states in legs 1 and 3. On the other hand, B terminal spans legs 9, 10, and 11 so that a pulse applied to B will reverse the flux saturation states in legs 2, 3, and 4. Thus, a pulse at only A unblocks both sides of the logicor; but, since the ac output windings are connected in series bucking, the net ac output signal is zero. However, a pulse at only B will reblock the right side of the logicor but will unblock the left side and this results in an ac output signal. Pulses at both A and B reblock both sides of the logicor and thus, no ac output signal is generated. The logical operations which the core of Fig. 26(b) perform are given by

$$AB^1 + AB + A^1B^1 = e_0^1 \quad (26a)$$

$$A^1B = e_0. \quad (26b)$$

To complete the requirements of a selective system, a "00" core is illustrated in Fig. 26(c). Only a single three-hole topology is required for "00" selection. In this case, the reset signal unblocks the core. However, a signal at either A or B , or signals at both A and B , will block the logicor. Consequently, the "00" device performs the following selective functions:

$$A^1B^1 = e_0 \quad (27a)$$

$$AB^1 + A^1B + AB = e_0^1. \quad (27b)$$

Selective logicors may be directly cascaded, if it is desired to build up the system capacity, by connecting the ac output of one stage to the ac input of the second stage, etc. Thus, if an N -call channel is required, the number of selective logicors, m , which are required is

$$m = 1/2 \log_2 N. \quad (28)$$

Hence, a 64-call system requires three selective logicors. In an experimental 16-call system utilizing two six-hole logicors of the type illustrated in Fig. 19, the discrimination between desired and undesired signals; *i.e.*, the unblock-to-block ratio of the cores, was in the order of 10 db. The typical number of turns around each leg was in the order of 50 and typical current requirements for reversal of the flux saturation states in the control legs were in the order of 30 ma (peak). In the experimental circuit, the ac signal frequency was approximately 50 kc and the pulse rate was varied between 0–20 k pps.

A principal feature of the ferrite logicor is that a single multihole disk may be used to realize fairly complex logical functions. For example, the quadripole parity checker performs a logical operation which requires nine elemental building blocks, as illustrated in Fig. 22. To realize the same operation by use of direct-coupled transistor circuits would require as many as 12 transis-

tors.⁶ A second feature which makes the logicor attractive is the fact that a single core topology may be used for many different circuit functions by variation of the winding configurations. Thus, the six-hole core of Fig. 19 may be used to perform such diverse operations as single-pole double-throw switching, sequential gating, "exclusive or" logic, odd-parity checking, binary half-adding, and binary code selection.

CONCLUSION

The transfluxor is a ferrite device which uses a multiple aperture topology to perform ac gating functions. When the device is fabricated from high-remnant material, the gating function is combined with memory. It is possible to gate the transfluxor "on" and "off" with pulses of unlimited amplitudes by use of a three-or four-hole topology. Thus, the gating process is uncritical. In order to utilize the advantages of driving the transfluxor from an ac voltage source, an auxiliary single-hole core may be used in the driving circuit. The driver core functions as a current limiting device which, nevertheless, allows considerable loading of the transfluxor and, in addition, serves to compensate the ac circuits against variations of the B - H characteristics due to ambient temperature changes. The unblock-to-block ac signal ratio of the transfluxor may be compensated against departures in squareness of the B - H characteristics by use of ac compensation windings. By utilizing the various compensation techniques described above in combination with a four-hole topological design, experimental transfluxors have been operated successfully over an ambient temperature range in excess of 200°C. Unblock-to-block ac signal ratios of at least 25 db have been maintained over this entire range.

Multihole ferrite cores may be used to perform more complex logic operations than simple on-off gating by winding the device with several pulse inputs so that several flux paths may be controlled by external signals. Such ferrite devices are called logicors. Three-hole logicors have been designed which perform such functions as sequential gating and "exclusive or" logic. In addition, six-hole cores have been designed which are capable of complex logical operations such as binary half-adding, quadripole-input odd-parity checking, and selective response to binary codes.

ACKNOWLEDGMENT

The authors are thankful to G. Palmer of the Dielectric and Magnetic Materials Subsection of the Electronics Laboratory for his cooperation in providing the required ferrite materials for this investigation. In addition, the suggestions of H. Putsch, R. Goldner, and A. P. Stern and the laboratory assistance of A. Klisz and J. V. O'Hern of the Advanced Circuits Subsection are gratefully acknowledged.

⁶ R. H. Beter, W. E. Bradley, R. B. Brown, and M. R. Rubinoff, "Direct-coupled transistor circuits," *Electronics*, vol. 28, pp. 132-136; June, 1955.

Polarization Reversal and Switching in Guanidinium Aluminum Sulfate Hexahydrate Single Crystals*

HARRY H. WIEDER†

Summary—The ferroelectric switching properties of GASH ($(\text{CN}_2\text{H}_8)_2\text{Al}(\text{SO}_4)_2 \cdot 6\text{H}_2\text{O}$) were studied under sinewave and pulse conditions. The results indicate that the polarization reversal process is analogous to that found in barium titanate single crystals. The activation fields are of the same order of magnitude in the two ferroelectrics, although the domain mobility of GASH is 30 to 100 less than that of BaTiO_3 at room temperature. Neither a threshold field nor a true coercivity was found for GASH and the hysteresis losses in this material are less by a factor of 10 in comparison with barium titanate. The upper frequency limit for observing ferroelectric phenomena appears to be about 25–50 kc in both materials.

It is concluded that while GASH has some advantages over BaTiO_3 as a possible electronic component in terms of lower hysteresis losses, ease of crystal growth, and lower electromechanical activity, its use at the present stage of development must be limited to low speed (less than 1 kc) switching circuits.

INTRODUCTION

THE recently discovered ferroelectric sulfates¹ have many of the characteristic properties of polarization reversal and bistability associated with ferroelectric barium titanate crystals. Holden, *et al.*,² have indicated the similarities between some of the switching properties of guanidinium aluminum sulfate hexahydrate (GASH) and those found for barium titanate.³ We chose to study in detail the switching properties of GASH and to ascertain its possible utility as an electrical and electronic component.

Like other ferroelectrics, a section of a GASH crystal having its polar axis perpendicular to the main faces on which metal electrodes are applied will behave as the electric analog of a ferromagnetic material. Specifically, if a sinusoidally varying potential be applied to a GASH crystal prepared in the above manner and the integrated charge be measured across a large capacitor in series with the crystal, then a dynamic display of the instantaneous relation between charge and potential will show a hysteresis loop similar to that between magnetic flux and magnetic field. Such a hysteresis loop encountered for GASH is shown in Fig. 1. In terms of classical physics, it displays the dynamic relation between the displacement D and the electric field E . The displacement

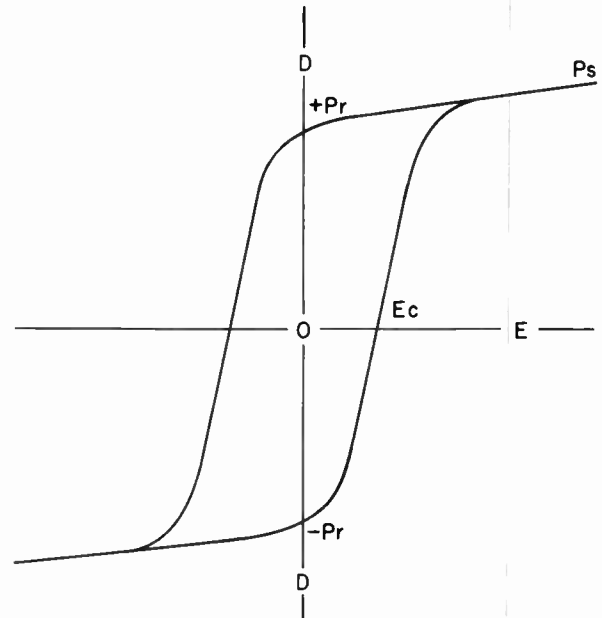


Fig. 1—Hysteresis loop of a ferroelectric GASH crystal at 60 cps. D and E are the electric displacement and electric field, P_s is the spontaneous polarization and P_r the remanent polarization respectively. E_c is the apparent coercivity.

is related to the orientation of the electric dipoles within the crystal by the polarization vector P . For a sufficiently large applied field, the polarization reaches a saturation value and the maximum attainable dipole orientation is represented by the spontaneous polarization P_s .

At $E=0$, the displacement $D = E + 4\pi P$, consists of a remanent polarization $\pm P_r$, the sign of the polarization depending upon the direction in which the loop is traversed. A positive electric field applied to the crystal when the latter is at $-P_r$, will switch the crystal, *i.e.*, when the field is removed it will return to state $+P_r$, and the crystal will absorb a charge $Q = 2P_s \cdot A$, where A is the electrode area. A negative electric field will, however, return the crystal to $-P_r$, the absorbed charge being negligibly small. In essence, the above described property makes GASH useful as a binary memory device since it obviously has two stable states of polarization which can be identified by means of properly coded pulses. Also, since one may define a dielectric constant ϵ (since GASH is essentially a dielectric) one must necessarily differentiate between the dielectric constant ϵ_R measured at low electric fields where the dipole motion is reversible and a differential permittivity ϵ_D defined as the slope of the hysteresis loop at any point. The prop-

* Original manuscript received by the IRE, February 28, 1957; revised manuscript received, May 9, 1957.

† U. S. Naval Ordnance Lab., Corona, Calif.

¹ A. N. Holden, B. T. Matthias, W. J. Merz, and J. P. Remeika, "New class of ferroelectrics," *Phys. Rev.*, vol. 98, p. 546; April, 1955.

² A. N. Holden, B. T. Matthias, W. J. Merz, and J. P. Remeika, "Properties of GASH and some of its isomorphs," *Phys. Rev.*, vol. 101, pp. 962–966; February, 1956.

³ W. J. Merz, "Domain formation and domain wall motion in ferroelectric BaTiO_3 single crystals," *Phys. Rev.*, vol. 95, pp. 690–698; August, 1954.

erty of changing dielectric constant with electric field has been suggested as the basis for employing ferroelectrics such as GASH as saturable reactors and dielectric amplifiers.

In whatever manner ferroelectrics such as GASH are to be employed, it is important that an evaluation of the speed of polarization reversal and its dependence upon internal and external crystalline parameters be available. The dependence of the rate of polarization upon the magnitude of the electric field and the existence of a threshold field, if such can be found, are especially important switching criteria.

In the case of barium titanate, no threshold field and hence no true coercivity was found experimentally.^{4,5} For engineering purposes especially for computer applications, it is desirable that a ferroelectric material be obtained having a threshold field E_0 such for $E \leq E_0$ no polarization reversal should occur.

EXPERIMENTAL

GASH crystal sections were cleaved perpendicularly to the ferroelectric axis from a large crystal grown from water solution using the description of Holden, *et al.*,² as a guide. The cleaved crystals were examined for surface irregularities and only those having parallel plane faces were retained. The crystals were then diced into squares having an area of 0.03 cm². The range of thickness ran from 0.01 to 0.05 cm. After evaporating silver electrodes on the major surfaces, only those crystals were subjected to further tests that had completely symmetrical 60-cps hysteresis loops. A total of 12 crystals were thus selected. In addition, seven more crystals were obtained from Dr. H. Jaffee of the Brush Laboratories. The latter had circular electrodes of vacuum deposited silver of 0.35 cm² in area. The thickness of these crystals ranged from 0.03 to 0.05 cm. The subsequently described experimental results are characteristic of these 19 crystals and to a large extent it is felt that the results apply to ferroelectric GASH crystals in general.

SINEWAVE MEASUREMENTS

The sinewave tests consisted in displaying a hysteresis loop oscillographically and measuring the spontaneous polarization and coercivity as a function of the driving frequency for each crystal. The results indicate the similarity between barium titanate and GASH. At low audio frequencies (less than 1 kc) the spontaneous polarization, obtained from an extrapolation of the linear portion of the hysteresis loop, is frequency independent. The magnitudes are in good agreement with the values reported by Holden.² The highest value of P_s at +25°C was found to be 0.35 $\mu\text{coulomb/cm}^2$; the lowest value was $P_s = 0.31 \mu\text{coulomb/cm}^2$. Fig. 2 shows the depend-

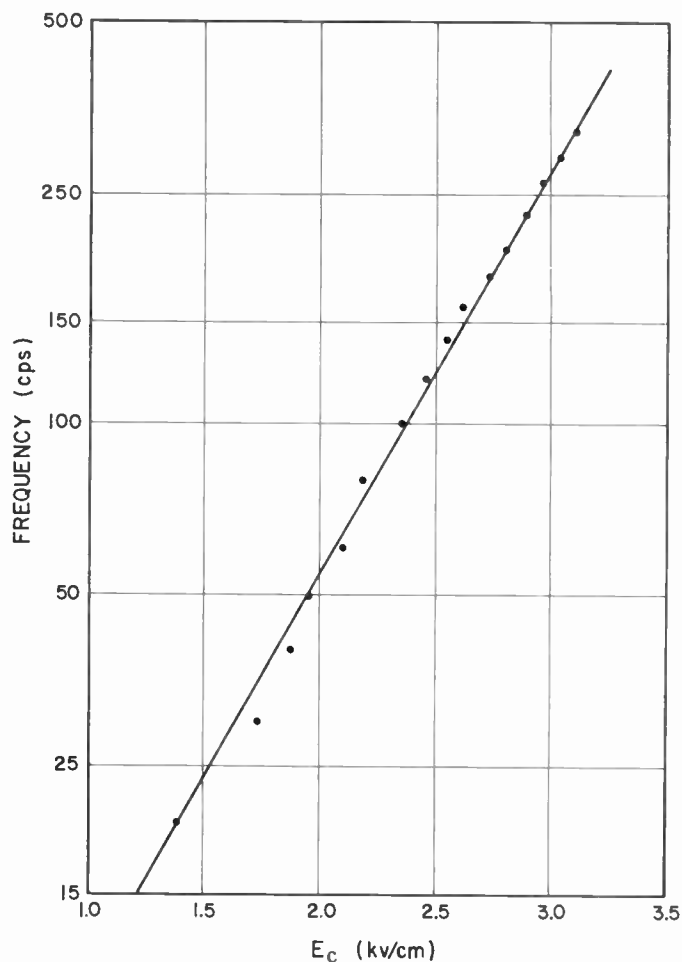


Fig. 2—Coercivity as a function of driving frequency for a GASH crystal 0.05 cm thick.

ence of the coercivity as a function of frequency for a particular sample. We define the coercivity as the magnitude of the electric field E_c when the polarization passes through zero and the maximum value of the sinusoidal driving field E_{max} is large enough to drive the crystal into the saturation (*i.e.*, spontaneous polarization) region. It was found that the coercivity of GASH decreases with frequency down to quasistatic conditions. The lack of a true coercivity such as found for ferromagnetic crystals might be considered in terms of the same slow polarization reversal mechanism discussed by Landauer, *et al.*,⁶ and by the author⁴ in the case of barium titanate.

Fig. 3 (next page) shows the dependence of the coercivity measured at 60 cps upon the reciprocal crystal thickness. This might be considered as evidence of a space charge layer in GASH in analogy to barium titanate.⁷ In the following section, this will be taken into

⁶ R. Landauer, D. R. Young, and M. E. Drougard, "Polarization reversal in the BaTiO₃ hysteresis loop," *J. Appl. Phys.*, vol. 27, pp. 752-758; July, 1956.

⁷ W. J. Merz, "Switching time in ferroelectric BaTiO₃ and its dependence on crystal thickness," *J. Appl. Phys.*, vol. 27, pp. 938-943; August, 1953.

⁴ H. H. Wieder, "Retarded polarization phenomena in BaTiO₃ crystals," *J. Appl. Phys.*, vol. 27, pp. 413-416; April, 1956.

⁵ H. H. Wieder, "Activation field and coercivity of ferroelectric BaTiO₃," *J. Appl. Phys.*, vol. 27, pp. 367-369; March, 1957.

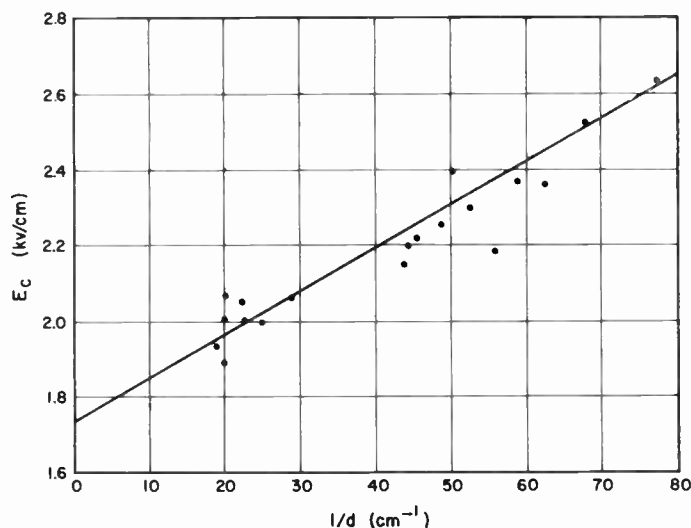


Fig. 3—Coercivity at 60 cps measured as a function of the reciprocal thickness ($1/d$) of the crystal samples. The coercivity decreases for an increase in crystal thickness indicating the presence of a nonferroelectric layer within the crystal.

account in discussing polarization reversal under pulse conditions.

The hysteresis losses within the volume of the ferroelectric crystal in going around the hysteresis loop may be obtained from a graphical integration of the experimentally obtained hysteresis loop areas as a function of frequency. The validity of this may be ascertained from the classical equation⁸ relating the amount of work W per unit volume of a dielectric, for a change in displacement $d\bar{D}$, brought about by the application of an external field E :

$$W = \frac{1}{4\pi} \int_D E \cdot d\bar{D}. \quad (1)$$

Fig. 4 shows the hysteresis losses for a particular crystal sample in the audio frequency range. A comparison between GASH and a similar BaTiO_3 crystal is illustrated in Table I. It shows that the hysteresis losses W of BaTiO_3 in the tetragonal crystal phase⁹ at $+25^\circ\text{C}$ and at 60 cps are higher than those of GASH.

As a first approximation, we can take the product $2E_c P_s \approx W$ as representative of hysteresis losses and as can be seen from Table I, these values are in reasonable agreement with the graphically integrated loop areas. At a constant temperature, the rate of change of hysteresis losses with frequency is therefore proportional to the rate of change of coercivity, *i.e.*,

$$(\partial W / \partial \omega) = 2P_s (\partial E_c / \partial \omega) \quad (2)$$

and energy equivalent to the area of the hysteresis loop is dissipated in the form of heat within the crystal.

⁸ C. J. F. Bottcher, "Theory of Electric Polarisation," Elsevier Publishing Co., Amsterdam, Holland; 1952.

⁹ H. H. Wieder, "Ferroelectric hysteresis in BaTiO_3 single crystals," *J. Appl. Phys.*, vol. 26, pp. 1479-1482; December, 1955.

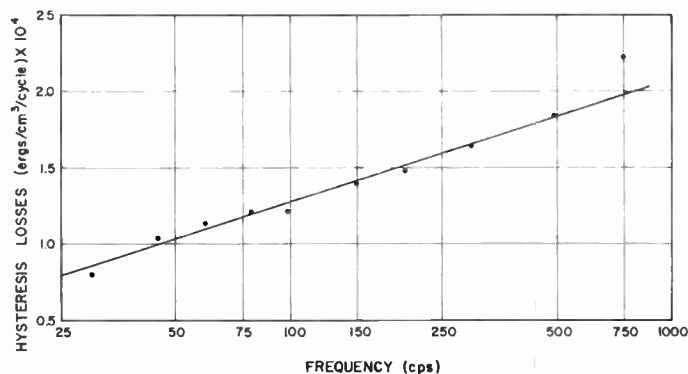


Fig. 4—Hysteresis losses obtained from a graphical integration of the area of hysteresis loops at low audio frequencies for a sample 0.021 cm thick.

TABLE I

A COMPARISON BETWEEN SOME OF THE PROPERTIES OF GASH AND BaTiO_3 SINGLE CRYSTALS AT $+25^\circ\text{C}$

Ferroelectric	P_s $\mu\text{coulombs/cm}^2$	E_c kv/cm	W ergs/cm ³ /cycle	$2P_s E_c \approx W$
BaTiO_3	26	0.75	2.7×10^5	3.9×10^5
GASH	0.35	2.2	1.2×10^4	1.5×10^4

PULSE MEASUREMENTS

Pulse measurements on GASH crystals were accomplished by applying a train of rectangular voltage pulses of successive opposite polarities in such a manner that each pulse reverses the sign of the previous remanent polarization. The amplitude of these pulses and their duration had to be respectively large enough and of sufficient duration to cause the amount of reversed polarization to be substantially $2P_s$. For pulse rise times less than $0.1 \mu\text{second}$, polarization reversal can be regarded as taking place in a steady state field E of the pulse whose duration T is much longer than the time τ_s required for polarization reversal. The intervals between pulses must be long enough for the crystal to reach an equilibrium state between successive pulses.

For pulse amplitudes between 1 kv/cm and 8 kv/cm of crystal thickness, an electromechanical pulse generator was employed to give pulses having a rise time of $0.01 \mu\text{second}$. A positive pulse of 600 milliseconds duration was followed by an interval of 600 milliseconds in which the crystal was shorted. Thereafter a negative pulse of 600 milliseconds completed the cycle.

These pulses were applied to a ferroelectric crystal mounted in a sample holder in series with a 170-ohm resistor. The switching current transient developed across the resistor was displayed on an oscilloscope allowing an evaluation of switching time τ_s . A representative switching transient found for GASH crystals is shown in Fig. 5. We define τ_s as the time required for the transient switching current (dp/dt) to return to a very

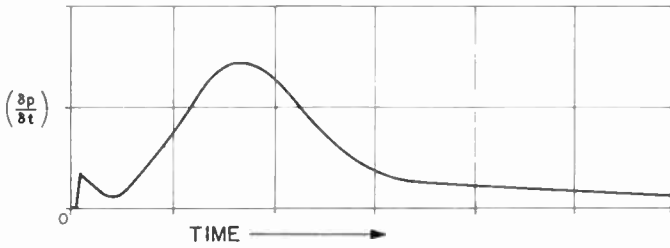


Fig. 5—Switching transient of a 0.021-cm-thick GASII crystal; horizontal scale = 100 μ seconds/division, pulse amplitude $E = 3.3$ kv/cm.

small value in the presence of an applied field E and that the integrated area under the transient have the value

$$\int_0^{\tau_s} \left(\frac{\partial p}{\partial t}\right) dt \simeq 1.41 P_s. \quad (3)$$

The results obtained for a representative sample are plotted in Fig. 6. In agreement with Holden, *et al.*,² it can be seen that for higher fields the reciprocal switching time ($1/\tau_s$) increases linearly with applied field. For this region we can speak of polarization reversal in terms of a domain wall mobility μ such that

$$\mu \simeq \frac{d}{\tau_s(E - E')} \quad (4)$$

with d being the crystal thickness and E' the extrapolated linear plot of E for $\tau \rightarrow \infty$. For the 19 crystals used in the present experiments, the calculated values of μ showed large variations: the highest value $\mu = 0.08$ ($\text{cm}^2/\text{volt second}$) was obtained for a thick crystal, $d = 0.05$ cm, the lowest value $\mu = 0.02$ ($\text{cm}^2/\text{volt second}$) was obtained for a thin, $d = 0.013$ cm, crystal. While this would seem to indicate an additional dependence of μ upon d , the relatively large oscillation of values in between the above indicated maximum and minimum and the few samples used preclude the establishment of a definite interrelation. At any rate, a comparison with barium titanate³ in the tetragonal phase at $+25^\circ\text{C}$ ($d = 0.005$ cm) shows that the mobility of GASII is considerably less than the quoted mobility ($\mu \simeq 2.5$ $\text{cm}^2/\text{volt second}$) of the former material.

At low pulse amplitudes, the empirical relation⁴ between τ_s and E in the case of BaTiO_3 is given by

$$\tau_s = \tau_0 \exp(\alpha/E). \quad (5)$$

τ_0 is a constant having the dimension of time and α is an activation field probably determined by the rate of nucleation of 180° domains. A relation similar to (5) may be written for GASII. Fig. 7 shows this by a plot of $\log \tau_s$ vs $1/E$ for the same crystal whose switching properties at high field values was shown in Fig. 6. From plots such as Fig. 7, the activation field α was determined for each crystal. Subsequently we noticed that the activation field shows a strong dependence upon the

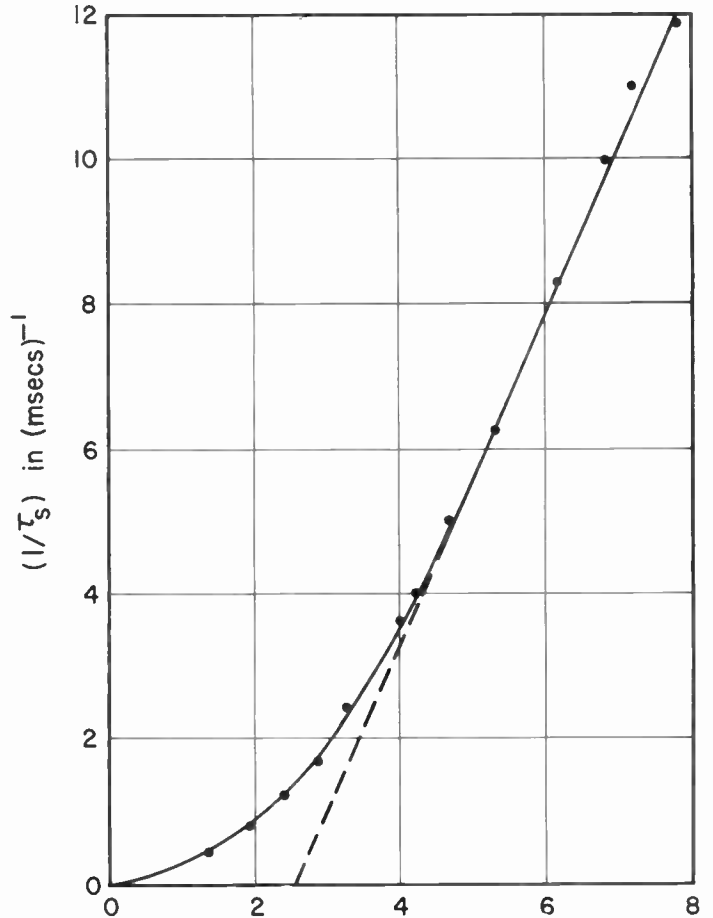


Fig. 6—Reciprocal switching time ($1/\tau_s$) as a function of pulse amplitude E for a 0.021-cm-thick crystal.

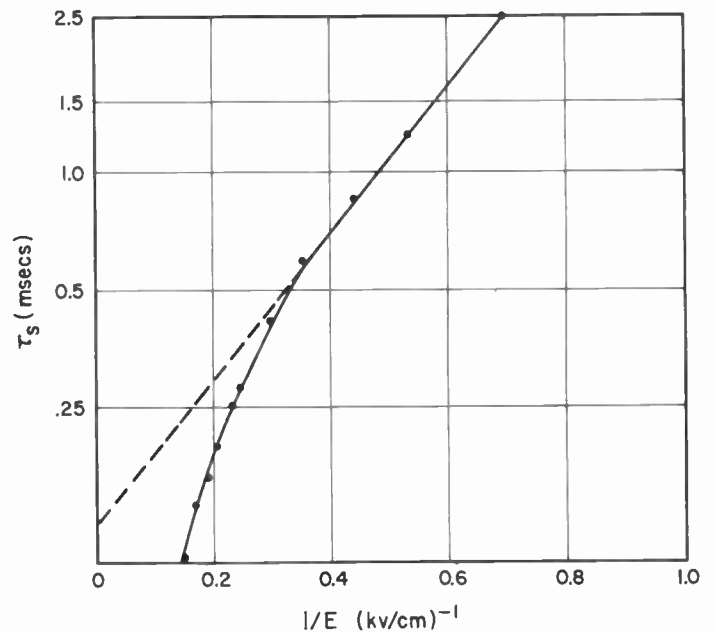


Fig. 7—A plot of the relation $\tau_s = \tau_0 \exp(\alpha/E)$ for the curved portion of Fig. 6. The slope of the line is the activation field, $\alpha = 4.1$ kv/cm.

reciprocal crystal thickness ($1/d$) as shown in Fig. 8. This would suggest the existence of a space charge layer in GASH in analogy to BaTiO_3 . The relation proposed by Merz⁷ for the latter is based on the argument that a field applied to a BaTiO_3 crystal is divided between two capacitors in series. One represents a nonferroelectric space charge layer having a dielectric constant ϵ_L and thickness d_L , the second capacitor is the bulk ferroelectric whose dielectric constant is ϵ_B and thickness is d_B . A calculation of the thickness of the space charge layer d_L yields

$$d_L \approx \frac{1}{2} \frac{\gamma \cdot \epsilon_L}{\alpha_0 \cdot \epsilon_B} \quad (6)$$

The parameter γ is the slope of the line of Fig. 8, α_0 is its intercept, ϵ_B and ϵ_L are respectively the dielectric constants of the bulk of the ferroelectric and the space charge layer. In the case of GASH, the reversible dielectric constant measured in the direction of the ferroelectric axis at a frequency of 1 mc is $\epsilon_R \approx 6$. In any other axial orientation $\epsilon_R \approx 4$. The crystalline anisotropy is evidently much lower in GASH than in BaTiO_3 . We assume that the dielectric constant of the nonferroelectric layer in GASH is that of the nonoriented material, *i.e.*, $(\epsilon_L/\epsilon_B) \approx 4/6$. From Fig. 8, we obtain the values of $\gamma \approx 44$ volts and $\alpha_0 \approx 2.5$ kv/cm. Therefore using (6), $d_L = 5.9 \times 10^{-3}$ cm, the value of d_L in GASH appears to be larger by a factor of 10 in comparison with the calculated d_L of BaTiO_3 . An alternative explanation of Fig. 8, as well as Fig. 3, may be given in terms of a dehydrated nonferroelectric layer in the vicinity of the electrodes. The latter is produced during the vacuum deposition of the electrodes when the hot metallic particles come in contact with the crystal surface. Experiments still in progress tend to support the latter possibility.

QUASI-STATIC MEASUREMENTS

For electric fields less than 1 kv/cm, the pulse method described in the previous paragraph is not suitable for a measurement of polarization reversal. The switching currents are too small and the reversal time too long for effective observation of differentiated switching transients. Instead, an electric field is applied to the ferroelectric in series with a $1 \mu\text{fd}$ polystyrene capacitor and the integrated charge on this capacitor is measured as a function of time by means of an electrometer and timing mechanism. The apparatus is the same as that used for the tracing of quasi-static loops and has been described elsewhere.⁴ By making use of (3), the switching time τ_s can be defined unambiguously. A plot of τ_s vs $1/E$ from such measurements is shown in Fig. 9. It pertains to the same crystal whose plot is shown in Fig. 7 at higher fields. The agreement between values of the activation fields obtained in this manner is quite good:

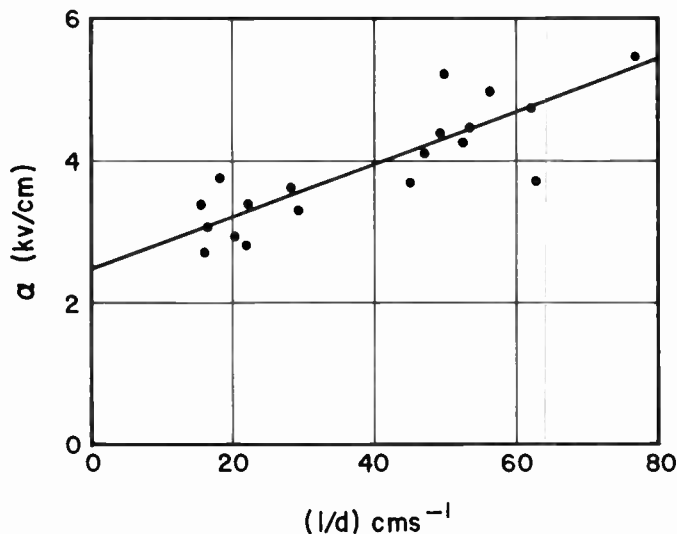


Fig. 8—The activation, field α , depends upon the reciprocal crystal thickness. In conjunction with Fig. 3, this suggests the existence of a nonferroelectric layer within GASH crystals.

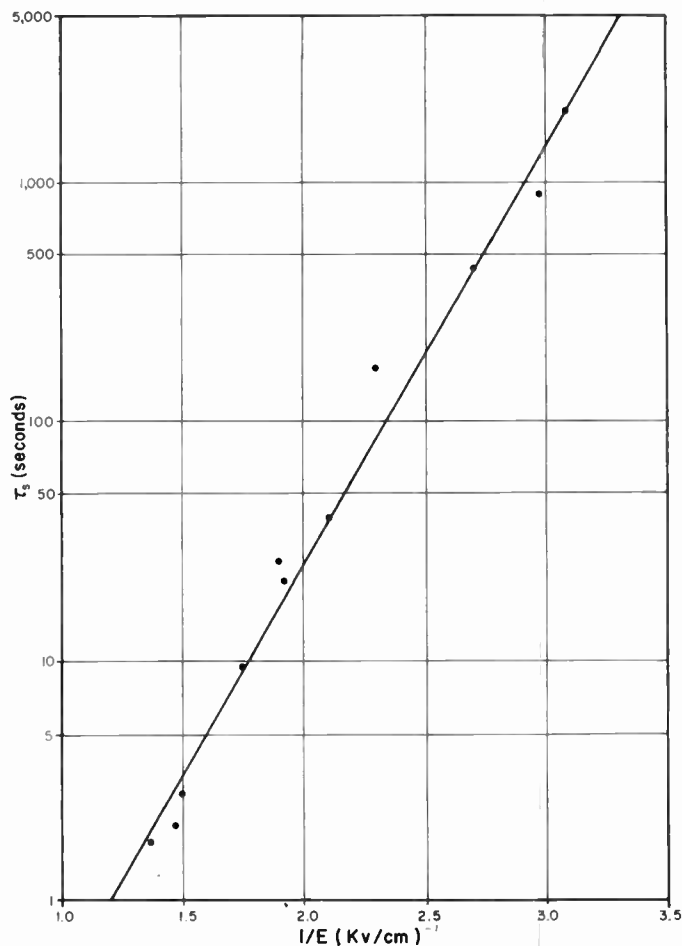


Fig. 9—The switching time obtained at low fields by quasi-static methods still has the same logarithmic dependence upon E as Fig. 5. The same crystal was used as for Figs. 5 and 6, and the slope here is $\alpha = 4.2$ kv/cm.

$$\begin{aligned}\alpha(\text{pulse}) &= 4.1 \times 10^3 \text{ volts/cm,} \\ \alpha(\text{quasistatic}) &= 4.2 \times 10^3 \text{ volts/cm.}\end{aligned}\quad (7)$$

No evidence of a threshold field α_0 could be found down to a value of $E=0.3$ kv/cm. Therefore, it appears that even fields smaller by a factor of six than the 60-cps coercivity of a particular crystal, if allowed to remain on GASH crystals for a sufficiently long time, will ultimately cause a complete reversal of polarization.

DISCUSSION

The lack of a cohesive general theory of ferroelectricity restricts us to an evaluation and comparison of empirical relationships which hold for both GASH and BaTiO₃. Optical and electrical observations indicate that polarization reversal in barium titanate takes place by a domain nucleation and subsequent domain wall motion in the direction of an externally applied electric field.³ Similar observations were made on a number of other ferroelectrics having quite different crystal structures whether perovskites such as KNbO₃,¹⁰ or hydrogen-bonded crystals such as KH₂PO₄.¹¹

Although optical observations were not made on GASH, we assume *a priori* that a domain nucleation followed by growth of these domains by means of domain wall motion accompanies the electrically observed polarization reversal. While the domain mobility was shown to be considerably slower in GASH in comparison with BaTiO₃, the activation field is smaller respectively by only a factor of two. It would appear that domain nucleation does not vary greatly in both materials if α is indeed related to nucleation as suggested^{3,12} by Merz.

The factor γ (6) representing the rate of change of the activation field α with reciprocal crystal thickness is nearly the same in both materials: $\gamma(\text{BaTiO}_3) = 45.8$ volts and $\gamma(\text{GASH}) = 44$ volts respectively.

While the slower polarization reversal is a deterrent to the use of GASH as a circuit component, the lower hysteresis losses, very much lower dielectric constant ϵ_R and apparently very low electromechanical activity make its use attractive in comparison with BaTiO₃. Not the least consideration is the ease of growing crystals from a water solution as compared to the high temperature growth from the melt to BaTiO₃.

One of the most significant advantages of GASH is its

lack of fatigue, *i.e.*, the decrease in the amplitude of the switching transient under repeated pulsing such as encountered in BaTiO₃. The fatigue effect is still under study in the latter material and its causes are as yet not completely known.

The upper frequency limit of polarization reversal appears to be in the vicinity of 50 kc for both materials. The high fields required to drive the ferroelectrics into saturation apparently cause large dielectric heating losses and these combined with electrostriction effects destroy the crystals. This is particularly true in the case for BaTiO₃ which has high electromechanical coupling coefficients.

CONCLUSION

The measurements described in this paper illustrate the similarity between GASH and ferroelectric crystals of different physical and chemical structures, especially the better known BaTiO₃. It is shown that:

1) No threshold field may be found in GASH and the adherence to the exponential relation $\tau_s = \tau_0 \exp(\alpha/\epsilon)$ down to very low fields makes it unlikely that a practical value is attainable. The lack of such a threshold and the lack of a true "coercivity" would make it necessary that some additional gating be provided if GASH be used as an element in a ferroelectric memory matrix.

2) While the activation fields measured in GASH at +25°C are of the same order of magnitude as those of tetragonal barium titanate, the domain mobility appears to be considerably lower in the former ferroelectric. Nevertheless, the upper practical limit of driving frequency of 25 to 50 kc is the same in both materials.

3) The hysteresis losses in GASH are smaller by approximately a factor of ten as compared to BaTiO₃ paralleling the decrease in P_s .

4) A space charge, or dehydrated layer exists in GASH and constitutes the probable explanation of the dependence of α and E_c upon crystal thickness.

5) The low dielectric constant, low electromechanical activity, lack of polarization fatigue, and ease of crystal growth ought to interest the designer in search of low-duty cycle bistable ferroelectric elements, but a great deal of additional work is required to establish its proper place as a reliable solid state electronic component.

ACKNOWLEDGMENT

The support of the Navy Bureau of Ordnance through the Foundational Research Program is gratefully acknowledged. The author is also indebted to D. A. Collins for able assistance in the experimental phases of this work.

¹⁰ H. H. Wieder, "Wall motion and polarization reversal in ferroelectric KNbO₃," *Bull. Amer. Phys. Soc.*, vol. 1, p. 254; June, 1956.

¹¹ T. Mitsui and J. Furuichi, "Domain structure of Rochelle salt and KH₂PO₄," *Phys. Rev.*, vol. 90, pp. 193-202; April, 1953.

¹² E. A. Little, "Dynamic behavior of domain walls in BaTiO₃," *Phys. Rev.*, vol. 98, pp. 978-984; May, 1955.



Straight-Field Permanent Magnets of Minimum Weight for TWT Focusing—Design and Graphic Aids in Design*

MYRON S. GLASS†, MEMBER, IRE

Summary—A convenient design formula has been derived which enables one to estimate readily the minimum amount of magnetic material which will satisfy a given set of field strength requirements on the axis of a tubular permanent magnet. Such a magnet is suitable for focusing the beam of a traveling-wave tube (tw) with coaxial rf fittings if small holes are provided in the side of the magnet to admit the coaxial lines.

The calculation is further expedited by the use of design graphs, based upon the formula, from which one can read off directly the required cross section area at the middle of the magnet. From this value one may calculate the average cross section, volume, and weight of magnetic material. A correction factor has been derived which also enables one to apply the results for the simple tubular magnet directly to the case of magnets specially shaped to fit around waveguide.

The validity of the formula and of the associated design graphs has been confirmed by tests upon a series of magnets. These magnets covered a considerable range of field requirements and of size, varying in weight from three to twenty pounds.

INTRODUCTION

THE traveling-wave tube (tw) is emerging rapidly from the laboratory and is taking its place in various engineering applications. In most of these applications the associated equipment, including the focusing magnet, must be kept small and light. While periodic focusing¹⁻⁴ satisfies the requirement of magnet weight reduction, there are still many cases, particularly when waveguides must be coupled directly to tw's, where periodic focusing is very difficult. Straight-field focusing, because of its simplicity and convenience, becomes the likely choice of the circuit designer when the size and weight of the magnets are acceptable.

The literature on periodic focusing has emphasized the light weight of the periodic magnets as compared with some of the larger and heavier straight-field magnets which were perhaps not always correctly designed for minimum weight. This tends to promote a general impression that straight-field magnets are universally and necessarily large and heavy. A lack of published in-

formation, in convenient form, on the design of minimum weight permanent magnets for straight-field focusing has permitted this impression to stand uncorrected.

While it is true that some twt focusing requirements are such that straight-field magnets become much larger and heavier than periodic magnets, it is equally true that in other cases the difference in weight is negligible. One twt, to which we refer later, is focused by a magnet which weighs about three pounds. Assuming that the periodic magnet weighs about half as much, the small difference in weight of the complete circuit provides little incentive for the circuit designer to overcome the technical difficulties of periodic focusing. Since the choice between the two focusing methods may depend largely upon the minimum weight for which the straight-field magnet can be designed, it becomes important to provide a convenient method of estimating this weight.

A convenient and efficient magnet design for focusing twt's consists of a tubular magnet mounted coaxially with respect to the tube and terminated by pole pieces which are apertured to receive the tube. The tubular configuration may be extensively reshaped to adapt it to space requirements of the associated circuit components without greatly affecting the field strength distribution on the axis. In magnets so designed it is evident that the length of the magnet is equal to the internal air gap between the pole pieces, and that, therefore, the field strength in the gap must be equal to the demagnetizing field. It is also evident that the useful air gap is bounded by the inner wall of the magnet. These circumstances reduce the number of variables which enter into the calculations.

There is an explicit relation between the specified conditions (diameter, length, and field strength) in the air gap and the amount of magnet material required to satisfy these conditions. Most of the steps in tracing this relation are straightforward and can be followed easily with the aid of a slide rule. One particular step, however, is tedious to calculate by the usual means. Reducing this step to a graphic solution has minimized the effort. We have also found it convenient to add other graphs to expedite some routine steps of the solution. We thus arrive at a simple and rapid graphic procedure for the design of minimum weight magnets to satisfy straight-field focusing requirements.

In order to confirm the validity of the graphic method,

* Original manuscript received by the IRE, February 28, 1957.

† Bell Telephone Labs., Inc., Murray Hill, N. J.

¹ A. M. Clogston and H. Heffner, "Focusing of an electron beam by periodic fields," *J. Appl. Phys.*, vol. 25, pp. 436-447; April, 1954.

² J. T. Mendel, C. F. Quate, and W. H. Yocom, "Electron beam focusing with periodic permanent magnet fields," *Proc. IRE*, vol. 42, pp. 800-810; May, 1954.

³ K. K. N. Chang, "Optimum design of periodic magnet structures for electron beam focusing," *RCA Rev.*, vol. 16, pp. 65-81; May, 1955.

⁴ K. K. N. Chang, "Periodic magnetic field focusing for low noise traveling-wave tube," *RCA Rev.*, vol. 16, pp. 423-331; September, 1955.

we have designed and tested magnets suitable for focusing various traveling-wave tubes. The quantitative design of the magnets has been derived directly from the graphs, as shown in the following section. The measured field strength produced by these magnets has agreed closely with the design values, within the limits of variation of the magnet materials. In order further to evaluate these magnets we have incorporated them in micro-wave amplifiers built around representative twt's.

In the discussion of the graphic design method, we illustrate our remarks with references to two particular amplifiers. These two are cited because they happen to include the smallest (3-pound) and also the largest (20-pound) magnets which have been designed with the aid of the charts and subsequently used to focus twt's.

In Table I are descriptive data identifying the two amplifiers.

TABLE I

Amplifier Type	1917	1789
Operating Frequency, Megacycles	10,700-11,700	~6000
Required Field, Strength-Oersteds	475	610
Gap Length, Inches	5.75	7.50
Gap Diameter	1.60	2.50

In Fig. 1 the two are shown for comparison of size and physical appearance.

The three-pound focusing magnet used in the 1917 amplifier appears in Fig. 2. The magnet is seen to be an assembly of two identical halves. A separate half-magnet shown in the foreground reveals the contours of the inner surface. Thus the magnet is seen to consist of a pair of bar magnets with median protuberances which, in the assembly, contact at the middle to act as spacers. From the middle they taper outwardly to provide clearance for the transverse waveguides. The twenty-pound magnet used in the 1789 amplifier has the same general shape.

The magnet configuration described above provides a tapering cross section which decreases from a maximum at the middle to about 60 per cent of the maximum at the ends. This is found to be the correct taper to provide approximately uniform field strength within the magnet and consequently along the length of the gap. A typical distribution of axial field strength for the 1917 magnet is shown in Fig. 3. The fact that the field strength is higher than the value specified in Table I results from the circumstance that the magnetic strength of Alnico 5, currently obtained from our supplier, is higher than the values shown by the published curves.

Experience has shown that for good focusing, it is required that the magnetic flux lines be accurately straight. The maximum tolerable perpendicular component of field, or cross-field, is about 1 oersted. In the field provided by the magnets alone one measures

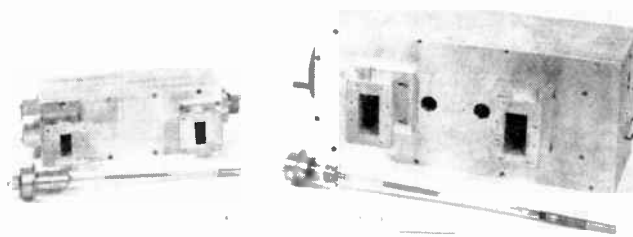


Fig. 1—Experimental twt circuits. Left—11,000-mc twt and circuit. The built-in permanent magnet supplies focusing field strength of 500 oersteds along 5 3/4-inch air gap. Right—6000-mc twt and circuit. The focusing field strength is 610 oersteds along 7 1/2-inch air gap.



Fig. 2—Details of magnetic structure. Left—Field straightener assembly consists of permalloy disks separated by aluminum spacers. The permalloy disks must be held accurately perpendicular to the axis. Middle—This pair of magnets weighs three pounds. It produces a field of 500 oersteds along the common axis in the 5 3/4-inch gap between polepieces. Right—Single magnet, showing inner contours.

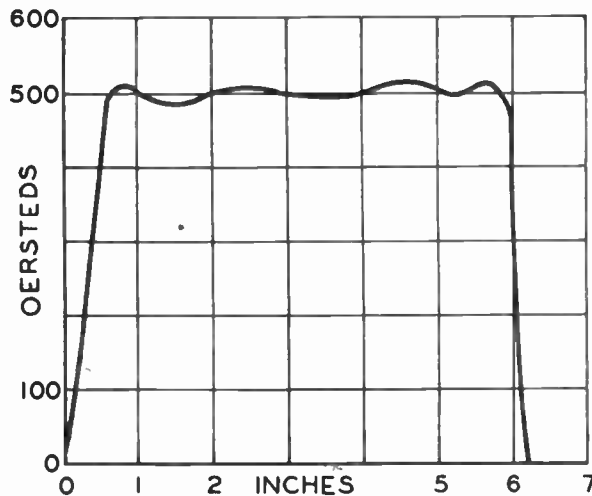


Fig. 3—Field strength distribution along axis of magnet pair shown in Fig. 2.

cross-fields as large as 10 oersteds. These are corrected by the use of field straighteners. A partially disassembled field straightener is shown with the magnet in Fig. 2. It consists of an array⁵ of apertured disks of permalloy with aluminum spacers, assembled on a hollow mandrel through which passes the traveling wave tube. The permalloy disks in this configuration serve to reduce the cross-fields to acceptable levels, less than 1 oersted, but have little effect on the axial field strength.

⁵ This type of field straightener was suggested several years ago by C. C. Cutler.

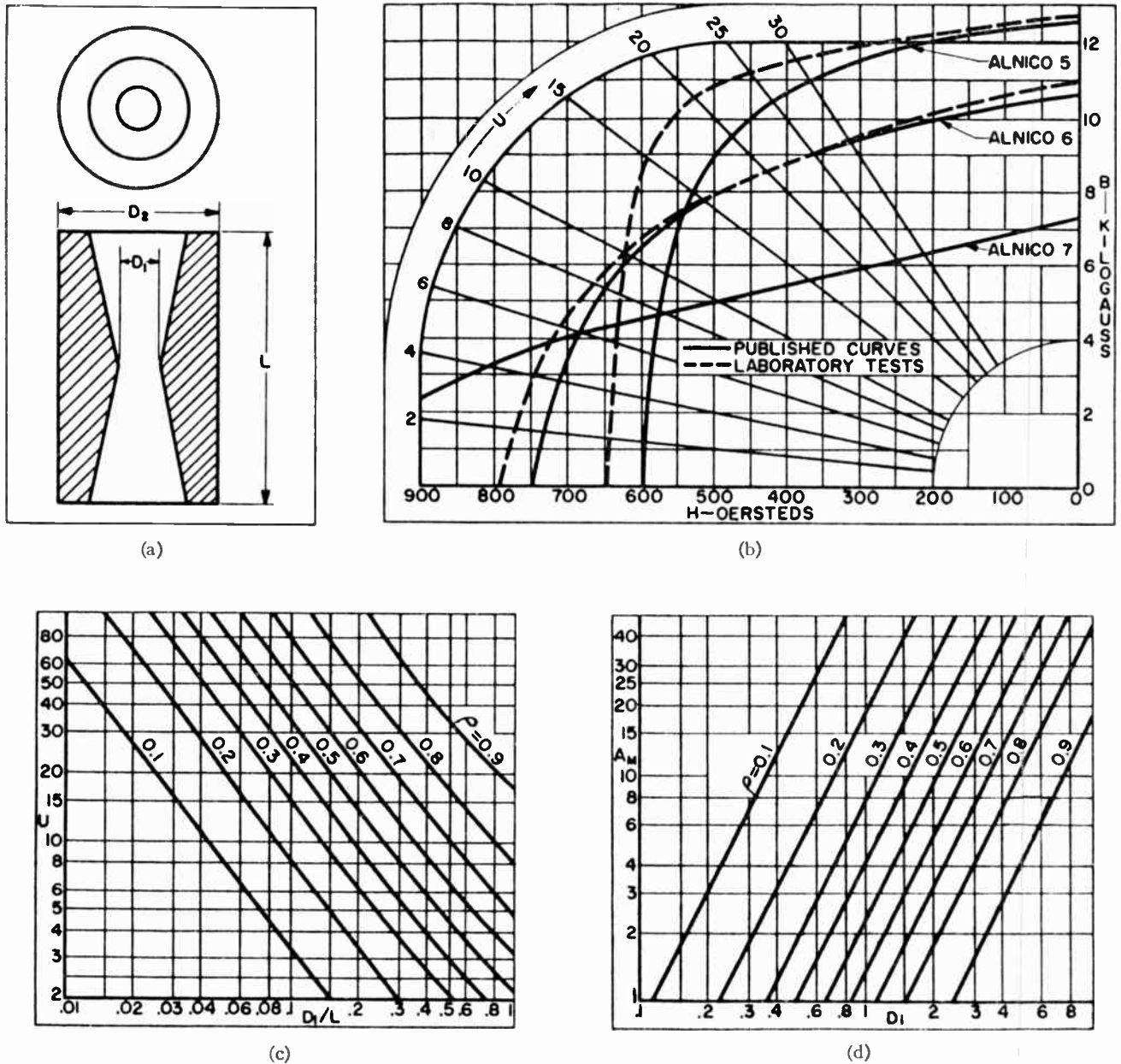


Fig. 4—Assume $H=610$; $D_1=2.5$ inches; $L=7.5$ inches. To find the required median section perpendicular to the axis of the tubular magnet shown in (a): from (b) obtain the value $U=10$ for $H=610$ on “published” curve for Alnico 6. In (c) insert $U=10$ and $D_1/L=0.33$ and obtain $\rho=0.58$. In (d) insert $\rho=0.58$ and $D_1=2.5$ and obtain $A_m=10$ square inches. ($\rho=D_1/D_2$.) This is the required solution for the median section of the magnet. Once this is known, other dimensions and the required weight of magnet may be readily calculated by slide-rule operations. “Laboratory tests” on Alnicos now on hand (b) indicate that magnets of current production may be somewhat stronger than the assumed value of H .

The shape of the magnet used in the circuits, and illustrated in Fig. 2, is inconvenient for analytic treatment. For that reason, we treat it as approximately equivalent to a tubular magnet, Fig. 4(a), which is assumed to have the same taper of section from middle to ends. We then set up a graphic design technique which enables us to determine quickly the required cross sectional area at the middle of such a magnet. Once this median section is known, the other dimensions and the required weight of magnet material may be easily calculated. Finally, it is shown in the last section, and it has been confirmed experimentally, that a magnet specially

shaped as shown in Fig. 2 to provide clearance for transverse waveguides requires 30 per cent more magnet material than the tubular magnet of Fig. 4(a).

One should probably note in passing that the tubular magnet with tapered section has also been analyzed by de Bennetot.^{6,7} He developed mathematical means to arrive at values of field strength to be expected at points along the axis of a tubular magnet of specified

⁶ M. de Bennetot, “Sur le calcul des aimants permanents de forme tubulaire,” *Annales de Radioélectricité*, pp. 193-216; April, 1954.

⁷ M. de Bennetot, “Aimants permanents pour tubes électroniques en hyper fréquences,” *L'Onde Électrique*, pp. 341-342; August-September, 1955.

material and geometry. His analysis does not offer, however, a solution of the reciprocal problem of estimating dimensions and weight of the magnet which will satisfy the specified conditions. While our graphic method is aimed primarily at the latter problem, one may also carry the computations through the graphs in reverse order, and may solve for field strength on the axis for magnets of known dimensions and of the same general configuration.

THE GRAPHIC DESIGN PROCEDURE

Approaching the problem of design of a focusing magnet, one usually finds certain requirements and dimensions to be already fixed. The field strength, H , is set by the focusing requirements of the tube. The minimum length of air gap is determined from the geometry of the tube. The inside diameter, D_1 of Fig. 4(a), must be large enough to accommodate the field straightener. These considerations fix the values of H and D_1 , and also L , since the magnet has the same length as the gap. From these given conditions and requirements one wishes to derive other design dimensions, and the required weight of magnet.

We have found it convenient in the analytic treatment to introduce the symbol, U ,⁸ to represent the ratio $B/(-H)$ where H is field strength in oersteds and B is magnetic induction in Gauss at the operating point on the demagnetization curve for the magnet. We have also found it convenient to set up a graph, as in Fig. 4(b), where lines representing a range of values of U are superimposed upon demagnetization curves for various useful magnet materials.

The first step in graphic design derives from Fig. 4(b) the preferred magnetic material and the value of U at the operating point for this material. One introduces the required value of H in this graph and, for minimum weight, selects the magnet material which has largest value of B for this value of H . For example, to get a field of 500 oersteds one would choose Alnico-5 over the two other Alnicos in the graph. At the indicated operating point on the demagnetization curve of the selected material one reads out the indicated value of U .

The actual operating point on the demagnetization curve is determined entirely by the permeance of the environment in which the magnet finds itself. If there are no other magnetic materials close by, the permeance is determined entirely by the geometry of the magnet itself. This establishes an explicit relation between the geometry of the magnet and the operating point on its demagnetization curve. This relation, which is traced out in the concluding section of this paper, is represented graphically in Fig. 4(c). Here values of U are plotted against the ratio D_1/L for various values of ρ . Since ρ is defined as the ratio of diameters, D_1/D_2 , it is evident that this graph includes all the controlling

dimensions of the magnet, and does indeed represent a useful relation between magnet geometry and operating point on the demagnetization curve.

For the second step in the graphic procedure, one inserts in Fig. 4(c) the specified value of D_1/L and the value of U previously obtained from Fig. 4(b). At the point of coincidence of these values, one may read out directly the required value of ρ . This graphic solution eliminates the need for a large amount of tedious calculation which would otherwise be required.

It is perhaps evident to the reader that, once we have evaluated ρ , the additional calculation required to obtain the other dimensions of design and magnet weight may be carried out readily with the slide rule. We have found it convenient, however, to use the graph of Fig. 4(d) to obtain directly the required cross section area at the middle of the magnet. In this graph the area, A_m , of the median section is plotted against D_1 for various values of ρ .

Now, it may be helpful to review the complete design process as illustrated by two representative cases. In Table II the design data are summarized for the focusing magnets used in the two circuits illustrated in Fig. 1. In the top box are given the required values of H , L , and D_1 . In the middle box are given the results of the three steps of the graphic method of solution. Finally, in the bottom box are shown the additional steps needed to obtain the required weight of the magnet.

TABLE II

		1917	1789
Given Conditions	H	475	610
	L	5.75 inch	7.5 inch
	D_1	1.6	2.5 inch
	D_1/L	0.28	0.33
From Graphs	U	20	10
	Material	Alnico 5	Alnico 6
	ρ	0.7	0.58
	A_m	2.1 in ²	10.0 in ²
Slide Rule	A_{corr}	2.7	13.0
	A_{avg}	2.16	10.4
	Vol	12.4 in ³	78 in ³
	Wt	3.2 pounds	20.3 pounds

The reader will recall that the specially shaped magnets, shown in Fig. 2, require 30 per cent more material than the more ideally shaped magnet of Fig. 4(a), which was the basis of the calculation. The tabulated value, A_{corr} , is 30 per cent larger than A_m . One also recalls that the section area tapers down at the ends to 60 per cent of the value at the middle. The tabulated quantity, A_{avg} , is the average value, 80 per cent of the corrected maximum value. This multiplied by the length gives the volume. The density figure used in calculating the weight is 0.26 pound per in³ for the Alnicos used in these two magnets.

It is perhaps evident to the reader that in the design of tubular magnets similar to Fig. 4(a) one would not

⁸ This term is seen to have the dimensions of negative permeability.

add the 30 per cent correction factor, but the other steps would be the same as those shown in the illustrative examples. This would also be true for tubular magnets with small deviations from the configuration of Fig. 4(a). For example, one might consider the case of a tubular magnet with straight cylindrical bore and external taper to reduce the end section to 60 per cent of the medial section. It appears reasonable, and it has been confirmed experimentally, that the results of the graphic design procedure are applicable, without correction, to this configuration if one again interprets D_1 as the inner diameter and D_2 as the outer diameter of the median section.

ORIGINS OF THE GRAPHIC DESIGN METHOD

Derivation of the Relation Shown Graphically in Fig. 4(c)

If a bar of magnetic material is inserted within a uniform field of strength II' , for example inside a solenoid, the magnetization of the bar is described by the equation

$$II = II' - \left(\frac{N}{4\pi}\right)(B - II) \quad (1)$$

in which

II = magnetizing force in the bar

B = flux density in the bar

$N/4\pi$ = demagnetizing factor, a function of the length-to-diameter ratio of the magnet.⁹

If the bar is of material suitable for a permanent magnet and if the magnetizing field is removed there is a residual state of magnetization which is described by reducing II' to zero in (1) giving

$$-II \left(1 - \frac{N}{4\pi}\right) = B \left(\frac{N}{4\pi}\right). \quad (2)$$

If the field II' is strong enough to saturate the bar, then the values of B and II will fall on the characteristic demagnetization curve for the material, and (2) may be rewritten

$$U = \frac{B}{-II} = \frac{1 - N/4\pi}{N/4\pi}. \quad (3)$$

For convenience we let

$$F(N) = \frac{1 - N/4\pi}{N/4\pi} \quad (4)$$

and write

$$U = F(N) \quad (5)$$

to describe the operating point of the bar magnet.

⁹ R. M. Bozorth and D. M. Chapin, "Demagnetizing factors of rods," *J. Appl. Phys.*, vol. 13, pp. 320-326; May, 1942. This material is reviewed briefly in Bozorth's book "Ferromagnetism."

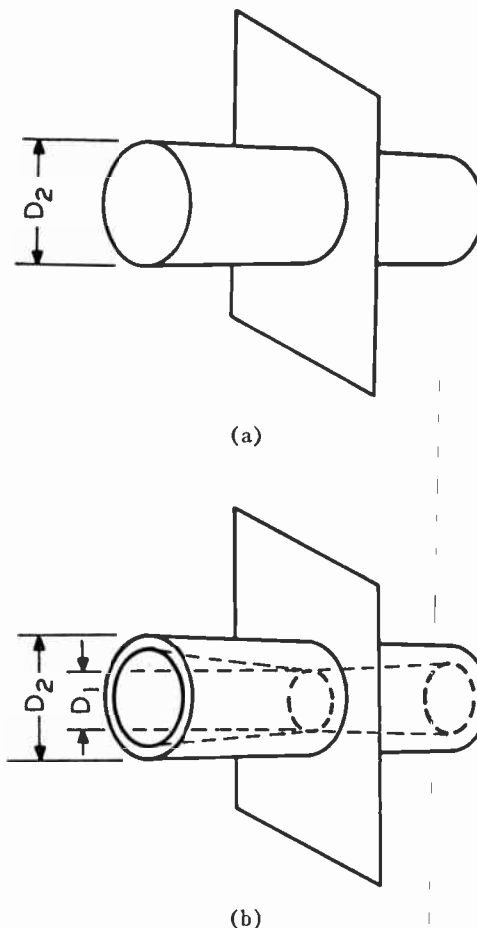


Fig. 5—(a) Cylindrical bar magnet. (b) Tapered tubular magnet.

Now one may consider a plane [see Fig. 5(a)] intersecting the bar at the middle and perpendicular to the axis. It is evident that the flux threading through the section of the magnet cut by the plane must be equal to the total flux external to the bar threading through the plane. The external flux will be equal to the product of the external permeance by the magnetomotive force, that is, $-IILP_{\text{ext}}$.¹⁰ The flux passing through the median section of the bar is equal to the product of the flux density by the median cross section area, that is, BA_m . All this may be summarized in the equation

$$-IILP_{\text{ext}} = BA_m. \quad (6)$$

Since

$$A_m = \frac{\pi}{4} D_2^2 \quad (7)$$

¹⁰ This expression implicitly assumes that H is constant along the length of the magnet. This is not a good assumption for a bar magnet, particularly one which is long and slender. However, since the end result of this derivation is applied to a magnet design in which H is (by design) constant along the length, one feels safe in treating it as a constant here.

one may combine equations (5, 6, 7) to obtain

$$P_{\text{ext}} = \frac{\pi}{4} F(N) \frac{D_2^2}{L}. \quad (8)$$

Since the external permeance is determined by external geometry it seems evident that the solid rod and hollow cylinder of Fig. 5, having identical external dimensions, will also have the same external permeance. But in the case of the tubular magnet there is also a small internal permeance, P_{int} , given approximately by the equation

$$P_{\text{int}} = \frac{\pi}{4} (D_1^2/L). \quad (9)$$

The total flux in air which the tubular magnet must supply at the median plane will be

$$\text{total flux} = -HL(P_{\text{ext}} + P_{\text{int}}). \quad (10)$$

This total flux must also thread the magnet section at the median plane, so that

$$-HL \frac{\pi}{4} \frac{D_2^2 F(N)}{L} + \frac{\pi}{4} \frac{D_1^2}{L} = BA_m. \quad (11)$$

In the tubular magnet the area of the median section is given by

$$A_m = \frac{\pi}{4} (D_2^2 - D_1^2) = \frac{\pi}{4} D_2^2 (1 - \rho^2). \quad (12)$$

Combining (11) and (12) one obtains

$$-H \frac{\pi}{4} D_2^2 [F(N) + \rho^2] = B \frac{\pi}{4} D_2^2 (1 - \rho^2)$$

which readily reduces to

$$U = \frac{B}{-H} = \frac{F(N) + \rho^2}{1 - \rho^2} \quad (13)$$

for the tubular magnet. As one would expect, if ρ is reduced to zero, (13) is converted back to (5) for the solid bar.

In (13) one finds an explicit relation between magnet operating point and magnet geometry. It is therefore a means by which one may convert magnetic operating point requirement, as expressed by U , into dimensional requirements. Conversely it may be used to find the probable field strength of a magnet of known dimensions. In order to facilitate these applications of (13), it is displayed graphically in Fig. 4(c). It will be noted that for convenience the ratio D_1/L is used on the graph replacing the term $F(N)$ used in the equation. This substitution is made readily in preparing the graph, with the aid of the Bozorth-Chapin⁹ data for the cylindrical magnet. In selecting values from the Bozorth-Chapin chart it is important to select each value from a curve

representing a value of permeability comparable with the value of U which one is plotting.

It should perhaps be noted in passing that the Bozorth-Chapin data on the demagnetization factor apply to solid rods of uniform cross section. In such a magnet the field strength is somewhat weaker at the middle than at the ends. If the magnet is very long and slender this effect would reach such proportions that one would hesitate to apply these data to the solution of our problem where a tapered section holds the field strength nearly constant along the length of the magnet. In our experience, however, the length-to-diameter ratio of these focusing magnets has not been great enough to introduce observable error from this cause.

The Correction Factor

In the magnet designs illustrated in Table II we added 30 per cent of the values of cross section and weight estimated for the tubular magnet. We justified this by saying that the modified shape which is convenient to use in our microwave amplifiers is less efficient magnetically than the tubular magnet which was analyzed.

In the modification of the tubular magnet to accommodate transverse waveguides at the ends, it is necessary to make each half of the magnet essentially a flat bar where it bridges the waveguide. For this reason, and also for convenience in packaging, the external shape of the magnet becomes square rather than round. This change in shape provides an easy approach to a rough appraisal of the weight correction factor made necessary by the modification.

If a square and a circle enclose equal areas, the periphery of the square measures 1.13 times the circumference of the circle. Hence, the external permeance of the square section is about equivalent to the external permeance of a circular section of diameter 13 per cent greater than the diameter of the reference circle. From (8) one notes that the external permeance is proportional to the square of the diameter of the external surface. This proportionality is modified somewhat by the fact that the $F(N)$ term is also a function of geometry. Also the small internal permeance remains unchanged. As a first approximation, however, one may regard the external permeance as $(1.13)^2$ or 1.28 times the permeance of a round section enclosing equal area, and specify the addition of an equal percentage of magnetic material. We have for convenience rounded off this correction factor at 30 per cent.

ACKNOWLEDGMENT

For helpful discussions of this work, the author is indebted to E. D. Reed and W. E. Danielson. For the mechanical design of the complete structures or circuits in which the satisfactory performance of these magnets was demonstrated, he is indebted to W. C. Sylvernal.

Some New Circuits for High-Power Traveling-Wave Tubes*

M. CHODOROW†, FELLOW, IRE, AND R. A. CRAIG‡, MEMBER, IRE

Summary—A discussion of new types of slow-wave structures, in which the coupling between sections is obtained largely by negative mutual inductance, is given in this paper. Since this type of coupling can be used to give “fundamental” amplifier operation with relatively high impedance, the devices are somewhat unusual in the field of high-power traveling-wave tubes.

Several structures which make use of this type of coupling are examined in a qualitative manner, and the results of “cold tests” on each model are given. In particular, one device, the so-called “clover-leaf” structure, is investigated in some detail. Curves of impedance, C , and gain at megawatt power levels are included. Some discussion of the practical problems involved in the design of an amplifier using this circuit is presented to serve as a guide for those interested in the construction of high-power traveling-wave tubes.

INTRODUCTION

DURING the past several years interest has arisen in the field of high-power traveling-wave tubes.

These tubes are, in general, pulse operated and may have peak power outputs of several megawatts with duty cycles ranging from a fraction of a per cent to several per cent. The transition from klystrons to traveling-wave tubes (twt's) is necessary if there is a need for instantaneous tuning or even continuous moderate tuning rates, since mechanical tuners are liable to fail after many tuning cycles.

Since many of the same basic components such as cathodes, collectors, etc., are used in both high-power klystrons and traveling-wave tubes, we can say that the primary difference between the two is in the interaction circuit and the associated couplers for transferring energy to and from the circuit.

Two basic types of slow-wave structures have received considerable attention as the interaction circuits for traveling-wave tubes. These are the helix and the periodically-loaded waveguide, which is a band-pass microwave filter.

The helix has many advantages when used as a traveling-wave propagating structure. It is by nature a broad-band device to which it is relatively easy to couple over a wide frequency range, and it is quite simply constructed. Attenuation may easily be added at various places along the helix to prevent the tube from oscillating when used as an amplifier.

However, twt's that employ helices as the propagating structures suffer one fundamental limitation: the relatively low power output. While output powers of several kilowatts have been obtained, this seems about the limit (at least in the 10-cm wavelength range, with correspondingly lower limits for higher frequencies).

The reason for this limitation on power is a simple one. In order to increase the power output of a tube, one must increase the power in the beam, *i.e.*, increase the accelerating voltage and current in the beam. In order to maintain the power density in the beam at reasonable levels it is necessary to increase the beam and helix diameters. While the increased helix diameter is satisfactory at high voltages as far as interaction with the beam is concerned, the increased velocity and diameter means that the helix will be a very open structure with much of the energy stored in the space-harmonic fields. Thus, the fundamental helix impedance will be greatly reduced, and the tendency toward backward-wave oscillations considerably increased. The only alternative (with a single helix) is to return to the smaller helix diameter and the higher power densities in the beam. Because of its limited cooling possibilities, the helix is limited in the amount of power it can dissipate, and a definite ceiling is placed on the power output of amplifiers which make use of a helix as an rf circuit.

Certain modified helix structures can increase the impedance of the device at higher power levels even with large diameters. Among these structures are the bifilar helix and the cross-wound helix, but even they will have power-handling limitations determined by the poor cooling characteristics. It would seem, therefore, that other slow-wave structures with better dissipation characteristics might show more promise as high-power twt's.

Besides helices, loaded waveguides or transmission lines have been most often used as the circuits for twt's. These devices are filter-type circuits consisting of waveguides with some sort of periodic loading to slow the wave velocity down to that of the electrons in the beam. They have the advantage over the helix-type structures of being much more rugged and capable of dissipating much larger amounts of heat, since the entire structure is of metal that can be easily cooled. Also, since the structures are large compared to most helix-type circuits, and are rigid, self-supporting devices, it is quite easy to maintain a high degree of uniformity from section to section by using ordinary machining practices. Therefore, a given circuit can be reproduced with identical properties with comparative ease.

* Original manuscript received by the IRE, January 21, 1957; revised manuscript received, May 20, 1957. The work reported in this paper was done at Stanford University and was prepared under Office of Naval Research contract N6ONR 251-32 NR-372-362, jointly supported by the U. S. Signal Corps, U. S. Air Force, and U. S. Navy (ONR, Bureau of Ships, and Bureau of Aeronautics).

† Microwave Lab., Stanford University, Stanford, Calif.

‡ General Electric Microwave Lab., Palo Alto, Calif.

In analyzing such structures one can consider them as linear arrays of coupled resonant cavities, or coupled slotted vanes, depending on the type of loading used. The obvious limitation of circuits of this type is the narrow bandwidth due to the resonances of the obstacles which are used for loading the guide. However, suitable design of the loading elements can give adequate bandwidth for high-voltage operation.

This paper describes a new class of propagating circuits suitable for use in pulsed high-power tw tubes in which the electrons interact with the fundamental space component of the propagating wave, and which are capable of giving bandwidths of the order of 10 to 20 per cent. Most of the data given are for dimensions suitable for operation at about 100 kv, but the same type of circuit with other dimensions could be suitable for much lower voltages and possibly greater bandwidths, although the impedances may not be as great as at the high voltages described here. Basically, the structures described here consist of sets of coupled cavities in which magnetic coupling between adjacent cavities is accomplished in such a way that it is equivalent to negative mutual coupling between resonant circuits in a filter. The use of negative mutual coupling gives a pass band characteristic in which the fundamental space component has a forward phase velocity, whereas with ordinary mutual coupling,¹ the fundamental component of the wave has backward phase velocity, and therefore interaction with the electrons must be with the first space harmonic. A general analysis of the impedance properties, and of the energy storage for coupled cavities, indicates that impedance for the space harmonic will be considerably less than for the fundamental. Therefore, there is a great advantage to be had by using a circuit in which the fundamental arrangement has a forward phase velocity.

An alternative way of getting a fundamental component with a forward phase velocity is to use capacitive coupling² (electric) between cavities. However, capacitive coupling is always through and around the beam aperture, and for most structures attempted to date there have always been conflicts in requirements between aperture size for suitable interaction with the electron beam and aperture dimensions to give adequate coupling. By using magnetic coupling, this problem is avoided. In the circuits to be described below two general methods have been used to get negative mutual coupling. The cavities that are coupled have a basic mode in which there is a Z component of the electric field (where Z is in the direction of beam propagation) and transverse components of the magnetic field. Various versions of the cavities, to be described, will have different cross sections: circular, rectangular, and distortions thereof. Normally, if such a series of cavities

were lined up with the same angular orientation and slots cut in the dividing wall between them, the magnetic coupling between the slots would be such as to give a positive mutual coupling with a propagation characteristic such that the fundamental component had a negative phase velocity.¹ One general method used here is to rotate the cavities relative to each other in such a way as to reverse the direction of the magnetic field.³ The other method involves inverted coupling loops in adjacent cavities in the coupling slot, and therefore gives the effect of negative mutual coupling.

IMPEDANCE PROPERTIES OF SPACE HARMONICS

The reasons for preferring interaction with the fundamental component of the wave propagating in this kind of loaded circuit can best be understood by considering the relative interaction impedances for the various space harmonics. The general circuit we are concerned with consists of a series of cylindrical cavities which are adjacent to each other with a centrally located hole for the electron beam to pass through. The way to couple such cavities is either through the central hole, in which case one gets a pass band characteristic such as is shown in Fig. 2(d) (or the upper curve of Fig. 1, next page), or through a slot near the circumference, in which case one gets magnetic coupling and a pass band characteristic as shown in Fig. 2(c) (or the lower curve of Fig. 1). We shall discuss the nature of the coupling later; here we are concerned with the nature of the space harmonics in the two cases, and primarily in the relative impedances of the useful components for these cases. The case of Fig. 2(d) we shall call "fundamental structure," and for this case we are assuming that the electron will interact with the fundamental component of the wave; for the case of Fig. 2(c), called the "space harmonic structure," the electrons will interact with $n = +1$ component.⁴

The method of analysis follows Pierce.⁵ While this analysis may not give exact numerical values, it certainly can be relied on to give some idea of the relative amplitudes of the various space harmonics. We compare two circuits, both operating at the same voltage, and

³ R. A. Craig, "Study of Periodic Structures for High-Voltage Traveling-Wave Tube Operation," TR-No. 36 (N6onr-25132) Stanford University (ERL and ML); November 2, 1954.

⁴ The notation used is the common one but we briefly summarize it here. In a periodic structure according to Floquet's theorem, any cartesian field component (and in particular E_z , which acts on the electrons) can be written as a sum of space harmonics.

$$E_z = \sum E_m = \sum_{-\infty}^{\infty} A_n F_n(x, y) e^{-i\beta_n z}$$

$$\beta_n = \beta_0 + \frac{2\pi n}{L} \quad n = 0, 1, 2 \dots \quad (18)$$

For the "fundamental structure" the interacting space harmonic is

$$A_0 F_0(x, y) e^{-i\beta_0 z} \quad 0 < \beta_0 L < \pi.$$

For the "space harmonic structure" considered here, the interacting space harmonic is

$$A_1 F_1(x, y) e^{-i\beta_1 z} \left\{ \begin{array}{l} \pi < \beta_1 L < 2\pi \\ -\pi < \beta_0 L < 0. \end{array} \right.$$

⁵ J. R. Pierce, "Traveling-Wave Tubes," D. Van Nostrand Co., New York, N. Y., p. 94; 1950.

¹ M. Chodorow and E. J. Nalos, "The design of high-power traveling-wave tubes," Proc. IRE, vol. 44, pp. 649-659; May, 1956.

² J. C. Slater, "Microwave Electronics," D. Van Nostrand Co., New York, N. Y.; 1950.

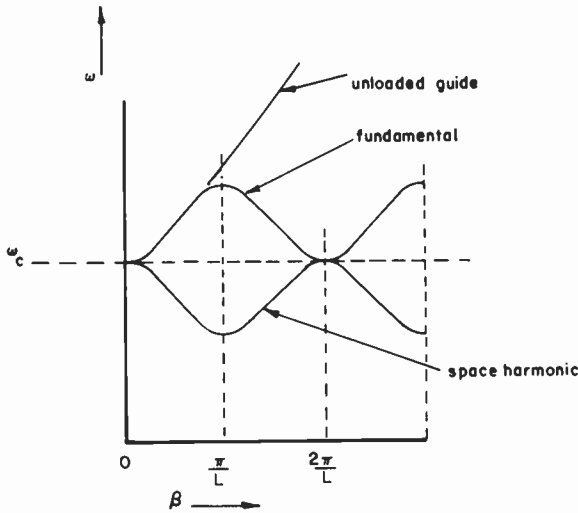


Fig. 1—Frequency as a function of propagation constant in periodic structures.

therefore at the same phase velocity. The interaction impedance is given by

$$\frac{|E_{zn}|^2}{\beta_n^2 W v_o} \tag{1}$$

Here W represents the energy stored/unit length, and v_o is the group velocity. It is assumed that this will be evaluated on the cavity axis. For both circuits there will be a factor which takes into account the variation in the field with radial position of the electrons, and for good performance in both cases, it is necessary to pick the radius of the aperture sufficiently small so the variation of interaction across the cross section is not too great. However, whatever the size of the aperture permitted by any such consideration, it will be the same in both cases, since for each the field across the aperture varies as the Bessel function $I_0(\gamma_n r)$

$$\gamma_n^2 = \beta_n^2 - k^2 \tag{2}$$

where

$$k = \frac{\omega}{c} = \text{free space propagation constant} \tag{3}$$

γ_n will be the same in both circuits if the phase velocity is the same for both. For the same bandwidth of operation, the group velocity will also have to be the same for two circuits. Therefore, to optimize either circuit, one must optimize the factor

$$\frac{|E_{zn}|^2}{W} \tag{4}$$

in order to yield the maximum impedance for that structure. If we consider that the propagating structure consists of a series of gaps with periodic spacing L , gap spacing l , and voltage V across each gap, then it can easily be shown that the amplitude of the space harmonic is given by

$$|E_{zn}|^2 = \frac{M^2 V^2}{L^2}, \tag{5}$$

where

$$M = \sin \frac{\beta_n l}{2} / \frac{\beta_n l}{2} \tag{6}$$

To calculate the energy storage per unit length, we shall make the assumption that the energy stored per gap can be calculated approximately by considering the gap as a planar capacity. In that case the energy per gap becomes

$$W_0 \frac{V^2}{l} \tag{7}$$

where W_0 is a proportionality constant. The stored energy per unit length then becomes

$$W_0 \frac{V^2}{L} \tag{8}$$

The corresponding Pierce impedance can then be written as

$$\left[\frac{\sin(\beta_n l / 2)}{\beta_n l / 2} \right]^2 \frac{\beta_n l}{\beta_n L} \frac{1}{(\beta_n^2 W_0 v_o)} \tag{9}$$

For any given structure, then, we must select the values of L and l to optimize this impedance for the space harmonic of interest. We have written this impedance in terms of the transit angle $\beta_n l$ across the gap and the transit angle $\beta_n L$ from gap to gap. For fundamental operation the transit angle between gaps is roughly in the range from $\pi/2$ to π , whereas for space harmonic operation it is in the range from $3\pi/2$ to 2π . It has been shown by Pierce that if

$$\beta_n L > \frac{3\pi}{4}, \tag{10}$$

the impedance is optimized by having

$$\beta_n l = \frac{3\pi}{4} \tag{11}$$

On the other hand, if

$$\beta_n L = \frac{3\pi}{4}, \tag{12}$$

then the expression is optimized by having

$$\beta_n l = \beta_n L \tag{13}$$

These results determine how the periodic spacing L is to be apportioned between gaps and drift space. The results imply that on fundamental operation one has essentially zero drift space between gaps ($l=L$), whereas for operation in the first space harmonic where $\beta_n L$ is about $\frac{3}{4}$ of a cycle, the optimum apportionment is to divide the space equally between gap and drift space. This means that for space harmonic operation the factor $\beta_n l / \beta_n L$ is equal to 0.5 whereas for fundamental operation it is equal to unity. Also, M^2 is also slightly larger

(about 1.2:1) for the case of fundamental operation. The net result, subject to the approximations used (planar gaps for energy storage, etc.), is that the impedance of the fundamental structure is somewhat more than twice as great as that of the space harmonic structure. This gives a factor of about 1.25 to 1.3 in the Pierce interaction parameter C . Moreover, it will make a difference of about 1.6 in QC which will also improve the gain performance of the fundamental operation as compared to space harmonic.

Basically, the advantage of operation on the fundamental component over the space harmonic is due to the fact that for a given voltage per gap, which gives the same effect per gap for the two structures, there is an equal length of wasted space in the space harmonic structure where no interaction takes place, so that the field averaged over the length of a unit cell is only half as great. Otherwise stated, for the same *average* field in the two structures, the space harmonic field has to be twice the average value over half of the path and zero over the other half. This results in the average energy stored per unit length being twice as great. In practice, using re-entrant cavities in a space harmonic structure rather than planar gaps would reduce this factor slightly.

COUPLING OF CAVITIES

As previously stated, with the structures such as shown in Fig. 2, coupling adjacent cavities through the central aperture [Fig. 2(d)] gives a pass band shape like the upper curve in Fig. 1, which has a higher interaction impedance of the useful wave component than the lower curve which corresponds to coupling through a side slot [Fig. 2(c)]. Unfortunately, to get adequate bandwidth may require too large a central aperture for *uniformity* of interaction with the beam.⁶ This is a separate requirement, and in comparing impedances in the previous section it was assumed that the radius of the aperture for the various circuits was the same. If the beam aperture and coupling aperture coincide there may be conflicting requirements on the aperture size.

It would be desirable if one could get the pass band such as shown in Fig. 2(d) by using magnetic coupling with slots close to the wall, rather than using the same aperture both for the beam and for the coupling.

The equivalent circuit for ordinary magnetic coupling between cavities is shown in Fig. 3. In terms of such an equivalent circuit, the pass band shown in Fig. 2(d) can be obtained by reversing the windings of every other inductance to give negative mutual inductance. To analyze what has to be done to slot coupling between cavities to get this effect, it is convenient to examine the effect of slot coupling on the two band edges ($\beta L = 0, \pi$). One can determine the two frequencies at the band edges for a structure of this kind by putting shorts across the midplanes of two adjacent cavities, thus

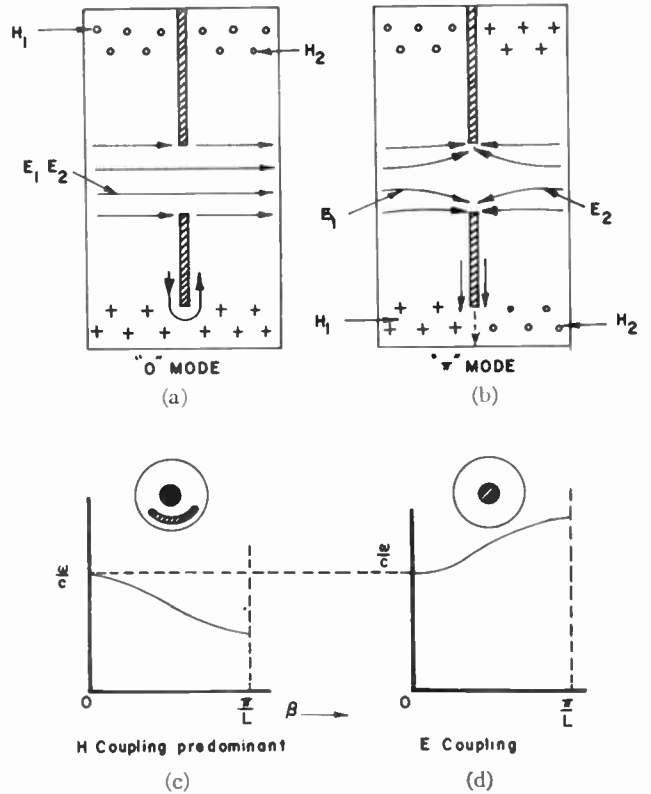


Fig. 2—Brillouin diagrams for E and H -field coupling.

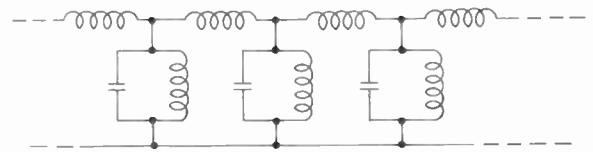


Fig. 3—Equivalent circuit of space harmonic structure.

getting a shorted length of the propagated circuit consisting of two half sections. This will have two resonant frequencies: one for $\beta L = 0$ in which the fields are shown in Fig. 2(a), and the other for $\beta L = \pi$ with the field shown in Fig. 2(b). In the first case the magnetic fields on opposite sides of the wall are in the same direction; in the second case they are in opposite directions. These two modes, which give the frequencies at the edges of the pass band, will be called the 0 and π phase modes respectively. For a structure, Fig. 2(d), in which the fundamental component has a forward phase velocity, the π mode is at a higher frequency than the zero mode, and conversely for a structure with a fundamental having a negative phase velocity. Analyzing this kind of cavity, we can see why the slot on the axis gives one type of circuit, while a slot near the periphery gives another kind. A slot on the axis results in the reduction of capacity for the π mode, and therefore it will be at a higher frequency than that of the zero mode which is not perturbed by the hole. Similarly, a slot at the circumference causes no perturbation in the frequency of the zero mode, because the H fields on both sides of the slot are in the same direction, and removing the wall

⁶ H. A. Bethe, "Theory of diffraction by small holes," *Phys. Rev.*, vol. 66, pp. 163-182; October, 1944.

makes no difference. Stated in terms of the currents, one can say that the current is flowing down on one side of the wall and up on the other, and when the slot is cut in the wall the currents on opposite sides are of such magnitude and direction that continuity of current is maintained with no perturbation, as can be seen from the figure. On the other hand, for the π mode, the H fields on opposite sides of the slots are oppositely directed, and the currents on both sides of the wall are each going toward or away from the slots simultaneously. When a slot is cut in the wall, the currents on both sides have to flow around the slot as shown in Fig. 4. One can say that this increases the effective inductance of the cavity, and therefore lowers its frequency. Another way of saying the same thing is that, with the current flowing in the direction shown, the magnetic field in the vicinity of the slots is reduced, and this reduction is the same as if the volume of the cavity were increased in a region of strong magnetic field. This acts to push the frequency down, making the π mode lower than the zero mode, and giving the pass band characteristic shown in Fig. 2(c).

Therefore, it can be seen that, if it is possible to so distort the magnetic fields in the two adjacent cavities so that in the zero mode the magnetic fields parallel to the slot are oppositely directed (or the corresponding currents across the slot on both sides of the wall flow in the same direction), this would result in the zero mode being depressed relative to the π mode; but in the π mode the fields would be parallel and the currents oppositely directed with no perturbation. In circular cavities, of course, this cannot be done. But if one distorts the cavity by making its cross section something other than a circle, and then orients adjacent cavities properly, it is possible to find regions in which the projection of the magnetic field along some particular direction will be oppositely directed to the projection of the magnetic field on the other side, even though the general sense of rotation of the field lines in the adjacent cavities is the same. Therefore, a slot cut along such a line will have fields oppositely directed on opposite sides, and the currents across the slots will also have the correct behavior, that is, have the component normal to the slot flow in the same direction on both sides. Such cavities and the results of detailed measurements are described below. Another and more obvious way of getting negative mutual coupling between cavities is to use coupling loops. Coupling loops such as shown in Fig. 5 will produce mutual inductance and a pass band very much like Fig. 2(c). If, however, the coupling loop is an S shape as shown in Fig. 21, then the result is negative mutual coupling, and the pass band is shown in Fig. 2(d). This was apparent quite early in the course of this program, and some tests were actually made using a coupling loop made of a copper strap. However, it did not seem a very practical method of providing coupling, as the problem of maintaining tolerances on such coupling loops seemed rather difficult and the use of slots looked quite promising. A method

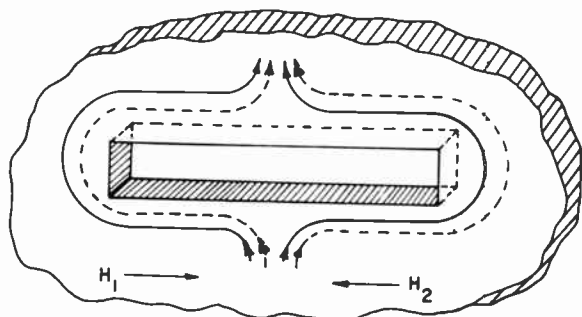


Fig. 4—Current paths for H field parallel to slot, but in opposite directions on each side of plane containing the slot.

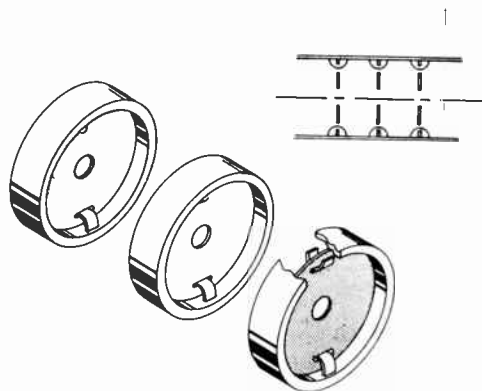


Fig. 5—Cavities coupled by loops which provide mutual inductance.

has now been devised of producing such coupling loops which seems reproducible. Results on this structure are also briefly described.

Rectangular Cavities

A very simple structure which will give the desired type of coupling is illustrated in Fig. 6. The 0 mode is shown, and it is easy to see that there is a component of magnetic field in each cavity that is parallel to the slot, but that the direction of H_1 is opposite to that of H_2 . Thus, the 0 mode will be lowered in frequency by the coupling through the slots, whereas the π mode will depend on the coupling through the center hole, and will not be changed by the slots.

One can derive expressions for the fields in such a structure and determine the relative effects of slot width and length on the coupling between cavities.³

Experimentally, rectangular cavities coupled together by both capacitive and negative mutual inductive coupling have demonstrated conclusively that the principle of such coupling is sound and the behavior of the perturbation of the 0 and π modes is as expected. Bandwidths of the order of 10 per cent or higher can be expected for operation as a filter. As an amplifier, operation would be in the fundamental wave with a TM waveguide mode of propagation with only a percentage of the filter pass band being utilized. The experimental results and theoretical calculations show that long slots give greater coupling, but this means that the ratio of cavity

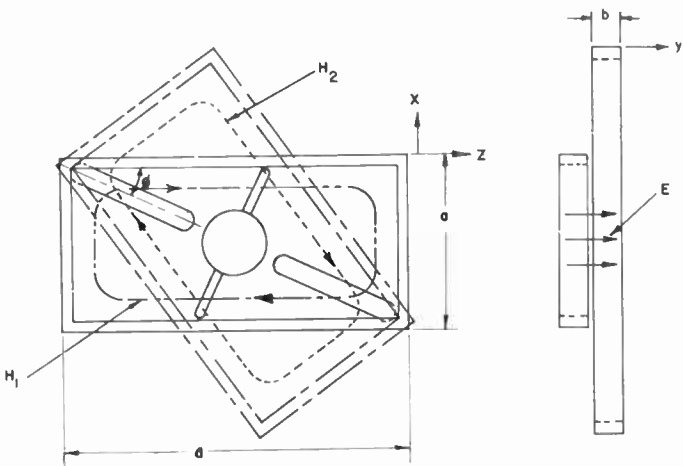


Fig. 6—Rectangular structure coupled by negative mutual inductance.

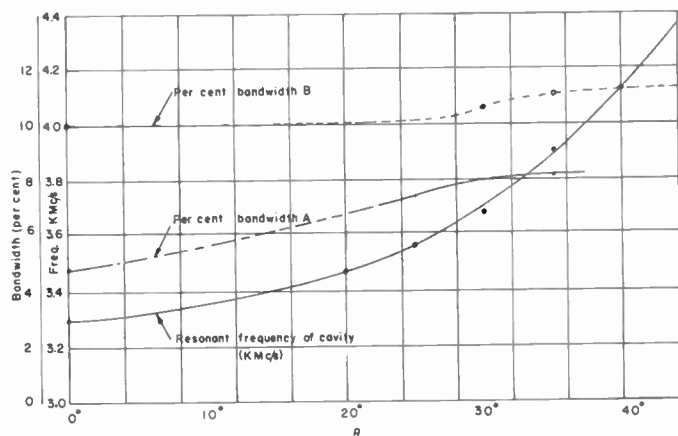


Fig. 8—Bandwidth and resonant frequency vs θ for parallelogram cavities shown in Fig. 7.

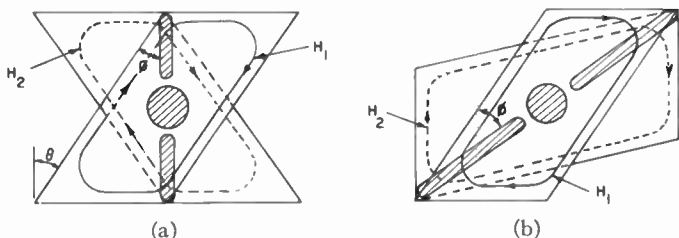


Fig. 7—Parallelogram structures with slots (a) short diagonals and (b) along long diagonals.

width to cavity length becomes small for a given resonant frequency. Therefore the electric field will tend to become nonuniform over the beam cross section, and the device will not be very efficient as an amplifier.

Parallelogram Structures

In the foregoing, we found that rectangular cavities must be quite narrow in order to have a small angle between the slots and the magnetic field lines if large coupling is to be obtained through the slots. In order to decrease the angle ϕ , and lengthen the slots without changing the effective width of the cavity, one can deform the rectangular cavity into a parallelogram. Thus, with slots cut in the window along the major diagonal of the cavities, two major improvements over the rectangular structure result: 1) a smaller angle ϕ , and 2) a correspondingly longer slot. Both of these should give increased bandwidth. The component of magnetic field along the ends of the cavities, which serves only to reduce the frequency of the π mode, is now more effective, however. If the slots are placed in the shorter diagonal of the structure, this component is less effective, but the slots are then shorter than before, and the desired coupling is thereby reduced. Fig. 7 illustrates both possible configurations.

Experimental tests made for a range of values of ϕ from 0° to 45° gave a range of bandwidths for two different windows that were considerably wider than for

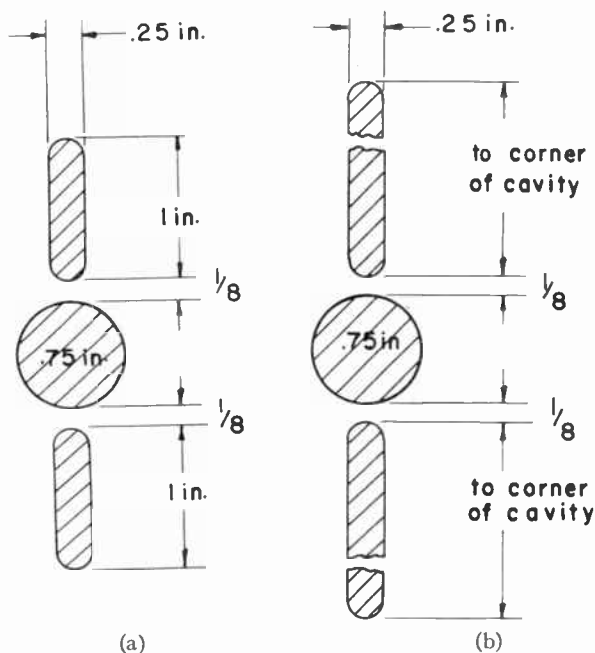


Fig. 9—(a) Window dimensions used for curve A in Fig. 8, (b) Window dimensions used for curve B in Fig. 8.

the simple rectangular structure. The results are presented graphically in Fig. 8. Curve A is measured with a window which has 1-inch by $\frac{1}{8}$ -inch slots as illustrated in Fig. 9. Curve B is measured with the other window which differs only in that the slots extend completely to the corners of the cavity for all values of the angle θ .

In summary, we conclude that the cavities made in the shape of parallelograms are capable of giving larger bandwidths when used with windows or irises which allow negative mutual inductance coupling than are rectangular cavities of the same resonant frequency. However, the increase in bandwidth obtained is not sufficient to make the devices extremely useful for traveling-wave tubes. Since the maximum bandwidth that can be obtained from the center hole alone is about 4 or 5 per cent, the slots would give very good cold bandwidth if it were possible to add more of them to the

structure so that equal amounts of coupling could be obtained through each one.

The Hourglass Structure

The next step in the program of increasing the number of useful coupling slots in a negative mutual inductance coupled structure was to make cylindrical cavities with walls pushed in on opposite ends of a diameter. This device is shown in Fig. 10. The shape of an individual cavity leads to the name "hourglass," and this structure will be referred to by that name.

Principle of Operation: From Fig. 10 one can see that the indented cavity walls cause the magnetic field to pass a slot with a fairly large component parallel to it when the cavity is resonating in what would be called the TM_{010} mode in a cylindrical cavity. Since cavity 2 is rotated 90° with respect to cavity 1, the magnetic fields for the zero mode will have large components in opposite directions in adjacent cavities. Thus the coupling is similar to that obtained in the rectangular and parallelogram structures, but there are now four useful slots instead of two. The component of field which corresponds to H_x in the rectangular structure now makes a large angle with respect to the slot, and thus does not adversely affect the frequency of the π mode to any extent. While no attempt has been made to arrive at a criterion for determining the resonant frequency of this cavity, it is apparent that a square cavity with sides deformed into the structure shown in Fig. 10 will have a higher resonant frequency than the original square cavity. In practice it has been found that the slots will not be resonant in the pass band. If the sides of the cavity are pushed in further to raise the resonant frequency, the distance between them will become smaller, and the axial electric field will become nonuniform across the center hole.

Experimental Results: The test structure was made from rings of 4.5-inch diameter. The resonant frequency of the cavities was 2780 mc in the TM_{010} mode of a cylindrical cavity. Bandwidth between the zero and π modes was 380 mc or about 14 per cent, with only 60 mc (2.2 per cent) of this bandwidth due to capacitive coupling through the center hole.

The hourglass structure shows considerable promise as a traveling-wave-tube circuit, since the bandwidth, while not extraordinary, is adequate for some applications and can very likely be improved by refinements in the design. Impedance, while not measured, should be very good since the size of the coupling hole is small with respect to the other cavity dimensions.

Added bandwidth was obtained by increasing the number of slots, as can be seen by comparing the results to those of the rectangular and parallelogram structures. Doubling the number of slots has essentially increased the bandwidth obtained from negative mutual inductance coupling alone from about 6 per cent to nearly 12 per cent.

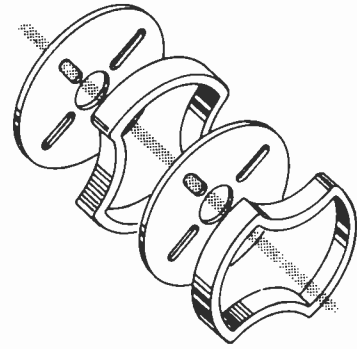


Fig. 10—"Hourglass" structure.

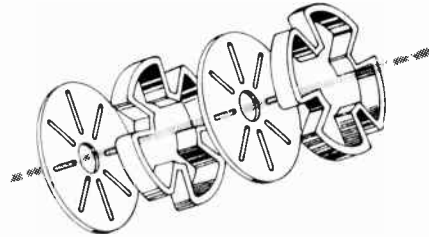


Fig. 11—"Clover-leaf" structure.

The Clover-Leaf Structure

When one contemplates methods of altering the hourglass structure in order to increase the coupling by making the magnetic field component parallel to the slot larger in magnitude, one can think of pushing cavity walls more toward the center of the structure in appropriate places. However, this may not be practical in these existing structures because of the proximity of the center coupling hole to the walls. An alternative designed to provide good coupling at the slots, as well as to provide more slots than the previous structures, is that illustrated in Fig. 11. The cavity consists of a cylindrical pipe with the walls indented at 90° intervals around the periphery. The indentations will henceforth be identified as "fingers."

In the TM_{01} cylindrical waveguide mode, the magnetic field lines are circumferential, so that the fingers cause a large radial component of this field to appear adjacent to each one. The inclusion of a slot adjacent to a finger will then allow a large amount of magnetic coupling to occur through each slot. Cavity 2 is rotated 45° with respect to cavity 1, so that the H fields in the zero mode will have opposite directions on either side of the slot. The situation is illustrated in Fig. 11. The coupling is again negative mutual inductance. The appearance of the magnetic field lines when viewed from the end of the cavity is similar to that of a four-leaf clover, hence the name, "clover-leaf structure."

Physical Construction: Several test cavities were constructed with fingers of various sizes to determine their effect on resonant frequencies and bandwidths between the zero and π modes for identical windows. In several cavities the diameter was arbitrarily set at $4\frac{1}{2}$ inches. The resonant frequency of a cylindrical cavity of

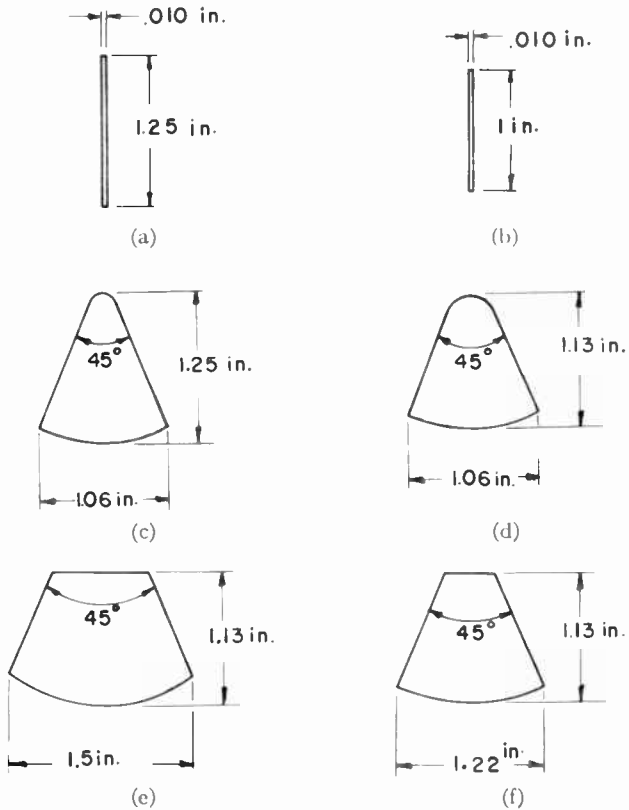


Fig. 12—Resonant frequency of TM_{010} cavity mode for 4.5-inch diameter cavity loaded with fingers of dimensions shown. (a) $f_0 = 3070$ mc; (b) $f_0 = 2630$ mc; (c) $f_0 = 3320$ mc; (d) $f_0 = 3010$ mc; (e) $f_0 = 3345$ mc; (f) f_0 not measured.

this diameter resonating in the TM_{010} mode is 2010 mc; the finger dimensions must be set so that this frequency is raised to somewhat above 3000 mc if the band-pass is to be centered there. Fig. 12 shows fingers of various sizes and the resonant frequencies of the cavities formed from the ring with four identical fingers mounted at 90° intervals around the interior of the ring.

The slots should be as long as possible to obtain maximum coupling. However, they must not be so long that they become resonant in the pass band or extremely odd results occur. Assuming there is a maximum length of slot that can be used without obtaining resonance, the position of the slot is dictated by the amount of bandwidth one can obtain with the slot in various positions. It turns out that to get the optimum bandwidth the slot should be as near the center hole as possible. The width of the slot was fixed at $\frac{1}{4}$ inch, as further increases in width do not add a great deal to the bandwidth (Fig. 13). Also, this width should be sufficient to prevent any breakdown across the slot due to the component of electric field that appears there whenever the power is flowing through it.

Pass Band Measurements: Several tests were made to determine the width of the pass band between the zero and π modes of several structures made with various size fingers and various types of windows. The results of the tests taken largely on two half sections are given in Fig. 14, which shows the percentage band-

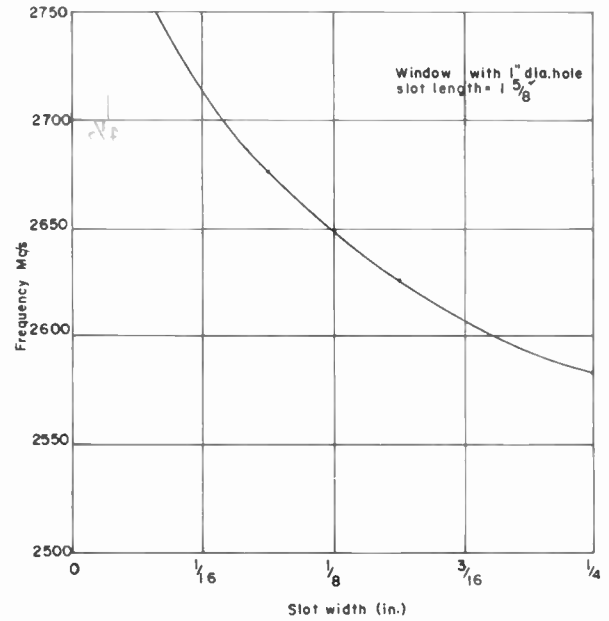


Fig. 13—Variation in lowest cutoff frequency vs slot width of a clover-leaf structure.

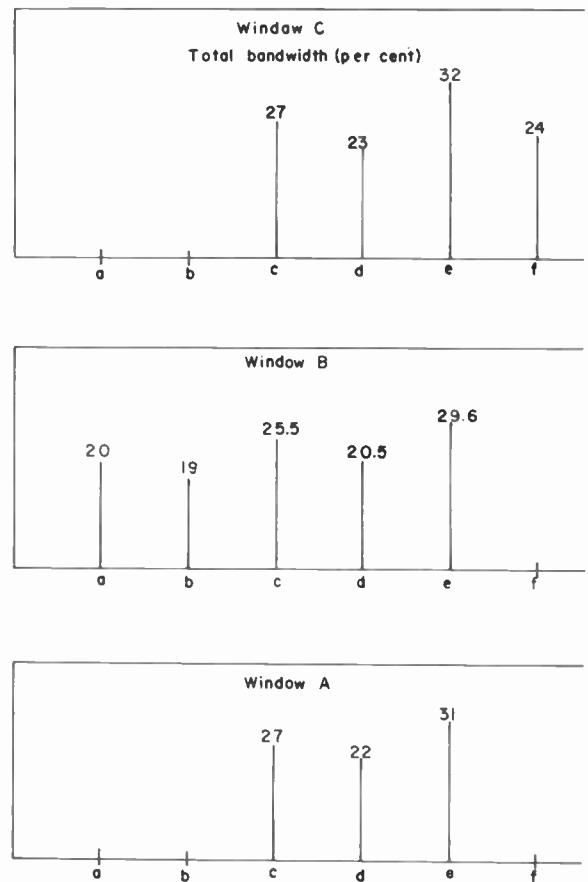


Fig. 14—Percentage bandwidth obtained with various types of fingers for three different windows.

width for the various types of fingers, and for several different windows. The windows used are shown in Fig. 15. The percentage bandwidth is defined as:

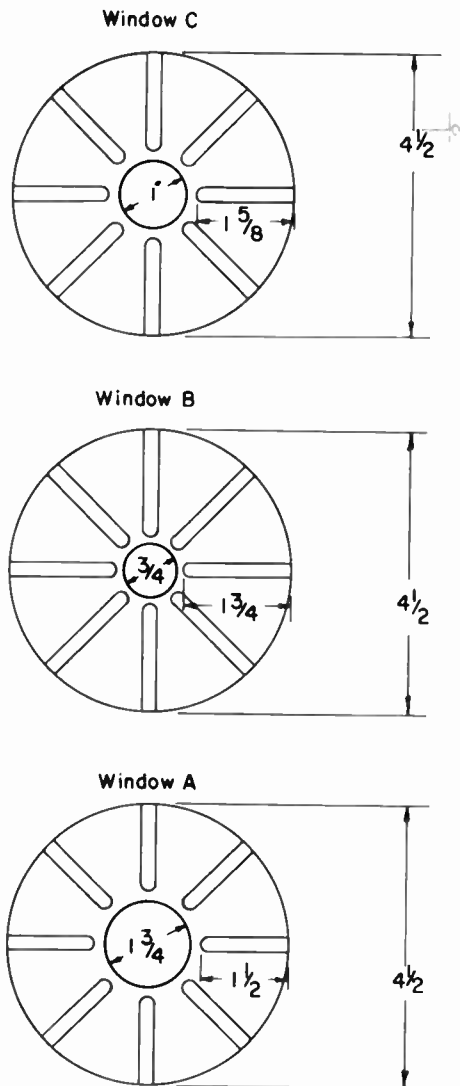


Fig. 15—Different types of windows used for tests of clover-leaf structures.

$$\frac{2(f_{\pi} - f_0)}{f_{\pi} + f_0} \times 100 \tag{14}$$

where

f_0 = frequency of the zero mode

f_{π} = frequency of the π mode.

The combination of window and finger which was used in impedance tests was not that which gave the best bandwidth; it was a fair compromise between bandwidth and other factors. The finger used with window C of Fig. 15 was that shown in Fig. 12(f). Tests showed that this combination would avoid the presence of the next higher (TM_{110}) mode in the desired pass band. The effect of this mode extending into the pass band is discussed in a later section.

The shape of the pass band of the clover-leaf structure was determined by resonant cavity techniques for structures with two different types of fingers and windows using the results shown in Fig. 16, where fre-

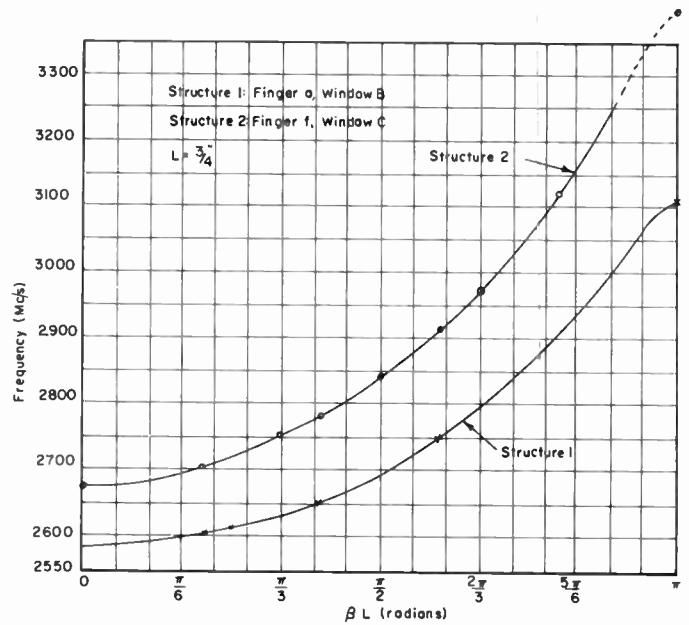


Fig. 16—Frequency vs phase shift per section for two different clover-leaf structures.

quency is plotted as a function of βL . It is important to note the shape of the pass band which is approximately the same for both structures. It is quite likely that all the structures of this type will have similarly shaped pass bands, and very little additional experimental information (other than the two cutoff frequencies) will be needed to predict the performance of the device as an rf circuit for a traveling-wave tube.

In order to determine the slope near the π mode a structure was made of about 16 sections, and the pass band was measured at intervals of phase shift of $\pi/16$ radians per section. Two such structures were constructed. The first one had an anomaly in the pass band which did not appear when making tests on only three or four sections. Fig. 17 shows the appearance of this anomaly. It was found that the slots in this structure were of such length that they could be resonant in a TEM type of transmission line mode near the upper end of the pass band. For such resonant slots the equivalent circuit for the structure becomes that shown in Fig. 18, and a conventional circuit analysis will indicate that with the resonant frequencies of the two types of circuits close together, the variation of the pass bands and their characteristics will be quite different than for the case of the slot resonance far from the cavity resonance. Also, with the closely spaced resonances, the field distribution may be such that some stop bands may not be easily detectable. A second structure had the slots shortened in order to move the resonance of the slot to a frequency out of the pass band of interest. This was done with the sacrifice of some bandwidth. Unless an anomaly actually occurs in the pass band of the structure, the same general shape pass band is obtained under almost all conditions; the difference in slot lengths, and the difference in the shapes of the fingers,

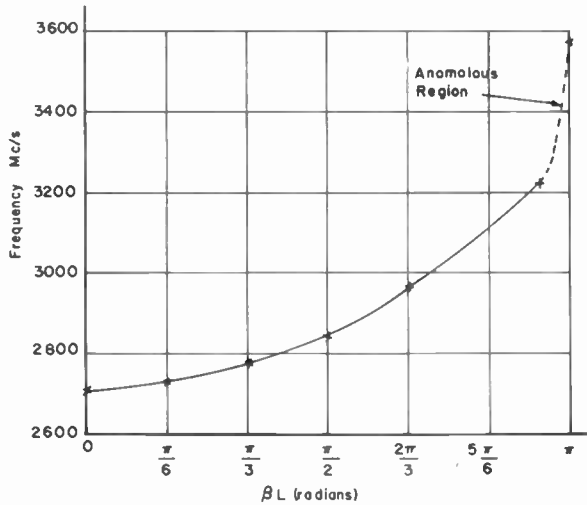


Fig. 17—Pass band of a clover-leaf structure showing an anomalous region.

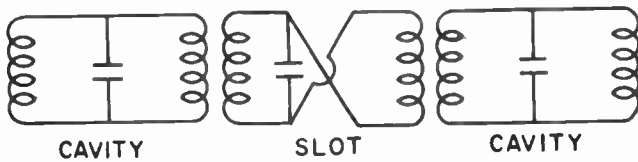


Fig. 18—Equivalent circuit of negative mutual structure with resonant slots.

is not too important in the (general) shape of the propagation characteristic.

Impedance Measurements: The circuit impedance for each structure is determined by methods described in various places in the literature.⁷⁻¹¹ In general, for each circuit, two separate resonators were constructed: one of two sections such as that shown in Fig. 19, and one of three sections. Thus, we could measure E^2/W at the 0, $\pi/2$, and π modes in the two-section length, and at the 0, $\pi/3$, $2\pi/3$, and π modes in the three-section length. These two lengths could be clamped together to form one length of five sections for the purpose of measuring E^2/W at six resonant frequencies to get a better idea of the variation over the width of the pass band. Fig. 20 shows the values of v_0 and v_p over the pass band as calculated from the curves of Fig. 16.

The Interlaced Structure

Another structure has been devised which also has negative mutual inductance coupling as shown in Fig.

⁷ T. Moreno, "A New Type Directional Coupler for Waveguides," Sperry Gyroscope Co. Rep.; July 17, 1946.

⁸ W. W. Hansen and R. F. Post, "On the measurement of cavity impedance," *J. Appl. Phys.*, vol. 10, pp. 1059-1061; November, 1948.

⁹ E. J. Nalos, "Measurement of circuit impedance of periodically loaded structures by frequency perturbations," *Proc. IRE*, vol. 42, pp. 1502-1511; October, 1954.

¹⁰ C. H. Papas, "On Perturbation Theory of Electromagnetic Cavity Resonators," TR-No. 3 (Nonr-22014), Calif. Inst. Tech.; March, 1954.

¹¹ L. C. Maier, "Field Strength Measurements in Resonant Cavities," TR-No. 143, Mass. Inst. Tech. Res. Lab. of Elec.; November 2, 1949.

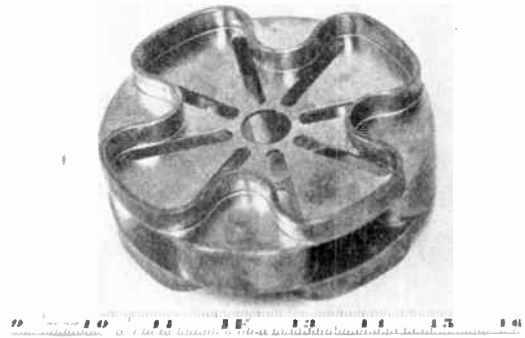


Fig. 19—Photograph of brazed two-section clover-leaf cavity.

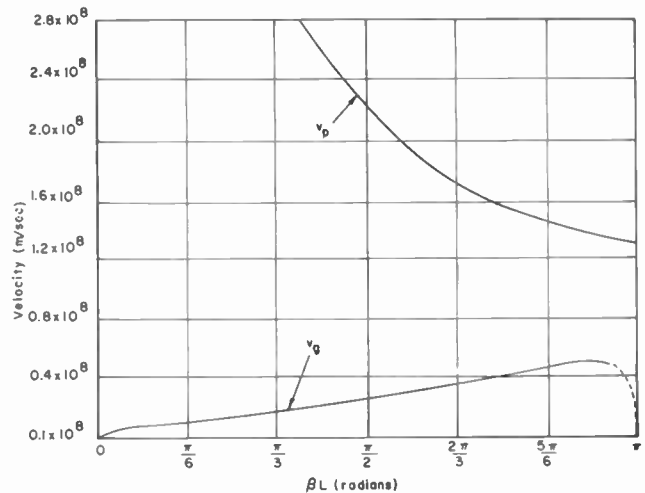


Fig. 20—Velocities in a clover-leaf slow-wave circuit.

21. It consists of using reversed coupling loops to couple adjacent cavities. This is a method of producing the equivalent circuit of Fig. 18. It is to be expected that such reversed loops will give pass band characteristics like the slots in the clover leaf.¹²

An extension of the principal outline above is the addition of many loops around the entire structure. The metallic wall between the loops can be omitted without any deleterious effects in performance. The resulting section is shown in Fig. 22.

A pass band on several sections of the circuit was measured by resonant methods, and is plotted in Fig. 23. The cutoff frequency of the unloaded pipe is indicated on this figure for reference purposes. The pass band is not affected by rotation of the respective cavities, *i.e.*, the loops can be mirror images from one cavity to the next, or a direct translation, with no apparent differences in performance.

¹² This turns out to be true in practice but the end of the pass band which is strongly perturbed (*i.e.*, 0 mode pushed down or π mode up) will depend on the location of the loop resonant frequency relative to the cavity resonance and the results must be interpreted cautiously. We are indebted to P. Dunn and L. Mullett of A.E.R.E., Harwell, who devised a similar circuit for a proton accelerator for pointing out some of the idiosyncracies of such coupling loops.

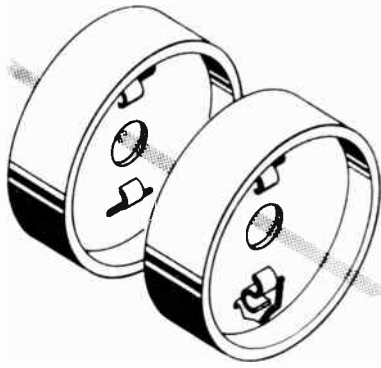


Fig. 21—Simplified diagram showing negative mutual coupling.



Fig. 22—Schematic of "interlaced" negative mutual structure.

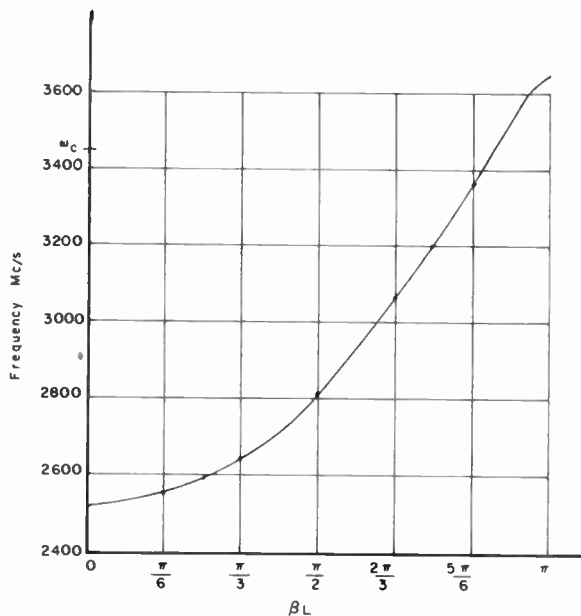


Fig. 23—Pass band of a typical interlaced structure.

The impedance of this circuit is roughly the same as that of the clover leaf when measured by a metallic plunger. This fact is extremely encouraging in view of the additional bandwidth which the "interlaced" type of circuit has shown compared to the others tested.

Further tests are planned in order to determine the effect of varying the number of loops in the cavity, their

shape, and the area that each loop intercepts, on the bandwidth and electronic impedance. The circuit appears promising enough to warrant further investigation as a circuit for high-power traveling-wave tubes.

PREDICTED PERFORMANCE OF THE CLOVER-LEAF STRUCTURE

Of the several structures discussed thus far, it was decided to investigate the clover-leaf more completely as a possible twt circuit. Detailed measurements were made on several slightly different clover-leaf circuits, and the results were combined to give a gain vs frequency characteristic. In the following part, the methods of calculation and the approximations made in each are outlined in some detail.

The circuit impedance $E_0^2/\beta^2 W v_0$ was determined experimentally for the clover-leaf structures by perturbation techniques, and the values of v_0 found from Fig. 20. All structures tested were designed for operation at a voltage near 100 kv. The voltage determines the section spacing (the spacing between disks). All of these structures are quite dispersive, that is, there is a wide difference in the phase and group velocity over the entire pass band. This means that synchronization will ordinarily occur over a small frequency band.¹³ The value of β is known from the geometry of the structure and the measured pass band characteristic; the only remaining factor to be found is E_0^2/W . The results are plotted in Fig. 24 as a function of βL .

Calculation of Gain

Once the value of $E_0^2/\beta^2 W v_0 = E_0^2/\beta^2 P$ has been determined, it is a simple matter to calculate the gain parameter C from the relation

$$C^3 = \frac{E_0^2}{2\beta^2 P} \frac{I_0}{4V_0} \quad (15)$$

using the known perveance. The impedance $E_0^2/2\beta^2 P$ is plotted as a function of βL , the phase shift per section, in Fig. 25, and C is plotted against the same abscissa with beam voltage as a parameter in Fig. 26. As expected, the impedance varies widely over the pass band. In an elementary analysis one finds that it becomes infinite at each cutoff frequency since, in a lossless structure, the group velocity is infinite there. However, since the cavity Q is finite (*i.e.*, some loss is present), the attenuation increases as the group velocity decreases according to the relation

$$\alpha = \frac{\omega}{2Q_0 v_g} \quad (16)$$

¹³ However, with the dimensions suitable for these high voltages, the impedance of these structures and also the gain parameter C is quite high. QC , the space charge parameter, will be correspondingly small and this combination of very high C and small QC will result in uniform gain over a much wider deviation from synchronizing than with more conventional values of these parameters.

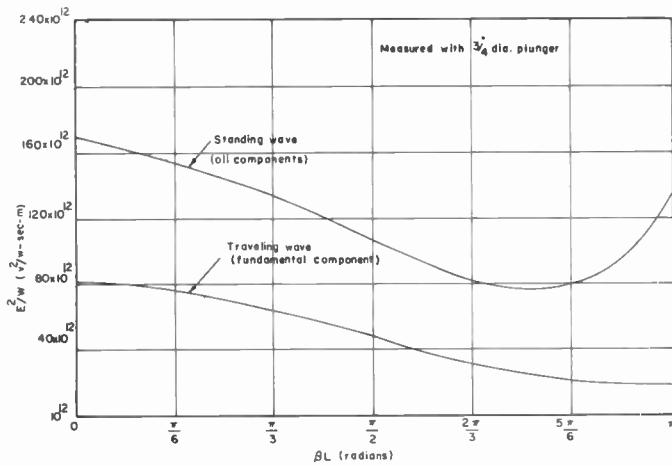


Fig. 24—Plot of E^2/W for a clover-leaf structure.

Having determined the value of C over the frequency band, one can then use standard methods to complete the gain calculation.⁵ A length for the rf circuit of 50 cm was chosen so that a gain of approximately 20–30 db would result when 15-db total loss was uniformly distributed over the length. We have not concerned ourselves with the problem of efficiency at this point, or the loss would be distributed in some other fashion. The value of BCN has been calculated for a typical clover-leaf structure, and is plotted vs frequency with beam voltage as a parameter in Fig. 27. Since the gain in db is expressed as

$$G = A + BCN \tag{17}$$

we have only to compute A which can be done by means of published curves.^{14,15} Typically, A may vary from -6 to -12 db.

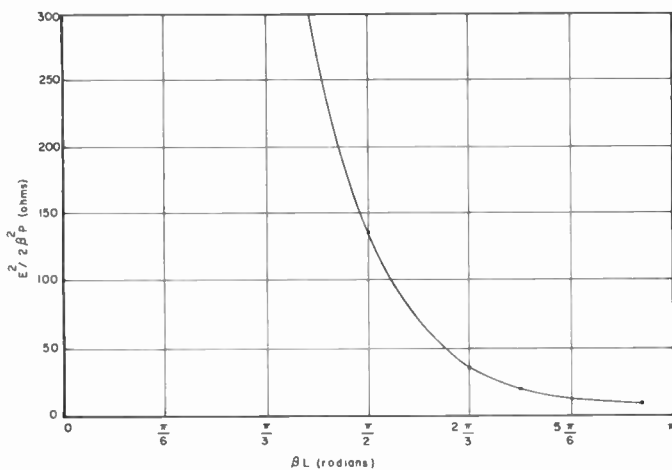


Fig. 25—Circuit impedance of a clover-leaf circuit in fundamental mode.

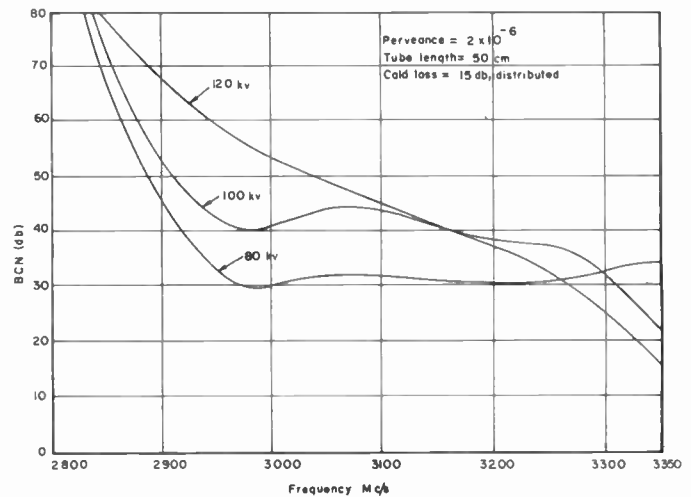


Fig. 27—Gain of a clover-leaf twt.

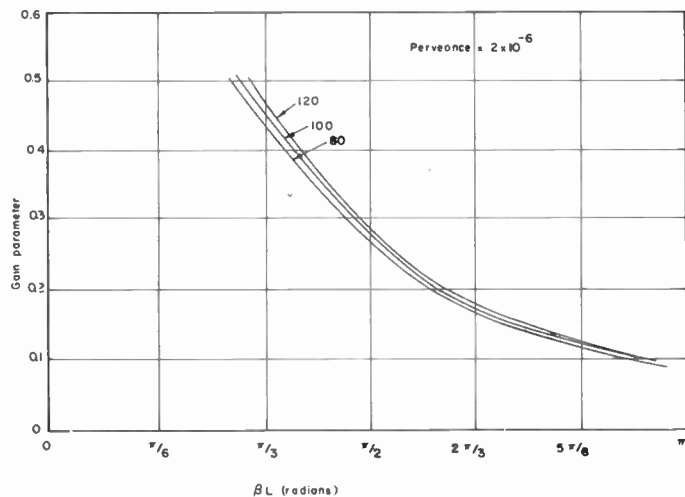


Fig. 26—Gain parameter of a clover-leaf structure.

The gain characteristic appears to be fairly flat over a 10 per cent frequency band. The high gain of the low-frequency end of the device is a result of increasing C and decreasing QC with an assumed constant value of attenuation. In actual practice the increased attenuation near the band edge may make these calculated values unrealistic.

Higher-Order Modes: Any waveguide has an infinite number of propagating modes with various field configurations which satisfy Maxwell's equations. A loaded waveguide can be expected to have similar modes, each divided into a series of pass and stop bands because of the periodic loading. The clover-leaf structure will have all the TM modes (which are the ones of interest) per-

where α is the attenuation constant, and Q_0 is the unloaded Q of the structure. Thus, the gain will likely be finite at these points.

¹⁴ G. R. Brewer and C. K. Birdsall, "Normalized Propagation Constants for a Traveling-Wave Tube for Finite Values of C ," Hughes Aircraft Co. (Res. and Dev. Labs.), TM-No. 331; October, 1953.

¹⁵ C. K. Birdsall and G. R. Brewer, "Traveling-Wave Tube Propagation Constants for Finite Values of C ," Hughes Aircraft Co. (Res. Labs.) TM-No. 396; June 23, 1955.

turbed to a higher frequency than the unloaded circular guide, but each mode will be perturbed differently by the fingers, and thus the percentage frequency change will be different.

The question which immediately comes to mind is that concerning the possibility of interference between two modes when the cavities are connected by irises to make an rf circuit for a twt. One might expect that the lowest pass bands of the TM_{010} and TM_{110} resonant cavity modes might interfere for long coupling slots and relatively large fingers in the cavities; experimental tests confirm this expectation.

It was found that the lowest resonant frequency of the TM_{110} mode was relatively unaffected by changes in the slot width, but was greatly affected by the change in size of the center hole. Small increases in the size of the center hole decrease the slot length, and thus decrease the bandwidth, since relatively little electric coupling occurs through the center hole.

Tests made with several different fingers and windows

indicate that the maximum bandwidth obtainable in the TM_{01} waveguide mode pass band without overlap with the TM_{11} mode is about 700 mc at 3000-mc center frequency. However, for the TM_{11} mode there is relatively little axial electric field in the beam aperture, and what little exists there is in opposite directions on either side of the beam, so there is no net coupling to a truly axial beam.

Tests to date do not indicate that there are any great difficulties with the presence of the TM_{11} mode in the pass band, but we merely mention it here as a fact that should not be overlooked in the design of these structures.

Efficiency: Since the efficiency is intimately related to various parameters which are themselves interrelated, it is quite difficult to compute accurately. Leaving out the attenuation problem, all experimental and theoretical considerations of efficiency made to date indicate that a high C , low QC tube such as calculated here might have a very high efficiency.



CORRECTION

Johannes Labus, author of the paper "Space-Charge Waves Along Magnetically-Focused Electron Beams," which appeared on pages 854-861 of the June, 1957 issue of PROCEEDINGS, has brought the following errors to the attention of the editors.

In (31), page 860, i_z and i_ϕ should be replaced by Δi_z and Δi_ϕ .

In the sentence preceding (37), page 861, H_z should be replaced by ΔH_z .

On Multimode Oscillators with Constant Time Delay*

VIKTOR MET†

Summary—Special emphasis is paid to narrow-band systems with a small number of modes, and to high switching speed.

Sufficient stability conditions presented have been derived by use of a first-order Taylor approximation, which substantially reduces algebraic complexity. The system may deviate considerably from quasi-linearity.

Graphical interpretation of stability and transients permits application to curve data and is believed to give an easily visualized explanation for experimental observations. Mode switching speeds of 7 m μ sec could be achieved with an S-band bistable oscillator.

INTRODUCTION

PROPERTIES of oscillators with several degrees of freedom have been extensively described in literature.¹⁻¹¹ Van der Pol discusses the case of two degrees of freedom,^{1,2} and more recently various experimental and theoretical investigations have been reported.³⁻¹¹

The expression "frequency memory" has been connected with multimode oscillators, indicating one of their fundamental characteristics: A suitable instruction signal, *i.e.*, the mode frequency to be memorized, switches such an oscillator from one mode to another. More than two stable states are directly available without complicating the basic circuit. This is an advantage over analog memory devices operating in the ampli-

tude domain. Still, circuits incorporating wide bandwidth and minimum delay are prerequisite for high-speed operation, but the bandwidth has to cover a certain range of rf frequencies, and we have a natural application of broad-band microwave devices.

As a first step towards a multimode memory, technical realizability of bistable oscillators at microwave frequencies has been investigated and is reported here. The conclusions made in previous analyses had to be modified and extended, according to selectivity in the recirculation loop and deviation from quasi-linearity.

To demonstrate the basic mode-switching phenomena with least complexity, a graphical approach will be represented to render useful qualitative as well as explicit results.

Most of the theoretical analysis lacks mathematical rigor due to the complicated nature of the problem. Transient effects will be neglected for the stability criteria, and since we shall allow for fast growth and considerable nonlinearity, the results cannot be expected to be as accurate as for quasi-linear systems. It will turn out that our results are closely related to Cunningham's work,⁹ and that our system exhibits distinct limit-cycles of different frequencies, the choice of which will depend on initial conditions.

FORMULATION OF THE PROBLEM

A basic multimode oscillator consists of a broad-band amplifier and a suitable feedback network, as shown in Fig. 1. Proper termination of adjacent components in the loop is assumed.

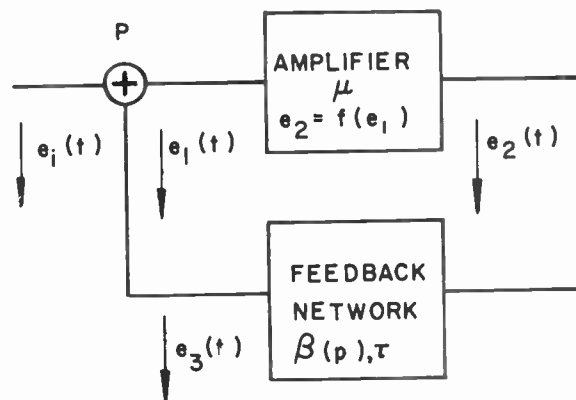


Fig. 1—Basic recirculation system.

For convenience, the amplifier is specified to have neither frequency dependence nor delay. In its linear region it provides gain μ in the loop, and saturation occurs for large levels due to nonlinear effects. Trans-

* Original manuscript received by the IRE, December 10, 1956; revised manuscript received, May 13, 1957.

† General Electric Microwave Lab., Palo Alto, Calif.

¹ B. van der Pol, "An oscillation hysteresis in a triode generator with two degrees of freedom," *Phil. Mag.* (London), vol. 43, p. 700; 1922.

² B. van der Pol, "The nonlinear theory of electric oscillation," *Proc. IRE*, vol. 22, p. 1051; September, 1934.

³ T. B. Warren, Confidential Technical Rep. No. 25 (NR 377 362); August 20, 1953. Reference to this work is made in the following reports of the Elect. Res. Lab., Stanford University:

R. W. De Grasse, "Stability of Multi-Mode Oscillatory Systems," Tech. Rep. No. 18; August 9, 1954.

K. Amo, "Signal-to-Noise Discrimination in Amplitude Limiters," Tech. Rep. No. 17; August 2, 1954.

M. E. Disman, "Registers and Counters Based on Frequency Memory," Tech. Rep. No. 19; August 16, 1954.

H. C. Lee, "Linear Analysis of Multi-Mode Oscillatory Systems," Tech. Rep. No. 20; July 26, 1954.

⁴ W. A. Edson, "Multiple resonance effects in oscillators," *Proc. of the Natl. Elect. Conf.*, vol. 9, pp. 171-177; 1954.

⁵ W. A. Edson, "Frequency memory in multi-mode oscillators," *IRE TRANS.*, vol. CT-2, pp. 58-67; March, 1955.

⁶ W. J. Cunningham, "Nonlinear Oscillators with Constant Time-Delay," Rep., Dunham Lab., Yale University; August, 1955.

⁷ F. E. Pickel and P. H. Rogers, "A Study of Recirculation as a Frequency Memory Device," Tech. Rep. No. 46, Eng. Res. Inst., University of Michigan; March, 1955.

⁸ W. A. Edson, "Frequency Memory Using a 15 Mc/s Fused Quartz Delay-Line," Tech. Rep. No. 25, Stanford University; February 21, 1955.

⁹ W. J. Cunningham, "Graphical solution of certain nonlinear differential-difference equations," *J. Franklin Inst.*, vol. 261, pp. 621-629; June, 1956.

¹⁰ H. C. Lee, "A Flip-Flop Circuit Based on Frequency Memory," Tech. Rep. No. 81, Stanford University; January 30, 1955.

¹¹ L. D. Smithy, "The Traveling-Wave Amplifier as a Multimode Oscillator," Thesis, U. S. Naval Postgraduate School, Monterey, Calif.; 1956.

mission through the amplifier shall be completely described by the function $e_2=f(e_1)$.

The natural modes of the system are determined by the properties of the feedback network. Following previous notations, a transfer function $\beta(p)$ and a constant delay τ are defined, which corresponds to separation into a lumped-constant network and an ideal delay-line.

The junction P provides a means to impress an external driving signal $e_i(t)$, which we shall refer to as instruction signal.

LINEARIZED ANALYSIS OF THE MULTIMODE OSCILLATOR

For sufficiently small signals $e_1(t)$ we may neglect higher order terms in the series expansion of e_2 , and we have

$$e_2(t) = \mu e_1(t). \tag{1}$$

From definition of the junction P we obtain the feedback equation

$$e_1(t) = e_3(t) + e_i(t), \tag{2}$$

and with

$$e_3(t) = \mathfrak{D}[e_2(t - \tau)], \tag{3}$$

where \mathfrak{D} defines a differential operator equivalent to $\beta(p)$ in time domain, we can write

$$e_1(t) = \mathfrak{D}[\mu e_1(t - \tau)] + e_i(t). \tag{4}$$

This represents a linear differential-difference equation, which is readily converted into an algebraic equation by applying the Laplace transform:

$$E_1(p) = \mu\beta(p)e^{-p\tau}E_1(p) + E_i(p), \tag{5}$$

where $E_1(p) = \mathcal{L}[e_1(t)]$ and $E_i(p) = \mathcal{L}[e_i(t)]$.

To find the natural modes p_n of the system we ask for values $E_1 \neq 0$ if $E_i = 0$, and from (5) we obtain

$$p_n = \sigma_n + j\omega_n = \frac{1}{\tau} \{ \log |\mu\beta(p_n)| + j[\arg \mu\beta(p_n) + 2n\pi] \}. \tag{6}$$

The steady states of the nonlinear system correspond to particular pairs of conjugate complex roots of (6), after nonlinear effects have shifted a pair onto the $j\omega$ -axis. The corresponding frequencies ω_n shall be referred to as mode frequencies. In this situation all other roots lie further in the left half of the complex frequency plane due to small signal discrimination properties.¹² With $\sigma_n = 0$, and as $\beta(p_n) = \beta(j\omega_n)$, (6) is readily solved in this case:

¹² It is tacitly assumed here that small signal discrimination provides stability. All nonlinear effects are assumed to be of a purely resistive nature and merely reduce the loop gain for all signals, simultaneously creating new frequencies. For specified driving conditions we may define an equivalent linear resistive network for the nonlinear amplifier, and include generators for the new frequencies.

$$\omega_n = \frac{1}{\tau} [2n\pi + \arg \mu\beta(\omega_n)] \doteq \frac{2n\pi}{\tau} \text{ for } n \gg 1, \mu > 0, \tag{7}$$

since $\arg \beta(p_n) \ll 2n\pi$. Experimental observations show that the ω_n thus defined are useful approximations for the steady states of the recirculation system.

The mode spacing $\delta\omega_n$, which is of some practical interest, is readily obtained as

$$\delta\omega_n = (\omega_{n+1} - \omega_n) = \frac{1}{\tau} (\arg \beta_{n+1} - \arg \beta_n + 2\pi). \tag{8}$$

For narrow-band systems the contribution of the transfer-phase terms in (8) cannot be neglected and causes decreased mode spacing. On the other hand, for systems with a large number of modes and flat gain, $(\arg \beta_{n+1} - \arg \beta_n) \ll 2\pi$ and

$$\delta\omega_n \doteq \frac{2\pi}{\tau}. \tag{9}$$

To estimate σ_n one has to consider that $\beta(p)$ may have poles and zeros in the region close to the $j\omega$ axis, and hence may vary appreciably over a small neighborhood near a specific value p . For flat $\beta(\omega)$ these singularities may be sufficiently remote and an approximation $\beta(p) \doteq \beta(j\omega)$ is then permissible. Then with (6) $\sigma_n = 1/\tau \log |\mu\beta(j\omega_n)|$, which means that the exponential growth factor is proportional to $1/\tau$ and $\log |\mu\beta_n|$.

If an instruction signal $e_i(t)$ is switched on at $t=0$, a step perturbation corresponding to the recirculation time τ occurs. A series representation may be obtained with the aid of the Laplace transform, but the phenomenon is readily visualized directly if a "flat" system with infinite bandwidth is assumed.

Then for

$$e_i(t) = \begin{cases} 0 & t < 0 \\ A_i \cos \omega t & t \geq 0, \end{cases}$$

and with the total phase shift associated with ω a multiple of π , one immediately obtains the series

$$e_1(t) = A_i \cos \omega t \sum_{n=0}^{N-1} (\mu k)^n, \quad N\tau \leq t < (N+1)\tau, \tag{10}$$

for the $(N+1)$ st interval.

The quantity μk is a real constant in the special case and equals $\mu\beta$. The sign of μk denotes favorable or unfavorable phase condition. The amplitudes converge for $|\mu k| < 1$, or net loss in the loop. For $|\mu k| > 1$, or net gain in the loop, the amplitudes diverge.¹³

In previous papers it has been found convenient to think in terms of mode spacing rather than recirculation time, as far as switching speed of physical systems was

¹³ It is interesting to note that the amplitudes associated with a frequency, for which the phase condition is unfavorable, increase in the fashion of a divergent, alternating series. This illustrates the fact, that the nonlinear characteristic determines the stable state in the physical case, and that the linear solution might describe a disturbance only.

concerned. Obviously the direct relationship is between switching speed and effective recirculation time. In narrow-band systems, this effective recirculation time will be larger than τ , by an amount given by the group delay and transient time of the lumped-constant part of the feedback network. This has to be considered if mode spacing is related to switching speed, using (9). Assuming minimum transient time of the corresponding networks, larger mode spacing will imply smaller effective delay, and higher switching speed. If the spacing between two modes of a system shall serve to denote switching speed, another obvious consideration is that there are to be no suppressed modes between the two, as may be caused by insufficient loop gain for certain frequencies.

For maximum switching speed the effective loop delay should be minimized. After eliminating all possible constant delay, the transfer phase may be properly shaped in narrow-band devices, to minimize the group-delay in the frequency range of interest.

Consider a two-mode system obtained from an ideal, flat one by insertion of a band-pass filter of proper bandwidth into the recirculation loop. Loop gain and phase characteristic are plotted in Fig. 2 for both cases.

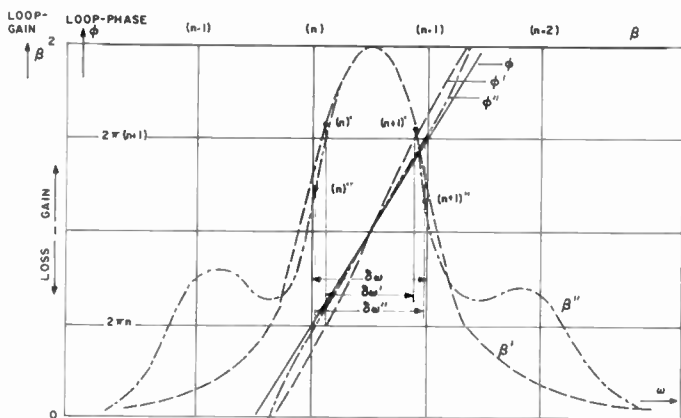


Fig. 2—Gain and associated phase characteristics.

The filter causes increased slope of the phase characteristic in the region of interest and $\delta\omega' < \delta\omega$. A simple approximation shows 33 per cent mode compression for a filter bandwidth equal to the “flat” system mode spacing. The compression may be reduced using a scheme given by Bode,¹⁴ which is indicated by the characteristics β'' , Φ'' . Proper shaping of the gain outside of the region of interest results in phase correction as indicated. For more than two modes, stability restrictions imposed on the gain characteristic will make application of this scheme more difficult, but proper phase equalization to obtain uniform mode spacing would be highly desirable.

¹⁴ H. W. Bode, “Network Analysis and Feedback Design,” D. Van Nostrand Co., New York, N. Y.; 1945.

NONLINEAR ANALYSIS OF THE MULTIMODE OSCILLATOR

Approximation of the Nonlinearity

We specify the nonlinear characteristic by a power series in e_1 as

$$e_2(t) = f[e_1(t)] = \sum_{\nu=0}^{\nu=\infty} a_{\nu} [e_1(t)]^{\nu}. \tag{11}$$

The loop shall be chosen to permit $2M+1$ mode frequencies in a frequency band $[\omega_{-M}, \omega_M]$. All frequencies outside of this region are dissipated in the feedback network. For $\omega_M > \omega_{-M}$ and $\omega_{-M} = \frac{1}{2}\omega_M + \epsilon$ a mode distribution can be prescribed, such that even terms of the power series render no contribution in this frequency range and may be neglected.¹⁵ This only has to be considered for terms of powers larger than three, since the second power term is automatically excluded from contribution in the interval $[\omega_{-M}, \omega_M]$. Thus, in most cases van der Pol's approximation^{1,2}

$$e_2(t) = a_1 e_1(t) + a_3 e_1^3(t) \tag{12}$$

will describe the phenomena to be investigated with sufficient accuracy, since usually the coefficients of powers larger than three will be quite small. According to our notation for the small signal gain we specify $a_1 = \mu > 0$, and $a_3 < 0$, to obtain a saturation type characteristic.

Transmission of a set of sinusoids is described by substituting

$$e_1(t) = \sum_{m=-M}^{m=M} A_m \cos \theta_m, \tag{13}$$

into (11) or (12), where $\theta_m = \omega_m t + \phi_m$.

Since we are primarily interested in systems which have a set of sustained sinusoids as steady states, transmission of small signals in presence of one large signal is of particular importance. To answer questions about stability we expand (11) into a Taylor series of the variables A_m , and will at the most include second-order terms of small quantities. Assuming one amplitude, A_0 , to be large and constant we obtain

$$e_2(t) \cong e_2(t) \Big|_{A_m=\Delta_m} + \sum_{m=-M}^{m=M} (A_m - \Delta_m) \frac{\partial e_2(t)}{\partial A_m} \Big|_{A_m=\Delta_m} + \frac{1}{2} \sum_{m=-M}^{m=M} (A_m - \Delta_m)^2 \frac{\partial^2 e_2(t)}{\partial A_m^2} \Big|_{A_m=\Delta_m} + \dots \tag{14}$$

For most stability considerations we may disregard the last term of (14). The derivatives are readily obtained from (11), and for the case of one large signal,

$$\Delta_m = \begin{cases} 0 & m \neq 0 \\ A_0 & m = 0. \end{cases} \tag{15}$$

¹⁵ Frequencies $\omega_{-m} + a\epsilon$ and $\omega_m - b\epsilon$, a and b being natural numbers, arise from the even terms and are excluded from the set of mode frequencies.

If second-order terms are to be considered and (15) is used to evaluate (14), we have to remember that all crossterms involving products of two different small amplitudes are lost.

Two-Signal Transmission

We restrict our investigations to transmission of one large and one small signal for the moment, and specify amplitudes A_L , A_s , and angles θ_L , θ_s .

For van der Pol's approximation (12), we obtain from (13), (14), and (15)

$$e_2(t) \doteq \sum_{\nu=0}^{\nu=1} a_{(2\nu+1)} [A_L \cos \theta_L]^{(2\nu+1)} + (2\nu + 1)A^{2\nu}L A_s \cos^{2\nu} \theta_L \cos \theta_s]. \quad (16)$$

Evaluating and discarding third-harmonic terms in accordance with our assumptions of selectivity we have

$$e_2(t) \doteq \left(\mu + \frac{3}{4} a_3 A^2_L \right) A_L \cos \theta_L + \left(\mu + \frac{3}{2} a_3 A^2_L \right) A_s \cos \theta_s + \frac{3}{4} a_3 A^2_L A_s \cos (2\theta_L - \theta_s). \quad (17)$$

Having considered first-order contributions of small signals, we recognize terms at ω_L and ω_s , as well as at a new frequency $(2\omega_L - \omega_s) = \omega_{-s}$. If certain pairs of mode frequencies are symmetrically located about ω_L , the frequency of the large signal, we realize that such pairs may mutually enforce each other if special phase conditions are met. The proof of this statement follows immediately from writing an analogous equation to (17) for ω_L and ω_{-s} , which will contain a term of frequency ω_s . This is Warren's³ three-signal effect, which we will discuss separately. Let us assume here that no three mode frequencies of the system constitute such symmetrical pair located about the center frequency, and that a certain minimum deviation from symmetry is guaranteed. Thus we introduce a sufficient margin to eliminate entrainment effects, which still could permit mutual enforcement for small deviations from symmetry.

For the specific values of A_L and A_s we consider (17) to be the definition of an equivalent linear network for the nonlinear fourpole. This enables us to investigate transmission at each frequency separately. Defining $e_2|_{\theta_\nu}$ as the factor of $\cos \theta_\nu$ in (17), we can write

$$e_2|_{\theta_L} = \left(\mu + \frac{3}{4} a_3 A^2_L \right) A_L \quad (18)$$

and

$$e_2|_{\theta_s} = \left(\mu + \frac{3}{2} a_3 A^2_L \right) A_s \quad (19)$$

Since $a_2 < 0$ and $\mu > 0$, we realize that transmission is more favorable for the large signal A_L than for the small signal A_s . This phenomenon has been termed small signal discrimination of the nonlinear fourpole.

Introducing the steady-state transfer coefficient of the feedback network $k_\nu = |\beta(\omega_\nu)|$ we evaluate (3) as

$$e_3|_{\theta_\nu} = k_\nu e_2|_{\theta_\nu}, \quad (20)$$

and substituting into (18) and (19) we obtain

$$e_3|_{\theta_L} = k_L \left(\mu + \frac{3}{4} a_3 A^2_L \right) A_L, \quad (21)$$

and

$$e_3|_{\theta_s} = k_s \left(\mu + \frac{3}{2} a_3 A^2_L \right) A_s. \quad (22)$$

For the large signal A_L the feedback equation has to hold, and evaluating (2) with $e_i(t) = 0$, and making use of the fact that ω_L as a mode frequency satisfies (7), one has

$$A_L = k_L A_L \left(\mu + \frac{3}{4} a_3 A^2_L \right). \quad (23)$$

For $\mu k_L > 1$ (23) has nontrivial real solutions and

$$A^2_L = \frac{4}{3a_3} \left(\frac{1}{k_L} - \mu \right), \quad (24)$$

which is the familiar result of van der Pol's analysis.^{1,2}

Stability with respect to growth of the small signal is readily checked with (22) after substituting (24):

$$e_3|_{\theta_s} = k_s \left(\frac{2}{k_L} - \mu \right) A_s, \quad (25)$$

and we find that for

$$\left| \frac{2k_s}{k_L} - \mu k_s \right| < 1 \quad (26)$$

the loop gain for the small signal is less than one. This implies that disturbances of frequency ω_s cannot grow in presence of sustained oscillation at ω_L . Specifying $k_L = 1$, which is no loss in generality since we still may prescribe μ , (26) may be written

$$-1 < k_s(2 - \mu) < 1. \quad (27)$$

For specified μ and k_L (27) states that k_s must not exceed a certain maximum value, defined by this equation.

To check stability with respect to growth of the large signal we specify $\theta_L = \theta_s$ in (16), and after substituting (24) we obtain

$$e_3|_{\theta_s} = A_L + (3 - 2\mu k_L) A_s, \quad (28)$$

where A_s now is a small disturbance at frequency ω_L , and $\omega_s = \omega_L$. The stability condition is represented by

$$|3 - 2\mu k_L| < 1. \quad (29)$$

Both (29) and (26) constitute sufficient conditions for stability of sustained oscillation at ω_L , with A_L as defined in (24). The necessity of the lower bound (-1) in (27), and an analogous equation derived from (29), cannot be claimed. Depending on the particular situation it may be replaced by $(-Q)$, $Q > 1$. This is intuitively clear since the disturbance would have to change sign in successive intervals of length τ , and cannot exist in systems of restricted bandwidth.

Since ω_L and ω_s may represent any two of the given set of mode frequencies, our result is quite general. For all combinations possible we will find that the k_ν will have to satisfy a condition $k_{\min} < k_\nu < k_{\max}$ to assure stability for each individual pair. Since we may always disregard the contributions from the third term of (27), according to our assumption of no symmetry between any three mode frequencies, we may superimpose the two-signal test. Thus we can demonstrate stability of the large signal A_L with respect to a linear combination of all mode frequencies, the most general case possible.

One could also show that upon substitution of (13) into (12), and writing an analogous equation to (23) for each component, one obtains a system of simultaneous equations describing the possibilities of simultaneous oscillation at several mode frequencies. The validity of (26) would assure that all amplitudes A_ν except one have to be zero for real solutions to exist. We merely list this statement without proof, which would follow a straightforward procedure.

Three-Signal Interaction

We shall now proceed to the investigation of the phenomenon which we recognized upon closer inspection of the frequency balance, specified by (17). Specifically, we shall state the stability conditions for a symmetrical pair of small signals $A_s \cos \theta_s$ and $A_{-s} \cos \theta_{-s}$ in presence of the large, sustained signal $A_L \cos \theta_L$, under the assumption $|\omega_L - \omega_s| = |\omega_L - \omega_{-s}|$.

Again we obtain from (12), (13), (14), and (15)

$$e_2 \Big|_{\theta_{-s}} = \mu A_{-s} + \frac{3}{2} a_3 A_{-s} A^2_L + \frac{3}{4} a_3 A_s A^2_L \frac{\cos(2\theta_L - \theta_s)}{\cos \theta_{-s}} \tag{30}$$

$$e_2 \Big|_{\theta_L} = \mu A_L + \frac{3}{4} a_3 A^3_L \tag{31}$$

and

$$e_2 \Big|_{\theta_s} = \mu A_s + \frac{3}{2} a_3 A_s A^2_L + \frac{3}{4} a_3 A_{-s} A^2_L \frac{\cos(2\theta_L - \theta_{-s})}{\cos \theta_s} \tag{32}$$

The stable amplitude for the large signal is specified by (24), and stability with respect to the large signal requires (29) to hold. To check stability of the large signal

with respect to the symmetrical pair of small signals we follow Warren's approach:³

If A_{-s} and A_s are equal and positive we can make (30) and (32) identical. Furthermore, if

$$\phi_s + \phi_{-s} = \phi_L + (2N + 1)\pi \tag{33}$$

we have $\cos(2\theta_L - \theta_s) = -\cos \theta_{-s}$ and $\cos(2\theta_L - \theta_{-s}) = -\cos \theta_s$, and both expressions assume a maximum value, since $a_3 < 0$.

$$e_3 \Big|_{\theta_{-s}, \theta_s} = \frac{k_s}{k_L} A_s = \frac{k_s}{k_L} A_{-s}, \tag{34}$$

which means that the symmetrical disturbance may grow for

$$k_s > k_L. \tag{35}$$

It is interesting to note that the growth of the symmetrical disturbance depends on k_s/k_L only, and is independent of the small signal gain μ .

For $k_s < k_L$ the three-signal effect cannot appear, and the center mode is stable.

Warren states that the frequency characteristic of the loop has to be concave downward for stability with respect to the three signal effect. This curvature has to be prescribed in accordance with (26), and cannot exceed a certain maximum degree, if stability of some modes is not to be lost. For our stability tests we evaluated the steady-state loop gain for the small signal, and concluded stability if it turned out to be less than one. The degree of nonlinearity will be of no influence due to the resistive nature assumed, but transients would have to be considered for rates of growth of the order of τ . We may argue though, that transients will merely slow down the process of growth of a disturbance, and that our results are still valid, as crude an approximation as they might be.

GRAPHICAL METHOD OF ANALYSIS AND QUALITATIVE TREATMENT OF MODE SWITCHING

Two-Signal Transmission in a Normalized Cubic Nonlinearity

For our van der Pol approximation of the nonlinearity

$$e_2(t) = a_1 e_1(t) + a_3 e_1^3(t) \tag{36}$$

we may always normalize e_1 and e_2 to convert (36) into

$$\bar{e}_2(t) = \frac{3}{2} \bar{e}_1(t) - \frac{1}{2} \bar{e}_1^3(t). \tag{37}$$

The normalized voltages \bar{e}_1 and \bar{e}_2 are defined as $\bar{e}_2 = e_2/e_{2\max}$ and $\bar{e}_1 = e_1/e_1(e_{2\max})$. We still have the linear transmission parameter $\beta(p)$ at our disposal to prescribe an arbitrary small signal gain in the loop, if we permit $|\beta(p)| > 1$. Again we shall define $k_m = |\beta(\omega_m)|$ to be the steady state transmission factor. The choice of k_m and the physical interpretation of the normalized voltages

will then specify the degree of nonlinearity in the circuit. This is true, since for fixed a_1 in (36) the small signal gain is determined by k_m ; a_1 , e_{2max} and $e_1(e_{2max})$ specify a_3 .

Since the normalized characteristic corresponds quite well to typical parameters of physical systems, we may associate direct practical meaning to the results to be obtained.

All the following stability tests shall be based on sufficiency of small signal discrimination and absence of the three-signal effect, which according to Warren³ means concave downward loop gain characteristic vs frequency.

For two signals (13) reduces to

$$\bar{e}_1(t) = A \cos \theta_0 + B \cos \theta_1, \quad (38)$$

where A and B have been introduced for the A_v for convenience. Substituting into (37) we have

$$\begin{aligned} \bar{e}_2(t) \cong & \left(\frac{3}{2} A - \frac{3}{8} A^3 - \frac{3}{4} A B^2 \right) \cos \theta_0 \\ & + \left(\frac{3}{2} B - \frac{3}{8} B^3 - \frac{3}{4} B A^2 \right) \cos \theta_1 \\ & - \frac{3}{8} A B [A \cos (\theta_0 - \theta) + B \cos (\theta_0 + 2\theta)], \quad (39) \end{aligned}$$

where $\theta = \theta_1 - \theta_0$, with $\omega_1 - \omega_0 = \delta$.

In Fig. 3 magnitudes and frequencies of components of (39) are illustrated. On a spectrum analyzer this distribution has been observed in a physical case, where ω_0 represented sustained oscillation and ω_1 a small instruction signal. With a square-law detector an apparent beat frequency is observed. This is a convenient method of measuring frequency of oscillation by "straddling" it with a small signal of known, variable frequency.

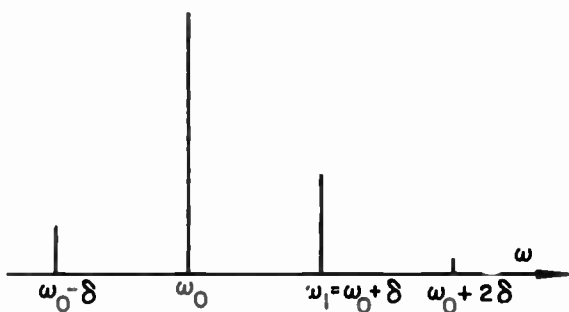


Fig. 3—Frequency distribution of the two-signal transmission for cubic nonlinearity.

Inspection of (39) shows that the family of curves $W = (3U/2 - 3U^3/8 - 3UV^2/4)$ characterizes transmission of ω_0 or ω_1 in the nonlinear fourpole. U may be either A or B , and V either B or A respectively. An index A or B for W shall denote the choice of A or B for U , and consequently B or A for V . Thus the two sets of curves W_A and W_B are conveniently combined in one set W , and interpretation of U and V specifies the particular set (Fig. 4).

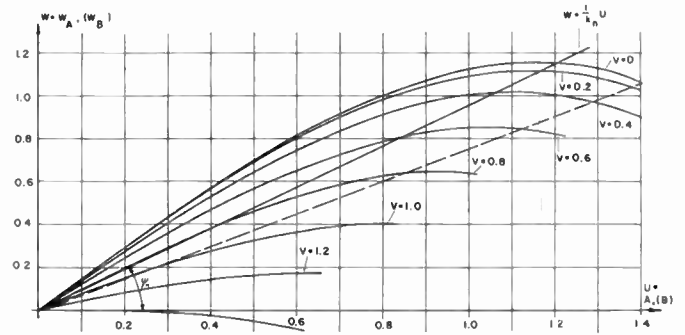


Fig. 4—Two-signal discrimination characteristic.

Recirculation Viewpoint

The feedback equation for the steady state is defined as

$$\bar{e}_1(t) = k_n \bar{e}_2(t - \tau) + \bar{e}_i(t), \quad (40)$$

and (37) holds simultaneously.

Eq. (37) may be interpreted as definition of equivalent linear transmission coefficients for each individual component of (37). If only mode frequencies are considered, the time dependence is readily removed from (40), and for the two-signal case, one obtains for each single frequency

$$U = k_n W(U, V) + U_i. \quad (41)$$

For oscillation at ω_0 and $U_i = 0$, $U = A$, (41) defines the stable level of A . The corresponding straight line has been drawn in Fig. 4. Depending on k_n in (41) the feedback line intersects $W_A(A, 0)$ to render the point of stability. Of course $1/k_n$ must be smaller than

$$\left. \frac{\partial W(A, 0)}{\partial A} \right|_{A=0}$$

to assure net gain in the loop. Reducing the loss of the feedback network corresponds to decreasing of ψ_n in Fig. 4.

An instruction signal of frequency ω_0 will synchronize the oscillation, and $\bar{e}_3(t)$ will be in phase with the instruction signal by definition of mode frequencies in terms of τ , after all transient amplitudes are sufficiently small. Eq. (41) may then be written as:

$$A = k_0 W_A + A_i = k_0 W_A + k'_0 W_A = k''_0 W_A, \quad (42)$$

where k''_0 will depend on W_A . Since $k'_0 > 0$ one has $k''_0 > k_0$, and hence

$$\frac{1}{k''_0} < \frac{1}{k_0} \quad \text{and} \quad \psi''_0 = \tan^{-1} \left(\frac{1}{k''_0} \right) < \psi_0''.$$

In presence of an instruction signal of the frequency of the oscillation, the stable point is shifted on the $W_A(A, 0)$ curve. A straight line connecting it with the origin in the $W_A(A)$ diagram may be interpreted as a new feedback line with decreased slope $1/k''_0$. The change in saturation causes decreased or increased out-

put level, depending on the location of the stable point with respect to the maximum of W_A . Variation of the output level in this fashion has also been observed experimentally.

Stability Criteria

Eq. (39) and Fig. 3 show that two new frequencies are generated in the region of interest by the two-signal effect. This is true for the cubic polynomial and is a reasonable approximation for all other cases of practical importance. If these two frequencies may be disregarded, as in systems with nonuniform distribution of the mode frequencies ω_m , stability may be checked on an arbitrary two-signal basis and superposition holds.

Again assuming A to be the large signal, one obtains from (41) and (39) for $A_i=0$ and $B \ll 1$

$$\left(\frac{3}{2} - \frac{1}{k_0}\right)A - \frac{3}{8}A^3 = 0. \tag{43}$$

Graphically this may be interpreted as the straight-line intersection with $W_A(A, 0)$.

An incremental amplitude B is subjected to loop gain given by the slope of the curve $W_B(A, B)$ for the particular level A and at $B=0$, and the feedback coefficient k_1 .

Eq. (39) renders

$$W_B = \left(\frac{3}{2}B - \frac{3}{8}B^3 - \frac{3}{4}BA^2\right), \tag{44}$$

and differentiating (44)

$$\frac{\partial W_B}{\partial B} = \left(\frac{3}{2} - \frac{9}{8}B^2 - \frac{3}{4}A^2\right), \tag{45}$$

For $B \ll 1$

$$\left.\frac{\partial W_B}{\partial B}\right|_{B=0} \doteq \left(\frac{3}{2} - \frac{3}{4}A^2\right), \tag{46}$$

which specifies the desired slope. Buildup of B from zero level would mean

$$\left|k_1 \frac{\partial W_B}{\partial B}\right|_{B=0} > 1,$$

or net loop gain for ω_1 . The assumption of sustained oscillation at ω_0 implies a relation between k_0 and A , and combining (46) with (43) we obtain

$$k_1 \left.\frac{\partial W_B}{\partial B}\right|_{B=0} = k_1 \left(\frac{2}{k_0} - \frac{3}{2}\right). \tag{47}$$

For stability of A we have

$$\left|\frac{2k_1}{k_0} - \frac{3}{2}k_1\right| < 1, \tag{48}$$

which is but a restatement of (26). According to (26) we could specify a "forbidden region" in Fig. 4. Stability of

the large signal as defined by (29) also imposes such restriction, and the feedback line has to lie above the dotted line in Fig. 4. As mentioned before we might still have stability below the dotted line, but this would require more accurate investigations, to be demonstrated.

Mode Switching

The results obtained so far show that the small signal discrimination properties of a system sustaining a single sinusoid have to be changed, if a signal with small amplitude is supposed to build up in presence of a large one of different frequency. Both signals correspond to mode frequencies of our system.

Now for mode frequencies the impression of an instruction signal may be interpreted as a reduction of loss in the loop for this particular frequency, (42). It will be shown that this modifies the small signal discrimination in the desired way. Then an instruction signal of amplitude less than that of the sustained oscillation may switch the system to the corresponding mode frequency, but there appears a well-defined threshold level.

To verify these statements a two-mode system with $k_1 = k_0 = k$ is considered and small levels of the instruction signal $B_i \cos \omega_1 t$, ω_1 being a mode frequency, are assumed for the time being. Sustained oscillation shall have been established in the loop at ω_0 , corresponding to a level A_{k_0} specified by the feedback coefficient k . This situation is illustrated by two graphs derived from Fig. 4, as shown in Fig. 5(a) and 5(b).

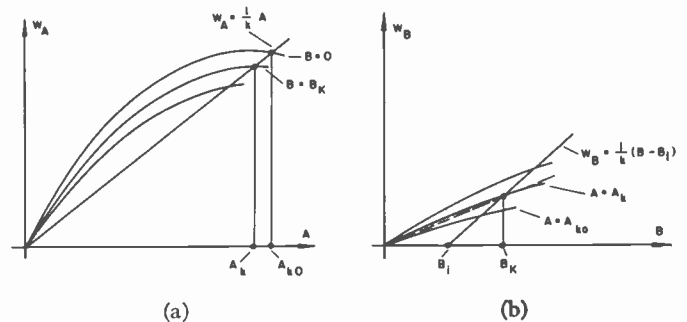


Fig. 5—Stability for large and small signal.

Experimentally it has been observed that a small instruction signal B_i , of amplitude insufficient to switch the system from ω_0 to ω_1 , causes a stable state where sustained oscillation at ω_0 exists in presence of ω_1 , the impressed frequency.

This corresponds to

$$A_k = k \left(\frac{3}{2}A_k - \frac{3}{8}A_k^3 - \frac{3}{4}A_k B^2\right), \tag{49}$$

which is the definition of the stable level of A in the presence of B . (For a sufficiently large B , this equation has no positive, real solution for A_k , which means that the system has switched to ω_2 .)

For $B \ll 1$ one obtains from (44)

$$W_B = \frac{3}{2} \left(1 - \frac{A^2}{2} \right) B. \quad (50)$$

In Fig. 5(b) this corresponds to replacement of the curves labeled A by the straight lines defined in (50). Thus a linearized system, as far as ω_1 is concerned, is obtained.

Stability requires B_K , the stable level associated with ω_1 , to be

$$B_K = kW_B + B_i,$$

which follows from (41).

With (50) this renders

$$B_K = \frac{B_i}{1 - K}, \quad K = \frac{3k}{2} \left(1 - \frac{A_k^2}{2} \right), \quad (51)$$

and (49) has to hold simultaneously.

K is a number less than one and denotes the equivalent linear transmission coefficient for ω_1 in presence of stable oscillation at ω_0 , with level A_k . For positive K the effective level B_K at the input of the nonlinear fourpole is greater than B_i . The fact that ω_1 is a mode frequency has been taken into account in (51) by assigning proper algebraic signs. In a "flat" system the transient caused by switching on ω_1 with amplitude B_i at $t=0$ would be readily expressed in a series expansion analogous to (10). For B_i sufficiently small, A_k may be considered a constant, and the series converges for $|K|$ less than 1. For small instruction signals this linearized analysis is a practical approximation, and the transient behavior is analogous to that of the linearized system in the second section.

A similar buildup will occur even though (50) cannot be maintained due to larger B_K . Still an impressed B_i may produce a $B_K > B_i$. If B_K is sufficiently large, A_k will be reduced accordingly, and finally the system will switch to ω_1 . The existence of this threshold effect could also have been anticipated from (47), which is realized to be smaller than one by a finite and well-defined amount.

Due to the impressed signal the feedback line for its frequency is shifted to the right in Fig. 5(b) by an amount B_i . For a level B_i , too small to produce switching, two separate line intersections determine the stable levels for small and large signal. In Fig. 5(a) the original feedback line intersects the A curve labeled B_K to render A_k , and in Fig. 5(b) the shifted feedback line intersects the B curve labeled A_k at $B = B_K$. This last value could also be interpreted as intersection with the dotted line in Fig. 5(b), which is obtained from the original feedback line by reducing $1/k$ to $1/k''$, according to (42).

Graphical Determination of Stability

Once k and B_i are specified, an iteration method is used to determine the steady-state levels A_k and B_K .

In a physical system the actual step-buildup will bear some resemblance to the iterative steps, but the fact that non-zero recirculation time is involved causes more complicated transients. The stable equilibriums assumed for the construction are established after several recirculations only and thus, in an actual buildup, the system always "lags" with respect to the construction. In Fig. 6, B_i first is assumed to be zero, which renders $A_k = A_{k0}$. Then the transmission of ω_1 is given by curve A_{k0} in the corresponding $W_B(B)$ diagram. (The two sets of curves W_A and W_B are identified in Fig. 6.) The straight line $W_B = 1/k(B - B_i)$ is drawn, and its intersection with curve $W_B(A_{k0}, B)$ determines B_{K1} , the first value of B_K in the iterative process. B_{K1} would cause A_k to drop to A_{k1} , if it would be the stable input-level B_K . The process is repeated for A_{k1} and convergence occurs quite rapidly, or it is realized that the system switches to ω_1 , as in Fig. 6. For the present assumptions a $B_i = 0.3$ is sufficient to switch a system from stable oscillation, of input level 1.2 at ω_0 , to ω_1 .

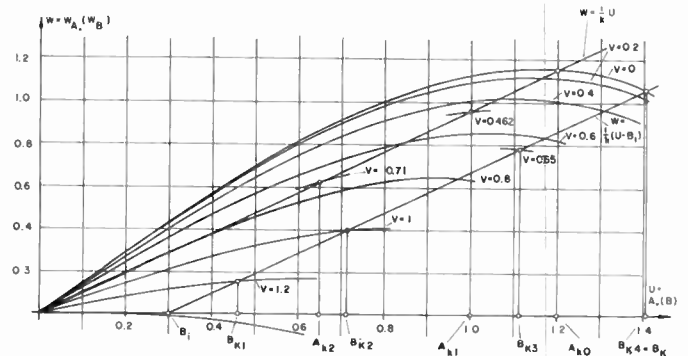


Fig. 6—Graphical determination of stability. $B_i = 0.3$ switches the system from stable oscillation with input level $A_{k0} = 1.2$.

For switching, B_i has to be chosen large enough to bring the effective input level B_K to a value, for which the corresponding A curve can no longer intersect the feedback line. This is just a restatement of previous conclusions.

The graphical method may conveniently be applied to nonlinear characteristics specified by curve data.

Narrow-Band Systems

If selectivity is present in the loop to restrict the number of modes, the contribution of the selective elements to the over-all transient has to be considered for even an approximation. In a two-mode oscillator, which will be described in the experimental part, a filter restricts loop gain to two mode frequencies. To effectively suppress all other modes, the bandwidth of the filter has to be of the order of the mode spacing. Since the transient time is $1/\Delta f$, minimum instruction time $\tau + (1/\Delta f)$ has to be expected. This agrees well with the experimental observation of instruction within 1.5 to 2 recirculations.

EXPERIMENTAL WORK

The basic scheme of an S-band recirculation system is given in Fig. 7, and conventional components represented the specific elements in early experiments.

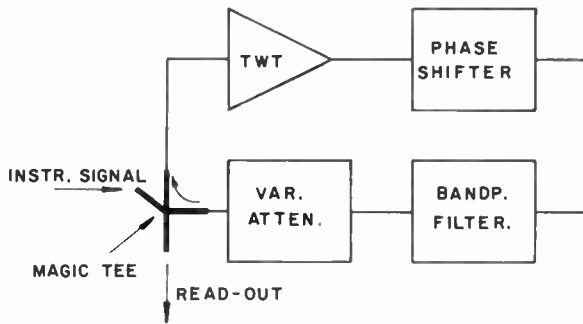


Fig. 7—Experimental recirculation system.

Extensive open-loop measurements were made to check various filter adjustments. Mode spacings of 50 mc could be obtained with bistable and tristable oscillators.

To increase the mode spacing, the time delay in the loop had to be reduced. The main limitation for this lies in the active element, a Huggins-type traveling-wave tube. Construction of special narrow-band slow-wave circuits and design for minimum transit-time would be desirable.¹⁶ This has not been considered for the present experiments.

Independently of other work¹¹ an electron coupling scheme using a conventional helix-type tube has been devised to render a very compact recirculation system. Four separate couplers were placed along the tube, and the three regions thus formed are sufficiently decoupled in the reverse direction by attenuators and directional properties of the system (Fig. 8). The feedback assembly forms a compact unit which fits into the capsule of the traveling-wave tube (Fig. 9). The loops of the coaxial cavity are adjusted for 300-mc/3-db bandwidth and the insertion loss is negligible. Two modes at 2790 and 2985 mc, corresponding to a mode spacing of 195 mc, could be established.

If the additional transit delay is tolerable, as for series time operations, coupler 1 may be spaced close to the gun, and appreciable gain is available for the instruction signal. Couplers 3 and 4 are spaced quite closely, since the beam is saturated in this region. Gain and phase may be varied by adjustment of the helix voltage and the beam current.

The effective loop delay for a mode spacing of 195 mc is 5.1 μ sec, and mode switching could be accomplished within 7 μ sec, for sufficiently large level of the instruction signal.

¹⁶ In a conventional sense, large bandwidth is often directly associated with high speed. For regenerative processes, however, it is important to consider at what expense of transit time this bandwidth has been obtained.

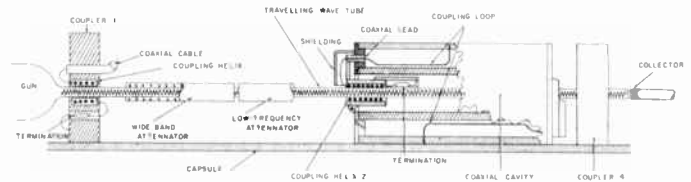


Fig. 8—Detailed view of the bistable oscillator assembly.

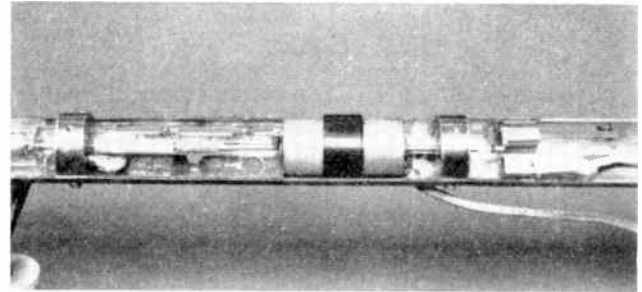


Fig. 9—Assembled feedback unit.

The observed oscillations were quite stable and reproducible. A block diagram for a binary counter, a possible application, is shown in Fig. 10.

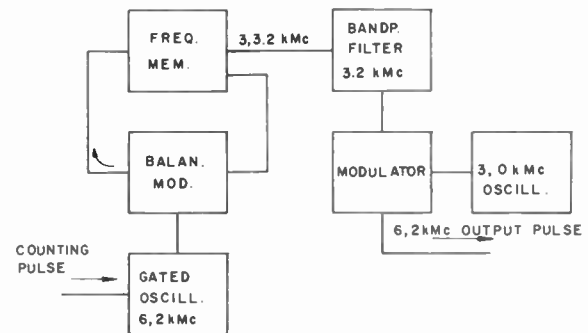


Fig. 10—Block diagram of a binary counter.

CONCLUSION

If the regenerative properties of the multimode oscillator are to contribute to fast mode switching waveforms, minimum delay of the feedback loop and maximum small signal gain μ are required. Thus speed implies a certain deviation from quasi-linearity. Under the assumption of negligible third-harmonic transmission in the loop, which condition is readily met in physical cases, it is shown that sustained oscillation at any of a set of sinusoids is still possible. The standard stability checks are extended to above situation of increased nonlinearity and the sufficient conditions obtained show good correspondence with experimental results. Graphical methods are employed to demonstrate threshold and switching phenomena with the least complexity. The feasibility of high-speed bistable oscillators, which may be thought of as the analogy to multivibrators in the frequency domain, could be demonstrated on an S-band system.

ACKNOWLEDGMENT

The author wishes to thank Dr. W. A. Edson of the General Electric Microwave Laboratory, Palo Alto, Calif. for valuable discussions on the subject of multi-mode oscillators. The contributions of his colleague, M. P. Forrer, General Electric Microwave Laboratory, on the experimental investigations performed are also acknowledged.

LIST OF SYMBOLS

e_1, e_2, e_3, e_i = Voltage time functions in the feedback loop.
 E_1, E_i = Laplace transforms of time functions.
 τ = Constant delay of the feedback network.
 $\beta(p)$ = Transfer function of the feedback network.
 $\mathcal{D}[\]$ = Transfer differential operator representing $\beta(p)$ in time domain.

$e_2 = f(e_1)$ = Nonlinear characteristic.
 μ = Small signal transmission factor of the nonlinearity.
 $p = \sigma + j\omega$ = Complex frequency.
 $p_n = \sigma_n + j\omega_n$ = Natural modes of the linearized system.
 ω_n = Steady state or mode frequency of nonlinear system.
 $\delta\omega_n$ = Mode spacing.
 $\theta = \omega t + \phi$ = Time angle.
 k = Steady-state transmission factor of the feedback network.
 A, A_n, B = Amplitude coefficients.
 A_k, B_k = Steady-state levels for A and B .
 A_L = Amplitude of a large signal.
 A_s = Amplitude of a small signal.
 U, V, W = Normalized amplitudes.
 K = Equivalent loop transmission factor for the small signal.
 Δ_m = Evaluation parameter for Taylor series.

A Reactance Theorem for Antennas*

CURT A. LEVIS†, ASSOCIATE, IRE

Summary—A rigorous expression for the frequency derivative of the input reactance or susceptance of an arbitrary antenna is derived by integration of Maxwell's equations. This expression is shown to depend on the polarization properties of the far field of the antenna and on a quantity which may be interpreted as the electromagnetic energy stored in its near field. The theorem gives a precise theoretical foundation to an intuitive analysis, based on network theorems, which has been used with some success to predict the bandwidth properties of antennas.

INTRODUCTION

RELATIONS between the impedance behavior of lumped circuits and the energy stored in their elements have been of considerable importance in network theory.¹ Their contribution has been not so much to direct calculation as to an insight into the behavior of resonant circuits, the sharpness of resonance being dependent on the circuit Q , which is proportional to the ratio of stored to dissipated energy. These relations have been extended to microwave circuits, where certain integrals involving electric and magnetic field quantities are interpreted as electric and magnetic

stored energy.^{2,3} Since many antennas are narrow-band devices with definite resonance properties, it is natural that these concepts were extended also to antenna theory. In discussing the impedance of such antennas, it has become customary to speak of Q and stored energy even though these quantities are difficult to define rigorously, for, in the case of antennas, all of space must be considered and the apparent stored energy becomes infinite under the usual steady-state assumptions.

Various devices have been used to circumvent this difficulty. Chu⁴ calculated a lower bound for the stored energy of antennas on the basis of an approximate equivalent circuit for each radiated spherical mode. Counter⁵ divided the total electromagnetic fields into "radiation" and "local" fields. "Radiation" fields are assumed to contribute only to a flow energy which must be subtracted from total energy in order to obtain the stored energy from which Q can be calculated. A defect of this method

* Original manuscript received by the IRE, January 2, 1957; revised manuscript received, April 30, 1957. The research in this paper was performed under a contract with the Air Res. and Dev. Center, Wright-Patterson AFB, Ohio.

† Antenna Lab., Dept. of Elec. Eng., Ohio State Univ., Columbus, Ohio.

¹ E. A. Guillemin, "Communication Networks," John Wiley & Sons, Inc., New York, N. Y. vol. II, ch. 6; 1935.

² S. Ramo and J. R. Whinnery, "Fields and Waves in Modern Radio," John Wiley & Sons, Inc., New York, N. Y., p. 423 ff; 1953.

³ C. G. Montgomery, R. H. Dicke, and E. M. Purcell, eds., "Principles of Microwave Circuits," McGraw-Hill Book Co., Inc., New York, N. Y., ch. 5; 1948.

⁴ L. J. Chu, "Physical Limitations of Omnidirectional Antennas," Tech. Rep. 64, Res. Lab. of Electronics, Mass. Inst. Tech.; 1948.

⁵ V. A. Counter, "Miniature Cavity Antennas," Rep. No. 2, Contract No. W 28-099-ac-382, Microwave Lab., Stanford Univ., June 30, 1948.

is that the flow velocity must be postulated; Counter assumed a value $(\mu\epsilon)^{-1/2}$ at all points of space.

The approach to be taken here will develop from Maxwell's equations a rigorous formula for the frequency derivative of the reactance or susceptance of an antenna. This formula contains certain integrals which are suggestive of stored energy, but such interpretations must be made cautiously. The reactance or susceptance derivatives also are shown to depend on certain polarization properties of the antenna. Such a connection has been established for particular configurations before;⁶ it is exhibited here as a very general property. The formulas do not lend themselves readily to computation. They are more likely to be useful in furnishing additional insight into antenna resonance phenomena.

INTERPRETATION OF CERTAIN ELECTRO-MAGNETIC QUANTITIES

Certain electromagnetic quantities which appear in the theorem are of interest because of their possible interpretation as physically meaningful quantities. The mks system of units⁷ will be used and a time dependence $e^{j\omega t}$ will be implied.

Mean Power Flow

The normal component of the Poynting vector $\frac{1}{2} \text{Re} (\mathbf{E} \times \mathbf{H}^*)$, when integrated over a closed surface, gives the mean power flow across the surface. This does not rigorously establish the quantity

$$\mathbf{P} = \frac{1}{2} \text{Re} (\mathbf{E} \times \mathbf{H}^*) \quad (1)$$

as a rate of *local* mean power flow,⁸ and some authors have vigorously rejected such an interpretation.^{9,10} Others have found it very useful. At any rate, if one wishes to *postulate* that energy is stored in electromagnetic fields and that a power flow through space does take place, then \mathbf{P} is its most widely accepted measure. In the far field, the power density decreases as R^{-2} where R is the distance from the point of observation to the antenna. It is therefore convenient to define a power flow per unit solid angle (subtended at the antenna) by

$$P_{\Omega} = \frac{1}{2} R^2 \text{Re} (\mathbf{E} \times \mathbf{H}^*), \quad (2)$$

so that P_{Ω} is independent of the distance from the antenna to the point of observation.

⁶ T. H. Crowley, "Relations between Impedance and Polarization," Project Rep. 339-21, Antenna Lab., Ohio State Univ. Res. Foundation, prepared under Contract W 33-038 ac21114, Air Res. and Dev. Center, Wright-Patterson AFB.

⁷ J. A. Stratton, "Electromagnetic Theory," McGraw-Hill Book Co., Inc., New York, N.Y. p. 16 ff; 1941.

⁸ *Ibid.*, pp. 131-137.

⁹ R. W. P. King, "Electromagnetic Engineering, Vol. I: Fundamentals," McGraw-Hill Book Co., Inc., New York, N. Y., pp. 188-193; 1945.

¹⁰ M. Mason and W. Weaver, "The Electromagnetic Field," Univ. of Chicago Press, Chicago, Ill., p. 264 ff; 1929.

Energy Density

The quantities $\frac{1}{2}\mu\mathbf{H}\cdot\mathbf{H}^*$ and $\frac{1}{2}\epsilon\mathbf{E}\cdot\mathbf{E}^*$ are the most widely accepted measures of the average energy stored in oscillating magnetic and electric fields, respectively. These interpretations are subject to the same criticisms as that concerning the mean power flow.

Phase

The phase of a linearly-polarized field vector \mathbf{F} is easily defined by writing the vector in polar form. Let

$$\mathbf{F} = |\mathbf{F}| e^{i\phi} \mathbf{u}, \quad (3)$$

where \mathbf{u} is a unit vector. Then ϕ is taken as a measure of the phase of \mathbf{F} . A formula for ϕ is

$$\phi = \frac{1}{2} \text{Im} \ln (\mathbf{F} \cdot \mathbf{F}). \quad (4)$$

This formula can also be applied in the case of elliptically-polarized fields and is proposed as a definition for the phase of such fields.

Group Velocity

The velocity of energy or signal propagation is a difficult subject even for simple unbounded media.¹¹ The group velocity is closely related to energy propagation. For plane waves in unbounded media and for singly propagating modes in cylindrical waveguides, this velocity is given by

$$v_g = (d\beta/d\omega)^{-1} \quad (5)$$

where β is the propagation constant. In terms of the phase of the field components this can be written as

$$v_g = (-s \cdot \nabla \partial\phi/\partial\omega)^{-1} \quad (6)$$

where the wave under consideration is a pure traveling wave, s is a unit vector in the direction of \mathbf{P} , and ϕ is computed by (4) from \mathbf{H} for TM waves, from \mathbf{E} for TE waves, and from either for TEM waves. Eq. (6) is a more complicated expression than (5), but it is more general since it deals directly with the fields.

Polarization

In the far field of an antenna its polarization properties are functions of direction only. Some of these properties can be specified directly in terms of the field vectors without recourse to any coordinate system. One such quantity is the axial ratio, r , defined as the ratio of the major to the minor axis of the polarization ellipse. The orientation of the major axis cannot be specified without a coordinate system, but a change of orientation can. To illustrate, let α be the directed angle between some arbitrary axis, perpendicular to the propagation direction (say the e_2 axis in Fig. 1), and the major axis of an elliptically-polarized wave. Count α positive if it is in the same direction as the rotation of the electric field vector with time. Obviously, α is independent on the

¹¹ Stratton, *op. cit.*, pp. 330-340.

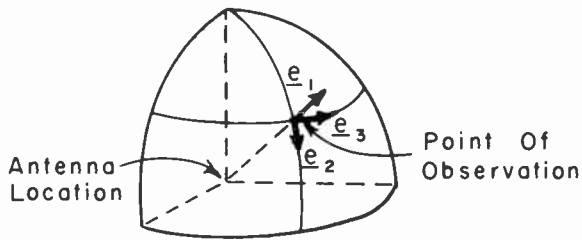


Fig. 1.

choice of axis, but the rate of orientation change, $d\alpha/d\omega$, is not. It will be denoted by σ ,

$$\sigma = d\alpha/d\omega. \tag{7}$$

STATEMENT OF THE THEOREM

The theorem can be stated in three related but not fully equivalent forms. Let v denote the input voltage at the antenna terminals and i the input current. Let

$$Z = R + jX = Y^{-1} = (G + jB)^{-1} \tag{8}$$

be the input impedance, and r the axial ratio. Then one form of the theorem is

$$\begin{aligned} \frac{|i|^2}{4} \frac{dX}{d\omega} = & \int_V \left[\frac{1}{4} (\mu \mathbf{H} \cdot \mathbf{H}^* + \epsilon \mathbf{E} \cdot \mathbf{E}^*) \right. \\ & \left. + \frac{1}{2} \text{Re} (\mathbf{E} \times \mathbf{H}^*) \cdot \nabla \frac{\partial}{\partial \omega} \phi_H \right] dV \\ & + \int_{\Omega} P_{\Omega} \frac{2r}{r^2 + 1} \sigma d\Omega, \end{aligned} \tag{9}$$

where

$$\phi_H = \frac{1}{2} \text{Im} \ln (\mathbf{H} \cdot \mathbf{H}), \tag{10}$$

the volume integral is to be taken over all of external space, and the integral with respect to Ω over all possible directions. The symbol $\partial/\partial\omega$ which appears in (9) denotes partial differentiation with respect to angular frequency. Current is here considered as an independent variable; physically, the operation $\partial/\partial\omega$ corresponds to the divided difference between two readings taken under identical conditions except for an infinitesimal increase in the frequency of the generator accompanied by a readjustment of its strength such that the magnitude of the input current stays constant, and with the understanding that the phase of all field quantities always is to be referred to the input current.

The first two terms within the brackets suggest interpretation as the mean magnetic and electric energy densities discussed in the previous section. The last term contains the product of power density and generalized group velocity. The volume integral is therefore very similar in form to that suggested by Counter, the only difference being in the "energy flow velocity" factor where the generalized group velocity takes the place of

Counter's $(\mu\epsilon)^{-1/2}$. The last integral represents the total radiated power times a weighed average of certain polarization properties as a function of direction, the weight being the power density. This integrand vanishes for linear polarization.

In line with this interpretation, (9) can be rewritten as

$$\begin{aligned} \frac{|i|^2}{4} \frac{dX}{d\omega} = & \int_V \{ U_H + U_E - v_{\theta H}^{-1} P \} dV \\ & + P_T \left(\frac{2r}{r^2 + 1} \sigma \right) \end{aligned} \tag{11}$$

where

- $U_H = \frac{1}{4} \mu \mathbf{H} \cdot \mathbf{H}^*$ represents local magnetic energy
- $U_E = \frac{1}{4} \epsilon \mathbf{E} \cdot \mathbf{E}^*$ represents local electric energy
- $v_{\theta H}^{-1} P$ represents local flow energy
- P_T is the total radiated power
- P is the magnitude of the Poynting vector \mathbf{P}
- r is the axial ratio
- $v_{\theta H}$ is calculated by (6) from the \mathbf{H} vector,

and the symbol (\quad) denotes the weighted average described above.

It should be noted that (9) is rigorous (the derivation is given in the Appendix), but the interpretation suggested in (11) is arbitrary. For instance, one may wish to interpret the volume integral as representing "stored energy," but the conclusion that it is therefore always positive would be erroneous. It is a well-known fact that linearly-polarized antennas may have negative reactance slopes, therefore the volume integral may be negative. This example shows that the interpretations should be made cautiously and within the framework of (9).

Another form of the theorem is the exact dual of the first, viz.,

$$\begin{aligned} \frac{|v|^2}{4} \frac{dB}{d\omega} = & \int_V \left[\frac{1}{4} (\mu \mathbf{H} \cdot \mathbf{H}^* + \epsilon \mathbf{E} \cdot \mathbf{E}^*) \right. \\ & \left. + \frac{1}{2} \text{Re} (\mathbf{E}^* \times \mathbf{H}) \cdot \nabla \frac{\partial}{\partial \omega} \phi_E \right] dV \\ & + \int_{\Omega} P_{\Omega} \frac{2r}{r^2 + 1} \sigma d\Omega, \end{aligned} \tag{12}$$

where

$$\phi_E = \frac{1}{2} \text{Im} \ln (\mathbf{E} \cdot \mathbf{E}) \tag{13}$$

and $\partial/\partial\omega$ in (12) now represents differentiation with the input voltage considered as an independent variable. Examination of the left sides of (9) and (12) shows that the two forms should give identical results, but with opposite sign, when

$$X = 0 = B. \tag{14}$$

A third form is

$$\begin{aligned} \frac{|i|^2}{4} \frac{X}{|Z|} \frac{d|Z|}{d\omega} &= \frac{|v|^2}{4} \frac{B}{|Y|} \frac{d|Y|}{d\omega} \\ &= \int_V \left[\frac{1}{4} (\mu \mathbf{H} \cdot \mathbf{H}^* + \epsilon \mathbf{E} \cdot \mathbf{E}^*) + \frac{1}{2} \operatorname{Re} (\mathbf{E}^* \times \mathbf{H}) \cdot \nabla \frac{\partial}{\partial \omega} \phi_P \right] dV \\ &\quad + \int_{\Omega} P_{\Omega} \frac{2r}{r^2 + 1} \sigma d\Omega \end{aligned} \quad (15)$$

where

$$\phi_P = \frac{1}{2} \operatorname{Im} \ln (\mathbf{E} \times \mathbf{H} \cdot \mathbf{s}) \quad (16)$$

and $\partial/\partial\omega$ treats the product $(v \cdot i)$ as an independent variable. Here the terms involving impedance and admittance derivatives vanish at resonance.

It should be noted that the factor which plays the role of energy velocity differs in the three forms. Thus a single unambiguous expression for the velocity of energy propagation away from an antenna does not emerge from the present analysis. Calculation of the velocity term unfortunately requires more knowledge of the frequency behavior of the field than is usually available. For this reason, the theorem is likely to be a more conceptual than a computational aid.

The volume integrals in (9), (12), and (15) extend over all of external space. However, if a finite integration volume is used, the error behaves no worse than R_n^{-1} , where R_n is the nearest distance from the antenna to the boundary of the integration volume. This follows directly from the derivation (see Appendix), since only terms of this order are neglected. The far-zone fields therefore do not contribute significantly to the stored energy integral.

The proof of the theorem is rather involved and is presented as an Appendix. Only the first form is proved. Modifications for the others are indicated, and they can be derived without difficulty.

APPENDIX

PROOF OF THE THEOREM

To prove the theorem, two lemmas are needed. A time dependence $e^{j\omega t}$ will be implied throughout.

Lemma 1

In a lossless, source-free, isotropic region V bounded by a surface S with outward unit normal \mathbf{n} and containing no nonlinear electric or magnetic materials,

$$\begin{aligned} \int_S (\mathbf{H}^* \times \mathbf{E}' + \mathbf{H}' \times \mathbf{E}^*) \cdot \mathbf{n} dS \\ = j \int_V (\bar{\mu} \mathbf{H} \cdot \mathbf{H}^* + \bar{\epsilon} \mathbf{E} \cdot \mathbf{E}^*) dV, \end{aligned} \quad (17)$$

where the prime denotes partial differentiation with respect to ω , $\bar{\mu} = \mu + \omega\mu'$, and $\bar{\epsilon} = \epsilon + \omega\epsilon'$. To prove the lemma, V is divided into subregions V_j such that any sur-

faces at which μ or ϵ are discontinuous become boundaries of the subdivisions. In each subregion, Maxwell's equations are satisfied,

$$\nabla \times \mathbf{E} = -j\omega\mu\mathbf{H}, \quad (18)$$

$$\nabla \times \mathbf{H} = j\omega\epsilon\mathbf{E}. \quad (19)$$

The conjugates and partial derivatives of each side of these equations can be taken and the resulting relations combined to obtain

$$\begin{aligned} \mathbf{E}' \cdot \nabla \times \mathbf{H}^* - \mathbf{H}^* \cdot \nabla \times \mathbf{E}' + \mathbf{E}^* \cdot \nabla \times \mathbf{H}' - \mathbf{H}' \cdot \nabla \times \mathbf{E}^* \\ = j(\bar{\epsilon}\mathbf{E} \cdot \mathbf{E}^* + \bar{\mu}\mathbf{H} \cdot \mathbf{H}^*). \end{aligned} \quad (20)$$

By use of a vector identity, the left side of (20) becomes $\nabla \cdot (\mathbf{H}^* \times \mathbf{E}' + \mathbf{H}' \times \mathbf{E}^*)$ and by integrating over V_j and using Gauss' theorem, a set of formulas similar to (17) is obtained, except that they apply to the individual subregions rather than the region V itself. If a summation on j is then performed, the volume integrals sum into a volume integral over all of V . Let S_{jk} be the boundary surface common to V_j and V_k . For each S_{jk} there will be two surface integrals, one arising from the application of Gauss' theorem to V_j and similarly one from V_k . Since the tangential components of \mathbf{E} and \mathbf{H} are continuous across S_{jk} , and since the outward normals are oppositely directed in the two integrals, the sum of the internal surface integrals vanishes and it is found that only the external boundaries contribute. Their contribution amounts to an integration over all of S . This proves the lemma.

Lemma 2

Let S_2 be a spherical surface of radius R centered at some point on the antenna and sufficiently large to enclose the entire antenna and all discontinuities. Beyond S_2 , the medium will be assumed homogeneous. Let \mathbf{n}_2 be the unit outward normal to S_2 . Then

$$\begin{aligned} \int_{S_2} (\mathbf{E}' \times \mathbf{H}^* + \mathbf{E}^* \times \mathbf{H}') \cdot \mathbf{n}_2 dS_2 \\ = 2 \int_{S_2} (\mu/\epsilon)^{1/2} (\mathbf{H}' \cdot \mathbf{H}^*) dS_2 + O(R^{-1}), \end{aligned} \quad (21)$$

where $O(R^n)$ denotes terms of the order of R^n . (More precisely, $F(R) = O(R^n)$ means that the quantity $|R^{-n}F(R)|$ is bounded for very large positive values of R . In the case of vector functions, this must be true for each component.) The terms of order R^{-1} do not contribute significantly if S_2 is chosen in the far field of the antenna. The lemma is proved by expanding the antenna field in terms of outgoing spherical waves.¹² Using the coordinate system of Fig. 1, the field components of each mode satisfy

¹² Stratton, *op. cit.*, ch. 7.

$$\begin{aligned}
 H_1 &= O(R^{-2}), & E_1 &= O(R^{-2}) \\
 H_2 &= O(R^{-1}), & E_2 &= (\mu/\epsilon)^{1/2}H_3 + O(R^{-3}) \\
 H_3 &= O(R^{-1}), & E_3 &= -(\mu/\epsilon)^{1/2}H_2 + O(R^{-3}) \\
 H_1' &= O(R^{-1}), & E_1' &= O(R^{-1}) \\
 H_2' &= O(R^0), & E_2' &= (\mu/\epsilon)^{1/2}H_3' + O(R^{-2}) \\
 H_3' &= O(R^0), & E_3' &= -(\mu/\epsilon)^{1/2}H_2' + O(R^{-2}) \quad (22)
 \end{aligned}$$

and this is therefore also true of the total fields. Expansion of the integrands in (21) in terms of components and use of (22) proves the lemma.

To prove the theorem, consider the electromagnetic field radiated by an antenna such as shown in Fig. 2 or

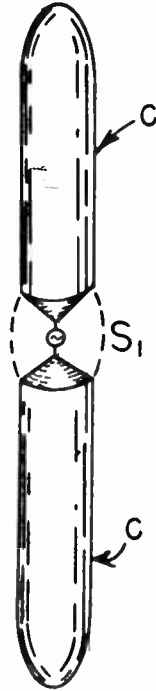


Fig. 2.

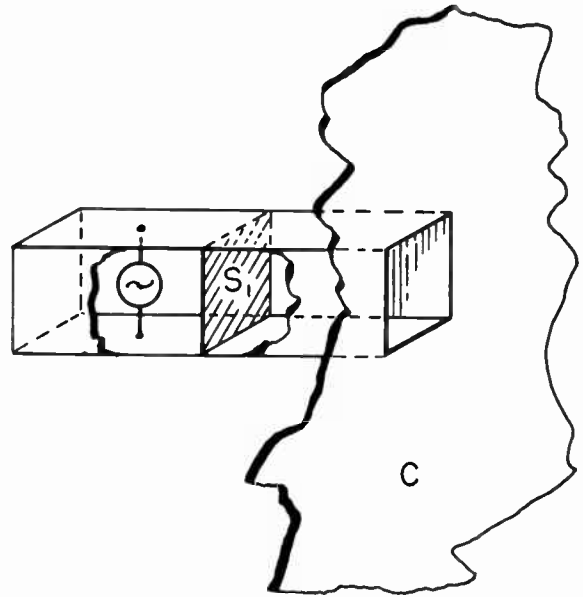


Fig. 3.

In Fig. 3, energy is supplied through a waveguide (or coaxial line) propagating a single mode. \$S_1\$ is a transverse plane where the impedance will be defined. Denote by \$\mathbf{e}_1\$ the normalized vector function which characterizes the transverse electric field components of the propagating mode at \$S_1\$. (The dimensions associated with \$\mathbf{e}_1\$ are meters\$^{-1}\$.) The general transverse electric field at \$S_1\$ is then given by

$$\mathbf{E}_T = v\mathbf{e}_1, \quad (26)$$

a relation which defines the voltage \$v\$. Let the propagation direction at \$S_1\$ be given by the unit vector \$\mathbf{n}_1\$. The transverse components of the magnetic field are then specified by

$$\mathbf{H}_T = i\mathbf{n}_1 \times \mathbf{e}_1, \quad (27)$$

and this relation defines the current, \$i\$. The impedance is defined by (25) as before. In both models, \$S_2\$ is a spherical surface which encloses the antenna at a very large distance from it, \$C\$ represents conducting surfaces of the antenna, and \$V\$ is the volume enclosed by \$S_1\$, \$C\$, and \$S_2\$.

The fields in \$V\$ and on its boundaries are functions of position, frequency, and excitation. In specifying excitation, one can specify \$v\$, or \$i\$, or their product—but not independently since the ratio \$Z\$ is a function of only the antenna geometry and frequency. Thus one of the ways of specifying completely the functional dependence of the fields in \$V\$ is to write

$$\mathbf{E} = \mathbf{E}(i, x, y, z, \omega), \quad (28)$$

$$\mathbf{H} = \mathbf{H}(i, x, y, z, \omega), \quad (29)$$

where \$x, y, z\$ are the Cartesian coordinates of the point at which the fields are evaluated in some reference system whose origin we shall take somewhere in the antenna structure. All variables in (28) and (29) are

Fig. 3. The terminal surface \$S_1\$ is chosen so that an antenna impedance can be defined. In Fig. 2, it encloses a conical gap across which excitation is applied to the antenna conductors, \$C\$, which are assumed to conduct perfectly. The gap is small, and the fields about it are uniform. The voltage \$v\$ is defined by

$$v = \int \mathbf{E} \cdot d\mathbf{l}, \quad (23)$$

where the integration is to be performed from one conductor across the gap to the other. A similar definition for the current \$i\$ is

$$i = \oint \mathbf{H} \cdot d\mathbf{l}, \quad (24)$$

with the path of integration circumferentially around the gap. The impedance is, of course, the ratio

$$Z = v/i. \quad (25)$$

considered independent. Application of lemma 1 to the fields in V , and noting that tangential \mathbf{E} vanishes on C , yields

$$\begin{aligned}
 & - \int_S (\mathbf{H}^* \times \mathbf{E}' + \mathbf{H}' \times \mathbf{E}^*) \cdot \mathbf{n}_1 dS_1 \\
 & = j \int_V (\bar{\mu} \mathbf{H} \cdot \mathbf{H}^* + \epsilon \mathbf{E} \cdot \mathbf{E}^*) dV \\
 & + \int_{S_2} (\mathbf{E}' \times \mathbf{H}^* + \mathbf{E}^* \times \mathbf{H}') \cdot \mathbf{n}_2 dS_2. \quad (30)
 \end{aligned}$$

The left-hand integral can be reduced to $i^*v' + i'v^*$. Since the prime denotes *partial* differentiation with respect to ω , and since i is considered as an independent variable in (28) and (29),

$$i' = 0 \quad (31)$$

and

$$v' = i \frac{dZ}{d\omega}. \quad (32)$$

Lemma 2 applies directly to the right-hand integral. If one denotes the volume integral in (30) by

$$4E_T = \int_V (\bar{\mu} \mathbf{H} \cdot \mathbf{H}^* + \epsilon \mathbf{E} \cdot \mathbf{E}^*) dV, \quad (33)$$

the result is

$$\begin{aligned}
 & |i|^2 \frac{dZ}{d\omega} \\
 & = j4E_T + 2 \int_{S_2} (\mu/\epsilon)^{1/2} (\mathbf{H}' \cdot \mathbf{H}^*) dS_2 + O(R^{-1}). \quad (34)
 \end{aligned}$$

Since

$$\text{Re}(\mathbf{H}' \cdot \mathbf{H}^*) = \frac{\partial}{\partial \omega} (\mathbf{H} \cdot \mathbf{H}^*), \quad (35)$$

the real part of (34) merely states that an increase in input resistance represents an increase in radiated power for constant current input. The imaginary part is

$$\begin{aligned}
 & \frac{|i|^2}{4} \frac{dX}{d\omega} \\
 & = E_T + \frac{1}{2} \int_{S_2} (\mu/\epsilon)^{1/2} \text{Im} (\mathbf{H}' \cdot \mathbf{H}^*) dS_2 + O(R^{-1}). \quad (36)
 \end{aligned}$$

The quantity $(\mathbf{H}' \cdot \mathbf{H}^*)$ can be expanded by a vector identity

$$\begin{aligned}
 \mathbf{H}' \cdot \mathbf{H}^* & = \frac{(\mathbf{H} \cdot \mathbf{H})(\mathbf{H}' \cdot \mathbf{H}^*)}{(\mathbf{H} \cdot \mathbf{H})} \\
 & = \frac{1}{(\mathbf{H} \cdot \mathbf{H})} [(\mathbf{H} \cdot \mathbf{H}')(\mathbf{H}' \cdot \mathbf{H} + (\mathbf{H} \times \mathbf{H}') \\
 & \quad \cdot (\mathbf{H} \times \mathbf{H}^*)], \quad (37)
 \end{aligned}$$

$$\mathbf{H}' \cdot \mathbf{H}^* = \frac{1}{2} (\mathbf{H} \cdot \mathbf{H}^*) \frac{\partial}{\partial \omega} \ln (\mathbf{H} \cdot \mathbf{H}) + G \quad (38)$$

where

$$G = \frac{(\mathbf{H} \times \mathbf{H}') \cdot (\mathbf{H} \times \mathbf{H}^*)}{\mathbf{H} \cdot \mathbf{H}}. \quad (39)$$

The quantity G is closely related to certain polarization properties of the field. For instance, a necessary and sufficient condition for linear polarization is $\mathbf{H} \times \mathbf{H}^* = 0$. In fact, it will be shown that in the far field G can be expressed entirely in terms of the power density and polarization properties. To show this, one expands the fields in terms of their components and uses (22) to obtain

$$G = \frac{(H_2 H_3' - H_3 H_2')(H_2 H_3^* - H_3 H_2^*)}{H_2^2 + H_3^2} + O(R^{-3}). \quad (40)$$

The polarization at any point of the field is given by¹³

$$p = j \frac{E_3}{E_2} = -j \frac{H_2}{H_3} + O(R^{-1}). \quad (41)$$

Then to an accuracy of order R^{-3} ,

$$H_2 H_3^* - H_3 H_2^* = j(p + p^*) \frac{(\mathbf{H} \cdot \mathbf{H}^*)}{1 + pp^*}, \quad (42)$$

$$H_2^2 + H_3^2 = H_3^2(1 - p^2), \quad (43)$$

$$H_2 H_3' - H_3 H_2' = -j H_3^2 p', \quad (44)$$

and

$$G = \frac{p'(p + p^*)(\mathbf{H} \cdot \mathbf{H}^*)}{(1 + pp^*)(1 - p^2)}. \quad (45)$$

The parameter p is dependent on the choice of local coordinate vectors to which the field components are referred, but from (39) it is apparent that G is independent of this choice. To arrive at a more basic physical picture of G , one can employ the q -plane representation¹³ by transforming according to

$$p = (1 - q)/(1 + q). \quad (46)$$

In terms of the new parameter,

$$G = -\frac{1}{2} (\mathbf{H} \cdot \mathbf{H}^*) \frac{(1 - qq^*)}{(1 + qq^*)} \frac{d}{d\omega} \ln q. \quad (47)$$

The axial ratio r of the polarization ellipse is given by

$$r = \pm \frac{1 + |q|}{1 - |q|}, \quad (48)$$

and its orientation angle α with respect to the \mathbf{e}_2 axis (paragraph entitled "Polarization") by

¹³ V. H. Rumsey, "Techniques for handling elliptically polarized waves with special reference to antennas, part I—transmission between elliptically polarized antennas," *PROC. IRE*, vol. 39, pp. 535-40; May 1951. Correction in *PROC. IRE*, vol. 43, p. 733; June 1955.

$$\alpha = \mp \frac{1}{2} \text{Im} \ln q, \quad (49)$$

where the upper sign applies to right-hand and the lower to left-hand polarization.¹⁴ Accordingly,

$$\text{Im } G = 2(\mathbf{H} \cdot \mathbf{H}^*) \frac{r}{r^2 + 1} \sigma + O(R^{-3}), \quad (50)$$

and (38) yields

$$\begin{aligned} \text{Im} (\mathbf{H}' \cdot \mathbf{H}^*) &= (\mathbf{H} \cdot \mathbf{H}^*) \phi_{H'} + 2(\mathbf{H} \cdot \mathbf{H}^*) \frac{r}{r^2 + 1} \sigma \\ &+ O(R^{-3}). \end{aligned} \quad (51)$$

This result will now be used in (36),

$$\begin{aligned} \frac{|i|^2}{4} \frac{dX}{d\omega} &= E_T + \frac{1}{2} \int_{S_2} \left(\frac{\mu}{\epsilon} \right)^{1/2} (\mathbf{H} \cdot \mathbf{H}^*) \phi_{H'} dS_2 \\ &+ \int_{S_2} \left(\frac{\mu}{\epsilon} \right)^{1/2} (\mathbf{H} \cdot \mathbf{H}^*) \frac{r}{r^2 + 1} \sigma dS_2 \\ &+ O(R^{-1}). \end{aligned} \quad (52)$$

In the first integral $(\mu/\epsilon)^{1/2} (\mathbf{H} \cdot \mathbf{H}^*)$ can be replaced by $\text{Re} (\mathbf{E}^* \times \mathbf{H}) \cdot \mathbf{n}_2$ with error of the order of (R^{-1}) . Since $\phi_{H'}$ vanishes on S_1 , because of (31), and tangential \mathbf{E} vanishes on C , this integral can be extended over these surfaces as well. Once more applying Gauss' theorem yields

¹⁴ "IRE Standards on Radio Wave Propagation, Definition of Terms"; 1942.

$$\begin{aligned} \int_{S_2} (\mu/\epsilon)^{1/2} \mathbf{H} \cdot \mathbf{H}^* \phi_{H'} dS_2 \\ = \int_V \nabla \cdot [\text{Re} (\mathbf{E}^* \times \mathbf{H}) \phi_{H'}] dV. \end{aligned} \quad (53)$$

By a vector identity

$$\begin{aligned} \nabla \cdot [\text{Re} (\mathbf{E}^* \times \mathbf{H}) \phi_{H'}] \\ = \text{Re} (\mathbf{E}^* \times \mathbf{H}') \cdot \nabla \phi_{H'} + \phi_{H'} \nabla \cdot \text{Re} (\mathbf{E}^* \times \mathbf{H}), \end{aligned} \quad (54)$$

but $\nabla \cdot \text{Re} (\mathbf{E}^* \times \mathbf{H})$ vanishes in any region where Maxwell's equations in the form of (18) and (19) are satisfied. Therefore

$$\begin{aligned} \int_{S_2} (\mu/\epsilon)^{1/2} (\mathbf{H} \cdot \mathbf{H}^*) \phi_{H'} dS_2 \\ = \int_V \text{Re} (\mathbf{E}^* \times \mathbf{H}) \cdot \nabla \phi_{H'} dV. \end{aligned} \quad (55)$$

Eq. (55), together with (52) and (33), proves the theorem in the form of (9) when R is allowed to increase without limit.

The other forms are proved very similarly. One difference is the interpretation of $\phi_{H'}$ in (53). In the far field, \mathbf{E} and \mathbf{H} are essentially in phase at all frequencies, and consequently $\phi_{E'}$ or $\phi_{P'}$ may be substituted for $\phi_{H'}$ in this equation. Another difference arises out of (28) and (29); for the second form of the theorem, one uses v instead of i as the independent variable, and for the third form, the product (vi) replaces i in these equations.

Heat Loss in Grooved Metallic Surface*

ENRIQUE A. MARCATIL†

Summary—This paper describes an elementary and powerful way to calculate the conduction current losses in metallic waveguide walls, that have parallel periodic grooves of semicircular cross section, when the diameter of the circles is small with respect to the wavelength, but long with respect to the skin depth. The helix circular-electric waveguide falls in this class, and its circular-electric-wave losses have been estimated.

The method consists in guessing judiciously the solution of Maxwell's equations close to the wall. It turns out that with the first two obvious guesses, close approximations to the rigorous solution are obtained for grooves at right angles and parallel to the tangential magnetic field.

* Original manuscript received by the IRE, February 20, 1957.

† Bell Telephone Labs., Inc., Holmdel, N. J.

INTRODUCTION

IT IS KNOWN that the power dissipated by conduction current in a waveguide or cavity is approximately¹

$$P = \frac{1}{2\delta g} \int_S |H_t|^2 ds \quad (1)$$

in which δ is the skin depth, g the conductivity of the metal wall of which S is its boundary, and $|H_t|$, the

¹ S. A. Schelkunoff, "Electromagnetic Waves," D. Van Nostrand Co., Inc., New York, N. Y., p. 320; 1947.

intensity of the magnetic field tangential to the wall calculated assuming $g = \infty$.

Eq. (1) is a very good approximation, provided that the radius of curvature of any element of S is large compared to the skin depth, and consequently, the calculation of the heat loss is reduced essentially to the boundary value problem of finding $|H_t|$.

Consider now a tube of circular cross section made by winding a helix with a pitch equal to the diameter of the wire. The inside of the tube is a waveguide and if the diameter of the wire is small compared to the wavelength, the normal modes far from cutoff can be defined assuming that the tube behaves like a circular cylindrical waveguide of diameter equal to the inside diameter of the helix. The approximation of the helix to a cylinder is very good for the macroscopic problem of calculating phase constants, but in general a poor one for the microscopic determination of $|H_t|$. Before finding $|H_t|$, several simplifications will be made.

- 1) Since the diameter of the wire is very small with respect to the wavelength and the modes are far from cutoff, the Bessel functions that define the electromagnetic field in the neighborhood of the wall will be approximated by circular functions. This means that only for the purpose of calculating $|H_t|$, the tube may be rectified and the wall to be considered is made of an infinite number of parallel straight wires infinitely long with their axes contained in a plane.
- 2) Only TEM waves polarized parallel or perpendicularly to the grooves and impinging perpendicularly to the wall will be considered. Therefore, the pitch is ignored and the results obtained will be applicable only in regions of semicircularly grooved wall where the tangential magnetic field is parallel or perpendicular to the groove, (Fig. 1).



Fig. 1—Semicircularly grooved walls impinged by TEM fields.

- 3) The last approximation is actually the method used to solve the boundary value problem. The method consists in assuming that the field is described by the first terms of the Fourier series that would be needed for the exact solution. By judicious selection of each term, the metallic boundary turns out to be similar to the semicircularly grooved one.

The method described has been already used,² but for

² J. C. Maxwell, "Electricity and Magnetism," Cambridge, London, Eng., 3rd ed., vol. 1, sec. 203; 1904.

the particular problem we are solving, the solution is so simple and full of information that the author thought it was worth writing down in detail.

MAGNETIC FIELD PERPENDICULAR TO THE GROOVE

Consider the following electromagnetic field that satisfies Maxwell's equations,

$$E = \sin \frac{2\pi}{\lambda} z + A \exp \left(- \sqrt{\left(\frac{2\pi}{a}\right)^2 - \left(\frac{2\pi}{\lambda}\right)^2} z \right) \cdot \cos \frac{2\pi}{a} x \quad (2)$$

$$H_x = \frac{1}{i\mu\omega} \frac{\partial E}{\partial z} \quad (3)$$

$$H_z = - \frac{1}{i\mu\omega} \frac{\partial E}{\partial x} \quad (4)$$

E is the electric field in the y direction; λ , the free space wavelength; a , a period of the field along x ; μ , the magnetic permeability, and ω , the angular pulsation. The exponential dependence of time is understood.

If $(a/\lambda) \ll 1$, the electric field for $z \ll (\lambda/2\pi)$ becomes

$$E \cong \frac{2\pi}{\lambda} z + A \exp \left(- \frac{2\pi}{a} z \right) \cos \frac{2\pi}{a} x \quad (5)$$

and the description of the metallic boundary is obtained making $E=0$, that is

$$\frac{2\pi}{\lambda} \bar{z} + A \exp \left(- \frac{2\pi}{a} \bar{z} \right) \cos \frac{2\pi}{a} \bar{x} = 0 \quad (6)$$

where \bar{x} and \bar{z} are the cartesian coordinates of the surface. Calling

$$\frac{2\pi}{a} \bar{z} = \zeta \quad (7)$$

$$\frac{2\pi}{a} \bar{x} = \xi \quad (8)$$

$$A = - \frac{a}{\lambda} \zeta_0 \exp \zeta_0 \quad (9)$$

and separating variables, (6) becomes

$$\frac{\zeta}{\zeta_0} \exp (\zeta - \zeta_0) = \cos \xi \quad (10)$$

For each value of the new arbitrary constant ζ_0 , this equation represents a cylindrical surface with generatrix parallel to the y axis and directrix given by (10). Several members of this family of curves have been plotted in Fig. 2. The range of ξ has been selected from 0 to π since $\cos \xi$ is an even function with respect either to $\xi=0$ or $\xi=\pi$.

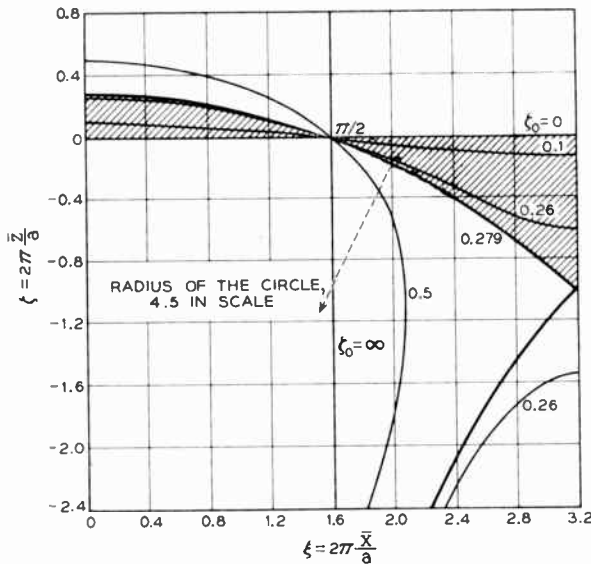


Fig. 2—Grooved wall cross sections for one correction term. Conduction current parallel to grooves.

For the sake of completeness, it must be said that for negative values of ξ_0 , the curves obtained are symmetrical to those already drawn, with respect to the line $\xi = \pi/2$, and consequently they do not need to be reproduced.

Of all the half periods of the metallic wall cross section in Fig. 2, only those given by $0 \leq \xi_0 < 0.279$ (shaded area), and particularly that corresponding to $\xi_0 = 0.279$ as a limiting case will be considered from now on, the reason being that for the continuous part of these curves, $|\zeta| \leq 1$, and consequently, the condition $\bar{z} \ll (\lambda/2\pi)$ imposed previously, is fulfilled.

Now it is possible to discuss the physical meaning of (2), (3), and (4). Far from the wall, that is for $z \rightarrow \infty$, the field is a standing TEM wave and the short circuit equivalent to the metallic wall is located in $z=0$ no matter what the value of A is. Since by (9), $|A| \ll 1$, the second term of (2), (3), and (4) becomes a correction only important for small values of z . This correction changes the cross section of the boundary surface from a straight line to a periodic curve that is sinusoidal for $-(A\lambda/a) \ll 1$, and that for $(A\lambda/a) = -1/e$, that is, for $\zeta_0 = 0.279$, becomes very similar to an arc of circle which has been drawn in Fig. 2 (dotted line) for comparison purposes.

Whatever the value of ζ_0 , all curves of Fig. 2 coincide in correspondence of the equivalent plane short circuit located in $\zeta = 0$. From the figure it is evident that for $\zeta_0 \cong 0.279$, a small change in the top of the groove corresponds to a large one in the bottom of it, the physical reason being that for $\zeta_0 \neq 0$ the wall is made of a succession of cutoff waveguides; the deeper the grooves, the longer the cutoff waveguides and consequently, the shape of the bottom of them becomes unimportant.

CONDUCTION CURRENT LOSSES FOR GROOVES PERPENDICULAR TO TANGENTIAL MAGNETIC FIELD

Because of the presence of the grooves, conduction current loss $P(\zeta_0)$, is different from the value $P(0)$ that the same standing wave would dissipate on a flat surface. The unitary increase of heat loss is

$$\frac{\Delta P}{P(0)} = \frac{P(\zeta_0) - P(0)}{P(0)} \tag{11}$$

Each value of P , calculated from (1), is a very good approximation as long as the radius of curvature of any element of the cross section is large compared to the skin depth. The only region where this condition is not satisfied is for $\bar{z}_0 = 0.279$ at $\xi = \pi$, but its contribution to the loss is that of a small area compared to the rest of the cross section, and consequently the error introduced may be neglected. Since in (1)

$$|H_t|^2 = |H_x|^2 + |H_z|^2 = |H_x|^2 \left[1 + \left(\frac{d\zeta}{d\xi} \right)^2 \right]$$

$$ds = \sqrt{(d\bar{x})^2 + (d\bar{z})^2} = d\bar{x} \left[1 + \left(\frac{d\zeta}{d\xi} \right)^2 \right]^{1/2}$$

(11) becomes from (3), (5), and (9)

$$\frac{\Delta P}{P(0)} = \frac{1}{\pi} \int_0^\pi [1 + \zeta_0 \exp(\zeta_0 - \zeta) \cos \xi]^2 \left[1 + \left(\frac{d\zeta}{d\xi} \right)^2 \right]^{3/2} d\xi - 1 \tag{11'}$$

The integration has been made graphic-numerically except for $|\zeta_0| \ll 1$, since in that case $|\zeta| \ll 1$, and being $\exp \zeta \cong 1$, the integration can be made analytically.

Fig. 3 shows graphically (11) using as abscissas the

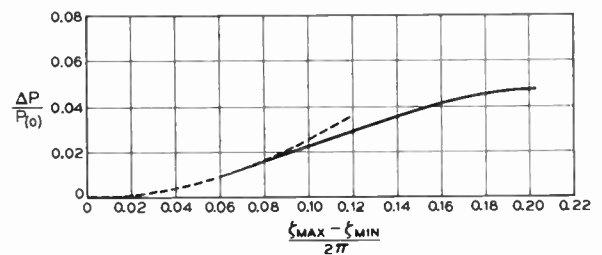


Fig. 3—Unitary heat loss increase for conduction current parallel to grooves of Fig. 2.

ratio of the depth of the groove to the period. The fundamental results are:

- 1) $\Delta P/P(0)$ is a function of the ratio of the depth of the groove to the period, so geometrical similar grooves have the same heat loss, as long as the period is large with respect to the skin depth and small with respect to the wavelength.

- 2) Grooves parallel to the conduction current have unitary heat loss increase of the order of a few per cent.
- 3) If a flat metallic surface is grooved in the direction of the conduction current the equivalent short circuit moves toward the metal ζ_0 .

As a second approximation, consider the following electromagnetic field:

$$E = \sin \frac{2\pi}{\lambda} z + M \exp \left(-\sqrt{\left(\frac{2\pi}{a}\right)^2 - \left(\frac{2\pi}{\lambda}\right)^2} z \right) \cos \frac{2\pi}{a} x$$

$$\cos \xi = -\exp(\zeta - \zeta_{\min}) \left\{ \frac{1}{4} \frac{1 + 2\zeta_{\min}}{1 + \zeta_{\min}} \mp \sqrt{\left(\frac{1}{4} \frac{1 + 2\zeta_{\min}}{1 + \zeta_{\min}}\right)^2 - \frac{\zeta}{2(1 + \zeta_{\min})} + \frac{\exp[2(\zeta_{\min} - \zeta)]}{2}} \right\} \quad (20)$$

$$+ N \exp \left(-\sqrt{\left(\frac{4\pi}{a}\right)^2 - \left(\frac{2\pi}{\lambda}\right)^2} z \right) \cos \frac{4\pi}{a} x \quad (12)$$

$$H_x = \frac{1}{i\mu\omega} \frac{\partial E}{\partial z} \quad (13)$$

$$H_z = -\frac{1}{i\mu\omega} \frac{\partial E}{\partial x} \quad (14)$$

These expressions are similar to (2), (3), and (4) only that another term of the Fourier expansion has been added.

Assuming $(a/\lambda) \ll 1$, the electric field in $|z| \ll \lambda$ becomes

$$E = \frac{2\pi}{\lambda} z + M \exp \left(-\frac{2\pi}{a} z \right) \cos \frac{2\pi}{a} x + N \exp \left(-\frac{4\pi}{a} z \right) \cos \frac{4\pi}{a} x \quad (15)$$

and the metal surface capable of satisfying the boundary value of this field is

$$\zeta + \exp(-\zeta + \zeta_1) \cos \xi + \exp(2\zeta + \zeta_2) \cos 2\xi = 0 \quad (16)$$

where ζ_1 and ζ_2 are arbitrary constants, $\zeta = (2\pi/a)z$, $\xi = (2\pi/a)x$, and x and z are the coordinates of the directrices of the cylindrical metallic surfaces. Because there are two arbitrary constants, there is a double infinity of possible curves represented by (16), but we are interested in those that, like curve $\zeta_0 = 1$ of Fig. 2 have a discontinuity in the derivative at ξ equal to any odd number of π . This discontinuity corresponds to $H_x = 0$ at the bottom of the grooves. Consequently from (13) and (15), after the familiar change of variables, and for $\zeta = \zeta_{\min}$ and $\xi = (2n+1)\pi$ with $n = \pm 0, 1, 2, 3 \dots$

$$H_x = 0 = 1 + \exp(-\zeta_{\min} + \zeta_1) - 2 \exp(-2\zeta_{\min} + \zeta_2) \quad (17)$$

is obtained.

For the same points of discontinuity, (16) becomes

$$\zeta_{\min} - \exp(-\zeta_{\min} + \zeta_1) + \exp(-2\zeta_{\min} + \zeta_2) = 0 \quad (18)$$

From (17) and (18), $\exp \zeta_1$ and $\exp \zeta_2$ are found to be only functions of ζ_{\min} and (16) becomes

$$\zeta + (1 + 2\zeta_{\min}) \exp(\zeta_{\min} - \zeta) \cos \xi + (1 + \zeta_{\min}) \exp[2(\zeta_{\min} - \zeta)] \cos 2\xi = 0 \quad (19)$$

Separating variables,

Since we are looking for deep grooves, selecting $|\zeta_{\min}| > 1$, the fraction before the square root is positive. The consequence is that since $\cos \xi$ has positive as well as negative values the negative sign of the alternative choice must be selected. For the points at the bottom of the grooves, $\xi = (2n+1)\pi$ and $\zeta = \zeta_{\min}$, (20) becomes

$$-1 = -\frac{1}{4} \frac{1 + 2\zeta_{\min}}{1 + \zeta_{\min}} + \frac{1}{4} \frac{3 + 2\zeta_{\min}}{1 + \zeta_{\min}}$$

and after some algebra

$$\zeta_{\min} = -\frac{3}{2}$$

Carrying this expression to (20), the equation of the wall cross section is

$$\cos \xi = -\exp(-\zeta + 1.5) \cdot [1 - \sqrt{1 + \zeta + \frac{1}{2} \exp[-2(1.5 + \zeta)]}] \quad (21)$$

and its geometry is shown in Fig. 4 together with a circle (dotted line) for comparison purposes.

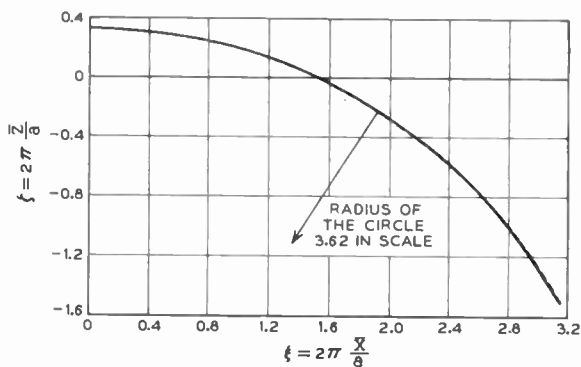


Fig. 4—Grooved wall cross section for two correction terms.

Again, the unitary increment of power dissipated on the wall on account of the grooves (21), was calculated graphic-numerically from the expression

$$\frac{\Delta P}{P(0)} = \frac{1}{\pi} \int_0^\pi [1 + 2 \exp(-1.5 - \zeta) \cos \xi + \exp(-3 - 2\zeta) \cos 2\xi]^2 \cdot \left[1 + \left(\frac{d\zeta}{d\xi}\right)^2\right]^{3/2} d\xi - 1. \quad (22)$$

The result is

$$\frac{\Delta P}{P(0)} = 0.069.$$

Now it is possible to plot $\Delta P/P(0)$ against relative groove depths, $(\zeta_{\max} - \zeta_{\min})/r$ for three wall cross sections made of successive arcs of circles of radii r (Fig. 5). The coordinates of these points are:

$$1) \quad \frac{\zeta_{\max} - \zeta_{\min}}{r} = 0 \quad \text{and} \quad \frac{\Delta P}{P(0)} = 0$$

corresponding to a flat surface and the electromagnetic field has no correction term.

$$2) \quad \frac{\zeta_{\max} - \zeta_{\min}}{r} = \frac{1.279}{4.5} = 0.284 \quad \text{and} \quad \frac{\Delta P}{P(0)} = 0.049$$

corresponding to one correction term.

$$3) \quad \frac{\zeta_{\max} - \zeta_{\min}}{r} = \frac{1.833}{3.62} = 0.505 \quad \text{and} \quad \frac{\Delta P}{P(0)} = 0.069$$

corresponding to two correction terms.

Observing Fig. 5, it becomes apparent that with these three points it is possible to extrapolate the result for a relative groove depth equal to 1. For this abscissa, $\Delta P/P(0) = 0.09 \pm 0.01$.³

MAGNETIC FIELD PARALLEL TO THE GROOVE

Consider the following electromagnetic field

$$H_y = \cos \frac{2\pi}{\lambda} z + A \exp\left(-\sqrt{\left(\frac{2\pi}{a}\right)^2 - \left(\frac{2\pi}{\lambda}\right)^2} z\right) \cos \frac{2\pi}{a} x$$

$$|E_s| = \sqrt{|E_x|^2 + |E_z|^2} = \frac{1}{\epsilon\mu} \frac{2\pi}{\lambda} \sqrt{\left(\frac{a}{\lambda} \zeta\right)^2 + \left[\frac{\lambda}{a} A \exp(-\zeta)\right]^2 - 2\zeta A \exp(-\zeta) \cos \xi}$$

³ When this paper was finished, the author found out that J. A. Morrison of Bell Telephone Labs. has worked out an exact solution for the increase of heat loss in the case of relative groove depth equal to 1, and his result is

$$\frac{\Delta P}{P(0)} = \frac{8}{\pi^3} \int_0^1 [K(k)]^2 dc - 1 = 0.085$$

where $c = k^2$ and $K(k)$ is the complete elliptic integral of the first kind and modulus k .

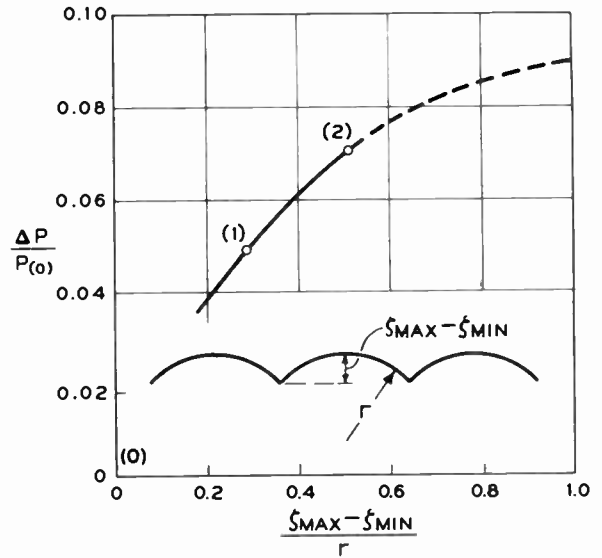


Fig. 5—Unitary heat loss increase for conduction current parallel to grooves. (0), (1), and (2) are the number of correction terms.

$$E_x = -\frac{1}{i\epsilon\omega} \frac{\partial H_y}{\partial x}$$

$$E_z = \frac{1}{i\epsilon\omega} \frac{\partial H_y}{\partial z} \quad (23)$$

For $(a/\lambda) \ll 1$ and on the surface of the metal, the field becomes with

$$H_y = 1 - \frac{1}{2} \left(\zeta \frac{a}{\lambda}\right)^2 + A \exp(-\zeta) \cos \xi \quad (24)$$

$$E_x = \frac{1}{i\epsilon\omega} \frac{2\pi}{\lambda} \left[\frac{a}{\lambda} \zeta - \frac{\lambda}{a} A \exp(-\zeta) \cos \xi \right] \quad (25)$$

$$E_z = \frac{1}{i\epsilon\omega} \frac{2\pi}{\lambda} \frac{\lambda}{a} A \exp(-\zeta) \sin \xi. \quad (26)$$

Far from the wall, the amplitude of the standing electric field is from (23) for $z \rightarrow \infty$

$$E = \frac{1}{\epsilon\omega} \frac{2\pi}{\lambda} \quad (27)$$

On the metallic surface the amplitude of the electric field obtained from (25) and (26) is

and the maximum possible value is

$$|E_s|_{\max} = \frac{1}{\epsilon\mu} \frac{2\pi}{\lambda} \left[\frac{a}{\lambda} \zeta + \frac{\lambda}{a} A \exp(-\zeta) \right] \quad (28)$$

From (27) and (28)

$$\frac{|E_s|_{\max}}{E} = \frac{a}{\lambda} |\zeta| + \frac{\lambda}{a} |A| \exp(-\zeta). \quad (29)$$

Assuming for the time being that

$$\frac{a}{\lambda} |\zeta| + \frac{\lambda}{a} |A| \exp(-\zeta) \ll 1, \quad (30)$$

the electric field on the metallic surface is very small and the transformation of conduction current into displacement current is negligible. The consequence is that the geometry of the wall is obtained making II_y a constant. From (24)

$$-\zeta^2 + 2\left(\frac{\pi}{a}\right)^2 A \exp(-\zeta) \cos \xi = B \quad (31)$$

where B is an arbitrary constant.

Establishing the location of the top of the grooves in

$$\zeta = 0; \quad \xi = 2n\pi, \quad n = \pm 0, 1, 2, 3, \dots$$

and the bottom of the grooves in

$$\zeta = \zeta_{\min}; \quad \xi = (2m + 1)\pi, \quad m = \pm 0, 1, 2, 3$$

the following results are obtained from (31)

$$A \frac{\lambda}{a} = -\frac{a}{\lambda} \frac{\zeta_{\min}^2}{2[1 + \exp(-\zeta_{\min})]} \quad (32)$$

$$\cos \xi = \left[1 - \left(\frac{\zeta}{\zeta_{\min}}\right)^2 [1 + \exp(-\zeta_{\min})] \right] \exp(\zeta). \quad (33)$$

Carrying (32) to (30), the inequality reads

$$\frac{a}{\lambda} \left[|\zeta| + \frac{\zeta_{\min}^2 \exp(-\zeta)}{2[1 + \exp(-\zeta_{\min})]} \right] \ll 1$$

and in the most pessimistic condition, that is, at the bottom of the groove and for $\exp(-\zeta_{\min}) \gg 1$,

$$\frac{a}{2\lambda} \zeta_{\min}^2 \ll 1. \quad (34)$$

As long as this inequality is fulfilled, (33) represents the cross section of the wall; several members of the family are plotted in Fig. 6.

CONDUCTION CURRENT LOSSES FOR GROOVES PARALLEL TO TANGENTIAL MAGNETIC FIELD

The unitary increase of heat loss due to the grooves is calculated from (11) and (1)

$$\frac{\Delta P}{P(0)} = \frac{\int_S |II_t|^2 ds - \int_{S_0} |II_{t0}|^2 ds}{\int_{S_0} |II_{t0}|^2 ds} \quad (35)$$

where II_t is the intensity of the magnetic tangential field on the grooved wall, $|II_{t0}|$, the intensity of the tangen-

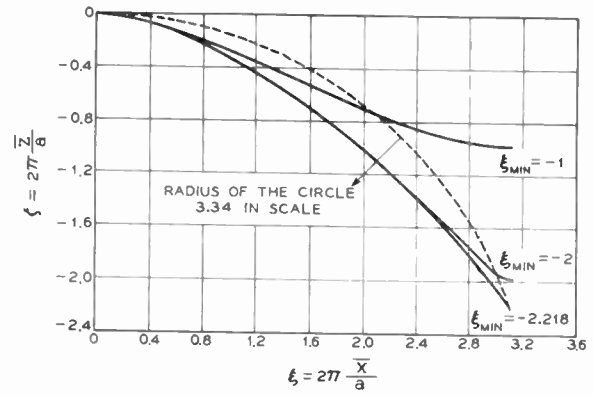


Fig. 6—Grooved wall cross section for one correction term. Conduction current perpendicular to grooves.

tial field if the wall is plane, S is the surface of the grooved wall, and S_0 the surface of the flat wall.

$|II_t|$ obtained from (24) and (32) is very close to unity and $|II_{t0}| = 1$ by definition, therefore (35) yields

$$\frac{\Delta P}{P_0} = \frac{S - S_0}{S_0} = \frac{l - a}{a} \quad (36)$$

where l is the length of the cross section per period.

Because of the fact that close to the short circuit the electric field is close to zero if (34) is satisfied, it is possible to conclude from (36) that whatever the shape of the curve, the unitary increase of heat loss is proportional to the unitary increase of cross section of the wall.

CONCLUSION

An elementary and accurate way has been shown to calculate the heat losses in metallic waveguide walls that have parallel periodic grooves of semicircular cross section when the diameter of each semicircle is small with respect to the free space wavelength and large with respect to the skin depth.

The conduction current loss is $\pi/2$ times the heat loss calculated with flat surface if the grooves are perpendicular to the conduction current and 1.09 ± 0.01 the heat loss calculated with flat surface if the grooves are parallel to the conduction current.

This last result is a good approximation to the experimental value obtained for a helical waveguide⁴ of 7/16-inch diameter carrying TE_{01} mode at 5.4-mm wavelength. The pitch is approximately two times the 0.00445-inch diameter of the wire and the conduction current loss plus the coupled power to the outside lossy jacket has been measured to be 1.1 times the value of heat loss for the circular cylindrical waveguide. Since the spaces between successive turns are cut off waveguides for circular electric modes, the coupled power is negligible and the excess loss is essentially due to the presence of grooves on the wall.

⁴ J. A. Young, unpublished work.

IRE Standards on Letter Symbols and Mathematical Signs, 1948 (Reprinted 1957)*

(57 IRE 21 S1)

NEW FOREWORD

THE MATERIAL contained in this printing is abstracted from the 1948 Standards on Abbreviations, Graphical Symbols, Letter Symbols and Mathematical Signs, now out of print. The abbreviations portion of that document has been superseded by Standard 51 IRE 21 S1, while the graphical symbols portion has been superseded by Standard 54 IRE 21 S1. The 1957 Symbols Committee and the Standards Committee have authorized reprinting of this remaining portion of the 1948 Standard in the belief that it will serve a useful purpose pending completion of a more comprehensive Standard being prepared by the Symbols Committee.

101. GENERAL PRINCIPLES OF LETTER SYMBOL STANDARDIZATION

101.1. General

In preparing manuscripts, it is suggested that authors give careful attention to the use of symbols from this and other standard lists and to the principles here given. Symbols used should be defined clearly. When a table of symbols is not given, it is desirable to make reference to the standard lists from which the symbols are taken. The many numbers, letters, and signs which are similar in appearance should be distinguished carefully.

101.2. Definitions

A *magnitude letter symbol* is a single letter, with subscript or superscript if required, used to designate the magnitude of a physical quantity in mathematical equations and expressions. Two or more magnitude symbols printed together always represent a product. Magnitude letter symbols are to be distinguished from the following:

101.21. *Abbreviations*, which are shortened forms of names and expressions employed in texts and tabulations. Neither the abbreviation of the name of the unit of a physical quantity nor the single-letter designation of the unit should ever be used in place of the magnitude symbol in an equation.

101.22. *Mathematical signs and operators*, which are characters used with magnitude symbols to denote mathematical operations and relations.

* Reprints of this Standard, 57 IRE 21 S1, may be purchased while available from the Institute of Radio Engineers, 1 East 79th Street, New York, N. Y., at \$0.60 per copy. A 20 per cent discount will be allowed for 100 or more copies mailed to one address.

101.23. *Graphical symbols*, which are conventionalized diagrams and letters used on plans and drawings.

101.24. *Chemical symbols*, which are letters and other characters designating chemical elements and groups.

101.3. Units

The same symbol should be used for the magnitude of the same physical quantity regardless of the units employed and regardless of special values occurring for different states, points, parts, times, etc. The units employed and the special values may be designated when necessary by subscripts, superscripts, or by upper and lower-case letters when both are specifically included as symbols in a standard list. The units used should be indicated when necessary. Sometimes different symbols are used for the components of a vector.

101.4. Subscripts

A subscript preferably should be a single character. It is commonly employed to indicate a specified value of a physical quantity, such as pressure or temperature. A multiple subscript, sometimes divided by a comma, refers to more than one state, point, part, time, etc. A subscript should not be attached to a subscript except in extreme cases.

101.5. Superscripts

A symbol with a superscript, such as a prime (') or a double prime (''), should be enclosed in parentheses, braces, or brackets before affixing an exponent. A complicated exponent (or any other expression frequently repeated) may be replaced by a single symbol selected to represent it. Reference marks should not be attached to symbols.

101.6. Conflicts

Conflicts which would occur when different physical quantities are assigned identical magnitude symbols in the same or different standard symbol lists may be resolved in one of the following ways:

101.61. For one or more of the conflicting uses, the given symbol may be employed with subscript or superscript selected by the author.

101.62. If one of the quantities has an alternate symbol in a standard list, it may be used.

101.63. A slight change in the name of the quantity may remove the conflict. For instance, one may use l for "length of radius" when r for "radius" conflicts with r used for the magnitude of another quantity.

101.7. *Unlisted Quantities*

The symbol chosen by an author for a physical quantity not appearing in any standard list should be one that does not already have a different meaning in the field of the text.

101.86. Abbreviations and names of units should be printed in roman type.

101.87. Mathematical signs and operators should be printed in roman type except when they are single letters, in which case they should be printed in italics.

101.88. *Examples of typographical standards:*

Item	Standard for Printed Page	Standard for Manuscript
Scalars	<i>E</i> (italic)	<u>E</u>
Vectors	E (bold roman)	<u>E</u>
Phasors	<i>E</i> (bold italic)	<u><i>E</i></u>
Conjugate phasors	<i>E</i>* (bold italic)	<u><i>E</i>*</u>
Absolute magnitude of phasor	<i>E</i> or (italic)	<u>E</u> or
	 E (bold italic)	<u> E </u>
Letter exponents and subscripts	<i>E^A, E_h</i> (italic)	<u>E^h</u> , <u>E_h</u>
Numbers	4 (roman)	4
Names and abbreviations of units	amp, m (roman)	amp, m
Names of functions and operators	cos, exp, (roman)	cos, exp,
	curl, log, div, grad	curl, log, div, grad
Exceptions to preceding item: Single-letter designations of functions and operators	<i>d, D_x, f(x)</i> (italic)	d, D _x , f(x)
	<i>Jo(x), j, a, P(n, r)</i>	Jo(x), j, a, P(n, r)

101.8. *Typography*

101.81. Letter symbols and letter subscripts, whether upper or lower case, should be printed in italic type unless definitely specified otherwise. On manuscript this is indicated by underlining each symbol which is to be italicized.

101.82. Letter symbols for scalar quantities are printed in italic type. When special type is used for vector quantities, the same letter in italic type should be used for the corresponding scalar magnitude of the vector quantity.

101.83. Letter symbols for vector quantities should be printed in bold roman type, unless the text deals only with the magnitudes of the vector quantities and not with their vector relations. On manuscript, bold roman type is indicated by wavy underlining.

101.84. Letter symbols for phasor quantities are printed in bold italic type. Phasor quantities are quantities whose values are expressed by complex numbers. The conjugate of a phasor may be designated by a star following the letter symbol of the phasor. On manuscript bold italic may be indicated by both straight and wavy underlines, such as ***A***.

101.85. Numerals are printed in roman type whether appearing as terms in equations, coefficients, exponents, or subscripts.

102. SPECIAL PRINCIPLES

102.1. *Applications to Electrical Circuits*

102.11. Instantaneous values of current, voltage, and power which vary with time are represented by the lower-case letter of the proper symbol.

Example: *i, e, p, i_o, e_a.*

102.12. Maximum, average, and root-mean-square values are represented by the upper-case letter of the proper symbol.

Example: *I, E, P, I_p, E_p.*

If necessary to distinguish between maximum, average, or root-mean-square values:

Maximum values may be represented by the subscript "m."

Example: *E_m, I_m, E_{pm}.*

Average values may be represented by the subscript "av."

Example: *E_{av}, I_{pav}.*

Root-mean-square or effective values may be represented by the upper-case letter without subscript.

Example: *E, I, E_o, I_p.*

102.2. *Applications to Electron Tube Circuits*

102.21. *External.* Values of resistance, impedance, admittance, etc., in the external circuit of an electrode may be represented by the upper-case symbols for the quantities with the proper electrode subscripts.

Example: $R_j, Z_j, Y_j, R_p, Z_p, Y_p, C_{gp}$.

102.22. *Inherent.* Values of resistance, impedance, admittance, etc., inherent in the tube may be represented by the lower-case symbol with the proper electrode subscripts.

Example: $r_{jk}, z_j, y_j, r_p, z_p, y_p, c_{gp}$.

102.3. Applications for Electron Tubes

102.31. Symbols for quantities in electrode circuits of electron tubes are developed from the proper quantity symbol and subscripts representing the electrodes concerned. When one of the electrodes concerned is the cathode, the subscript "k" may be omitted and the single subscript understood to mean "with respect to the cathode."

102.32. The electrode abbreviations to be used as subscripts are:

- j general (convention for any electrode)
- f filament
- h heater
- k cathode
- g grid (c also used: see 102.36)
- p plate or anode (b also used; see 102.36)
- s metal shell, or other self-shielding envelope
- d deflecting, reflecting, or repelling electrode (electrostatic type).

Example: $e_{jk}, e_j, E_{pk}, E_p, C_{gp}$.

102.33. Grid subscripts for multigrid tubes are developed by a numerical addition to the subscript. Grids are numbered according to position out from the cathode. When no numerical subscript appears, reference to the control grid is assumed.

Example: $e_{g1}, e_{g2}, c_{g1g2}, e_g$.

102.34. Deflection electrode subscripts for cathode-ray tubes are developed by a numerical addition to the subscript.

Example: $c_{d1d2}, e_{d1d2}, e_{d3d1}$.

102.35. In a double-subscript symbol, when the direction of the relationship is significant, the first subscript should designate the electrode circuit in which the effect (product of the multiplying operation) is measurable; and the second subscript should designate the electrode circuit in which the cause (operand or multiplicand) is measurable. This subscript sequence conforms to the mathematical convention for writing determinants from a set of fundamental Kirchlhoff's equations.

Example: g_{j2j1}, g_{vp}, g_{gp} .

102.36. When necessary to distinguish between components of current and voltage encountered in electron-tube circuits, the following symbols may be used. Their application to the case of a tube having a small varying component in the plate circuit is illustrated in the accompanying diagram in Fig. 1.

102.361. Instantaneous current and voltage values of a varying component may be represented by lower-case symbols with the subscripts "g" and "p" for grid and plate, respectively.

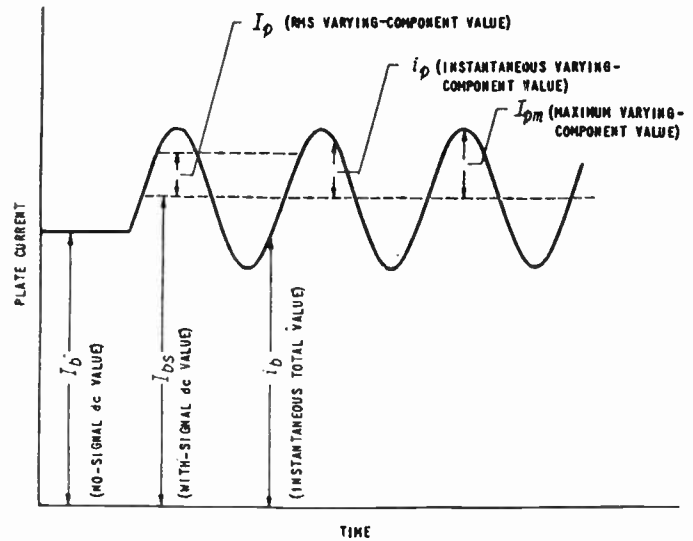


Fig. 1.

Example: e_p, i_g, e_{g3} .

102.362. Instantaneous total values of current and voltage (no-signal dc value plus varying-component value) may be represented by lower-case symbols and the subscripts "b" for plate and "c" for grid.

Example: i_b, e_c, i_{c2} .

102.363. Root-mean-square and maximum current and voltage values of a varying component may be represented by upper-case symbols and the subscripts given in 102.361.

Example: E_g, I_p, E_{pm} .

102.364. Values of current and voltage for the no-signal or static condition may be represented by upper-case symbols and the subscripts given in 102.362.

Example: E_{c3}, I_b, E_c .

102.365. Average values of current and voltage for the with-signal condition may be represented by the addition of the subscript "s" to symbols determined in accordance with 102.364.

Example: I_{bs}, E_{cs}, E_{bs} .

102.366. Supply voltages for electron tube elements may be represented by upper-case symbols and doubling the electrode subscripts indicated in 102.362 plus "ff" for the case of heater or filament supply.

Example: $E_{ff}, E_{cc}, E_{bb}, E_{cc2}$.

103. LIST OF LETTER SYMBOLS AND MATHEMATICAL SIGNS (IN ALPHABETICAL ORDER OF QUANTITY)

α	absorption factor
Y, Y, y	admittance
α	acceleration, angular
a	acceleration, linear
μ	amplification factor of an electron tube ($\mu = \mu_{pg}$) (see μ factor)
ω	angle, solid
θ	angle, transit
ω	angular frequency ($\omega = 2\pi f$)
ω_r	angular frequency, resonance

<i>A</i>	area	ϕ, θ	displacement, phase (phase angle)
α	attenuation constant ($\gamma = \alpha + j\beta$)	<i>D</i>	duty factor, duty cycle ($D = t_n f_n$)
<i>e</i>	base of Naperian or natural logarithms ($e = 2.718 \dots$)	η	efficiency
<i>B</i>	brightness, luminance ($B = \frac{dI}{dA \cos \theta}$)		elastance, self-elastance ($S = \frac{1}{c}$)
<i>C, c</i>	capacitance, (permittance)	E	electric field, electric field strength, electric intensity, electric field intensity
<i>X_C</i>	capacitive reactance	p	electric moment of a dipole
ϵ	capacitance, dielectric constant, dielectric coefficient	<i>E, e, V, v</i>	electromotive force, electric potential difference, voltage
<i>Z₀</i>	characteristic impedance, surge impedance charge, electronic ($e = 1.602 \dots \times 10^{-19}$ coulombs)	ϵ	emissivity
λ	charge, line density	ϵ_λ	emissivity, spectral
<i>Q, q</i>	charge, quantity of electricity (electric)	ϵ_t	emissivity, total
σ	charge, surface density of	<i>W</i>	energy, work
<i>p</i>	charge, volume density of (electric)	<i>U</i>	energy, internal or intrinsic
<i>p</i>	complex frequency, oscillation constant ($p = \delta + j\omega$)	<i>U</i>	energy, radiant
<i>G, g</i>	conductance	<i>H</i>	enthalpy, heat content
σ, ν	conductivity	<i>S</i>	entropy
<i>k</i>	conductivity, thermal	α	expansion, temperature coefficient of linear
<i>k</i>	coupling coefficient	exp	exponential function
<i>I, I, i</i>	current, electric	<i>F</i>	Faraday constant
<i>J, J</i>	current density, electric	H	field strength, magnetic (magnetic intensity, magnetizing force)
<i>A</i>	current density, sheet (linear current density)	<i>Q</i>	figure of merit of a reactor
<i>I_s, i_s</i>	current, saturation of a cathode, total electron emission	W	flux density, radiant
δ	damping constant, damping coefficient (decay constant) ($p = \delta + j\omega$)	ψ	flux, dielectric (displacement flux, flux of electric displacement)
<i>t_d</i>	deionization time	<i>F</i>	flux, luminous
J, J	density, current	Φ	flux, magnetic (flux of magnetic induction)
B	density, magnetic flux	Φ	flux, radiant ($\Phi = \frac{dU}{dt}$)
λ	density of charge, linear	F	force
σ	density of charge, surface	<i>f</i>	frequency
ρ	density of charge, volume	ω	frequency, angular ($\omega = 2\pi f$)
W	density of radiant flux	<i>f_c</i>	frequency, critical or cutoff
<i>A</i>	density, sheet current (linear current density)	<i>f_p</i>	frequency, pulse recurrence
<i>D</i>	derivative operator	<i>f_r</i>	frequency, resonance
<i>d, D</i>	diameter	ω_r	frequency, resonance angular
ϵ_0	dielectric constant, complex ($\epsilon_0 \approx \epsilon_r + j60\lambda\sigma$)	g, g	gravitational acceleration
ϵ	dielectric constant, dielectric coefficient, capacitance	<i>G</i>	gravitational constant
ϵ_v	dielectric constant of evacuated (free) space ($\epsilon_v = 8.855 \dots \times 10^{-12}$ farad per meter)	<i>H</i>	heat content, enthalpy
ϵ_r	dielectric constant, relative (specific inductive capacitance)	<i>Q</i>	heat, quantity of
ψ	dielectric flux, displacement flux (flux of electric displacement)	<i>q</i>	heat, rate of flow of
D	dielectric flux density, electric displacement	<i>t_k</i>	heating time, cathode
ϵ_i, η	dielectric susceptibility (intrinsic capacitivity) [$\epsilon_i = (\epsilon_r - 1)\epsilon_v$]	<i>I</i>	illuminance, amount of illumination
<i>d</i>	differential operator		
∂	differential operator, partial		
α	diffusivity, thermal		
D	displacement, electric (dielectric flux density)		
			$\left(E = \frac{dF}{dA}\right)$
		<i>Z₀</i>	impedance, characteristic (surge impedance)
		η	impedance of a medium, intrinsic
		Z, Z, z	impedance, self-impedance
		Δ	increment
		<i>L₁₂, etc.</i>	inductance, mutual

<i>L</i>	inductance, self-inductance	<i>m</i>	moment, magnetic
B	induction, magnetic (magnetic flux density) ($\mathbf{B} = \mu_r \mu_v \mathbf{H}$)	μ_{j3j2}	μ factor of an electron tube, relative effect of change on electrode "j3" to change on electrode "j2" (conditions of other electrodes to be specified) (see amplification factor)
<i>X_L</i>	inductive reactance	<i>L₁₂</i> , etc.	mutual inductance
E	intensity, electric (electric field strength, electric field intensity, electric field)	<i>e</i>	Naperian or natural logarithms, base of ($e = 2.718 \dots$)
<i>I</i>	intensity, luminous (candle power) $\left(I = \frac{dF}{d\omega} \right)$	<i>p</i>	number of poles
H	intensity, magnetic (magnetizing force, magnetic field strength)	<i>N</i>	number of turns or conductors
<i>J</i>	intensity, radiant ($J = \frac{d\Phi}{d\omega}$)	<i>n</i>	number per unit of measurement
B_i	intrinsic induction, magnetic polarization ($\mathbf{B}_i = \mathbf{B} - \mu_v \mathbf{H}$)	<i>D</i>	operator, derivative
<i>U</i>	internal or intrinsic energy	<i>d</i>	operator, differential
<i>l</i>	length	∇	operator, vector
<i>s</i>	length of path	∂	operator, partial differential
<i>Q</i>	light, quantity of	<i>j</i>	operator, 90° rotational, or $\sqrt{-1}$
ln	logarithm to base <i>e</i>	<i>a</i>	operator, 120° rotational
log	logarithm to base 10	<i>p</i>	oscillation constant, complex frequency ($p = \delta + j\omega$)
<i>B</i>	luminance (see brightness)	<i>T</i>	period
<i>K</i>	luminosity factor ($K = \frac{F_\lambda}{\Phi_\lambda}$)	μ_0	permeability, initial magnetic
<i>F</i>	luminous flux	μ	permeability, magnetic
<i>I</i>	luminous intensity ($I = \frac{dF}{d\omega}$)	μ_i	permeability, intrinsic magnetic (magnetic susceptibility), ($\mu_i = \mu_r - 1$) μ_v)
<i>S_F, S_P</i>	luminous sensitivity of a phototube	μ_r	permeability, relative magnetic
Φ	magnetic flux (flux of magnetic induction)	μ_v	permeability, magnetic, evacuated (free) space
B	magnetic flux density (magnetic induction), ($\mathbf{B} = \mu_r \mu_v \mathbf{H}$)	\mathcal{P}	permeance
H	magnetic intensity, magnetizing force (magnetic field strength)	<i>C, c</i>	permittance, capacitance
<i>m</i>	magnetic moment	β	phase constant, (wave number) wavelength constant ($\beta = \frac{2\pi}{\lambda}$)
μ	magnetic permeability	ϕ, θ	phase displacement, phase angle
μ_0	magnetic permeability, initial	π	pi, a ratio ($\pi = 3.14159 \dots$)
μ_v	magnetic permeability of evacuated (free) space	<i>h</i>	Planck constant ($h = 6.624 \dots \times 10^{-34}$ joule sec)
μ_r	magnetic permeability, relative	P	polarization, electric ($\mathbf{P} = (\epsilon_r - 1)\epsilon_v \mathbf{E}$)
B_i	magnetic polarization (intrinsic induction) ($\mathbf{B}_i = \mathbf{B} - \mu_v \mathbf{H}$)	<i>p</i>	poles, number of
μ_i	magnetic susceptibility (intrinsic magnetic permeability) ($\mu_i = (\mu_r - 1)\mu_v$)	<i>V, v, E, e</i>	potential difference, electric; electromotive force; voltage
A	magnetic vector potential	<i>V_r</i>	potential, electric scalar, retarded
A_r	magnetic vector potential, retarded	\mathcal{F}	potential, magnetic; magnetomotive force
H	magnetizing force, magnetic intensity (magnetic field strength)	A	potential, magnetic vector
\mathcal{F}	magnetomotive force, magnetic potential	A_r	potential, magnetic vector, retarded
<i>m</i>	mass	<i>P, p</i>	power, active power
<i>T_{H0}</i>	mercury condensate, temperature of	<i>P_p</i>	power, anode or plate dissipation
p	moment of a dipole, electric	<i>F_p</i>	power factor
<i>I</i>	moment of inertia	<i>P_g</i>	power, grid dissipation
		<i>P_i</i>	power, input
		<i>P_o</i>	power, output
		<i>p</i>	pressure
		γ	propagation constant ($\gamma = \alpha + j\beta$)
		<i>f_p</i>	pulse-recurrence frequency
		<i>Q, q</i>	quantity of electricity
		<i>Q</i>	quantity of electric charge
		<i>Q</i>	quantity of heat
		<i>Q</i>	quantity of light

U	radiant energy	k	thermal conductivity
Φ	radiant flux ($\Phi = \frac{dU}{dt}$)	α	thermal diffusivity
W	radiant flux density	t	time
J	radiant intensity ($J = \frac{d\Phi}{d\omega}$)	τ	time constant
R, r	radius	t_k	time of cathode heating
q	rate of flow of heat	t_d	time of deionization
X_C	reactance, capacitive	t_p	time of pulse duration
X_L	reactance, inductive	t_f	time of pulse fall
X, x	reactance, self-reactance	t_r	time of pulse rise
F_q	reactive factor	ϵ_t	total emissivity
P_q	reactive voltamperes (reactive power)	g_c	transconductance, conversion
ρ	reflection coefficient	g_{j2j1}	transconductance, effect in circuit of electrode "j2" to a change on electrode "j1"
\mathcal{R}	reluctance	g_n (also g_{op})	transconductance, inverse (inverse mutual conductance), effect in grid circuit to change on plate
ν	reluctivity ($\nu = \frac{1}{\mu}$)	g_m (also g_{pv})	transconductance, grid-plate (mutual conductance) effect in plate circuit to change on control grid
R, r	resistance	θ	transit angle
α	resistance, temperature coefficient of	τ	transmission factor
ρ	resistivity or specific resistance	∇	vector operator
f_r	resonance frequency	i	vector, unit (X -axis)
λ_r	resonance wavelength	j	vector, unit (Y -axis)
V_r	retarded electric scalar potential	k	vector, unit (Z -axis)
A_r	retarded magnetic vector potential	v	velocity
I_s, i_s	saturation current of a cathode, total electron emission	c	velocity of light in vacuum ($c = 2.998 \cdot \cdot \cdot \times 10^8$ kmps)
δ	secondary-emission ratio	V, v, E, e	voltage, electromotive force, electric potential difference
Z, Z, z	self-impedance, impedance	P_s	voltamperes (apparent power)
L	self-inductance, inductance	P_q	voltamperes, reactive (reactive power)
X, x	self-reactance, reactance	V	volume
s	sensitivity of a phototube, dynamic	ρ	volume density of electric charge
S_F, S_F	sensitivity of a phototube, luminous	β	wavelength constant, phase constant (wave number) ($\beta = \frac{2\pi}{\lambda}$)
S	sensitivity of a phototube, static		
S_{2870}, S_{2870}	sensitivity of a phototube, 2870° Kelvin tungsten		
s	slip (in electrical machinery)	λ_c	wavelength, critical or cutoff
c	specific heat, thermal capacity of unit mass	λ	wavelength in free space
ρ	specific resistance or resistivity	λ_r	wavelength, resonance
ϵ	spectral emissivity	W	work, energy
S	standing-wave ratio	E	Young's modulus of elasticity
\sum	summation		
σ	surface density of charge		
Z_0	surge impedance, characteristic impedance		
B, b	susceptance ($Y = G + jB$)		
ϵ_i, η	susceptibility, dielectric (intrinsic capacitvity) ($\epsilon_i = (\epsilon_r - 1)\epsilon_0$)		
μ_i, κ	susceptibility, magnetic (intrinsic magnetic permeability)		
T	temperature		
α	temperature coefficient of linear expansion		
α	temperature coefficient of resistance		
T_{Hg}	temperature of mercury condensate		
c	thermal capacity of unit mass, specific heat		

104. LIST OF LETTER SYMBOLS AND MATHEMATICAL SIGNS (IN ALPHABETICAL ORDER)

a	linear acceleration
a	120° rotative operator
A	area
A	sheet current density (linear current density)
A	magnetic vector potential
A_r	retarded magnetic vector potential
α	absorption factor
α	angular acceleration
α	attenuation constant
α	temperature coefficient of linear expansion

α	temperature coefficient of resistance	η	efficiency
α	thermal diffusivity	η	intrinsic impedance of a medium
		η, ϵ_i	dielectric susceptibility (intrinsic capacitance) ($\epsilon_i = (\epsilon_r - 1)\epsilon_0$)
B	brightness, luminance ($B = -\frac{dI}{dA \cos \theta}$)	F	Faraday constant
\mathbf{B}	magnetic flux density, magnetic induction ($\mathbf{B} = \mu_r \mu_v \mathbf{H}$)	\mathbf{F}	force
B, b	susceptance ($Y = G + jB$)	f	frequency
\mathbf{B}_i	magnetic polarization, intrinsic induction ($\mathbf{B}_i = \mathbf{B} - \mu_v \mathbf{H}$)	F	luminous flux
β	wavelength constant, phase constant (wave number) ($\beta = \frac{2\pi}{\lambda}$)	\mathcal{F}	magnetomotive force, magnetic potential
		f_c	critical or cutoff frequency
		f_p	pulse-recurrence frequency
		F_p	power factor
		F_q	reactive factor
		f_r	resonance frequency
C, c	capacitance (permittance)	G, g	conductance
c	specific heat, thermal capacity of unit mass	\mathbf{g}, g	gravitational acceleration
c	velocity of light in vacuum ($c = 2.998 \dots \times 10^8$ kmps)	G	gravitational constant
D	derivative operator	g_c	conversion transconductance
d, D	diameter	g_{j2j1}	transconductance, effect in circuit of electrode "j2" to a change on electrode "j1"
d	differential operator	g_m also g_{p0}	grid-plate transconductance (mutual con- ductance), effect in plate circuit to change on control grid
D	duty factor, duty cycle ($D = t_n f_p$)	g_n also g_{op}	inverse transconductance (inverse mutual conductance), effect in grid circuit to change on plate
\mathbf{D}	electric displacement, dielectric flux density	γ, σ	conductivity
∇	vector operator	γ	propagation constant ($\gamma = \alpha + j\beta$)
δ	damping constant, damping coefficient (decay constant) ($p = \delta + j\omega$)	H	heat content, enthalpy
δ	secondary-emission ratio	\mathbf{H}	magnetic intensity, magnetizing force (mag- netic field strength)
Δ	increment	h	Planck constant ($h = 6.624 \dots \times 10^{-34}$ joule sec)
∂	partial differential operator	\mathbf{I}, I, i	current
e	base of Napierian or natural logarithms ($e = 2.718 \dots$)	I	luminous intensity ($I = \frac{dF}{d\omega}$)
\mathbf{E}	electric field, electric field strength, electric in- tensity, electric field intensity	I	moment of inertia
E, e, V, v	electromotive force, electric potential differ- ence, voltage	\mathbf{i}	unit vector (X -axis)
e	electronic charge ($e = 1.602 \times 10^{-19}$ coulombs)	I_s, i_s	saturation current of a cathode, total electron emission
E	illuminance, amount of illumination ($E = \frac{dF}{dA}$)	\mathbf{J}, J	current density
E	Young's modulus of elasticity	\mathbf{j}	unit vector (Y -axis)
ϵ	capacitivity, dielectric constant, dielectric co- efficient	J	radiant intensity ($J = \frac{d\Phi}{d\omega}$)
ϵ	emissivity	j	90° rotative operator or $\sqrt{-1}$
ϵ_i, η	dielectric susceptibility (intrinsic capacitance) ($\epsilon_i = (\epsilon_r - 1)\epsilon_0$)	k	coupling coefficient
ϵ_λ	spectral emissivity	K	luminosity factor ($K = \frac{I'_\lambda}{\Phi_\lambda}$)
ϵ_0	complex dielectric constant ($\epsilon_0 \approx \epsilon_r + j60\lambda\sigma$)	κ, μ_i	magnetic susceptibility
exp	exponential function	k	thermal conductivity
ϵ_r	relative dielectric constant (specific inductive capacitance)	\mathbf{k}	unit vector (Z -axis)
ϵ_t	total emissivity		
ϵ_v	dielectric constant of evacuated (free) space ($\epsilon_0 = 8.855 \dots \times 10^{-12}$ farad per meter)		

L	inductance, self-inductance	Q, q	quantity of electricity quantity of electric charge
l	length	q	rate of flow of heat
\ln	logarithm to the base e	Q	quantity of heat
\log	logarithm to the base 10	Q	quantity of light
L_{12} , etc.	mutual inductance	R, r	radius
λ	line density of charge	\mathcal{R}	reluctance
λ	wavelength in free space	R, r	resistance
λ_c	critical or cutoff wavelength	ρ	reflection coefficient
λ_r	resonance wavelength	ρ	reflection factor
m	magnetic moment	ρ	resistivity or specific resistance
m	mass	ρ	volume density of electric charge
μ	amplification factor of an electron tube ($\mu = \mu_{\mu\mu}$) (see μ factor)	s	dynamic sensitivity of a phototube
μ	magnetic permeability	S	elastance, self-elastance ($S = \frac{1}{c}$)
μ_i, κ	magnetic susceptibility, intrinsic magnetic permeability ($\mu_i = (\mu_r - 1)\mu_0$)	S	entropy
μ_{j3j2}	μ factor of an electron tube, relative effect of change on electrode "j3" to change on electrode "j2" (conditions of other electrodes to be specified)	s	length of path
μ_0	initial magnetic permeability	S	standing-wave ratio
μ_r	relative magnetic permeability	s	slip (in electrical machinery)
μ_v	magnetic permeability of evacuated (free) space	S	static sensitivity of a phototube
N	number of turns or conductors	S_F, S_P	luminous sensitivity of a phototube
n	number per unit of measurement	S_{2870}, S_{2870}	2870° Kelvin tungsten sensitivity of a phototube
ν	reluctivity ($\nu = \frac{1}{\mu}$)	σ, γ	conductivity
ω	angular frequency ($\omega = 2\pi f$)	\sum	summation
ω	solid angle	σ	surface density of charge
ω_r	resonance angular frequency	T	temperature
p	electric moment of a dipole	t	time
P	electric polarization ($P = (\epsilon_r - 1)\epsilon_0 E$)	T	period
p	number of poles	t_d	deionization time
p	oscillation constant, complex frequency ($p = \delta + j\omega$)	t_f	time of pulse fall
\mathcal{P}	permeance	T_{Hg}	temperature of mercury condensate
P, p	power, active power	t_k	cathode heating time
p	pressure	t_p	time of pulse duration
P_u	grid dissipation power	t_r	time of pulse rise
P_i	input power	τ	time constant
P_o	output power	τ	transmission factor
P_p	anode or plate dissipation power	θ, ϕ	phase displacement, phase angle
P_q	reactive voltamperes (reactive power)	θ	transit angle
P_s	voltamperes (apparent power)	U	internal, intrinsic energy
Φ	magnetic flux (flux of magnetic induction)	U	radiant energy
ϕ, θ	phase displacement, phase angle	V, v, E, e	electric potential difference, voltage, electromotive force
Φ	radiant flux ($\Phi = \frac{dU}{dt}$)	v	velocity
π	pi, a ratio ($\pi = 3.14159 \dots$)	V	volume
ψ	dielectric flux, displacement flux (flux of electric displacement)	V_r	retarded electric scalar potential
Q	figure of merit of reactor	W	radiant flux density
		W	work, energy
		X, x	reactance, self-reactance
		X_C	capacitive reactance
		X_L	inductive reactance
		Y, Y, y	admittance
		Z, Z, z	impedance, self-impedance
		Z_0	characteristic impedance, surge impedance

Correspondence

The Use of Speech Clipping in Single-Sideband Communications Systems*

Clipping has been used extensively in radio communications systems because clippers reduce and regulate the peak value of an audio wave. Therefore, clipping allows the use of higher depths of modulation and provides a safeguard against overmodulation. Relatively simple clipper circuits may be used to increase the effective range of a communications transmitter.

Voice of America engineers, after conducting detailed studies of means of combatting jamming, reported that clippers provide signal-to-noise and interference improvements of approximately 9 db. VOA engineers further point out that clippers offer a basic advantage over compressors or limiters in that clippers operate instantaneously. Studies of many speech patterns show that high-frequency sounds, necessary for good intelligibility, normally occur immediately after low-frequency, high amplitude sounds. Compressors, which are quick to reduce gain and slow to restore gain, effectively reduce the amplitude of these high intelligibility, high-frequency sounds. Clippers, being instantaneous in operation, do not suffer from this limitation.

During the past few years there has been great interest shown in single-sideband transmission and it might be interesting to consider the application of clippers to single-sideband radio telephone transmitters. In the following, an analysis for determining the output wave form produced by a perfect single-sideband suppressed carrier transmitter, when fed a severely clipped audio wave, will be discussed. Since a severely clipped sine wave closely resembles a square wave, square waves are generally used as the basis for determining the operating characteristics of clipping systems and will be used in the following analysis.

The Fourier series, representing the square wave, shown in Fig. 1, is as follows:

$$e = \frac{2}{\pi} \left(\cos x - \frac{\cos 3x}{3} + \frac{\cos 5x}{5} - \frac{\cos 7x}{7} + \frac{\cos 9x}{9} \dots \right)$$

If this wave is used to 100 per cent amplitude modulate a transmitter, the spectrum shown in Fig. 2 results. This AM wave may be represented by the revolving phasor diagram shown in Fig. 3 for the instant $T=0$.

If the carrier and one sideband are eliminated, Fig. 4 results. The amplitude of this single-sideband wave is equal to the instantaneous sum of the inphase and quadrature components of the phasors. If we assume that the upper sideband is transmitted and the carrier is completely eliminated, the strongest component remaining will be the first-order upper sideband which will be used

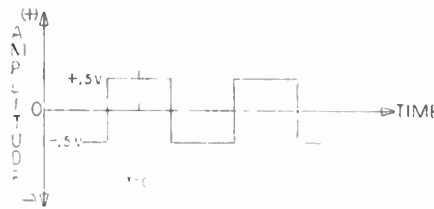


Fig. 1.

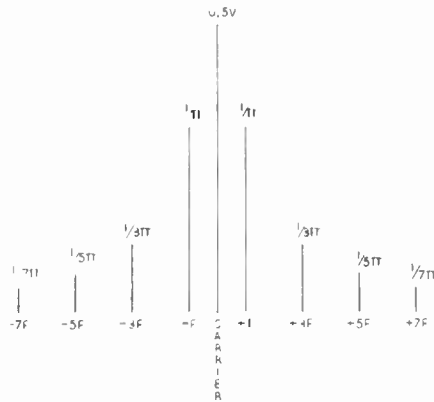


Fig. 2.

as a reference frozen phasor. Then the other components will rotate about this fundamental sideband component and by summing the inphase and quadrature components, we are able to arrive at the following relationship:

$$A(t) = (\text{in-phase}^2 + \text{quadrature}^2)^{1/2}$$

$$= \frac{1}{\pi} \left[\left(1 - \frac{\cos 2\omega t}{3} + \frac{\cos 4\omega t}{5} - \frac{\cos 6\omega t}{7} \dots \right)^2 + \left(\frac{\sin 2\omega t}{3} - \frac{\sin 4\omega t}{5} + \frac{\sin 6\omega t}{7} \dots \right)^2 \right]^{1/2}$$

where ω is equal to $2\pi F$ and F is equal to the fundamental frequency of the square wave.

It should be noted that this envelope function is composed of even harmonics whereas the square wave fed to the single-sideband generator is composed of only odd harmonics. The reason for this is that the carrier is eliminated and the strongest component remaining is the first-order sideband which is displaced from the carrier frequency by the fundamental frequency of the square wave.

This equation has two equal maximum amplitude points at $+90^\circ$ and -90° . Fig. 5 (opposite) is a phasor diagram for the $+90^\circ$ condition. It should be noted that when the fundamental sideband vector rotates 90° from its initial position, shown in Fig. 3, the third harmonic shifts three times 90° and the fifth harmonic swings five times 90° , etc. It

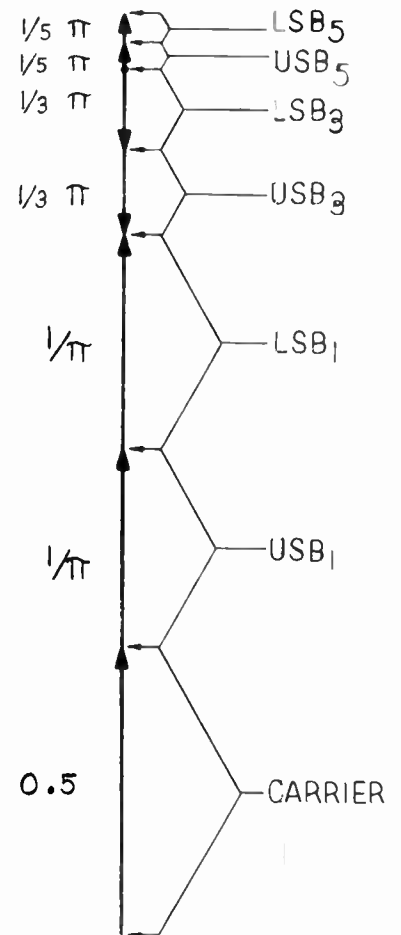


Fig. 3.

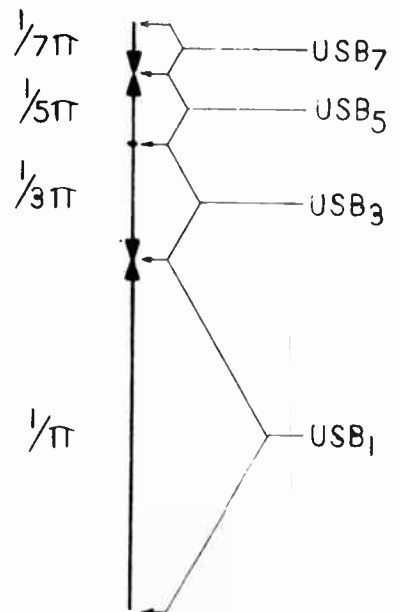


Fig. 4.

* Received by the IRE, April 25, 1957.

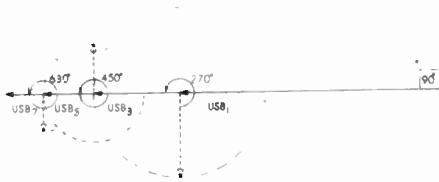


Fig. 5.

should be noted that all the sideband components line up in phase creating a large peak voltage.

The peak amplitude of the single-sideband wave is $2.02/\pi$ volts, when harmonics of the fundamental square wave frequency up to and including the 15th are considered. Thus, the peak amplitude is 2.02 times greater than the fundamental sideband frequency amplitude.

The peak amplitude of a conventional AM signal or a compatible single-sideband signal (CSSB) is $\pi/4$ times the amplitude of the fundamental component of the envelope. Thus, there is a total gain of 2.02 times $4/\pi$ or 8.2 db for CSSB over conventional single-sideband operation. However, there is a 6-db advantage of single-sideband suppressed or reduced carrier transmission over CSSB because of the carrier power saving, making a net gain of 2.2 db in favor of CSSB. In addition, CSSB, offers appreciable advantages in reduced cost and complexity of equipment because it allows the use of standard AM receivers. A more thorough comparison between the two systems has recently been published.^{1,2}

In conclusion, it would appear that the important advantages obtainable by the use of simple clipping systems may not be fully enjoyed by conventional reduced or suppressed carrier single-sideband systems.

LEONARD R. KAHN
Kahn Res. Labs.
Freeport, N. Y.

¹L. R. Kahn, "A Compatible Single-Sideband System," paper presented at the Second Annual Symposium on Aeronautical Communications, Utica, N. Y., October 9, 1956.

²L. R. Kahn, "Comparison of Compatible Single-Sideband with Other Single-Sideband Systems for Aeronautical Service," paper presented at the Washington Symposium sponsored by ARINC, Washington, D. C., February 1, 1957.

Fast Switching by Use of Avalanche Phenomena in Junction Diodes*

The literature on the transient behavior of semiconductor junction diodes has been centered mainly on the recovery transient that occurs on suddenly switching from the forward to the reverse direction. However, junction diodes also often exhibit a troublesome transient when switched from the reverse to the forward direction. This is particularly pronounced when the diode is switched into relatively high currents. A recent communication pointed out that

junction diodes could be switched much faster by operation around the avalanche breakdown voltage rather than by operation around zero bias, as is customary.¹ In that letter, the emphasis was on the recovery transient that normally occurs on cessation of the driving pulse, and it was demonstrated that this transient is insignificant when a diode is switched through the avalanche breakdown region from high to low current. The objects of this letter are to point out explicitly that a similar improvement should be obtained when switching through avalanche breakdown from low to high current, and to exhibit oscillographic evidence that such improvement is indeed realized.

For a P^+N junction whose operation can be described entirely in terms of a diffusion process, it can be shown that the diode voltage in response to an applied current step is

$$V(t) = (kT/q) \ln [1 + (I_0/I_s) \operatorname{erf}(t/\tau)^{1/2}]. \quad (1)$$

In (1), k = Boltzmann constant, T = absolute diode temperature, q = electronic charge, I_0 = magnitude of applied current step, I_s = diode saturation current, t = time, and τ = hole lifetime in the N region. The derivation of (1) assumes that the diode bulk resistance, R , is negligible. If it is not, a step term I_0R must be added to the right side of (1). Quite good experimental confirmation of (1) can be obtained if I_0 is small. A typical example of such agreement is shown in Fig. 1, for which the value of I_0 was about 50

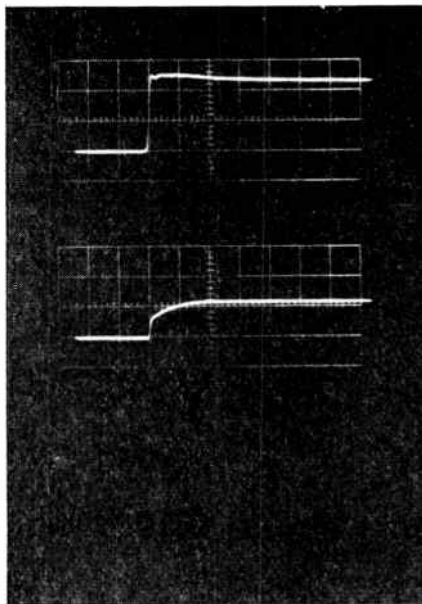


Fig. 1—Waveforms of low-level normal forward switching for a 1N461 diode. The sweep speed was 0.2 $\mu\text{sec}/\text{cm}$. The upper trace shows the generator voltage vs time (scale: 20 v/cm), from which an applied current step of 50 μa was obtained through a series resistor R (1 megohm). The lower trace shows the resultant diode voltage vs time (scale: 0.5 v/cm).

microamperes. The upper trace is that of the generator voltage step, and the lower trace shows diode voltage as a function of time in response to the current step obtained from

the generator through a relatively large resistance. It will be observed that the diode transient behavior is generally similar to that of a shunt combination of capacitance and resistance.

For much larger values of the applied current step, the character of the transient changes radically. The diode behavior changes from that of a capacitance-resistance arrangement to that of an inductance-resistance arrangement. There seems to be no quantitative theory available that describes the diode voltage response to large current steps. It has been pointed out, however, that the appreciable conductivity modulation which takes place at high carrier injection levels is probably the dominating mechanism here.²

It seemed to us that both forward and reverse transients, which occur when switching to or from high currents about zero bias, could be eliminated by switching about the avalanche breakdown voltage. The basis for our expectation was twofold: 1) the dielectric relaxation and drift times involved in driving into, as well as out of, the avalanche region are very short—of the order of 10^{-10} to 10^{-12} seconds; and 2) since there is no injection of minority carriers, the relatively long time associated with the conductivity modulation process characteristic of normal operation at high current levels is not involved.

To ascertain whether these ideas were well founded, a simple circuit arrangement was set up. It consisted of a Hewlett-Packard Type 212A pulse generator shunted by a 50-ohm resistor, in series with a resistor R and a diode. The input of a Tektronix Type 545 oscilloscope (with Type 53/54-K preamplifier) was connected across the diode to observe its voltage-vs-time behavior. With this simple arrangement, a diode could be switched from zero into its forward direction and back, and also, by reversing the diode polarity, from zero into its avalanche region and back. The positive output pulse from the generator was kept fixed at an amplitude of about 50 volts. The value of the series resistor R was kept high enough to ensure that constant-current step was applied to the diode in both modes of operation. The diode used to obtain Figs. 1 and 2 was a Hughes Type 1N461 silicon junction diode, selected for its sharp avalanche breakdown characteristic. Normal switching was obtained with the diode cathode grounded, whereas avalanche switching was obtained with the diode anode grounded. For the latter mode of operation, the value of R was reduced to permit a comparison at the same current level as used in normal switching.

As mentioned previously, the lower trace of Fig. 1 provides a good check of the theory on which (1) is based. No corresponding oscillogram of avalanche operation is provided here. At the very low level of applied current that was used—50 microamperes—the transient behavior in the reverse direction is determined principally by the charging current through the transition capacitance—of the order of 10 μmf for the diode employed—rather than by the avalanche breakdown conductance.

* J. E. Scobey, W. A. White, and B. Salzberg, "Fast switching with junction diodes," Proc. IRE, vol. 44, pp. 1880-1881; December, 1956.

²W. Shockley, "Electrons and Holes in Semiconductors," D. van Nostrand Co., Inc., New York, N. Y., p. 99; 1950.

* Received by the IRE, April 19, 1957.

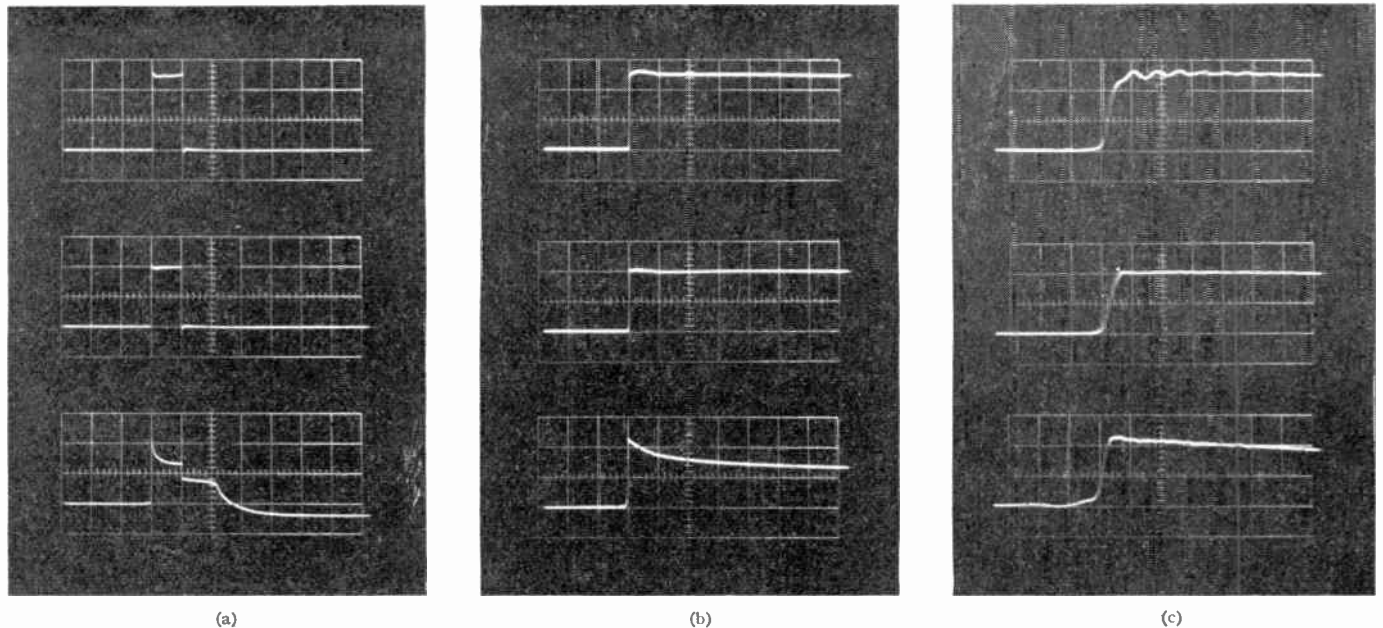


Fig. 2—(a)–(c) Waveforms of avalanche and normal switching for a 1N461 diode. The sweep speeds were 5.0 $\mu\text{sec}/\text{cm}$, 0.5 $\mu\text{sec}/\text{cm}$, and 0.04 $\mu\text{sec}/\text{cm}$, respectively. The upper traces show the generator voltage vs time (scale: 20 v/cm), from which an applied current step of 400 ma was obtained through a series resistor

R . The center traces show the resultant diode voltage for avalanche switching ($R=27$ ohms, scale: 20 v/cm) The lower traces show the diode voltage for normal switching ($R=120$ ohms, scale: 1 v/cm).

Fig. 2(a)–(c) illustrates avalanche and normal switching operation for an applied current step of about 400 milliamperes at three different sweep speeds. The upper traces in each figure show pulse-generator output voltage vs time, the center traces show diode voltage vs time for avalanche switching, and the lower traces show diode voltage vs time for normal switching. The marked overshoot of the leading edge of the forward transient that occurs in normal switching, clearly shown in the lower trace of Fig. 2(a), is completely absent in avalanche switching. Fig. 2(a) also shows that the severe recovery transient characteristic of the normal switching mode, which is known to be associated with minority carrier storage, is completely absent in the avalanche switching mode, even at the high current used. [The shape of the recovery transient in the lower trace of Fig. 2(a) is typical,³ except for its drop below the baseline. The latter feature resulted from the presence of a blocking capacitor in the pulse generator which caused the applied pulse to go slightly negative, instead of zero, for a short time.] Figs. 2(b) and 2(c) are similar to Fig. 2(a) except that, because of the higher sweep speeds used, the recovery transient does not appear. The center trace of Fig. 2(c) shows that switching into the avalanche region occurs with no observable transient. Thus, if the transient behavior of the avalanche switching mode is to be determined by these means within times less than the order of a few millimicroseconds, it will be necessary to utilize pulse generators and oscilloscopes with faster rise times than were available for our experiments. In addition, to avoid spurious circuit effects introduced by lead inductance and capacitance it will be

necessary to utilize the diodes designed for rf use.

In the above work, constant-current pulses were applied merely as a matter of practical convenience since the diode exhibits low steady-state resistance at the current level used. Equivalent results can be obtained, however, by applying constant-voltage pulses to the diode, and sampling the diode current as a function of time. For the normal switching mode, at low applied voltages, the current rises abruptly and then rapidly decays, within a time of the order of the hole lifetime, to its steady-state value. At relatively high applied voltages, the forward current transient appears as an abrupt rise, which is followed by a much more gradual rise to its steady-state value.⁴

As a matter of interest, in connection with the conductivity modulation process, a forward switching experiment was carried out on the Philco 1N263 germanium microwave mixer diode. In Fig. 3, the upper trace again shows the pulse-generator output voltage vs time, the center trace shows the diode voltage vs time in response to a current pulse of 400 milliamperes, and the lower trace shows the diode voltage in response to a current pulse of 40 milliamperes. As will be observed, the forward transient is significant for the high-amplitude current pulse, but is barely discernible for the low-amplitude pulse. The recovery transient is negligible, by comparison, in both traces.

Thus, it appears that a very marked improvement in the transient behavior can be obtained when normal high-level switching of junction diodes is replaced by switching about the avalanche breakdown voltage. Indeed, the duration of the transients in the avalanche mode of operation is so short as to

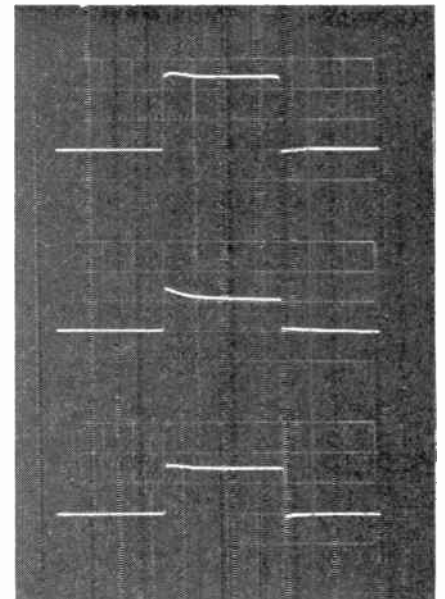


Fig. 3—Waveforms of high-level switching for a 1N263 microwave mixer diode. The sweep speed was 0.5 $\mu\text{sec}/\text{cm}$. The upper trace shows the generator voltage vs time (scale: 20 v/cm). The center trace shows the diode voltage vs time in response to an applied current step of 400 ma ($R=120$ ohms, scale: 2v/cm). The lower trace shows the diode voltage vs time in response to an applied current step of 40 ma ($R=1200$ ohms, scale: 0.5 v/cm).

challenge measurement by readily available pulse generators and oscilloscopes. Moreover, to realize the inherent high speed of avalanche operation, it will be necessary to modify the diode lead arrangement so that it does not constitute a limiting factor.

We wish to thank A. Barone for helping us with the experiments described above.

B. SALZBERG
AND E. W. SARD
Airborne Instruments Lab., Inc.
Mineola, N. Y.

³ B. Lax and S. F. Neustadter, "Transient response of a p - n junction," *J. Appl. Phys.*, vol. 25, pp. 1148–1154; September, 1954.

⁴ M. C. Waltz, "On some transients in the pulse response of point-contact germanium diodes," *PROC. IRE*, vol. 40, pp. 1483–1487; November, 1952.

Differentiating Devices*

Devices which can accurately differentiate or integrate time-varying electrical signals are utilized in many diverse applications, such as pulse circuits, analog computers, and systems which require sinusoidal signals in exact quadrature.

One type of circuit used for electronic differentiation is shown in Fig 1. The transfer function of this circuit in Laplacian operator form is:

$$\frac{E_o(s)}{E_i(s)} = \frac{-\left(\frac{K}{K+1}\right)RCs}{\left(\frac{RC}{K+1}\right)s + 1}$$

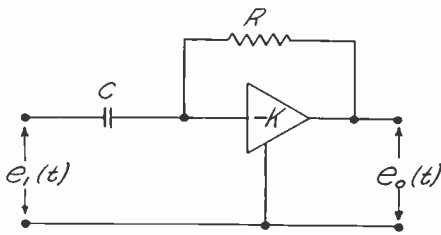


Fig. 1.

* Received by the IRE, April 26, 1957.

The derivation of this transfer function is predicated upon the following assumptions:

- 1) The circuit is not affected by the impedance of the input source or the output sink.
- 2) The circuit is not affected by the input and output impedances of the amplifier.
- 3) All elements operate within their linear ranges.

The transfer function approaches that of a perfect differentiator, *i.e.*, RCs , when the gain K is made very large, and the output is inverted.

A different circuit configuration, shown in Fig. 2, produces the following transfer function subject to the assumptions listed previously.

$$\frac{E_o(s)}{E_i(s)} = \frac{RCs}{RC(4-K)s + 1}$$

If the gain of the feedback amplifier is adjusted to a value of 4, the pole in the idealized transfer function is completely cancelled. In practice, a value very slightly less than the theoretical optimum is used to insure stability.

A powerful capability of the latter circuit derives from the ability to optimize K

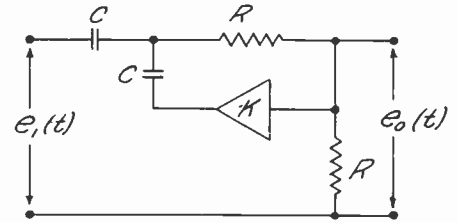


Fig. 2.

for certain classes of signals. For example, when the device is used as a 90° phase shifter for stable sinusoidal signals, small errors in K produce small errors in the output amplitude, but more significantly, small output phase errors. A dc signal proportional to the phase error can be derived from operation on the input and output signals, and this signal can be utilized to control K . This form of feedback error correction is applicable when the input signal has a predictable characteristic (*e.g.*, a carrier frequency component) which can be separated from random signal components.

Similar results are obtainable for integrating circuits.

CAPT. HERBERT B. VOELCKER, JR.
U. S. Army Signal Engineering Labs.
Fort Monmouth, N. J.

Contributors

Harold W. Abbott was born in Cohoes, N. Y., on September 9, 1927. After a period of service in the U. S. Navy, he received the B.S.E.E. degree from Union College, Schenectady, N. Y., in 1951.



H. W. ABBOTT

After graduation, he served a period of approximately three years in the U. S. Army Signal Corps and was engaged in a number of technical assignments.

Upon his release, he joined the General Electric Company's Engineering Training Program for one year.

Since 1954, Mr. Abbott has been active in the field of solid state circuits as a member of the Electronics Laboratory of the General Electric Co., Syracuse, N. Y.



Marvin Chodorow (A'43-SM'47) was born on July 16, 1913, in Buffalo, N. Y. He received the B.A. degree in physics from the University of Buffalo in 1934, and the Ph.D.

degree from the Massachusetts Institute of Technology in 1939.

During 1940 he was a research associate at Pennsylvania State College. Dr. Chodorow was an instructor of physics at the College of the City of New York from 1941 to 1943, when he became associated with the Sperry Gyroscope Co. as a senior project engineer. He remained at Sperry until 1947, when he joined the physics department of Stanford University, where he is now professor of applied physics and electrical engineering.

Dr. Chodorow is a member of the American Physical Society, and of Sigma Xi.

Dr. Chodorow is a member of the American Physical Society, and of Sigma Xi.



Robert A. Craig (A'50-M'57) was born on September 20, 1925, in Great Falls, Mont. He received the B.S. degree in electrical engineering from Montana State College, and began his graduate studies as a teaching and research assistant at the Electronics and Mi-

crowave Laboratories at Stanford University where he was awarded the M.S. and Degree of Engineer in E.E. in 1950 and 1951, respectively.

In 1951, he began work at Stanford University as a research associate in the Microwave Laboratory, where he was associated primarily with high-power twt research while continuing his graduate work on a part-time basis. In 1955, he received the Ph.D. degree in electrical engineering.

Dr. Craig joined the General Electric Microwave Laboratory in Palo Alto, Calif. in 1954 and since that time has been engaged in the development of high-power twt tubes.

He is a member of Tau Beta Pi, Phi Kappa Phi, and Sigma Xi.



Myron S. Glass (A'36-VA'39-M'55-SM'56) was born on May 25, 1902 in Eddyville, Iowa. He received the M.S. degree in physics

from the University of Chicago, in 1926. He joined the Technical Staff of Bell Telephone Laboratories the same year.



M. S. GLASS

magnetic focusing circuits for traveling-wave tubes.

From 1926 to 1941, Mr. Glass was engaged in development work on various electronic devices, principally cathode ray tubes and phototubes. From 1941 to 1954, he was engaged in development work on magnetrons.

Since 1954, he has been engaged in development work on

❖

Robert L. Jepsen (A'52) was born on June 16, 1920 in Valley, Wash. He received the B.S. degree in electrical engineering from Washington State College in 1944 and the Ph.D. degree in physics from Columbia University, in 1951.



R. L. JEPSEN

He was employed by the Radio Corporation of America, Lancaster, Pa., from 1944 to 1946 as a magnetron research and development engineer. Between 1946 and 1951, he was a research associate at the Columbia Radiation Laboratory where he was engaged in research on magnetrons. He joined Varian Associates as a research physicist in 1951, and has been director of the microwave tube research activity for over five years. His research studies have included klystrons, traveling-wave tubes, backward wave oscillators, ion oscillations, vacuum pumps, and molecular amplifiers.

Dr. Jepsen has published several papers on electron tubes, and holds patents in this field. He is a member of Tau Beta Pi and Sigma Xi.

❖

Curt A. Levis (S'48-A'53) was born in Berlin, Germany, 1926. He came to the United States in 1938 and entered Case



C. A. LEVIS

Institute of Technology in 1944. He spent two years as an electronic technician in the Navy, after which he returned to Case and received the B.S. degree in electrical engineering in 1949. From 1948 to 1949, he was employed as studio engineer at WSRS. He received the A.M. degree from Harvard University in 1950 and the Ph.D. degree in 1956 from Ohio State University, where he is now an assistant professor in the department of electrical

engineering and an associate supervisor at the Antenna Laboratory.

Dr. Levis is a member of Tau Beta Pi, Sigma Xi, Eta Kappa Nu, and Pi Mu Epsilon.

❖

Enrique A. Marcatili (M'56) was born in Córdoba, Argentina, on August 1, 1925. He was awarded the degree of Aeronautical Engineer in 1947, and the degree of Electrical Engineer, in 1948. He received a gold medal from the University of Córdoba for the highest scholastic record.



E. A. MARCATILI

He joined Bell Telephone Laboratories in 1954 after studying Čerenkov radiation in Córdoba, and since that time, has been engaged in waveguide research at Holmdel, N. J. Specifically, he has been concerned with the theory and design of branching filters in the millimeter region.

Mr. Marcatili is a member of the AFA (Physical Association of Argentina).

❖

Viktor Met was born on September 10, 1928 in Vienna, Austria. He received the Dipl. Ing. from Technische Hochschule, Vienna, in 1952 and was the recipient of a Fulbright Travel Grant in the same year. While working toward the M.S.E.E. degree, which he received in 1953 from the University of Minnesota, he was a teaching assistant at that University.



V. MET

Upon his return to Austria, he was a research assistant at Technische Hochschule. He received the degree of Dr. techn. in 1955. Since November, 1955, Dr. Met has been a member of the technical staff at General Electric Microwave Laboratory in Palo Alto, Calif.

❖

Jerome J. Suran (A'52-SM'55) was born in New York, N. Y. on January 11, 1926. After having served for three years with the U. S. Army during World War II, he received the B.S.E.E. degree from Columbia University, New York, N. Y., in 1949 and continued graduate studies there and at the Illinois Institute of Technology, Chicago, Ill.



J. J. SURAN

From 1949 to 1952, Mr. Suran was

employed in the field of control systems design and development by J. W. Meaker and Co., New York, N. Y. and in the field of fm communication research and development by Motorola, Inc., Chicago, Ill. Since 1952, he has been active in the area of solid-state circuits as a member of the Electronics Laboratory of the General Electric Company, Syracuse, N. Y.

Mr. Suran has a professional engineering license in the State of New York and is a member of the AIEE and the Research Society of America.

❖

Walter Welkowitz (S'46-A'49-M'55) was born in Brooklyn, N. Y., on August 3, 1926. He received the B.S. degree in electrical engineering from Cooper Union, New York, N. Y., in 1948. In 1949, he received the M.S. degree from the University of Illinois, Urbana, Ill., and in 1954, he was awarded the Ph.D. degree by that university for his work on the effects of high intensity sound on muscle tissue.



W. WELKOWITZ

In 1955, after a year as a researcher and lecturer at Columbia University's Graduate School of Engineering, Dr. Welkowitz joined Gulton Industries, Metuchen, N. J., where his work has led to the development of many new ultrasonic devices, including flowmeters and a wide variety of ultrasonic transducers and generating equipment.

A member of the Acoustical Society of America, Dr. Welkowitz is the author of several papers on the subject of ultrasonics and related acoustic topics. He recently developed an intracardiac heart microphone for cardiological research.

❖

Harry H. Wieder (S'47-A'50-M'55) was born in Romania on June 4, 1919. From 1941 to 1945, Mr. Wieder served in the U. S.



H. H. WIEDER

Army with a combat radio liaison group attached to the French Forces in North Africa and Europe. From 1945 to 1949, he attended the University of California, receiving the B.S. degree in physics.

From 1949 to 1953, Mr. Wieder was employed at the National Bureau of Standards on a number of classified projects, and continued graduate studies at the University of Maryland. Since 1953, Mr. Wieder has been associated with the U. S. Naval Ordnance Laboratory, Corona, Calif., where he heads the Dielectrics and Semiconductors Branch of the Physical Science Department.

Mr. Wieder is a member of the American Physical Society.

IRE News and Radio Notes

Calendar of Coming Events and Authors' Deadlines

- Automatic Control Conf., San Francisco, Calif., Aug. 19-20
 High Energy Symp., Oak Ridge, Tenn., Aug. 19-24
 WESCON, Fairmont Hotel and Cow Palace, San Francisco, Calif., Aug. 20-23
 URSI General Assembly, Boulder, Colo., Aug. 22-Sept. 5
 Symp. on Long Haul Communications, Honolulu, Hawaii, Aug. 27-29
 Special Technical Conference on Magnetic Amplifiers, Penn Sheraton Hotel, Pittsburgh, Pa., Sept. 4-5 (DL*: June 11, D. Feldman, Bell Tel. Labs., Whippany, N. J.)
 Industrial Electronics Symp., Morrison Hotel, Chicago, Ill., Sept. 24-25
 PGBTS Fall Symp., Willard Hotel, Wash., D. C., Sept. 27-28
 Nat'l Electronics Conference, Hotel Sherman, Chicago, Ill., Oct. 7-9 (DL*: June 1, V. H. Disney, Armour Res., Found., Chicago, Ill.)
 Computers in Control Symp., Chalfont-Haddon Hall Hotel, Atlantic City, N. J., Oct. 16-18
 IRE Canadian Convention, Exhibition Park, Toronto, Can., Oct. 16-18
 Conf. on Eng. Writ. & Speech, New York City, Oct. 21-22
 East Coast Aero & Nav. Conf., Lord Baltimore Hotel & 5th Reg. Armory, Balt., Md., Oct. 28-30
 PGED Meeting, Shoreham Hotel, Wash., D. C., Oct. 31-Nov. 1 (DL*: Aug. 15, W. M. Webster, RCA, Somerville, N. J.)
 PGNS Annual Meeting, Henry Hudson Hotel, New York City, Oct. 31-Nov. 1 (DL*: June 30, W. A. Higginbotham, Brookhaven Nat'l Labs., Upton, N. Y.)
 Annual Symp. on Aero Commun., Hotel Utica, Utica, N. Y., Nov. 6-8
 Radio Fall Meeting, King Edward Hotel, Toronto, Can., Nov. 11-13
 PGI Conference, Atlanta-Biltmore Hotel, Atlanta, Ga., Nov. 11-13 (DL*: July 15, R. L. Whittle, Fed. Telecommun. Labs., 1389 Peachtree St., N.E., Atlanta 9, Ga.)
 Mid-America Electronics Convention, Kan. City Mun. Audit., Kan. City, Mo., Nov. 13-14
 New England Radio-Elec. Mtg., Mechanics' Bldg., Boston, Mass., Nov. 15-16
 Conf. on Magnetism Sheraton-Park Hotel, Wash., D. C., Nov. 18-20 (DL*: Aug. 15, L. R. Maxwell, U. S. Nav. Ordnance Lab., White Oak, Silver Springs, Md.)
 Elec. Computer Exhibition, Olympia, London, England, Nov. 28-Dec. 4
 PGVC Conf., Hotel Statler, Wash., D. C., Dec. 4-5 (DL*: July 1, G. E. Woodside, Jr., 1145 19th St., N.W., Wash., D. C.)
 IRE Nat'l Convention, N. Y. Coliseum and Waldorf-Astoria Hotel, New York City, Mar. 24-27 (DL*: Nov. 1, G. L. Haller, IRE Headquarters, New York City)

* DL = Deadline for submitting abstracts



Receiving their Fellow awards from Rudolfo Soria, Chicago IRE Section Chairman, at the annual Chicago Section recognition banquet were (left) Rinaldo DeCola and (right) Eugene Mittelmann.



At the recent three-day joint RTCA-IRE symposium on air traffic control in Los Angeles were (left to right): V. J. Braun, Los Angeles IRE Section Chairman; R. E. Lee, Federal Communications Commissioner; J. T. Henderson, 1957 IRE President; J. T. Dellinger, RTCA Chairman; J. G. Bennett, Executive Assistant to the Presidential Air Safety Advisor.



The Professional Groups on Aeronautical & Navigational Electronics, and Military Electronics held a luncheon at Hotel Belmont-Plaza, New York City, March 19. Present were (left to right): Capt. C. L. Engleman, PGMIL Chairman; Maj. Gen. W. M. Morgan, Commander of the Air Force Cambridge Research Center; E. P. Curtis, Special Presidential Assistant for Aviation Facilities Planning; Joseph General, PGANE Chairman; and W. R. G. Baker, Professional Groups Committee Chairman.

PIONEER AWARD GOES TO HYLAND

The 1957 Pioneer Award was conferred upon L. A. Hyland, vice-president and general manager of Hughes Aircraft Company, by the IRE Professional Group on Aeronautical and Navigational Electronics.

The plaque which Hyland accepted before the IRE's National Conference on Aero Electronics honored him for his demonstration in the early 1930's that radio waves will reflect from objects, a basic radar discovery. He first observed and proved the principle of radar detection of aircraft while an associate engineer in the Naval Research Laboratory at Anacostia in 1931. In 1921 he had participated in the first blind landing of a flying boat by radio.



Left to right—L. A. Hyland and P. C. Sandretto, PGANE Awards Chairman.

Mr. Hyland is credited with more than forty inventions, including the shielded spark plug which made possible radio communications in aircraft by clearing up interference. He received the Distinguished Public Service Award, highest civilian honor of the United States Navy, in 1950. He is a member of the Society of Naval Engineers and the Society of Automotive Engineers.

HIGH-ENERGY SYMPOSIUM SET FOR AUG. 19-24 AT OAK RIDGE

A symposium on high-energy physics will be held in Oak Ridge, Tenn., Aug. 19-24. The symposium will be presented under the joint sponsorship of Oak Ridge National Laboratory and the Oak Ridge Institute of Nuclear Studies.

The six-day program will be conducted on an introductory level and will be addressed to scientists who have not previously been working in the field of high-energy or elementary-particle physics.

The lecturers and conference leaders taking part in the symposium are Maurice Neuman and L. Alvarez, University of California; Martin Block, Duke University; G. T. Zorn, Brookhaven National Laboratory; A. Pevsner, Johns Hopkins University; V. L. Fitch, Princeton University; and D. T. King, University of Tennessee.

Subjects on the program include the theory of elementary particles and their interactions, experiments using the nuclear-emulsion techniques and bubble chambers, and counter experiments.

Further information may be obtained from the University Relations Division, Oak Ridge Institute of Nuclear Studies, P. O. Box 117, Oak Ridge, Tenn.

MICHIGAN STUDENT WINS FIRST NEC AWARD IN ELECTRONICS

The winner, chosen in national competition, of the National Electronics Conference fellowship in electronics for the 1957-58 academic year, is Richard T. Denton, currently working toward a doctor's degree in electrical engineering at the University of Michigan. He received his master's and bachelor's degrees at Pennsylvania State University. Mr. Denton plans to study electronic systems analysis and design.

The award is the first to be given under

a recently adopted program for sponsoring advanced study in electronics. The NEC fellowship, worth \$2,500, is for a year of graduate study at any of eight colleges and universities participating in the conference.

These include Illinois Institute of Technology, Northwestern University, and University of Illinois as sponsors, and Michigan, Michigan State, Purdue, Notre Dame, and Wisconsin universities as cooperating institutions.

The sponsoring group also includes the IRE and American Institute of Electrical Engineers, with the Radio-Electronics-Television Manufacturers' Association and Society of Motion Picture and Television Engineers as participating members.

TRANSISTOR PAPERS REQUESTED

The 1958 Transistor and Solid-State Circuits Conference, to be held February 20-21, 1958, will be co-sponsored by the IRE Professional Group on Circuit Theory, AIEE Committee on Solid State Devices, IRE and AIEE Philadelphia Sections, and the University of Pennsylvania. The conference will be held at Irvine Auditorium and University Museum on the campus of the University of Pennsylvania.

Papers representing original contributions in the transistor and solid-state circuit fields are solicited for presentation at this two-day meeting. Abstracts of 500-1000 words should be furnished not later than October 11, 1957 to R. H. Baker, M. I. T. Lincoln Lab., Box 73, Lexington 73, Mass., or to J. G. Linvill, Stanford Research Lab., Stanford Univ., Stanford, Calif.

LUNCHEONS HIGHLIGHT INDUSTRIAL ELECTRONICS SYMPOSIUM

The Sixth Annual Industrial Electronics Symposium, sponsored by the IRE Professional Group on Industrial Electronics and Chicago Section, and the AIEE and its Chicago Section, will be held at the Morrison Hotel, Chicago, Sept. 24-25. Sixteen papers planned for presentation at this symposium will elaborate on the characteristics, use and integration of transducers into systems to measure and control complete processes.

A feature of the symposium will be speeches at two luncheons by J. D. Ryder, Dean of Engineering at Michigan State University, and A. E. Sperry, President of Panellit, Inc.

Advance registration for members of IRE and AIEE is urged. Checks for \$3.00 should be sent to Industrial Electronics Symposium, c/o L. A. Thacher, Electro Products Labs., 4501 N. Ravenswood Ave., Chicago, Ill. Non-members must register at the door for \$5.00; IRE-AIEE members may register at the door for \$4.00.

The symposium committee consists of: H. L. Garbarino, Co-Chairman; E. A. Roberts, Co-Chairman; E. Mittelmann, Program; J. N. Banky, Publicity; L. A. Thacher, Secretary-Treasurer; J. W. Grant, Arrangements; G. H. Brittain, Luncheons; P. W. Conway, Facilities; R. C. Crossley, Registration; A. L. Thayer, Printing; J. R. Wessling, Ladies' Program; R. S. Gardner, Harold Chestnut, C. E. Smith, R. M. Soria, and E. R. Whitehead.

Call for Papers

NOVEMBER 1 IS DEADLINE FOR 1958 IRE NATIONAL CONVENTION PAPERS

The 1958 IRE National Convention will be held at the Waldorf-Astoria Hotel and New York Coliseum, New York City, March 24-27, 1958.

Prospective authors are requested to submit all of the following by November 1, 1957.

- (1) 100-word abstract *in triplicate*, title of paper, name and address;
- (2) 500-word summary *in triplicate*, title of paper, name and address; and an indication of the technical field in which the paper falls.

The technical fields which may be covered are:

Aeronautical & Navigational Electronics
Antennas and Propagation
Audio
Automatic Control
Broadcast & Television Receivers
Broadcast Transmission Systems
Circuit Theory
Communications Systems
Component Parts
Education
Electron Devices
Electronic Computers
Engineering Management

Engineering Writing and Speech
Industrial Electronics
Information Theory
Instrumentation
Medical Electronics
Microwave Theory & Techniques
Military Electronics
Nuclear Science
Production Techniques
Reliability & Quality Control
Telemetry & Remote Control
Ultrasonics Engineering
Vehicular Communications

G. L. Haller, Chairman
1958 Technical Program Committee,
The Institute of Radio Engineers,
1 East 79 St., New York 21, N. Y.

Address all material to:

DOCTOR OF SCIENCE DEGREE CONFERRED UPON M. D. HOOVEN

M. D. Hooven (A'26-VA'39-SM'53), chief electrical engineer of the Public Service Electric & Gas Co., Newark, N. J., received the honorary degree of Doctor of Science, June 6, at the 41st commencement exercises of Newark College of Engineering. He was awarded this degree in recognition of his outstanding record as a professional engineer, good citizen and devoted servant to the advancement of his profession and engineering education.

Born in Weatherly, Pa., May 30, 1897, Mr. Hooven began his engineering education at Carnegie Institute of Technology, but left during World War I to serve as a member of the U. S. Army Signal Corps. Following the war, he resumed his education at Bucknell University, from which he graduated *magna cum laude* in 1920.

After serving as an engineer with the Westinghouse Electric & Manufacturing Co., under the tutelage of C. L. Fortescue, pioneer in high-voltage transmission design, and as radio engineer with the Robbins Electric Co., he joined Public Service in 1922.

Mr. Hooven is past president of the Montclair Society of Engineers and a member of Eta Kappa Nu. He is a fellow of the American Institute of Electrical Engineers which he served as director for four years and vice-president for two years. He is now its immediate past president.

He is a member of the American Society of Mechanical Engineers and the National Society of Professional Engineers. He is chairman of the liaison committee between the N.S.P.E. and the Engineers Joint Council, on which he also serves.

In engineering education, as separate from professional engineering groups, Mr. Hooven holds membership in the American Society for Engineering Education, and is a member of its Committee on Development of Engineering Faculties. He has also been active in the Engineers' Council for Professional Development as vice-president for one year and present president. He is the first chairman of the Committee on a Survey of the Engineering Profession.

R. J. ROCKWELL NAMED MARSTON MEDAL WINNER AT IOWA STATE

R. J. Rockwell (A'25-M'31-SM'43-F'45) was announced at the June Commencement exercises of Iowa State College as the 1957 winner of the Marston Medal. The medal is awarded annually in memory of the late Dean Anson Marston of the faculty of engineering to an alumnus of at least 30 years' standing in recognition of outstanding achievement in the field of engineering.

SYMPOSIUM ON AUTOMATIC CONTROL SET FOR AUGUST 19 IN SAN FRANCISCO

A Symposium on Automatic Control is being sponsored by the IRE Professional Group on Automatic Control with participation by the Instruments and Regulators Division of the ASME, and the Feedback Control Systems Committee of the AIEE. The Symposium will be held at the Mark

Hopkins Hotel in San Francisco on Monday, August 19, the day before WESCON. The program will consist of a morning technical session on Practical Applications in Nonlinear Control, during which four invited papers will be presented, and an afternoon panel discussion on Obstacles to Progress in Nonlinear Control. M. V. Long of the Shell Development Company will serve as chairman of the morning technical session, and Harold Chestnut will serve as moderator of the panel which will consist of John L. Bower of North American Aviation; Ernest G. Holzman of General Electric; O. J. M. Smith of UCLA; Charles F. Taylor of Daystrom; and George P. West of Ramo-Wooldrige.

On Tuesday and Wednesday, August 20-21, three technical sessions on automatic control will be presented as part of the WESCON technical program. These are being organized by the PGAC and consist of one session on each of the following topics: Nonlinear Control Systems, Sampled Data Control Systems, and Statistical Methods in Feedback Control.

The executive committee for the Symposium is comprised of: General Chairman, E. M. Grabbe; Technical Program, T. M. Stout; Publicity, J. M. Jones; Arrangements, H. S. Robinson; Technical Program (WESCON), A. M. Hopkin. Communications concerning the Symposium may be addressed to J. M. Jones, c/o Hughes Aircraft Company, Bldg. 6, Mail Station 2344, Culver City, Calif.

HARRY KRUTTER WINS DISTINGUISHED SERVICE CITATION

The Distinguished Civilian Service Award, the highest honor which the Secretary of Defense can bestow on civilians, has been presented to Harry Krutter (SM'47), Chief Scientist at the Navy's Air Development Center, Johnsville, Pennsylvania.

Dr. Krutter was previously honored last fall when he was presented with the Navy's Distinguished Civilian Service Award, which made him eligible for consideration for Defense Department recognition.

Secretary of Defense Charles Wilson recognized Dr. Krutter for "his outstanding scientific achievements in connection with the development of radar and electronic equipment now used in the country's airborne early warning equipment and for providing the nation with an important and timely improvement in its capability to defend itself."

Dr. Krutter has been associated with the Naval Air Development Center, the Navy's largest aeronautical research and developmental activity, since 1949.

ETA KAPPA NU ELECTS OFFICERS

At the recent annual meeting of Eta Kappa Nu at Cornell University, Ithaca, N. Y., the following officers were elected: C. T. Koerner (A'34-VA'39-M'55), Presi-

dent; Larry Dwon, Vice-President; C. H. MacDonald, Eastern Representative on the National Advisory Board; M. B. Reed (A'41-SM'48), Central Representative; and R. E. Nolte (M'48-SM'56), Western Representative.

Eta Kappa Nu Association is an electrical engineering honor society with a present membership of more than 28,000 persons selected for leadership qualities, attainments and activities. The society is known for its annual election of the "Outstanding Young Electrical Engineer," and its sponsorship of a movie on engineering careers.

PROFESSIONAL GROUP NEWS

The following PG Chapters were approved June 21 by the Executive Committee: PG on **Information Theory**, Boston Section; PG on **Military Electronics**, Northwest Florida Section; PG on **Reliability & Quality Control**, San Francisco Section.

The formation of a new IRE Professional Group on **Education** was approved by the IRE Executive Committee on April 10. The PG on Education becomes the 25th Group to join the Professional Group system. The following persons have been elected to serve as its first officers: J. D. Ryder, President; R. L. McFarlan, Vice-President; and J. G. Truxal, Secretary-Treasurer. The Group's assessment fee is \$3.00, effective July 1, 1957.

The formation of a new IRE Professional Group on **Engineering Writing and Speech** (PGEWS) was approved by the IRE Executive Committee at its meeting on May 14. This Group, the 26th IRE Professional Group, has as its objective "the study, development, improvement and promotion of the techniques of preparing, organizing for use, processing, editing, collecting, conserving, and disseminating any form of information in the electronics and related fields by and to individuals and groups by means of direct or indirect methods of communication."

At its first meeting, the Administrative Committee of the Group elected D. J. McNamara as chairman and Charles DeVore as vice-chairman. Miss Eleanor M. McElwee was appointed secretary and Herbert Michaelson was chosen treasurer.

In contrast to other IRE Groups which are concerned with specific branches of engineering research and development, the PGEWS will be concerned with the techniques used in written and oral communication of engineering information. Its objectives will include the development and promulgation of acceptable standards for writing, editing, illustrating, oral delivery, and the like, and the improvement of writing and speaking by engineers. It is believed that the Group will consist not only of engineers whose primary concern is with the presentation of technical information in written, oral, or graphic form, but also of other engineers who will join in order to participate in the services the Group can offer.

Plans are currently under way for a Group symposium to be held in the New York area in the early fall. Any IRE member may join the Professional Group on Engineering Writing and Speech by writing to the Technical Secretary at IRE Headquarters and asking that his name be added to the membership list.



H. KRUTTER

1957 Western Electronic Show and Convention

AUGUST 20-23, 1957, SAN FRANCISCO, CALIF.

The 1957 Western Electronic Show and Convention, held in alternate years at Los Angeles and San Francisco, is scheduled for the Cow Palace at San Francisco, Calif., Aug. 20-23. There will be 765 exhibits on display in three large exhibit halls, and 47 technical sessions will convene at the Cow Palace. A special evening session on controlled fusion research will be held at the Fairmont Hotel, San Francisco, August 21.

New to WESCON will be an international program which will present speakers and papers from abroad. This program, incidentally, is held with the cooperation of URSI, whose Twelfth International Assembly meets in Boulder, Colo. the following week. A Future Engineers' Show will serve also to display the best exhibits of science fairs previously held by western secondary schools. This show will be open to the public and awards will be given to the best student exhibitors.

Planned are field trips to the U. S. Army Nike installation; U. S. Naval Radiological Defense Lab.; Eitel-McCullough and Litton Industries, two manufacturers of electron devices; Ames Aeronautical Lab.; Univ. of Calif. Radiation Lab.; Ampex Corp. and Lenkurt Electric Co., two companies producing audio and instrumentation devices; the U.S.S. *Halibut* at Mare Island Naval Shipyard, the first nuclear-powered guided missile submarine; Data Processing Center of the Bank of America; California Academy of Sciences; Stanford Univ. Radio Propagation Field Station, Electronics Research Lab. and Microwave Labs.; and Lockheed Missile Research Labs.

Special events scheduled during the convention are: the All-Industry cocktail party in the Garden Court of the Sheraton-Palace during the evening of Aug. 20; the Distributor-Representative breakfast in the Terrace Room of the Fairmont Hotel on the morning of Aug. 22; the WESCON supper dance in the Garden Court of the Sheraton-Palace on the same evening; and the All-Industry Luncheon in the Gold Room of the Fairmont Hotel at noon on Aug. 23.

Ladies' activities will include a harbor cruise, a peninsula tour, a get-acquainted tea, a fashion show and luncheon, and a theater party to "Around the World in Eighty Days."

Registration at the 1957 WESCON will be handled only at the Cow Palace. Registration cards, previously mailed to IRE members, should be brought to the Cow Palace. The registration fee will be \$1.00 per person for everyone.

WESCON is sponsored jointly by the West Coast Electronic Manufacturers' Association, and the Los Angeles and San Francisco IRE Sections. General Chairman of the 1957 WESCON is D. B. Harris. His helpers are: B. M. Oliver, Convention Vice-Chairman; N. H. Moore, Show Vice-Chairman; H. M. Stearns, Secretary-Treasurer; C. F. Wolcott, B. S. Angwin, E. P. Gertsch, and H. P. Moore, members of WESCON's Board of Directors; Jack Ingersoll, Arrangements; D. A. Watkins, Technical Program;

J. J. Halloran and J. V. N. Granger, All-Industry Luncheon Co-Chairmen; D. H. Ross, Cocktail Party; A. J. Morris, Field Trips; K. R. Spangenberg, International Program; J. L. Corl and E. J. Schmidt, Registration Co-Chairmen; Chandler Murphy, Visitors' Housing; E. E. Ferrey, Public Relations; D. M. Perham, Historical Exhibit; S. F. Kiesel, Future Engineers' Show, Mrs. H. W. Smith, Jr., Women's Activities; C. N. Meyer, Visitors' Services; Don Larson, Business Manager; Mrs. J. W. Jarrett, Office Manager; and W. C. Estler, Public Relations Representative.

TUESDAY, AUGUST 20

9:30 A.M.—NOON

Session 1

Transistor Circuits

Chairman: J. G. Linvill, Stanford Univ.
A New Method of Designing Low-Level, High-Speed Semiconductor Logic Circuits, W. B. Cagle and W. H. Chen, Bell Tel. Labs.
A Wide-Band Transistor Feedback Amplifier, R. P. Abraham, Bell Tel. Labs.
Base Current Feedback in Transistor Output Pairs, W. F. Palmer and A. Anouch, Sylvania Elec. Prod.
A Multi-Stage Video Amplifier Design Method, J. J. Spilker, Jr., Stanford Univ.

Session 2

Microwave Components

Chairman: A. A. Oliner, Microwave Research Inst.
A New Waveguide Attenuator Element Utilizing Corrugated Metallic Surface Combined with Resistance Cord, Kiyoshi Morita and Kunihiro Suetake, Tokyo Inst. of Technology, Tokyo, Japan.
Three-DB Strip-Line Directional Couplers, J. K. Shimizu, Stanford Research Inst.
Waveguide to Stripline Couplers, P. J. Sferazza and H. Perini, Sperry Gyroscope Co.
A New Type of Directional Coupler for Coupling Coaxial Line to TE₁₀ Waveguide, R. F. Schwartz, Univ. of Pa.
Coupling of Rectangular Waveguides Having a Common Broad Wall Which Contains Uniform Transverse Slots, J. A. Barkson, Hughes Research Labs.

Session 3

Nonlinear Automatic Control Systems

Chairman: E. M. Grabbe, Ramo-Wooldrige Corp.
On the Design and Comparison of Contact Control Systems, I. Flugge-Lotz and E. H. Lindberg, Stanford Univ.
Phase Plane Trajectories as a Tool in Analyzing Nonlinear Attitude Stabilization for Space Missile Application, J. L. Halvorsen, Lockheed Missile Systems Div.
An Analysis of the Effects of Certain Nonlinearities on Servomechanism Performance, C. L. Smith and C. T. Leondes, UCLA.
Optimizing Control-Design of a Fully

Automatic Cruise Control System for a Turbo-Jet Aircraft, W. K. Genthe, John Oster Mfg. Co.

A General Method for Analyzing and Synthesizing the Closed Loop Response of a Linear and a Nonlinear Servomechanism, H. H. El-Sabbagh, Case Inst. of Technology.

Session 4

Component Part Design and Performance

Chairman: J. E. Fort, RCA.
Designing Relays for High Reliability, D. H. Cunningham, RCA.
A Stacked Ceramic Vacuum Relay, J. W. Daniels, Jennings Radio Mfg. Co.
Development of a Guided Missile Program Timer, B. F. Hubbard, Hubbard Scientific Labs.
Molded Metal Film Resistors, C. Wellard and S. J. Stein, International Resistance Co.
Vitreous Enamel Dielectric Capacitors—A Key to Reliability, B. L. Weller, Vitramon, Inc.

Session 5

Electronic Research Abroad

Chairman: R. R. Spangenberg, Stanford Elec. Labs.
Wave Propagation Research at the University of Sydney, V. A. Bailey, Univ. of Sydney, Australia.
Electronics Research at the University of Adelaide, L. G. H. Huxley, Univ. of Adelaide, Australia.
Electronics Research in the Philips Laboratories, D. B. H. Tellegen and H. Rinia, Philips Labs., Eindhoven, Holland.
The Electronics Research Program at Siemens and Halske, W. Veith, Siemens & Halske, Munich, Germany.
New Developments of the Strophotron, H. Haggblom and S. Tomner, Svenska Elektornor, Stockholm, Sweden.

Session 6

Information Theory

Chairman: Arnold Shostak, Office of Naval Research.
The Information Rate of the Human Channel, J. R. Pierce, Bell Tel. Labs.
Communication as a Game, N. M. Blachman, Sylvania Elec. Defense Lab.
Information Theory in the USSR, Paul Green, Lincoln Lab., M.I.T.
A Coded Facsimile System, W. S. Michel, W. O. Fleckenstein and E. R. Kretzmer, Bell Tel. Labs.
List Decoding for Noisy Channels, Peter Elias, M.I.T.

2:00 P.M.—4:30 P.M.

Session 7

Models for Systems

Chairman: W. H. Huggins, Johns Hopkins Univ.
Representation of Nonlinear Operators, L. A. Zadeh, Columbia Univ.
Propagation of Statistics in Systems, Bernard Widrow, M.I.T.

Mixed, Distributed and Lumped Systems, O. J. M. Smith, Univ. of Calif.

Panel discussion. Participants: L. A. Zadeh, Bernard Widrow, O. J. M. Smith, Brockway McMillan, Bell Tel. Labs., and W. K. Linvill, Inst. of Defense Analysis.

Session 8

Microwave Ferrite Devices

Chairman: A. L. Aden, Sylvania Microwave Physics Lab.

Multi-Element Ferrite Devices, Beaumont Davison, Case Inst. of Technology.

Mixing in Ferrites at Microwave Frequencies, P. H. Vartanian, Microwave Engr. Labs., and E. N. Skimal, Sylvania Microwave Physics Lab.

Viewpoints on Resonance in Ideal Ferrite Slab-Loaded Rectangular Waveguides, Harold Seidel, Bell Tel. Labs.

Microsecond Ferrite Microwave Switch, L. A. Blasberg and Harold Saltzman, Hughes Aircraft Co.

Ferrite Switches in Radar Duplexers, A. H. McEuen and J. P. Vinding, Cascade Research Corp.

Session 9

Computer Systems

Chairman: William Martin, Marchant Research Inc.

System Organization of the Mobidic Computer, John Terzian, Sylvania Elec. Prod.

The Nordic Computer, W. D. Rowe and T. A. Jeeves, Westinghouse Elec. Corp. Research Labs.

Interrogation in the Bismac System, O. H. Propster, Jr., RCA.

A Reliable Character Sensing System for Documents Prepared on Conventional Business Devices, D. H. Shephard, P. F. Bargh and C. C. Heasley, Jr., Intelligent Machines Research Corp.

Optimum Character Recognition System Using Decision Function, C. K. Chow, Burroughs Corp.

Session 10

Component Part Design, Control and Assembly

Chairman: M. A. Acheson, Sylvania Elec. Prod.

Circuit Components for High Voltage DC Power Supplies, Victor Wouk, Beta Electric.

Planning Your Components Process for Maximum Capacity, O. H. Jensen, Sylvania Elec. Prod.

An Investigation of the Effects of Humidity and Temperature on X.XX-P Printed Wire Boards, John Spaulding, General Electric Co.

Design Considerations for Ceramic Printed Circuit Packaging, J. H. Fabricius, Sprague Electric Co.

A Study of Dielectric Absorption Test Methods for Capacitors to be Used in Differentiating, Integrating and Time Constant Application, R. W. France, U. S. Electronic Development Corp.

Session 11

Engineering Management

Chairman: C. R. Burrows, Ford Instrument Co.

Engineer Management in Brazil, A. H. Schooley, Naval Research Labs.

Evaluating Scientists and Engineers for a Research and Development Activity, R. A. Martin, Hughes Research and Development Labs.

Your Self-Development into Supervision and Management, H. M. O'Bryan, Sylvania Elec. Prod.

The Transition from Engineer to Supervisor, H. M. Elliott, RCA.

Systems Engineering, I. L. Auerbach, Burroughs Corp.

Session 12

Antennas and Propagation

Chairman: J. B. Smyth, Smyth Research Assoc.

The Quarter-Wave Dipole, Bengt Josephson, Research Inst. of National Defense, Stockholm, Sweden.

General Design Considerations for Transponder TACAN Antenna, E. G. Parker and A. Casabona, Federal Telecommunication Labs.

Reflections from a Convex Surface, J. J. Brandstatter, Stanford Research Inst.

Summary of Tropospheric Path Loss Measurements at 400 MCPS over Distances of 25 to 830 Miles, J. H. Chisholm, W. E. Morrow, J. F. Roche and A. E. Teachman, M.I.T.

Effects of Super-Refractive Layers on Tropospheric Signal Characteristics in the Pacific Coast Region, A. P. Barsis and F. M. Capps, National Bureau of Standards.

WEDNESDAY, AUGUST 21

9:30 A.M.—NOON

Session 13

Semiconductor Devices I

Chairman: E. L. Steele, Motorola, Inc.
A Silicon PNP Fused-Junction Transistor, A. L. Wannlund and W. P. Waters, Hughes Aircraft Co.

Complementary High Speed Power Transistors for Computer and Transmission Application, R. W. Westberg and T. R. Robillard, Bell Tel. Labs.

Transistors by Grown-Diffused Technique, Boyd Cornelison and W. A. Adcock, Texas Instruments.

A Five-Watt, Ten-Megacycle Transistor, J. E. Iwerson, J. T. Nelson and F. Keywell, Bell Tel. Labs.

Diffused Fifty-Watt Silicon Power Transistors, Robert Anderson and Elmer Wolff, Texas Instruments.

Session 14

Electronics in High Speed Flight

Chairman: S. B. Batdorf.

Electronics in the B-52 Bomber, R. L. Shahan, Boeing Airplane Co.

Electronics in Aeronautical Research, J. A. White, Ames Aeronautical Lab.

Role of Electronic Trajectory Measurement Systems in Missile Test, Vernon Miller, White Sands Proving Ground.

Missile Aerophysics Phenomena of Electronic Import, Daniel Bershader, Lockheed Missile Systems Div.

Session 15

Sampled Data Control Systems

Chairman: A. M. Hopkin, Univ. of Calif.

Optimal Nonlinear Control of Saturating Systems by Intermittent Action, R. E. Kalman, Columbia Univ.

Additions to the Modified Z-Transform Method, E. I. Jury, Univ. of Calif.

Additional Techniques for Sampled Data Feedback Problems, G. M. Kranc, Columbia Univ.

Signal Flow Reductions in Sampled-Data Systems, J. M. Salzer, Magnavox Research Labs.

Conditional Feedback Systems Applied to Stabilization of Missile Pitch Attitude, D. R. Katt, Lockheed Missile Systems Div.

Session 16

Communications Systems Engineering

Chairman: J. W. Worthington, Jr., USAF.
A Detailed Description of the Synchronous Detection Process, John Webb, General Electric Co.

Design Principles of High Stability Frequency Synthesizers for Communications, N. H. Young and V. L. Johnson, Federal Telecommunications Lab.

Microwave Systems—Pipeline Style, F. V. Long, Texas Eastern Transmission Corp.

An Experimental Data Transmission System Speed Translator Using Magnetic Tape, W. A. Malthaner, Bell Tel. Labs.

Session 17

Military Research Requirements in Electronics

Chairman: Jobe Jenkins, Lockheed Missile Systems Div.

Role of Basic and Applied Electronics Research in the Defense Program, J. M. Bridges, Office of the Assistant Secretary of Defense.

Air Force Requirements in Basic and Applied Electronics Research, L. O. Hollingsworth, Air Force Cambridge Research Center.

Army Requirements in Basic and Applied Electronics Research, H. J. Merrill, Signal Engrg. Lab.

Navy Requirements in Basic and Applied Electronics Research, Arnold Shostak, Office of Naval Research.

Session 18

Microwave Antennas

Chairman: M. D. Adcock, Hughes Aircraft Co.

Mutual Coupling in Two-Dimensional Arrays, J. Blass and S. J. Rabinowitz, W. L. Maxson Corp.

Scattering of Microwaves by Figures of Revolution, J. S. Honda, Stanford Research Inst.

Pulsed Operation of Traveling-Wave Monopulse Arrays Utilizing Phase Comparison Techniques, C. E. Phillips, Convair.

Feed Optimization in Multi-Feed Antennas, J. A. Kuecken, General Electric Co.

Note on a Technique for Analyzing Three-Dimensional Scanning Antenna Performance, F. J. Gardiner, I-T-E Circuit Breaker Co.

2:00 P.M.—4:30 P.M.

Session 19

Semiconductor Devices II

Chairman: R. N. Noyce, Shockley Semiconductor Lab.

Resistance of Silicon Transistors to Neutron Bombardment, R. C. Gillis and J. W. Tarzwell, Autonetics.

Medium Power Silicon Rectifier, R. J. Andres and E. L. Steele, Motorola.

Diffused Silicon Diodes—Design, Characteristics and Life Data, Paul Zuk, J. H. Wiley and H. E. Hughes, Bell Tel. Labs.

Some Silicon Junction Diode Recovery Phenomena, T. E. Firlie, Hughes Aircraft Co.

The Nesistor—A Semiconductor Negative Resistance Device, R. G. Pohl, The Rauland Corp.

Session 20

Microwave Instrumentation

Chairman: S. B. Cohn, Stanford Research Inst.

Phase Stabilization to Microwave Frequency Standards, E. F. Davis, Jet Propulsion Lab.

The Theoretical Sensitivity of the Dicke Radiometer, L. D. Strom, Texas Instruments

Homoddyne Generator and Detection System, G. C. Mathers, Hewlett-Packard Co.

Frequency Translation by Phase Modulation, E. M. Rutz and J. E. Dye, Emerson Research Labs.

Equipment and Techniques for the Measurement of Radar Reflections from Model Targets, P. D. Kennedy, Ohio State Univ.

Session 21

Statistical Methods in Feedback Control

Chairman: O. J. M. Smith, Univ. of Calif.

Control System Optimization to Achieve Maximum Hit Probability Density, G. S. Axelby, Westinghouse Elec. Corp.

Statistical Analysis of Sampled Data Systems, G. E. Johnson, IBM Corp.

Nonlinear Amplitude-Sensitive Control Systems with Stochastic Inputs, D. W. C. Shen, Univ. of Pa.

Gain Modulation in Servomechanisms, J. F. Buchan and R. S. Raven, Westinghouse Elec. Corp.

Session 22

Symposium on Crystal Filters

Chairman: Leo Storch, Hughes Aircraft Co.

Historical Notes on Crystal Filters, A. R. D'Heedene, Bell Tel. Labs.

Present Design Approaches, D. I. Kosovsky, Hycon-Eastern.

Test Procedures and Instrumentation, Alvin Strouss, Bulova Watch Co.

Present Performance Limitations, W. R. Ives and D. L. Hammond, Scientific Radio Prod.

Future Design and Performance, L. Storch, Hughes Aircraft Co.

Session 23

Television and Radio Broadcasting

Chairman: J. L. Berryhill, KRON-TV.

Traveling Wave VHF Television Transmitting Antenna, M. S. O. Siukola, RCA.

Video Tape Recorder Symposium. Participants: Ross Snyder and Charles Ginsburg, Ampex Corp., and representatives of networks using the recorders.

Understanding the Artist's Problem in Telecasting, William Wagner, KRON-TV, San Francisco.

A Compatible Single-Sideband System Designed for the Broadcast Service, L. R. Kahn Research Labs.

A Stable Precision Television Demodulator, Herbert Hartmen, KCRA-TV, Sacramento.

Operation, Maintenance and Field Tests of Quadrature-Fed Antennas, Harry Jacobs, KGO-TV, San Francisco.

Session 24

Data Handling Devices

Chairman: L. C. Nofrey, Marchant Research, Inc.

Magnacard—A New Concept in Data Handling, R. M. Hayes and J. Wiener, Magnavox Research Lab.

Magnacard—Mechanical Handling Details, A. M. Nelson, H. Stern and L. Wilson, Magnavox Research Lab.

Magnacard—Magnetic Recording Studies, J. Burkig and L. Justice, Magnavox Research Lab.

A Very High Speed Punched Paper Tape Reader, A. M. Angel, Nat'l. Cash Register Co.

An Air-Floating Disk Magnetic Memory System, W. Farrand, North American Aviation.

8:00 P.M.—9:30 P.M.

Session 25

Controlled Nuclear Fusion

Chairman: Luis Alvarez, Univ. of Calif.

Controlled Nuclear Fusion, Herbert York, Livermore Lab., Univ. of Calif.

THURSDAY, AUGUST 22

9:30 A.M.—NOON

Session 26

Computers in Network Synthesis

Chairman: D. O. Pederson, Univ. of Calif.

Digital Computers and Network Theory, T. R. Bashkow and C. A. Desoer, Bell Tel. Labs.

Network Analysis and Synthesis by Digital Computer, W. Mayeda and M. E. Van Valkenburg, Univ. of Ill.

Computers in R-C Network Synthesis, S. Mason, M.I.T.

Digital Computers as Tools in Designing Transmission Networks, D. T. Bell, Bell Tel. Labs.

Session 27

Microwave Tubes I

Chairman: C. K. Birdsall, G. E. Microwave Labs.

Methods of Increasing Bandwidth of High Power Microwave Amplifiers, W. J. Dodds, T. Moreno and W. J. McBridge, Jr., Varian Assoc.

Wide Band Klystron Amplifiers, W. L. Beaver, R. L. Jepsen and R. L. Walter, Varian Assoc.

The SAL-89, A Grid Controlled Pulse Klystron Amplifier, J. D. Swearingen and C. Veronda, Sperry-Rand Corp.

A Gun and Focusing System for Crossed-Field Traveling-Wave Tubes, O. L. Hoch and D. A. Watkins, Stanford Univ.

Injection of Convergent Beams Focused by Periodic Magnetic Fields, Charles Susskind and J. L. Palmer, Univ. of Calif.

Session 28

Computer Circuit and Logical Design

Chairman: Jerre Noe, Stanford Research Inst.

The Transistor NOR Circuit, W. D. Rowe, Westinghouse Elec. Corp.

Flux Quantized Counter, J. R. Bacon and G. H. Barnes, Burroughs Corp.

Logic Design Symbolism for Direct Coupled Transistor Circuits in Digital Computers, J. B. O'Toole, Hughes Weapon Systems Development Labs.

A Mathematical Formulation of the Generalized Logical Design Problem, D. Ellis, Litton Industries.

A Five Microsecond Memory for UDOFT Computer, A. Ashley, Sylvania Elec. Proc.

Session 29

Automatic Instrumentation

Chairman: W. H. Fenn, Hughes Aircraft Co.

A New Concept for a Paper-Tape High-Information Rate Reader, Warren Welcome, Calif. Technical Industries.

Large Screen Bar-Graph Scope—A New Tool for Continuous Visual Monitoring of Multichannel Data, H. O. Wolcott, Federal Tel. & Radio Co.

Automatic Missile Check-Out Equipment, M. R. Beck and Robert White, Bendix Aviation Corp.

Rapid Automatic Check-Out Equipment for Maintenance of Weapon Systems, D. Y. Keim, Sperry Gyroscope Co.

Automatic Test Systems for Production, H. S. Dordick, RCA.

Session 30

Reliability Program

Chairman: O. B. Moan, Lockheed Missile Systems Div.

Reliability—A Practical Program, Morton Barov, Farnsworth Electronics Co.

Research-Insurance for the Future, R. M. Barrett, Air Force Cambridge Research Center.

Reliability and the Component Engineer, R. W. Brown, Boeing Airplane Co.

The AQL Myth, M. A. Acheson, Sylvania Elec. Prod.

Lessons to be Learned for a Unique Reliability Program, L. J. Blumenthal, Bell Aircraft Corp.

Session 31

Antennas

Chairman: D. C. Ports, Jansky & Bailey, Inc.

Space-Frequency Equivalence, W. E. Kock and J. L. Stone, Bendix Aviation.

Two-Dimensional Endfire Array with Increased Gain and Side Lobe Reduction, H. W. Ehrenspeck and W. J. Kearns, Air Force Cambridge Research Center.

The Split Reflector Technique for Broad-Band Impedance Matching of Center-Fed Antennas Without Pattern Deterioration, R. L. Mattingly, B. McCabe and M. J. Traube, Bell Tel. Labs.

Coupled Waveguide Excitation of Traveling Wave Antennas, W. L. Week, Univ. of Ill.

A New Satellite Tracking Antenna, C. J. Sletten, F. S. Holt, P. Blacksmith and G. R. Forbes, AFCRC.

2:00 P.M.—4:30 P.M.

Session 32**Passive and Active Circuits**

Chairman: J. M. Pettit, Stanford Univ.
The Design and Optimization of Synchronous Demodulators, R. C. Booton, Jr., and M. H. Goldstein, Jr., M.I.T.

The Extraction of Waveform Information by a Delay-Line Filler Technique, J. H. Park, Jr. and E. Glaser, Johns Hopkins Univ.

Stable Amplifiers Employing Potentially Unstable Transistors, G. S. Bahrs, Stanford Univ.

Synthesis of Active RC Transfer Functions by Means of Cascaded RC and RL Structures, I. Horowitz, Brooklyn Polytech. Inst.

Negative Impedance Circuits, W. R. Lundry, Bell Tel. Labs.

Session 33**Microwave Tubes II**

Chairman: D. A. Watkins, Stanford Univ.

Use of Multiple-Helix Circuits in 100-Watt CW Traveling-Wave Amplifiers, J. L. Putz and G. C. Van Hoven, General Electric Microwave Lab.

High Gain TWT for X-Band, Robert McClure, Sperry Gyroscope Co.

Development and Operation of Low-Noise Broadband Traveling-Wave Tubes for X- and C-Bands, F. B. Fank and F. M. Schumacher, General Electric Microwave Lab.

Shot Noise Amplification in Beams Beyond Critical Perveance, J. C. Twombly, Univ. of Colo.

Microwave Frequency Mixing and Division with Beam Type Tubes, R. W. DeGrasse, D. A. Dunn, R. W. Grow and G. Wade, Stanford Univ.

Session 34**Medical Applications of Super-Voltage Radiation**

Chairman: R. R. Newell, Stanford-Lane Hospital.

Some Considerations in the Choice of High Energy Machines for Therapy, Craig Nunan, Varian Assoc.

Medical Applications of the Linear Accelerator, Mitchel Weissbluth, Stanford Medical School.

Biological and Medical Applications of High Energy Protons, C. A. Tobias, Donner Lab., Univ. of Calif.

Medical Applications of the Synchrotron, Gail Adams, Univ. of Calif. Hospital.

Session 35**Instrumentation**

Chairman: P. D. Lacy, Hewlett-Packard Co.

A Survey of Equipment Used in Radioactivity Logging of Oil Wells, C. E. Williams, Ramo-Wooldridge Corp.

Millimicrosecond Photography with an Electronic Camera, E. C. Maninger and R. W. Buntentbach, Precision Technology, Inc.

Instrumentation Applications of the Video-Tape Recorder, E. L. Keller, Ampex Corp.

Design of a High-Speed Transistor Decimal Counter with Neon-Bulb Read-Out, R. D. Lohman, RCA.

A New Transfer-Storage Counter, R. W. Wolfe, Burroughs Corp.

Session 36**Vehicular Communications I**

Chairman: M. E. Kennedy, Los Angeles Dept. of Communications.

Qualitative Performance Evaluation of Land Mobile System, J. R. Neubauer, RCA.

High Power UHF Station Transmitter, Richard Ocko, General Electric Co.

Antennas for VHF Communications Systems, Ralph Bykerk, Tele-Beam Industries.

Frequency Cross Roads for the Mobile Services, Lester Spillane, San Francisco.

Session 37**Production Techniques**

Chairman: R. J. Stahl, Dalmo Victor Co.
Applications of Flying Spot Scanning Techniques to Automatic Inspection, H. P. Mansberg, Allen B. DuMont Labs.

Evaluation of Etched Circuit Boards from the Standpoint of Vibration, N. R. Dunbar, Autonetics.

Preassembled Component Modular Systems, J. D. Heibel, Erie Resistor Corp.

Capacitors for Automation, G. P. Smith, Corning Glass Works.

Use of Ceramic-Metal Seals, J. L. Hall, Thermo Materials, Inc.

FRIDAY, AUGUST 23

9:15 A.M.—11:45 A.M.

Session 38**Audio**

Chairman: Frank Lennert, Ampex Corp.
General Consideration on Phasing Two-Way Loudspeakers, J. K. Hilliard, Altec Lansing Corp.

A Wide Angle Loudspeaker of a New Type, Leonard Pockman, Ampex Corp.

Simplified Audio Impedance Measurements, Vincent Salmon and M. R. Berg, Stanford Research Inst.

Multi-Channel Audio Recorders, W. M. Fujii, Ampex Corp.

Methods of Recording Commercial Stereophonic Masters, R. J. Tinkham, Ampex Corp.

Session 39**Advances in Microwave Solid-State Devices**

Chairman: C. L. Hogan, Harvard Univ.
Microwave Atomic Amplifiers and Oscillators, George Birnbaum, Hughes Research Labs.

Measurements on Active Microwave Ferrite Devices, K. M. Poole and P. K. Tien, Bell Tel. Labs.

Maser Amplifier Characteristics for One- and Two-Iris Cavities, M. L. Stitch, Hughes Research Labs.

Microwave Properties and Applications of Garnet Materials, G. P. Rodrigo, Harvard Univ.

L-Band Isolators Utilizing New Materials, G. S. Heller, M.I.T. Lincoln Lab.

Session 40**Analog and Digital Computer Devices**

Chairman: Paul Morton, Univ. of Calif.
Rake, A High Speed Binary—BOD and

BCD Binary Buffer, G. F. Mooney and J. P. Hart, Rocketdyne.

Simulation of Transfer Functions Using Only One Operational Amplifier, A. Bridgman, Sylvania Elec. Prod.

Function Generation by Integration of Steps, E. H. Heinemann, Douglas Aircraft Co.

A Transistorized, Multi-Channel, Airborne Voltage-to-Digital Converter, R. M. MacIntyre, Ramo-Wooldridge Corp.

The Bizmac Transcoder, D. E. Beaulieu, RCA.

Session 41**Telemetry I**

Chairman: C. H. Hoepfner, Radiation, Inc.

An Airborne Filter for Low Distortion of FM Sub-Carriers, Warren Link, Lockheed Aircraft Corp.

Development of a High-Speed Transistorized Ten-Bit Coder, L. McMillian, Radiation, Inc.

A Transistorized PCM Telemeter for Extended Environments, R. E. Marquand and W. T. Eddins, Radiation, Inc.

A Stable Transistorized PDM Keyer, D. A. Williams, Jr., Bendix Aviation Corp.

Television as an Aid to Remote Sensory Perception, J. P. Day, Convair.

Session 42**Vehicular Communications II**

Chairman: A. A. MacDonald, Motorola, Inc.

Nine Hundred MC—A Potential Vehicular Communications Band, C. J. Schultz, Motorola, Inc.

Providing Mobile Coverage in Isolated Desert Terrain, R. L. Brinton, T. R. Ferry and E. L. Hare, Pacific Gas & Electric Co.

The Use of VHF Radio in Railroadings, J. W. Brannin, Southern Pacific Co.

A Selective Signaling System, Don Bentley, Electrical Communications.

Session 43**New Electronic Techniques for Industry**

Chairman: V. B. Corey, Donner Scientific Co.

Industrial Applications of Vacuum Relays, R. E. Johnston, Jennings Radio Mfg. Corp.

Electron Paramagnetic Resonance—A New Form of Spectroscopy, R. M. Sands, Varian Assoc.

Television in Radiography, A. R. Ogilvia, Sierra Electronic Corp.

Electronic Counting as an Industrial Tool, James Cunningham, Systron, Inc.

2:00 P.M.—4:30 P.M.

Session 44**Ultrasonic Engineering**

Chairman: T. A. Peris, Lockheed Missile Systems Div.

A Survey of Ultrasonic Generators, W. G. Cady, Pasadena, Calif.

A Novel Magnetostrictive Ultrasonic "Jack-Hammer" Type Rotating Drill for Boring Small Holes in Hard Materials, N. K. Marshall, Lockheed Missile Systems Div.

Non-Destructive Tests for Structural Adhesives, C. T. Vincent, Stanford Research Inst.

Considerations in I-F Filter Design, J. S. Turnbull, Collins Radio Co.

Session 45

Television Receivers and Televisual Devices

Chairman: J. M. Rosenberg, Litton Ind.

Securing 110-Degree Sweep for the Public Domain, W. D. Schuster and E. O. Stone, Sylvania Elec. Prod., and C. E. Torsch, The Rola Co.

A Brightness-Enhanced Color Receiver Employing Automatic Decoding in the Chromatron, R. H. Rector, Litton Industries.

21-Inch Direct-View Storage Tube, N. J. Koda, N. H. Lehver and R. D. Ketchpel, Hughes Research Labs.,

The Television Color Translating Microscope, V. K. Zworykin, RCA.

Automatic Fine-Tuning for Television Receivers, C. W. Baugh, Jr., Westinghouse Elec. Corp.

Session 46

Ionospheric Propagation

Chairman: T. J. Keary, Naval Electronics Lab.

Long-Range Auroral Backscatter Echoes Observed at 12 MC/S from College, Alaska, L. Owren and R. A. Stark, Univ. of Alaska.

Meteor Burst Communication—Part I: Oblique Path Meteor Propagation Results, W. R. Vincent, R. Wolfram, B. Sifford, W. Jaye and A. M. Peterson, Stanford Res. Inst.

Meteor Burst Communication—Part II: VHF Meteor Burst Communications System, W. R. Vincent, R. Wolfram, B. Sifford, W. Jaye and A. M. Peterson, Stanford Res. Inst.

Experimental Equipment for Communication Utilizing Meteor Bursts, R. J. Carpenter and G. R. Ochs, National Bureau of Standards.

High Frequency Multipath Analysis by the Short Pulse-Long Pulse Method, J. D. Lambert, Hughes Weapon Systems Development Labs.

Session 47

Telemetry II

Chairman: J. J. Dover, Air Force Flight Test Center.

A Transistorized High-Performance FM/FM System, William Fulton, Bendix Aviation Corp.

A Transistor-Magnetic Sub-Carrier Discriminator, G. H. Barnes and R. M. Tillman, Burroughs Corp.

A Low-Level Magnetic Commutator, D. C. Kalbfell, Kalbfell Electronix.

Missile Temperature Telemetering, Jay Cox, Lockheed Aircraft Corp.

Session 48

Nuclear Science

Chairman: W. W. Salisbury, Zenith Radio Research Corp.

The Varian Free Precession Magnetometer, M. E. Packard and T. L. Allen, Varian Assoc.

Radiation Effects on Silicon Diodes, J. W. Clark, H. L. Wiser and M. D. Petroff, Hughes Aircraft Co.

Particles and Accelerators, G. C. McFarland, High Voltage Engrg. Corp.

The Electrical Aspects of the UCRL 72C-Mev Synchrocyclotron, B. H. Smith, K. H. MacKenzie, J. Reidel, Q. Kerns, W. R. Baker, C. Park and R. L. Thornton, Radiation Lab., Univ. of Calif.

The Electrical Design of a Heavy-Ion Accelerator, Ford Voelker, Radiation Lab., Univ. of Calif.



Books

An Introduction to Cybernetics by W. R. Ashby

Published (1956) by John Wiley & Sons, Inc., 440 Fourth Ave., N. Y. 16, N. Y. 287 pages + 7 index pages + ix pages. Illus. 8½ X 5½. \$6.50.

Dr. Ashby, who is known to many engineers as the author of *Design for a Brain* and the father of the "homeostat," has written what he considers an easy *introduction* to cybernetics and not "merely a chat about cybernetics." The preface informs us that the book addresses itself to the "many workers in the biological sciences" who "are interested in cybernetics and would like to apply its methods and techniques to their own specialty." It is Ashby's contention that the basic ideas of cybernetics can be treated without reference to electronics and that they are fundamentally simple. Ashby expresses, furthermore, the conviction that although advanced techniques may be needed for advanced applications, a great deal can be done in the biological sciences by the use of quite simple techniques, provided they are used with a clear and deep understanding of the principles involved. He expresses the belief that by refining commonplace and well-understood concepts step by step, the biological worker who has no knowledge of mathematics beyond elementary algebra can be introduced to such cybernetics topics as feed-back, stability, regulation, ultrastability, information, coding, noise, and so forth.

Ashby divides his book into three major parts: Part I deals with the principles of mechanisms (including those that apply to determinate machines and very large systems). Part II, entitled, "Variety," deals with what is meant by information; it is designed to enable the reader "to proceed without difficulty to the study of Shannon's own work." Part III deals with regulation and control and provides "an explanation of the outstanding powers of regulation possessed by the brain, as well as the principles by which designers may build machines of like power."

The book is well written and equally well produced (with the exception of a rather curious index which includes entries such as borrowed knowledge, chair, chameleon, coffee, fly-paper, flying saucer, ghosts, Hitler, etc.). And yet, this reviewer cannot rid himself of a certain uneasiness in recommending it for the purpose for which Ashby wrote it, to wit: for those who want to achieve by self-study an actual mastery of the subject. Many admittedly easy exercises are scarcely designed to relieve this reluctance. When, in the chapter entitled, "The Black Box," exercise 6/16-2 asks the question, "To what degree is the Rock of Gibraltar a model of the brain?" it is with a sense of keen disappointment that one reads the answer, "It persists, so does the brain; they are isomorphic at the lowest level." Such exercises hardly do justice to the often insightful exposition that Ashby provides elsewhere.

The book's strongest point is, perhaps, that it brings the mathematically unsophisticated reader into some elementary

contact with a broad spectrum of mathematical raw materials for conceptual models. In this respect Ashby's book fills a void in the cybernetic literature in spite of its exceptionally scant bibliography.

Ashby's views of and aspirations for cybernetics as a mathematical discipline are revealed when he writes, "the truths of cybernetics are not conditional on their being derived from some other branch of science." In Ashby's view, cybernetics, whose subject matter is the domain of all possible machines, can, like mathematical physics, be indifferent to the criticism that it gives prominence to the study of nonexistent systems. Here Ashby becomes a victim of his own semantics. The position of esteem that mathematical physics occupies today must in large part be attributed to the fact that throughout the past three centuries scientists have learned to abstract from their experience aspects that are both mathematically manipulable and yet relevant to predicting and controlling an ever-widening range of physical phenomena.

Workers in the "soft"* sciences were deeply stirred by the cybernetic wave of the future. Here was a suggestion that they use new mathematical models and techniques that promised to be more applicable to problems of information, organization, perception, and perhaps even learning than the calculus had been. Here was a bridge to an era of computer technology with its potentialities of handling large quantities of data and of trying out complex conceptual models in reasonable time spans. Here was, finally, new hope for a rapprochement between scientists in these so-called soft areas with their more secure colleagues under the aegis of a possible unity of the communications sciences. Many of these hopes have been dashed, and much good will has been dissipated by those who, honestly, proclaimed that the problems of the biological and social sciences were on their way toward "solution" each time they had to their own satisfaction been able to transform "organized complexity" by the use of a more or less common-sense verbal device.

This reviewer is convinced that we must not relax our efforts but that we must on the contrary, dig in for a much longer pull. There are some tender shoots in areas in which models of modest scope and measurable phenomena are actually on speaking terms. We must intensify our explorations of mathematical models (such as in the theory of automata and continue to search for significant experiments that will take advantage of our newly-acquired armamentarium.

There are passages in Ashby's book that are not in marked disagreement with the above views. And yet, the tone of the whole book does not seem to convey the proper perspective of the road ahead. There are scientists whose current work is more or less directly inspired by the writings of Wiener, Shannon, etc., Should their work be labeled

* It might perhaps be more appropriate to call them the not-so-vertebrate sciences: their problems are tough rather than soft, but the fields lack a strong theoretical backbone.

as cybernetics and be introduced accordingly? This is certainly a matter of choice. Ashby has a perfectly good right to ignore these rather specific experiments and to substitute his own vision of the spectrum of problems that cybernetics will ultimately be capable of dealing with. But by not giving us at least one example of a truly successful application of a cybernetic model to a really tough biological problem, Ashby's book claims too much and proves too little.

W. A. ROSENBLITH
M.I.T.
Cambridge 39, Mass.

Elektronische Rechenmaschinen und Informationsverarbeitung ed. by A. Walther

Published (1956) by Verlag Friedr. Vieweg & Sohn, Braunschweig, Postfach 185, Germany. 229 pages + viii pages. Illus. 11½ X 8½. Paperbound. 25 DM.

Like many other proceedings of computer conferences, this volume covers a wide range of subjects, from the design to the application of digital computers. This one, however, has a decidedly cosmopolitan flavor. The authors come from eleven countries and their papers are printed in three different languages.

The title, *Electronic Digital Computing and Information Processing*, was that of a conference held in Darmstadt, Germany, in October, 1955. The organizer of the conference, Prof. A. Walther of Darmstadt, is also the editor of this book containing the sixty-four papers delivered at the conference. He has ably performed a most difficult job. The authors represent most of the major computing centers in Western Europe, as well as the United States and three eastern countries (the USSR, Czechoslovakia, and Eastern Germany). Prof. Walther has collected their papers into a readable and interesting volume.

Forty-five of the papers are in German, seventeen in English, and two in French. English-speaking readers will find that the linguistic hurdles have been lowered by the inclusion of English abstracts for papers not in English. A curious sidelight is the fact that the two Soviet papers appear in German while the three Czech papers are printed in English.

The book records an important conference and is thus of historical value. Many of the papers describe machines and techniques employed at various European computing centers. Others present research work of more general interest. The volume contains some unusual items, such as a demonstration that all arithmetic and logical computer operations can be built up from just one essential instruction containing only an address.

The technical material will be largely familiar to those who have followed developments in the U. S. What is, perhaps, most interesting to such readers is the account of the many computer projects which are carried on in Europe, and the resourcefulness displayed in the face of limited budgets.

WERNER BUCHHOLZ
IBM Corp.
Poughkeepsie, N. Y.

Theorie und Technik der Pulsmodulation by E. Hölzler and H. Holzwarth

Published (1957) by Springer-Verlag, Reichpietschauer 20, Berlin W. 35, Germany. 489 pages+3 appendix pages+7 pages of bibliography+6 index pages+xiv pages. Illus. 9½×6½. 57 DM.

The authors state in the preface of this book that their daily work at the Siemens & Halske Central Laboratories revealed time and again a widespread lack of information in the field of pulse techniques. They felt that it would be a worthwhile undertaking to give an up-to-date description of the state of the art with emphasis on pulse modulation, pulse transmission, and the effects of noise. On these topics the authors can speak with authority since they have done extensive work on pulse modulation systems for long-distance communication circuits.

A brief review of the contents of this book shows the comprehensive treatment of the material. The first chapter gives a review of amplitude and frequency modulation (AM and FM) including frequency band requirements, influence of phase and amplitude distortions and the effects of noise. A short qualitative description of pulse amplitude modulation (PAM), pulse phase and pulse duration modulation (PPM and PDM) and pulse code modulation (PCM) follows. The second chapter shows in detail how Fourier and Laplace transformations may be used to translate pulse phenomena from the time domain into the frequency domain. Subsequent sections are concerned with the discussion of three sampling theorems, quantization of signals, and attendant distortion. The third chapter contains a well written review of the principal circuits for pulse generation, pulse modulation, differentiation, integration, gating, clipping, clamping and others. The fourth chapter is devoted to a rather sophisticated analysis of pulse deformation after transmission through linear networks. Applying Bode's theorems to phase and attenuation characteristics of low-pass filters (and by frequency transformation to band-pass filters) the authors show how pulse deformation may affect the quality of transmission and produce crosstalk in time-sharing systems. As everywhere in this book, theoretical results are applied to practical cases, and suggestions are made to improve circuit performance. The influence of noise on PAM, PPM, PDM, and PCM is treated in the fifth chapter. Here the emphasis is on a careful analysis of the gain in signal-to-noise ratio through the use of specific modulation methods such as

PPM and PCM. The advantages of signal compression and expansion and the properties of combinations of two modulation methods (e.g. PPM-AM, PCM-AM, and PAM-FM) are also discussed. The sixth and final chapter supplements Chapter Three by describing complete pulse modulation systems such as a 24-channel PPM-AM communication system. Pulse measurements and component design are not covered.

The book is written for electrical engineers interested or active in pulse work. The style is lucid and concise. The analytical treatment in Chapters Two, Four, and Five can be followed without difficulty. Many numerical examples and over four hundred diagrams and figures assist the reader. The material covered is sufficiently general to be useful in many applications of pulse techniques such as radar, television, telemetering, and high speed digital computing. For those readers who are particularly interested in pulse modulation and its application to communication systems and microwave links this book should be an invaluable source of information.

W. H. VON AULOCK
Bell Tel. Labs. Inc.
Whippany, N. J.

Transistor Engineering Reference Handbook by H. E. Marrows

Published (1956) by John F. Rider, Inc., 116 W. 14 St., N. Y. 11, N. Y. 288 pages+2 index pages+viii pages. Illus. 12×9. \$9.95.

The author states in the introduction that, while many publications dealing with transistors are available, "the need to assemble and coordinate information on all the commercial aspects of the industry under one cover had led to the writing of this book."

The volume contains five sections. Section I is a "General Survey of Transistors." Following a chronology of important transistor developments, a short description of transistor materials, structures and fabrication techniques and a list of pertinent references is given. Characteristics and circuit properties of junction transistors are discussed next. A classified bibliography on transistor applications concludes the section. The material is complemented by forty figures and tables related mainly to transistor circuit design.

Section II occupies most of the volume and presents detailed data sheets (including characteristics and performance ratings) on some two hundred types of commercial

transistors which were available at the time when the book was written.

Section III contains reference data on circuit components used with transistors, such as audio transformers of various categories, IF and pulse transformers, capacitors, batteries, thermistors. A list of commercially available transistor test sets is also given.

Section IV lists the specifications and, in many cases, shows the circuit diagrams of some one hundred products utilizing transistors. Products described are various amplifiers, pulse generators and other oscillators, power converters, meters, flip-flops, communication equipment and radio receivers.

The volume is completed by a Manufacturers' Directory (Section V).

This reviewer is unable to display a great deal of enthusiasm for Section I. The material is too condensed to serve either as an understandable introduction to transistor physics and applications for the beginner or as a usable reference for engineers acquainted with the art. As the section stands, not even the little space occupied by it is used efficiently. For example, the author describes such experimental devices as filamentary transistors, field-effect transistors and fieldistors but makes no mention of drift-transistors and unijunction transistors. The model-circuits presented are not selected most judiciously to be representative of the contemporary art. There is some duplication: for example, instead of presenting a larger variety of flip-flops with a description of their respective merits, three essentially identical configurations are shown on page I-25; similarly, the configurations of Fig. 1-19 and 1-20 and those of Fig. 1-20A and 1-20B are identical.

The author did a very conscientious and useful job in compiling the material of Sections II, III and IV. These sections will be of considerable use to transistor circuit designers. It certainly is preferable to have information on transistors and associated components available in a single volume rather than to have to search for the material in countless specification sheets assembled in a multiplicity of folders.

It should, of course, be remembered that, due to the steady release of new and improved transistors and components, the value of the book is necessarily ephemeral. However, for the present, it will be found useful by many engineers.

A. P. STERN
General Electric Co.
Syracuse, N. Y.



Abstracts of IRE Transactions

The following issues of "Transactions" have recently been published, and are now available from the Institute of Radio Engineers, Inc., 1 East 79th Street, New York 21, N. Y. at the following prices. The contents of each issue and where available, abstracts of technical papers are given below.

Sponsoring Group	Publication	Group Members	IRE Members	Non-Members*
Broadcast & TV Systems	PGBTS-8	\$.90	\$1.35	\$2.70
Broadcast Transmission Systems	Vol. BTR-3, No. 1	1.40	2.10	4.20
Electron Devices	Vol. ED-4, No. 2	2.05	3.10	6.15
Engineering Management	Vol. EM-4, No. 2	1.00	1.50	3.00
Information Theory	Vol. IT-3, No.1	2.20	3.30	6.60
Reliability & Quality Control	PGRQC-10	1.20	1.80	3.60
Telemetry & Remote Control	Vol. TRC-3, No. 1	2.40	3.60	7.20
	Vol. TRC-3, No. 2	1.15	1.70	3.45
Vehicular Communications	PGVC-9	.75	1.10	2.25

*Public libraries and colleges may purchase copies at IRE Member rates.

Broadcast & TV Receivers

VOL. BTR-3, NO. 1, JUNE, 1957

Lyman R. Fink (p. 1)

A One Tube Crystal Filter Reference Generator for Color TV Receivers—R. H. Rausch and T. T. True (p. 2)

An Ultrasonic Remote Control for Home Receivers—R. Adler, P. Desmares, and J. Spracklen (p. 8)

A remote control system for TV receivers is described which employs ultrasound in the vicinity of 40 kc. Slowly decaying single-frequency signals are produced by striking aluminum rods with a hammer. The receiver employs limiting followed by frequency selection and integration to discriminate against acoustic interference.

Considerations governing the design of the mechanical sound transmitter are presented and a mass production technique for adjusting the mechanical resonant frequencies is described. The paper closes with a discussion of the ultrasonic microphone used in the receiver.

The Measurement of CRT Beam Apertures—E. J. Quinlan (p. 14)

Portable TV Design Considerations—F. R. Wellner and M. E. Jones (p. 18)

Techniques of Color Purity Adjustment in Receivers Employing the "Apple" Cathode-Ray Tube—R. C. Moore, A. Hopengarten, and P. G. Wolfe (p. 23)

A New Noise-Gated AGC and Sync System for TV Receivers—Part I—J. G. Spracklen and W. Stroh (p. 28)

A New Noise-Gated AGC and Sync System—Part II—G. C. Wood (p. 32).

Transistor Feedback Preamplifiers—R. P. Burr (p. 35)

Determination of Transistor Performance Characteristics at VHF—G. E. Theriault and H. M. Wasson (p. 40)

Broadcast Transmission Systems

PGBTS-8, JUNE, 1957

The Correction of Differential Phase Distortion in Color Television Transmitters—V. J. Cooper (p. 1)

Automatic Gain Control in TV Automation—M. H. Diehl, W. J. Hoffman, and W. L. Shepard (p. 6)

An automatic programming device depends on automatic gain control in typical TV applications. An "All-Electronic" agc with sufficient operational range for use as an integral part of a monochrome vidicon film center is described and compared to other gain control methods.

An automatic programmer also lends itself to the switching functions of a color film center, using the flying spot scanner principle. The simplicity of the All-Electronic agc method described emphasizes the superiority of the flying spot scanner system for TV station operation.

A 50-Watt Amplifier for Microwave Relays—L. W. Mallach (p. 10)

The significant problems encountered in the engineering development of a klystron amplifier system for 6000 megacycle microwave television relays are discussed and the final results and limitations of the system are set forth. All data submitted herewith is on the basis of laboratory results.

Video Transmission Testing Techniques for Monochrome and Color—J. R. Popkin-Clurman (p. 14)

Achievement of Practical Tape Speed for Recording Video Signals—C. P. Ginsburg (p. 25)

Electron Devices

VOL. ED-4, NO. 2, APRIL, 1957

On the Switching Transient in the Forward Conduction of Semiconductor Diodes—H. L. Armstrong (p. 111)

When a semiconductor diode is caused suddenly to pass forward current, the voltage across it shows a transient, overshooting its steady-state value. This transient behavior is analyzed with the help of a recently given theory of forward current and high-level minority carrier injection in the diodes, with special attention to types of diode often used in pulse circuits, where these transients may be important. The waveform of the transient is

calculated for a hypothetical diode with characteristics similar to some types in common use, and it is found to be very similar to those actually observed.

Temperature Characteristics of the Transfluxor—H. W. Abbott and J. J. Suran (p. 113)

Measurement of High-Frequency Equivalent Circuit Parameters of Junction and Surface Barrier Transistors—A. R. Molozzi, D. F. Page and A. R. Boothroyd (p. 120)

Methods are described for the determination of the high-frequency parameters of junction and surface barrier transistors and involve, in addition to the knowledge of the usual low-frequency parameters, measurement of the product of C_e and the extrinsic base resistance r_{b0} , r_{b0} itself, and the alpha cutoff frequency f_{α} . A previously described method is used to determine the product $r_{b0}C_e$, but new methods are described for the measurement of r_{b0} and f_{α} . The measurements are of "bridge" type, involving simple circuit adjustments for a response null at a single frequency.

Typical experimental results are given for transistors having f_{α} values as high as 85 mc, C_e values down to 2.3 pF and r_{b0} ranging from 45 to 400 ohms. The limits quoted for f_{α} and C_e refer to surface barrier transistors. Comparison with results derived by alternative methods of measurement show good agreement.

Dependence of Magnatron Operation on the Radial Centering of the Cathode—G. E. Becker (p. 126)

A modified Western Electric 4J52 magnatron has been constructed in which provision was made for displacing the cathode laterally in a controlled and measurable way while the tube was in operation. In all the tests which were made, it was found that the operation of the magnatron was best when the cathode was on center. As the cathode was displaced laterally in any direction the efficiency decreased, the frequency pushing increased, the spectrum deteriorated, and back-heating of the cathode increased, while the pulling figure, the Q 's, and the circuit efficiency remained unchanged. None of these quantities was sharply dependent on cathode position when the cathode was near center. Displacement of the cathode from center by a distance as large as 6 per cent of the nominal cathode-anode spacing produced negligible changes in operation, as far as the factors listed above are concerned. Preliminary and less precise results on starting-time jitter, and pulse-to-pulse amplitude and frequency jitter indicate that the same conclusion may be drawn about these factors.

Aperture Lens Formula Corrected for Space Charge in the Electron Stream—C. K. Birdsall (p. 132)

The aperture lens formula of Davisson and Calbick is rederived to include the effect of space charge forces. The correction is applied to a parallel flow Pierce gun, leading to the focal length reduction as a function of permeance, e.g., 30 per cent reduction at permeance 3×10^{-4} .

Some Characteristics of a Cylindrical Electron Stream in Immersed Flow—G. R. Brewer (p. 134)

The dc focusing characteristics of a cylindrical electron stream totally immersed in a uniform axial magnetic field are studied for the condition of laminar electron flow. The magnitude and wavelength of the beam radius perturbations and the angular velocity of precession of the electrons are determined as functions of the magnetic field, space-charge density, and initial injection slope.

Traveling-Wave Tube Propagation Constants—G. R. Brewer and C. K. Birdsall (p. 140)

A brief summary of some new computations of the incremental propagation constants for a traveling-wave tube is presented in the form of graphs.

The data includes values of the wave growth factor α_1 for larger values of the loss parameter d .

The computations for large values of the space-charge parameter QC and of the gain parameter C have revealed an anomalous propagation region for negative ranges of the velocity parameter b , which shows the transition from resistive-wall type interaction to the usual traveling-wave tube type interaction.

A Ceramic-Metal Voltage Reference Tube—J. W. Culp and P. Koskos (p. 144)

A glow discharge voltage reference tube constructed entirely of ceramic and metal has been developed. Minimum size (72), extreme ruggedness, and unusual electrical stability characterize the tube. Operating voltage is approximately 85 v.

Performance of the reference tube under conditions of shock, vibration, high temperature, and high altitude is described. Operating voltage stability over extended periods is demonstrated by presenting the results of precision measurements. Other aspects, such as temperature coefficient, ionization voltage, and the slope and smoothness of the voltage-current characteristic are discussed.

Traveling-Wave Tube Limiters—F. B. Fank and G. Wade (p. 248)

Good broad-band microwave limiters can be built by appropriately modifying conventional traveling-wave tubes. For example, with a single one-watt tube modified suitably the output power could be held constant to within $\pm \frac{1}{2}$ db over a range of input power of approximately 20 db. By modifying two such tubes in the proper way and using them in cascade the range of input power for limiting could be increased to greater than 45 db, and this accomplished over a 700-mc frequency range centered at S band. This was done with commercially available traveling-wave tubes. All the necessary modifications were made from outside the tube envelope.

Experimental results indicate that beam saturation for these tubes when operated conventionally occurs first under the attenuator section. By increasing the gain between the attenuator and the output coupler, the beam saturation can be made to occur first under the output coupler. This fact was of great use in the development of the limiters.

A High-Sensibility Cathode-Ray Tube for Millimicrosecond Transients—K. J. Germeshausen, S. Goldberg, and D. F. McDonald (p. 152)

A high-sensibility cathode-ray tube has been developed for the photographic recording of transients in the millimicrosecond region. The new cathode-ray tube uses a traveling-wave deflection system with magnetic focusing and attains a spot diameter of 0.001 inch. The first models have a sensibility of 0.026 volt/trace width and a writing speed of 10^{11} trace widths/second. Improved production models are expected to have sensibilities of less than 0.02 volt/trace width.

In this particular application, sensibility in volts per trace width and writing speed in trace widths per second are the significant performance characteristics. Analysis of the dependency of these on several important parameters in the general cathode-ray tube design shows that the use of a much smaller spot and display than is conventional results in large gains in sensibility.

Analysis also indicates that maximum sensibility is achieved with the deflection plates located in the lens region. Magnetic focusing is used to permit this optimum deflection plate location. To allow the choice of long plates with short effective transit time, a traveling-wave deflection system is employed. Post-

deflection acceleration is introduced to obtain high writing speeds.

A Power Series Solution of the Traveling-Wave Tube Equations—J. A. Mullen (p. 159)

A solution of the initial value problem for the three-wave formulation of the traveling-wave tube equations is obtained in the form of a series in powers of βCz , whose coefficients are evaluated recursively without solving the determinantal equation.

Design and Performance of a High Power Pulsed Magnetron—E. C. Okress, C. H. Gleason, R. A. White, and W. R. Hayter (p. 161)

This paper describes the salient features of a magnetron which attained by the spring of 1953 a peak power of up to 10 megawatts at 10 microsecond pulse duration and 17 kilowatts average power.

There was little previous knowledge or experience available for guidance at the time (1947) the development was started. Among the most important problems which had to be solved were: 1) the establishment of reliable criteria of π -mode stability as guides for high power magnetron design; 2) the development of a microwave window of sufficient bandwidth for lower order mode loading and which would permit operation of the tube at full power in air at atmospheric pressure; 3) the development of a cathode capable of withstanding high back bombardment power with reasonable life; 4) the development of methods for fabricating a large magnetron; 5) the elimination of voltage breakdown in various parts of the magnetron; 6) the development of a modulator to produce and measure 2- to 10-microsecond pulses up to 100 kilovolts and up to 400 amperes; and 7) the development of a calorimetric load of low thermal capacity for testing the magnetron at full power.

This paper is intended to assist the designers of magnetrons and systems to better appreciate: 1) the problems involved in the simultaneous attainment of multimegawatt power levels at long pulse durations, long wavelength and high duty; 2) what has been accomplished in this regime with magnetrons; and 3) that the experimental material given in the discussion is representative of an advance in magnetron art and not necessarily a limitation of what can be expected by way of performance from the pulsed magnetron.

Analysis of Coupled-Structure Traveling-Wave Tubes—Nathan Rynn (p. 172)

Until now there has been no general method available for taking into account the effect of the electron beam on coupled-structure couplers and attenuators for traveling-wave tubes. This paper presents an analytical procedure for this purpose based on the coupled mode approach of S. E. Miller and J. R. Pierce. It is valid for loosely coupled structures with small loss, only one of which is coupled directly to the beam. In addition to other relations, a general root equation is developed which takes into account loss in either or both of the coupled structures, space charge in the beam, and the possibility of different phase velocities in each structure. Typical plots of the incremental wave parameters are shown. An experimental verification of the theory is presented that shows that predictions made by means of it will be fair to good.

Backward-Wave Oscillator Starting Conditions—R. D. Weglein (p. 177)

Detailed calculations of the starting conditions for backward-wave oscillations were carried out in the region $0 < QC < 0.25$. The coupled-mode theory is called upon to explain the complex nature of the propagation constants for backward-wave interaction.

Backward-Wave Oscillators for the 8000-18,000-Megacycle Band—H. R. Johnson and R. D. Weglein (p. 180)

Design and construction of research models of two backward-wave oscillators, covering the

bands 7.6-12.4 and 11.6-18.0 kms, are described. These tubes are tuned purely electronically and cover their tuning ranges continuously with a power output of 25-mw absolute minimum. The highest electrode voltage used is 2100 volts; the over-all weight is about 7 pounds. These properties are achieved through a novel tube design which enables reduction of tube diameter where it is within the solenoid, and through use of a novel split magnet and rf match idea to enable reduction in necessary solenoid inner diameter.

Experimental Notes and Techniques (p. 185)

Program—Second Annual Technical Meeting on Electron Devices—[Sponsored by the Professional Group on Electron Devices, October 25-26, 1956, Shoreham Hotel, Washington, D. C. (p. 188)].

Contributors (p. 197)

Engineering Management

VOL. EM-4, NO. 2, JUNE, 1957

Selecting Research and Development Personnel for a Small Laboratory—Arnold Addison (p. 43)

In today's competitive labor market, it is not always a simple task to obtain research and development personnel. The engineering graduates from our colleges and universities are not sufficient to meet the staggering demands of American industry today.

Providing the most competition to the smaller research laboratories for urgently needed scientific manpower are large industrial and governmental organizations. Even so, if both salary and working conditions are favorable, personnel can be procured for these smaller organizations. This presentation discussed these important factors in developing a research and development program: 1) what areas of research and development do you wish to follow, 2) what kinds of research and development workers should you employ, and 3) where should you get your manpower?

Maintaining the Research and Development Personnel in a Small Laboratory—Arnold Addison (p. 46)

What you do with your engineering personnel after you get it is extremely important. Failure to understand management's responsibility in handling engineering personnel will result in a poor investment in the cost of selecting and subsequent training of such people. A realistic understanding of how not only to attract but hold your engineering personnel will pay dividends; you will hold the men you have so carefully chosen because certain basic needs have been met.

It is significant to note that this is not only a problem which faces the large industrial laboratories, but is also true of the small laboratories which at the present time are employing professional engineering people in large numbers.

Evaluating Engineers and Scientists for a Research and Development Activity—R. A. Martin and J. Pachares (p. 50)

Dilemma of Engineers in Management—A. N. Curtiss (p. 62)

The Science of Research Management—F. N. Stephens (p. 65)

Management and Engineering—Professionals of Progress—H. L. Richardson (p. 68)

Liaison Relations in Research and Development—A. H. Rubenstein (p. 72)

Personnel Selection and Training for Engineering Management—W. R. G. Baker (p. 79)

Engineering Management Challenge in Weapons Development—G. F. Metcalf (p. 82)

Information Theory

VOL. IT-3, NO. 1, MARCH, 1957

Philip M. Woodward (p. 2)

Entropy and Negentropy—P. M. Woodward (p. 3)

The IRE "Affiliate" Plan—A New Venture in Engineering Society Structure and Service—W. R. G. Baker (p. 4)

On the Estimation in the Presence of Noise of the Impulse Response of a Random, Linear Filter—G. L. Turin (p. 5)

A sounding signal is transmitted through a transmission medium which may be characterized as a linear filter whose impulse response is random, *i.e.*, drawn according to some probability law from an ensemble of possible impulse responses. To the output of the medium is added random noise; the resultant waveform is the received signal. A receiver is required to operate on this received signal so as to make a linear, minimum-mean-square-error estimate of the impulse response of the transmission medium.

Two problems concerned with the design of such a sounding system are considered in this paper. The first is the determination of the transfer function of the optimum linear estimating filter in the receiver. The second is the optimization of the spectrum of the transmitted sounding signal.

The Output Signal-to-Noise Ratio of Correlation Detectors—P. E. Green, Jr. (p. 10)

Expressions are derived for the output signal-to-noise ratio of a correlation detector when the two input functions to be correlated differ only by the presence of an arbitrary linear filter in each path, and the addition of noise to each. It is assumed that the signal and noises are Gaussian with arbitrary power density spectra, and the integration is performed by a filter of arbitrary transfer function. Two types of correlation detectors are distinguished, the low-pass detector in which the integrator is a low-pass filter, and the band-pass detector in which one of the two input functions is deliberately displaced in frequency by Δ and the integrator is therefore a band-pass filter tuned to Δ . Output signal-to-noise ratio expressions for the two types are almost identical.

Error Rates in Pulse Position Coding—L. L. Campbell (p. 18)

An expression for the error rate in a system using a binary pulse position code is derived. In the system considered, the pulses amplitude modulate a carrier and the resultant signal is contaminated by additive Gaussian noise. At the receiver the pulses are recovered by an envelope detector. If synchronization errors and post-detection filtering are neglected, it is shown that the probability of a binary error is approximated well by $1/2 \exp(-a^2/2)$, where a^2 is the peak input signal-to-noise power ratio. Finally, the error rate is derived for the case where the signal amplitude is subject to random fading. Some comparisons are made with error rates derived by Montgomery for other systems with and without carrier fading. It is found that when the signal is subject to fading the pulse position system is better than a comparable system using threshold detection.

The Part of Statistical Considerations in the Separation of a Signal Masked by a Noise—J. A. Ville (p. 24)

The object of this paper is to demonstrate that the stochastic considerations presently involved in signal detections are purely descriptive and are not sufficiently developed to reach the proposed aim.

On a Cross-Correlation Property for Stationary Random Processes—J. L. Brown, Jr. (p. 28)

Given two stationary random processes $x_1(t)$ and $x_2(t)$, the cross-correlation property of interest is the following: If one of the two processes is distorted by an instantaneous nonlinear device, then the cross correlation after the distortion is proportional to the cross-correlation function prior to the distortion.

Using an expansion of the second-order joint probability distribution $p(x_1, x_2)$ introduced by Barrett and Lampard, a necessary

and sufficient condition for the above cross-correlation property is given in terms of requirements on the expansion coefficients.

In certain cases, the constant of proportionality involved in the cross-correlation property is equal to the "equivalent gain" of the nonlinear device as defined by Booton. A necessary and sufficient condition for these two constants to be identical is formulated in terms of the expansion coefficients of $p(x_1, x_2)$. The class of distributions satisfying this condition is a subclass of the set of distributions for which the cross-correlation property is valid.

A Systematic Approach to a Class of Problems in the Theory of Noise and Other Random Phenomena—Part I—D. A. Darling and A. J. F. Siegert (p. 32)

The problem of finding the probability of distribution of the functional

$$\int_{t_0}^t \Phi(X(\tau), \tau) d\tau,$$

where $X(\tau)$ is a (multidimensional) Markoff process and $\Phi(X, \tau)$ is a given function, appears in many forms in the theory of noise and other random phenomena. We have shown that a certain function from which this probability distribution can be obtained is the unique solution of two integral equations. We also developed a perturbation formalism which relates the solutions of the integral equations belonging to two different functions $\Phi(X, \tau)$. If the transition probability density for $X(\tau)$ is the principal solution of two partial differential equations of the Fokker-Planck-Kolomgoroff type, the principal solution of two similar differential equations is the solution of the integral equations. As an example, we calculated the probability distribution of the sample probability density for a stationary Markoff process.

A Systematic Approach to a Class of Problems in the Theory of Noise and Other Random Phenomena—Part II, Examples—A. J. F. Siegert (p. 38)

The method of Part I is applied to the problem of finding the probability distribution of $u = \int_{t_0}^t K(\tau)x^2(\tau) d\tau$, where $K(\tau)$ is a given function and $x(\tau)$ is the Uhlenbeck process. The earlier methods of Kac and the author yielded the characteristic function of this distribution as the reciprocal square root of the Fredholm determinant D of an integral equation. The present method yields a second-order linear differential equation with initial condition only for D as function of t . For the special cases $K(\tau)=1$ and $K(\tau)=e^{-\alpha\tau}$ the characteristic function is obtained in closed form.

In Section III, we have verified directly from the integral equation the differential equation for D and some relations between D and the initial and end point values of the Volterra reciprocal kernel which appear in the joint characteristic function for $u, x(0)$ and $x(t)$.

On the Capacity of a Noisy Continuous Channel—Saburo Muroga (p. 44)

The capacity of a noisy continuous channel is discussed in both cases where the signal transmitted over the channel is expressible by a process with mutually independent random variables and where it is expressible by a Markov process. Unlike discrete channels, continuous channels impose certain restrictions on transmitter power in general. In the case of a continuous channel under disturbance of additive noise, a theorem on the capacity in terms of channel parameters is obtained and applied. Then in the general case of a Markov process a general procedure to calculate the capacity is shown.

Merit Criteria for Communication Systems—A. Hauptschein and L. S. Schwartz (p. 52)

Merit criteria are presented for the transmission of information through noisy channels.

The operational problem is formulated in such a way as to permit the minimum communication cost required to transmit a message over a communication system with a specified degree of reliability for given noise and loading (traffic density) conditions to be determined. The better system transmits the information at less cost. Cost values are shown to be functions of the basic merit parameters power, bandwidth and time, and the operational loading conditions. The formulation is general and can be applied to the evaluation of any modulation or coding system. Comparative evaluation of systems should result in performance indices which would permit judicious choice of systems for use in various operational situations.

First-Order Markov Process Representation of Binary Radar Data Sequences—G. C. Sponsler (p. 56)

Study of radar detection-trial data sequences has indicated the existence of interscan correlation. The theory of simple or first-order Markov chains is here applied to characterize the statistics of such sequences of correlated binary data consisting of detections (1's) and nondetections (0's) of a tracked target upon successive radar scans. Both stationary discrete and non-stationary continuous parameter processes are considered, for which relations are derived between four transition probabilities, β_i , and the absolute detection probability, β , and the so-called blip-scan ratio.

The discrete parameter, first-order Markov chain theory, presented first, is extended to the case wherein the blip-scan ratio may be expressed as a function of time. It is possible to employ the resulting nonstationary, continuous parameter solution to simulate radar data for aircraft flights of arbitrary patterns. Certain restrictions upon the admissible class of blip-scan functions are presented. In the case of the continuous parameter first-order process, the scan-to-scan correlation coefficient is shown to be restricted to positive values. An application is made to an automatic initiation problem.

Automatic Bias Control for a Threshold Detector—J. Dugundji and E. Ackerlind (p. 65)

A method for automatically controlling the threshold bias in a detector is described and analyzed.

In Section I, the threshold bias problem is described: bias is set for a constant false alarm rate (or a constant false alarm time). By "standard biasing" is meant the common practice of adjusting the required bias under the assumption that the noise is Gaussian and has a flat power spectrum.

In Section II, the error that is made by standard biasing, if it turns out the Gaussian noise does not have a flat power spectrum, is given.

In Section III, the automatic biasing method is given in the case where a constant false alarm time is required (its operation to maintain a constant false alarm rate is analogous). The device envisioned operates as follows: one bias level \bar{v}_0 is used as reference; the number of crossings per false alarm time T with positive slope of the noise envelope through \bar{v}_0 is averaged over a sufficiently long time to yield a stable value C . This count C serves to determine the threshold bias v . The level v changes only if the "long time" average count changes; it is specifically assumed that there is no response to instantaneous changes in C . It is shown that such a biasing method automatically adjusts to give a constant false alarm time (or rate), whenever the noise is Gaussian, and so has an advantage over the standard biasing method.

In Section IV, the efficiency of both methods for non-Gaussian noise is compared.

In Section V, the probability of detection of a short (relative to the averaging time)

"sure" signal with Rayleigh distributed amplitude is given when automatic biasing is used; due to the complexity of the expression obtained, no direct comparison has been made with the case where standard biasing is used.

Exact Integral Equation Solutions and Synthesis for a Large Class of Optimum Time Variable Linear Filters—J. S. Bendat (p. 71)

This paper presents the exact integral equation solution and synthesis for a large class of optimum time variable linear filters characterizing many physical problems. The signal random process is expressed in nonstationary Fourier series ensemble form, with certain statistical information assumed about its coefficients. The noise perturbation is represented by a damped exponential-cosine autocorrelation function, which is of major importance in fields of physics and engineering, such as radar, meteorology, and automatic control. For any finite operating period from 0 to t , the optimum time variable weighting function $h(\tau, t)$ is found to be of a separable form, consisting of functions of parameter τ multiplied by functions of parameter t , plus two delta function contributions at the beginning and end. Valid synthesis designs are developed for such separable weighting functions. Asymptotic synthesis techniques are formulated which cover special situations of long-time or short-time operation. The results are applied to two examples of practical interest.

Contributors (p. 81)

Reliability & Quality Control

PGRQC-10, JUNE, 1957

Reliability Indices for Missile Electronic Component Parts—T. S. Bills (p. 1)

Accelerated Life Testing of Capacitors—G. J. Levenbach (p. 9)

One of the problems facing the designer of modern electronic communication systems is the ultimate reliability to be achieved under service conditions. The required level of reliability together with the unavoidable complexity of present-day equipment calls for components having extremely low failure rates. Evaluation of the failure rates of such magnitude in the laboratory or pilot plant is practically impossible within a reasonable length of time and with a reasonable number of components. One way to meet this problem is the artificial reduction of the time to failure. This reduction of time or, in other words, the acceleration of life must be realistic to be of any value, which presents many problems in actual life testing.

In recent years several papers have been published concerning statistical methods applied to life tests showing an exponential distribution of time to failure. These methods have been used as the basis for the design of an experiment to explore the acceleration obtainable in testing capacitors of recent design. Some results of this experiment estimating acceleration factors corresponding to increases in applied voltages and ambient temperatures are presented.

Topology of Switching Elements vs. Reliability—J. P. Lipp (p. 21)

The topology of switching elements is explored from a probability or reliability standpoint. Arrays are indicated which offer a greater degree of reliability than any one of their elements, hence disproving the belief that circuit complexity necessarily lessens reliability. A further result is production of a simple mathematical technique adaptable to the solution of complex circuits in terms of reliability. Such "circuits" may actually consist of redundant communication paths as a more general interpretation of switching elements.

Dynamic Failure Control for Military Electronics—W. F. Luebbert (p. 34)

Failures in electronic equipment can cost

time, effort, supplies, money and even lives. Most reliability programs concentrate almost exclusively upon failure prevention; their main interest seems to be in developing failure resistant components and equipment. However, to assume that such an approach can eliminate all possibility of failure is unrealistic. It is much more practical to view the tendency to failure as ever-present and to place more emphasis upon control of failures and their effects (a concept including but not limited to prevention). There is a close analogy between the nondynamic approach to reliability and the "Maginot Line" type of military strategy, and between the dynamic failure control approach advocated here and the modern "Atomic War" type of strategy. The notorious "game" of Russian Roulette is used as an example, purposely far removed from electronics, of the dynamic approach to failure control and of the importance to dynamic failure control of thorough systems analysis.

In this article emphasis is upon the philosophy and foundations of the dynamic failure control viewpoint, and a minimum of formal rules and detailed suggestions are given. Yet it should be obvious that the dynamic approach would lead to increased emphasis upon the inhibition of failures by environment and application control, upon the possible usefulness of techniques to predict failures before they occur and upon the ability to detect, isolate and correct failures promptly. This approach also points toward the potential advantages of redundancy and dynamic failure compensation to permit over-all success in spite of part failure. Most of all it emphasizes the need for considering failures and their possible effects in over-all system planning. Equipment users can use the dynamic failure control approach to achieve operational reliability and effectiveness from unreliable equipment, while equipment designer-developers can use it to develop reliable equipment from unreliable parts.

(Papers Presented at the Radio Fall Meeting, October, 1956, Syracuse, N.Y.)

Factors in the Reliability of Germanium Power Transistors—A. B. Jacobsen (p. 43)

Naval Material Laboratory Transistor Reliability Study—R. E. Martin (p. 49)

Success Story—Transistor Reliability—1956—C. H. Zierdt, Jr. (p. 57)

Telemetry & Remote Control

VOL. TRC-3, No. 1, APRIL, 1957

(Proceedings of the 1957 National Symposium on Telemetering, April 14-16, 1957, Philadelphia, Pa.)

Introduction to the 1957 National Symposium on Telemetering

Phase Angle Analogs in Out-of-Sight Control Instrumentation—C. L. Parish (p. 1.1)

This paper describes the methods and techniques employed in real time display of telemeter data for missile control purposes. Emphasis is placed on the use of the electrical phase angle between two alternating voltages as the analogue of vehicle flight parameters such as altitude, airspeed, heading, etc. Attention is given to the advantages and disadvantages of the various transmission methods and the factors governing the choice of analogue for a particular function.

A system presently in use at Chance Vought Aircraft, Inc. is discussed from an application point of view. Methods of display and the effect on over-all accuracy are considered.

Some suggestions are given as to the logical extension of the system to provide semi-automatic landing of recoverable missiles.

A Wide-Band Microwave Link for Telemetering—R. E. Glass (p. 1.2)

The microwave link to be described operates in the 4-kmc frequency region and can be set up for any desired bandwidth between 40 to

250 megacycles. In its present state, the telemetering system uses a pulsed-frequency modulated carrier obtained by use of either a klystron or a voltage-tuneable magnetron. The receiver directly amplifies the carrier to a level of +27 DBM where it is amplitude limited and discriminated.

This system has been used in the field since January, 1955 and has proved to be quite reliable. Its use to date has been limited to measuring time intervals of 200 microseconds or less, and to faithfully reproducing pulse shapes requiring up to 250-mc bandwidth.

The various components utilized to accomplish the desired transmitting and receiving functions in this portion of the microwave band will be described.

A Low-Level, High-Speed Sampling System—J. P. Francis (p. 1.3)

Currently available equipment for the high-speed sampling of large numbers of low-level transducers such as strain gages and thermocouples tends to have serious limitations on accuracy and life, or on reliability and economy. A design of equipment for this purpose which is not so seriously limited is described. It combines commercially available units with certain components which have required development. It consists of a low-level multiplexer, dc amplifiers, a second stage of multiplexing at high level, a voltage-to-digital converter, and a recording unit. The design of the multiplexers is described. The low-level multiplexer has accuracy and life exceeding that of conventional units, and avoids the necessity for an amplifier on each input channel. The high level multiplexer has comparable accuracy at electronic speeds. These units are used as building blocks to provide for large numbers of input channels with a high degree of flexibility. Typical system features are described.

A Remote Control System for an Airborne Test Vehicle—Lyman Nickel (p. 1.4)

This paper describes a remote control system which provides continuously variable channels having an error of less than one per cent of full scale as well as a number of "on-off" or binary channels. This system is a method for transmitting and receiving control signals for an airborne test vehicle.

Petroleum Production Telemetering and Remote Control Systems—J. C. Stilley (p. 1.5)

The techniques and systems described in this paper clearly establish the advantages of a well designed telemetering and remote control system for the proper and safe operation of any pipeline or petroleum processing plant to enable the dispatcher or plant operator at a central control office to be informed of the operating condition of the equipment at the various pump, process or compressor stations along the pipeline or at the plant. This concentration of information data, enables a check and record of delivery schedules, efficiency of station operation, product losses, fail-safe conditions, alarm conditions and other pertinent general data. Digital or tone type telemetering provide an efficient and economical media for such systems.

Flight Test Data System Victor System 272—G. Luecke and G. E. Sandgren (p. 2.2)

This is an fm system designed specifically to record data aboard an aircraft under flight test and process the data to an acceptable and highly accurate form with reduction equipment located at a ground station. No telemetering link is required. Magnetic tape is the storage medium. The data outputs are time correlated.

FM information is recorded on a thirty track, 3,000 ft. 1½" magnetic tape for a maximum of forty minutes per reel. Twenty-five tracks are used for data, which include a voice channel. Four tracks are used for reference signals for error correction, for timing and calibration markers, and for addressing the

data on the tape with real time coding. One track is a spare.

Commercially available fm modulators of the resistance bridge controlled, voltage controlled or inductance controlled variety may be used with carrier frequencies at the RDB channels 8 to 13. As many as six carriers may be multiplexed onto each tape track. Standard inputs are used to calibrate the airborne modulators.

The ground reduction system uses the calibration information to automatically correct errors due to zero drift and sensitivity changes in system components. The ground system also corrects errors due to changes of tape velocity, commonly termed wow and flutter, by both mechanical and electronic devices.

Function generators provide a means for correcting nonlinear transducer curves to linear outputs.

Twenty-four demodulators and an audio channel will produce outputs for each playback pass of the tape. The demodulator outputs will drive oscillographs or strip chart recorders directly. At the same time, any one output may be fed to an analog to digital converter. The converter will digitize up to 1,000 samples per second and store the digitized information on an IBM 727 tape memory in a binary pattern suitable as a direct input to an IBM 704 computer. The data outputs from the demodulators are correlated in time to give a true indication of the time relationship of the signal inputs.

Real time addresses are on the tape every ten seconds and the playback of the tape readout can be programmed by using the addresses to start and stop the tape under search or read modes of operation. The tape readout may be started at any second interval. Readout over a particular section of tape may be repeated by selecting a repeat operating function.

The Transmission of Pulse Width Modulated Signals Over Restricted Bandwidth Systems—H. J. Heffernan (p. 2.3)

The apparent anomaly of transmitting PW signals, with pulse lengths as short as 90 microseconds, over restricted bandwidth systems with bandwidths in the order of 3 kc's, are discussed.

It has been shown that in reality, data is transmitted not as pulses of absolute length, but of relative length. However, resolution errors introduced using the techniques described do result in some increase in jitter.

No attempt has been made to compare operating thresholds or to make S/N comparisons as such figures as are now available would not be indicative of system performance when using optimized fm/fm discriminator output, low pass filters.

Extension of FM/FM Capabilities—H. O. Jeske (p. 2.4)

An experimental investigation has been conducted by Sandia Corporation to determine the feasibility of using the higher frequency fm subcarriers as carriers for a group of lower frequency fm subcarrier channels. The system tested was composed of eighteen channels being carried on three high-frequency subcarrier channels operated with a modulation index of one together with eight conventional fm/fm channels, or a total of twenty-six information channels per RF system. The maximum error due to nonlinearities in the transmission system was found to be ± 1.5 per cent when a modulation index of two is used. The system tested employed only conventional fm/fm components. From this investigation it is indicated that at least forty information channels per RF system may be employed using standard RDB subcarrier frequencies and that the response of information channels may easily be doubled over their normal ratings if extreme accuracy is not required.

Telemetry System for the X-17 Missile—J. A. Cox (p. 2.5)

This paper describes the circuits, components and packaging of a high performance airborne six-channel fm/fm telemetering system developed by the Lockheed Missile Systems Division for use in the Air Force X-17 Missile Program. The package, weighing $31\frac{1}{2}$ pounds and measuring 8 inches in diameter by 14 inches long obtains highly accurate information under the severe environmental conditions encountered by a hypersonic ballistic missile.

By utilizing time division multiplexing on four channels, 79 quantities are measured. A bridge-modulated subcarrier oscillator permits the use of variable reluctance transducers on commutated channels. Where possible, plug-in components were reduced in size by transistorization, printed wiring boards, and encapsulation techniques. The antenna coupling device is a radial folded cavity which carries the full structural load, and permits excitation of longitudinal r-f currents on the surface of the vehicle.

The philosophy and techniques associated with the development and application of this system resulted in many useful features providing exceptionally high information capacity, accuracy, reliability, and versatility.

Transistor Circuits Applied to Telemetering—J. H. Smith (p. 3.1)

The PDM portion of a PDM-FM telemeter system for missile operation is described with respect to design philosophy. The system approach has been used in order to produce a compatible marriage of circuitry to the required input and output devices. This has been particularly profitable in the case of the commutator and 70 kc transistor subcarrier oscillator. Transistor circuits have been applied in all cases except the subcarrier oscillator and this is now in the final development stage. This paper discusses several applications which have been successfully transistorized and are now in production. The solutions of problems associated with design for simplicity of circuits, minimum size and weight, ruggedness and reliability are covered.

A Low-Level Electronic Subcommutator—J. M. Walter, Jr. and J. H. Searcy (p. 3.2)

A Low-Level Electronic Subcommutator has been designed and developed by Radiation, Inc. This subcommutator (or commutator) uses the low-level switch described at the 1957 IRE National Convention and was a parallel development with the switch. Semiconductor devices were used extensively throughout the subcommutator, thus permitting miniaturization and ruggedization even though the circuits are extensive and complex. This paper explains the functioning of this subcommutator by describing the system for which it was designed, the circuits within the subcommutator, and its potential applications.

High-Speed High-Accuracy Multiplexing of Analog Signals for Use in Digital Systems—R. E. Marquand (p. 3.4)

Low Level Transistorized Chopper Amplifier—H. F. Harris and T. E. Smith (p. 3.5)

Low-level transistorized chopper amplifiers have been constructed for a specific missile application. With minor modifications, these amplifiers can meet the requirements for general usage. The chopper is capable of processing 900 signals per second at a common mode rejection of 1000:1. The gain is smoothly adjustable ± 20 per cent of full scale and the output is linear within 1 per cent of a straight line drawn between the end points. Operation is consistent over a temperature range of $+40^\circ\text{F}$ to 165°F with less than 10 per cent variation in gain. The amplifier's rise time is less than 300 microseconds. Input impedance is 25 k or better and output impedance is 5 k or less. Ripple is less than 10 millivolts peak.

Progress Report on a Solid State FM-FM Telemetering System—E. V. Politi (p. 3.6)

Program progress of hypersonic missiles and satellites is dependent upon advances in the

telemetering art, for instrumentation must be functional under the imposition of severe environmental extremes. Recently, a solid state fm-fm telemetering system has been developed that is immune to shock and vibration of considerable magnitude. Transistorized units of the solid state system described in this paper are inductance, resistance, and voltage controlled subcarrier oscillators, a missile roll indicator, and a mixing amplifier.

Operational Problems in Aircraft Telemetering—E. F. Shanahan (p. 4.1)

Data Processing, Analog or Digital—A. S. Westneat (Abstract) (p. 4.2)

Application of Telemetry to Flight Testing at Boeing Airplane Company, Wichita Division—A. J. C. Dettbarn (p. 4.3)

The Design Features of an Automatic Oscillograph Reader—D. L. Segel and Graham Tyson (p. 4.4)

The Northrop oscillograph reader is an automatic device designed and built to eliminate the previously laborious task of reducing data gathered from telemetering and other engineering tests. Most of the members of this convention are in fields of engineering that require oscillographic recording as a means of capturing data. It is assumed that most engineers are familiar with the old inaccurate system of sharpened pencils and fifty division to the inch rulers and to the era of data reducers with the so called calibrated eyeballs. The procedure in reducing an oscillograph record is to determine the displacement of each trace from a reference line and store this information so that at a later time, by means of a previously determined calibration curve, the displacement can be converted into terms of the original input variable.

Recently, several companies have brought forth devices employing manually operated movable crosshairs to represent the two coordinates of deflection and time. These employ analogue-to-digital converters to record the observed data on tabulators or punched cards. While these later machines have a great deal of appeal to the data reducer, any large amount of data to be reduced still represents a very tedious job with accuracies depending for the most part on the physical condition of the operator.

In order to produce results from a large amount of data with extreme accuracy, the automatic reader was developed. Initial work was started in October, 1953 and completion took place by October, 1954.

Space Ship Telemetry—Hans Scharla-Nielsen (Abstract) (p. 4.6)

A Direct Computer Controlled Data Editing System—B. M. Gordon (Abstract) (p. 5.1)

Handling PCM on the Ground—Some Problems, Some Solutions—T. Ilagan (Abstract) (p. 5.2)

Commutating Switch Development for Critical Applications—F. H. Gerring (Abstract) (p. 5.3)

Specification and Design of Mechanical Sampling Devices Relative to Telemetering System Requirements—E. B. Garretson and J. F. Brinster (p. 5.4)

A Telemetry Automatic Reduction System—TARE II—E. T. Hatcher (p. 5.6)

A Ruggedized RF Power Amplifier for Use in the 200 MC Telemetry Band—D. D. McRae (p. 6.1)

This paper discusses the design considerations involved in the development of a ruggedized 50-watt rf power amplifier, tunable over the frequency band of 215 to 245 megacycles. The amplification is accomplished in one stage, using an Eimac ceramic tetrode. The unit is capable of operating under severe airborne environmental conditions. Several novel features are incorporated in the amplifier design to match the circuitry to the ceramic tetrode. These features include a tuned input tank composed of two transmission lines, and a tuned

transmission-line output tank that has been curved to conserve space. The unit is blower cooled and requires approximately 100 cubic inches of housing volume in its present configuration.

Completely Transistorized Strain Gage Oscillator—W. H. Foster (p. 6.2)

Described is a completely transistorized strain gage oscillator (S.G.O.). Its primary use is in conjunction with a resistive-type strain bridge transducer to furnish a frequency modulated signal that is directly proportional to an applied force such as stress or pressure. It is expected that due to desirable characteristics it will find major application in the fields of telemetry and remote control, primarily in flight testing of aircraft and missiles. While the S.G.O. was designed primarily for airborne use, it also has applications in the fields of spectroscopy, thermodynamics, and mechanics.

The theory of operation of the S.G.O., including mathematical analyses, is described in considerable detail. Special emphasis is placed on the incorporation of transistors. The uses, applications, and performance of the S.G.O. are also discussed together with its electrical and physical characteristics. The transistorized S.G.O. was developed for the AFMTC as a portion of Project DATUM under USAF Contract No. AF 04(611)-683.

A New Transistor-Magnetic FM/FM Sub-Carrier Discriminator—G. H. Barnes and R. M. Tillman (p. 6.3)

An Electronic Commutator—P. Slavin (p. 6.4)

This paper will discuss the design and performance of a very small electronic commutator which uses symmetrical transistors and sub-miniature cold cathode tubes. Three variations of the basic design have been built having sampling rates of up to 2000 per second. The error increases with temperature and source impedance; the maximum error at 25°C with 2 K ohms source resistance being 15 millivolts. (on 5.0 volt range). Transistors as defined current switches and environmental test on cold cathode tubes are part of the paper.

A Transistorized Pulse Width Keyer—J. A. Riedel, Jr. (p. 6.5)

Notation and Characteristics of Two-Level Codes—G. Birkel, Jr. (p. 7.1)

Notations signifying various permutations of 2-level (binary) aggregates permit the tailoring of digital codes to fit particular hardware applications. Definitions of terms and permutation properties are followed by coding techniques and some applications. The techniques are illustrated by code tables that serve as examples for discussions in the text.

PDM Bandwidth Requirements—F. E. Rock (p. 7.2)

This paper is concerned with experimental and theoretical bandwidths of pulse duration modulation signals.

A theoretical evaluation of a hypothetical PDM system is examined and extrapolated into the region of standard hardware. The presentation takes the form of curves depicting bandwidth requirements. A look at the mathematics of the PDM curves is taken to show the effect of sampling speed and data frequency.

Experimental evaluations are presented in the form of spectrum photographs.

Theoretical Considerations of Practical Data Transmission Systems—F. M. Young (Abstract) (p. 7.4)

Noise and Bandwidth in PDM/FM Radio Telemetry—K. M. Uglow (p. 7.5)

A general equation for signal/noise output ratio in PDM/FM transmission is presented. Two special cases devised by Feldman-Bennett and Nichols-Rauch are derived and discussed. The performance of PDM/FM/FM is derived, and the advantages of PDM/FM/FM over PAM/FM/FM for very narrow-band subcarrier work are pointed out.

PCM Data Collecting and Recording System Designed for Airborne Use—P. Knight (p. 8.1)

A pulse-code modulated data-collecting and recording system has been developed especially for airborne applications. Up to 16 channels of analog data can be sampled at a rate of 150 times per second. The sampled information is converted to 8-bit binary code groups with an accuracy of ± 0.2 per cent and then recorded on magnetic tape. The system also provides for recording, along with the data, time history and voice information. This system is compatible with a UKR-7 ground processing system, resulting in a complete fast, automatic, and highly accurate data-reduction system.

Design of All Channel Ultra-Stable FM Discriminator—Sherman Rigby (p. 8.2)

Telemetry Receiving System at the Air Force Missile Test Center—H. A. Roloff (Abstract) (p. 8.4)

PDM-PAM Conversion System—R. L. Kuelin and W. T. Johnston (p. 8.5)

The requirements and methods for changing pulse amplitude modulation to pulse duration modulation are met by a PDM to PAM Converter. This unit functions over a wide range of input signals and can include, if desired, servo correction of zero and full scale references. As part of an integrated system, the converter is augmented with an all electronic commutator simulator, gate generators, and patching facilities. The converter features provisions for switching in the absence of up to five information channels, protection against generation of false master pulses, and a compensated duty-cycle circuit.

A Low Level Commutation System for Telemetry Application—Frank Shandelman, A. E. Hartung, and Harold Golden (p. 8.6)

Addendum—A Solid-State Pulse-Width Modulator—Henry Kaplan and M. A. Schultz (p. 3.3)

Simplifying FM Sub-Carrier Measurements by Digital Normalizing Techniques—John Humphries (p. 4.5)

A method has been developed of normalizing digital measurements of RDB sub-carrier frequencies so that the operator is never required to deal with frequency data. The method has the advantages of the high accuracy inherent in digital measurements together with extreme simplicity of operation and constant resolution for all RDB channels.

Telemetry Magnetic Tape Recorder/Reproducer—R. E. Hadady and S. Gilman (p. 5.5)

An entirely new magnetic recorder/reproducer system has been developed for telemetry use. Designed for 7-track, $\frac{1}{2}$ " tape and 14" reels, it is easily convertible to $\frac{1}{4}$ " and 1" tape (2 to 14 tracks). Primary design features are extreme accuracy (.05% peak wow and flutter), versatility (completely interchangeable analog, PDM and fm electronics, or any combination of these), and mechanical simplicity and reliability.

Coding for Suppression of Noise and Interference in Airborne PCM Telemetry Systems—H. F. Harmuth (p. 7.3)

For the transmission of data from aircraft and missiles to a ground station, compact, low-power equipment in the air is mandatory, but considerable complexity can be acceptable for the receiver. To transmit data reliably with low transmitter power under conditions of noise and interference normally encountered in air-to-ground transmissions, one may apply noise suppressing coding techniques such as PCM. In standard PCM a signal consists of a sequence of pulses with positive or negative amplitude, and the signals are detected by sampling the amplitudes and ascribing the value +1 to a positive amplitude and the value -1 to a negative amplitude. An improvement of about 7 db in signal-to-noise power ratio over this sys-

tem may be obtained by using a detection method based on correlation. The received signal is multiplied by a certain function, and the integral of this product taken over the length of the whole signal assumes the value +1 or -1. For each bit of information in the signal a different multiplying function is used. A signal with eight bits of information will thus be represented by eight integrals of value +1 or -1 each. This "integration system" behaves—as far as noise is concerned—like an "amplitude sampling system" having a bandwidth equal to one half times the pulse rate. Since amplitude sampling systems usually are operated with five times that bandwidth in order to keep the filter distortions sufficiently low, the gain of 7 db mentioned above is obtained.

Time Interval Telemetry System—Ned Wilde (p. 8.3)

Random nonrepetitive pulses space from 0.5 to several hundred microseconds apart originate in a moving source. These time intervals are to be measured and immediately displayed in digital form at a remote point located 10 to 20 miles from the vehicle. This application of telemetry techniques requires a system capable of transmitting, measuring and displaying the time intervals to an accuracy of ± 25 millimicroseconds in addition to providing a signal suitable for ground tracking of the source.

A system study was conducted followed by the construction of a laboratory prototype model to demonstrate the feasibility of performing the desired functions. The resulting telemetry system operated at a carrier frequency of 10 KMC, transmitting a CW tracking signal between timing pulses and no signal during a timing pulse. The transient decay time of the system at the beginning of a timing pulse became the rise time of that pulse at the input to the time interval measuring unit. The time is measured in discrete steps of 25 millimicroseconds with a maximum error of ± 1 step or ± 25 millimicroseconds. The time interval measuring and display units are completely electronic in nature. The stored information is permanently displayed on decade counters within a few microseconds after its occurrence and remained until the counters are manually reset. Additional pulses in the system did not affect a display.

Prior to measurement, the time interval information can be extracted from the system in analog form suitable for real time simulation or recording; after measurement, the information can be extracted in digital form suitable for computations or recording. It is believed that a system of this type could approach a potential accuracy of ± 10 millimicroseconds while maintaining the same degree of flexibility.

VOL. TRC-3, No. 2, MAY, 1957

The Chairman's Message (p.1)

Ballistic Missile Telemetry—L. L. Rauch (p. 2)

Teletel—E. L. Gruenberg (p. 5)

The original concept of telemetry has become too limited to include all that now exists in the modern fields of telemetry and remote control. Modern progress has resulted in the need for new concepts to embrace two new branches of development. The first, Teletest, encompasses the new art of remote experimentation with its problems of multiple measurement and recording. The second, Teletel, refers to the science of control at a distance.

The development of telemetry is reviewed and the distinguishing characteristics of the newer concepts are delineated. An interesting possible extension of Teletel to remote experimentation is pointed out. The recognition of the new concept of Teletel may stimu-

late progress in the field by unifying associated disciplines required to solve the newer problems.

A Survey of Progress Reported During 1955 in Telemetry and Remote Control—K. M. Uglow (p. 9)

Progress in the fields of telemetry and remote control reported during 1955 is summarized under the headings:

Data processing, data storage, digital transmission equipment, millivolt telemeter equipment, multiplexing methods and equipment, radio transmission, remote control, theory and analysis, transducers, and transistorized telemeter equipment.

The small proportion of it dealing with remote control is a reflection of the content of those technical sessions which have been sponsored by the IRE Professional Group on Telemetry and Remote Control.

A Note on the Frequency Distribution of A FM/FM Signal—P. B. Arustein (p. 13)

An approximate expression is derived giving the amplitude and phase of the individual frequency components of an fm/fm signal when the input is a sinusoid. The approximation is subject to the restrictions that the subcarrier frequency be large in comparison to the highest modulation frequency, and that the ratio of subcarrier deviation to subcarrier frequency be much less than unity.

Some qualitative properties of the frequency spectrum are pointed out and discussed, and illustrations of representative single subcarrier-frequency distribution are presented. Although subject to the above restrictions, the results are shown to be applicable to present day fm/fm telemetry techniques.

The Influence of Coding on Closed Loop Remote Control Systems—Zeev Bonenn (p. 16)

The effects of various simple coding methods on the stability of a remote control system are discussed. It is shown that these methods create stability problems and require better observation. Command and observation channels requirements are compared and it is shown that a compensatory relationship between them exists.

Noise and Bandwidth in FM/FM Radio Telemetry—K. M. Uglow (p. 19)

This paper discussed the derivation, limitations, and use of system equations relating input and output signal/noise ratios in fm detection with band-pass and with low-pass output filters and in fm/fm multiplex transmission. The fm/fm equation is:

$$(S/N)_D = (S/N)_C (3/4)^{1/2} (B_C/F_{UD})^{1/2} (f_{DC}/f_s) (f_{SD}/F_{UD})$$

where

$(S/N)_D$ is the output (data voltage) rms signal/noise ratio,

$(S/N)_C$ is the input (radio carrier channel) rms signal/noise ratio,

B_C is the input (radio carrier channel)

F_{UD} is the output (data voltage) low-pass filter bandwidth,
 f_{DC} is the peak deviation of the carrier due to the subcarrier,
 f_s is the center frequency of the frequency-modulated subcarrier, and
 f_{SD} is the peak deviation of the subcarrier due to the data voltage (assumed a sine wave).

System for Rapid Reduction of Telemetric Data—E. D. Heberling (p. 23)

This paper describes automatic telemetric data reduction equipment being developed by the Instrumentation Division at the U. S. Naval Ordnance Laboratory, Corona, Calif., under joint sponsorship of the Navy Bureau of Ordnance and Aeronautics. The design of some of the components has been completed and checked and will be described in detail in this report. The high-speed analog to digital converter is being procured from a commercial source. A high-capacity magnetic tape recorder is not currently available on the market for recording data at the maximum rate (30,000 samples per second) provided by other components of the system. It is expected that a suitable magnetic recorder will become available in the near future.

Transistorized Time Multiplexer for Telemetry—J. M. Sacks and E. R. Hill (p. 26)

A transistorized time multiplexer or commutator is described with applications to telemetry. The unit develops a commutated PAM signal corresponding to the IRIG standard for time multiplexing of an fm/fm signal. The channel input impedance is 500 k ohms and the channel response is accurate to ± 0.5 per cent of modulation range. The present unit includes 15 channels sampled 10 times per second, but channel switching rates up to at least 15 kc are feasible. Channel selection is achieved by two multivibrator rings operating a matrix of diode switches. The commutator consumes 1 watt from a single 45 volt supply, the accuracy being virtually unaffected by ± 20 per cent change in supply voltage. The unit will operate satisfactorily with channel accuracy maintained at ± 0.5 per cent and the commutating frequency changing less than 1 per cent in the temperature range 25°C. to 70°C.

An Automatic Test Set for FM/FM Telemetry Systems—H. A. McGee and P. S. Klasky (p. 30)

Techniques of automation are applied to the problem of preflight check-out of airborne telemetry systems. The result is a test set that measures and analyzes key system parameters without operator participation.

Operation of the subcarrier analyzer portion of the test set is described. Circuit details of pre-set binary counter chain, counter read-out matrix, and GO/NO-GO voltmeter are given. An example of typical test set packaging is shown.

Vehicular Communications

PGVC-9, JUNE, 1957

Foreword (p. 1)

Adjacent Channels and the Fourier Curse—J. S. Smith (p. 3)

This paper shows the results of measurements of adjacent channel interference due to wide and narrow band FM, AM, and SSBAM transmitters. A brief analytic discussion is made to illustrate why the expected results are obtained and a functional method of measurement is described. The measured transmitters were of a standard available commercial design except that in some cases filters were added for audio cutoff to show the possible improvement in performance due to restriction of audio band pass to the modulator.

Results indicated that at 20 kc, the narrowest spacing common in mobile radio use, there was little difference between the narrow systems of modulation. At closer spacings than 20 kc the SSB transmitter showed limitations due to noise. At closer spacings than 20 kc the results for FM were obscured by the limitations of the receiver selectivity.

Comparison of SSB and FM for VHF Mobile Service—H. Magnuski and W. Firestone (p. 12)

Mobile SSB and fm systems are compared on the basis of the same equipment size. The influence of the speech processing on the comparative results is discussed. It is concluded that SSB may provide a somewhat better range of operation with considerable spectrum saving but the S/N ratio in strong signal areas will be poorer.

Remarks will be strictly limited to the use of SSB for mobile service, voice communication in vhf band above 30 mc and not to other SSB applications.

There are two major questions to answer. 1. Will SSB be suitable for vhf mobile application and how well will it perform in comparison to fm or to put it bluntly, will all fm systems become obsolete overnight? The second question is: Why bother with SSB in the first place, will it really save the frequency spectrum and provide more channels?

This paper will try to cover the first question, the second will be only briefly mentioned; the answer to it is complex and not an obvious "yes," or "no."

In comparing SSB and fm some engineers previously based the comparison either on equal transmitter peak power or equal average power, or what not; some claim that SSB is better than fm by 9 db, some think it is 20 db or more better and some others think that it is no darn good at all. These figures are not questioned; they are all correct, relative to the assumptions made in comparing the systems.

Seventh National Conference, IRE Professional Group on Vehicular Communications, Single Side Band Panel Discussion—"Single Side Band AM for Mobile Communications?" (p. 19)



Abstracts and References

Compiled by the Radio Research Organization of the Department of Scientific and Industrial Research, London, England, and Published by Arrangement with that Department and the *Electronic and Radio Engineer*, incorporating *Wireless Engineer*, London, England

NOTE: The Institute of Radio Engineers does not have available copies of the publications mentioned in these pages, nor does it have reprints of the articles abstracted. Correspondence regarding these articles and requests for their procurement should be addressed to the individual publications, not to the IRE.

Acoustics and Audio Frequencies.....	1170
Antennas and Transmission Lines.....	1171
Automatic Computers.....	1171
Circuits and Circuit Elements.....	1171
General Physics.....	1173
Geophysical and Extraterrestrial Phenomena.....	1174
Location and Aids to Navigation.....	1175
Materials and Subsidiary Techniques..	1175
Mathematics.....	1179
Measurements and Test Gear.....	1179
Other Applications of Radio and Electronics.....	1180
Propagation of Waves.....	1180
Reception.....	1181
Stations and Communication Systems..	1181
Subsidiary Apparatus.....	1181
Television and Phototelegraphy.....	1181
Transmission.....	1182
Tubes and Thermionics.....	1182
Miscellaneous.....	1182

The number in heavy type at the upper left of each Abstract is its Universal Decimal Classification number and is not to be confused with the Decimal Classification used by the United States National Bureau of Standards. The number in heavy type at the top right is the serial number of the Abstract. DC numbers marked with a dagger (†) must be regarded as provisional.

ACOUSTICS AND AUDIO FREQUENCIES

- 534.13:539.2/.3].083 1995
Physical Acoustics and the Properties of Solids—W. P. Mason. (*J. Acoust. Soc. Amer.*, vol. 28, pp. 1197–1206; November, 1956.) Many of the techniques of physical acoustics can be used to study the elastic properties and internal friction of a wide range of materials. Several examples are discussed in detail.
- 534.2 1996
Dispersion Equation for Normal Waves in Stratified Media—L. M. Brekhovskich. (*Akust. Z.*, vol. 2, pp. 341–351; October–December, 1956.) A simple method of deriving the dispersion equation is shown and some particular cases are considered.
- 534.2 1997
Comparison of Methods of Calculating Pressure Fluctuations at a Diaphragm—H. Jung. (*Hochfreq. und Elektroak.*, vol. 65, pp. 37–41; September, 1956.) The derivation of pressure conditions based either on considerations of the statistical distribution of molecular impacts or on the natural frequencies in a one- or three-dimensional model leads to an equivalent result only if isothermal conditions are assumed.
- 534.2-14 1998
On the Pressure Dependence of Sound Absorption in Liquids—L. Liebermann. (*J. Acoust. Soc. Amer.*, vol. 28, pp. 1253–1255; November, 1956.) The absorption depends not only on the familiar shear viscosity, but also on bulk viscosity which relates to the dilation or compression of the liquid. The analysis is applied to water and ethyl alcohol.

- The Index to the Abstracts and References published in the PROC. IRE from February, 1956 through January, 1957 is published by the PROC. IRE, May, 1957, Part II. It is also published by *Electronic and Radio Engineer*, incorporating *Wireless Engineer*, and included in the March, 1957 issue of that journal. Included with the Index is a selected list of journals scanned for abstracting with publishers' addresses.
- 534.2-8 1999
Attenuation of Ultrasonic Waves of Finite Amplitude in Liquids—V. Narasimhan and R. T. Beyer. (*J. Acoust. Soc. Amer.*, vol. 28, pp. 1233–1236; November, 1956.) The attenuation was measured in water and in aqueous solutions of acetic and manganese sulphate. In contrast to the results of Towle and Lindsay (2809 of 1955), the results indicate that for water the rate of increase of α/v^2 with pressure decreases with increasing frequency.
- 534.21-14 2000
The Effect of Gas Bubbles on Sound Propagation in Water—J. D. Macpherson. (*Proc. Phys. Soc., London*, vol. 70, pp. 85–92, plate; January 1, 1957.) An investigation in the frequency range 15–100 kc.
- 534.22-14 2001
Rao's Rule and its Basis—B. B. Kudryavtsev. (*Akust. Z.*, vol. 2, pp. 331–340; October–December, 1956.) Rao's empirical relation connecting the velocity of sound in liquids and molecular volume (*Indian J. Phys.*, vol. 14, pp. 109–116; April, 1940) is discussed. Thirty-eight references including eleven to Russian literature.
- 534.232:538.65:621.318.134 2002
Performance of Ceramic Ferrite Resonators as Transducers and Filter Elements—van der Burgt. (See 2232.)
- 534.232:546.431.824-31 2003
Vibrations in Long Rods of Barium Titanate with Electric Field Parallel to the Length—C. V. Stephenson. (*J. Acoust. Soc. Amer.*, vol. 28, pp. 1192–1194; November, 1956.) The fundamental resonant and antiresonant frequencies are related to physical properties of the material. The theory was verified by experiment.
- 534.26 2004
Theory of Scattering of Sound by a Thin Rod—L. M. Lyamshev. (*Akust. Z.*, vol. 2, pp. 358–365; October–December, 1956.) An expression is derived for the sound pressure in the scatter field of a thin, infinitely long, elastic rod with circular cross section, taking into account the longitudinal and flexural vibrations.
- 534.26 2005
Some Results of the Theory of Diffraction of Sound at an Elastic Sphere—S. N. Rzhavkin. (*Akust. Z.*, vol. 2, pp. 366–371; October–December, 1956.)
- 534.26-14:534.88 2006
Theory of the Shadow Zone Diffraction of Underwater Sound—W. J. Noble. (*J. Acoust. Soc. Amer.*, vol. 28, pp. 1247–1252; November, 1956.) The theory of diffraction by a dark half-plane and an asymptotic expansion of the edge wave are used to calculate transmission anomalies. The dependence of the calculated tubes on range, wavelength, and depth agrees with observations.
- 534.613 2007
The Possibility of an Absolute Calibration of Emitters and Receivers of Sound by Radiation Pressure without the Use of a Radiometer—V. A. Zverev. (*Akust. Z.*, vol. 2, pp. 378–379; October–December, 1956.) Absolute calibration by a modulation method is outlined.
- 534.78 2008
Electronic Binary Selection System for Phoneme Classification—J. Wren and H. L. Stubbs. (*J. Acoust. Soc. Amer.*, vol. 28, pp. 1082–1091; November, 1956.) A system for automatic classification of spoken English into several groups of phonemes is described.
- 534.78 2009
Note on Pitch-Synchronous Processing of Speech—E. E. David, Jr., and H. S. McDonald—(*J. Acoust. Soc. Amer.*, vol. 28, pp. 1261–1266; November, 1956.) A gating system for reducing channel capacity based on the quasi-periodic nature of speech waveforms.
- 534.78 2010
Determination of the Speech Spectrum through Measurements of Superposed Samples—T. H. Tarnoczy. (*J. Acoust. Soc. Amer.*, vol. 28, pp. 1270–1275; November, 1956.) The application of a magnetic-recording technique to Hungarian speech is reported.
- 534.78:621.391 2011
The Information Content of Noise Sounds—F. Enkel. (*Nachrichtentechn. Z.*, vol. 9, pp. 493–498; November, 1956.) Analytical tests using logatoms were made to assess the importance of the continuous noise spectrum above 4500 cps and the dynamic structure of consonant sounds. Redundancy in normal speech is also discussed.
- 534.79 2012
The Cues of Constant Loudness for Continuous Tones and for Single Pressure Impulses—R. Feldtkeller. (*Frequenz*, vol. 10, pp. 356–358; November, 1956.) Brief discussion of a comparison of the curves. The impulses considered are of Gaussian shape, and their loudness is determined with reference to a 1-kc tone.
- 534.833.4 2013
Reactive Components in Sound Absorber Construction—C. Becker. (*J. Acoust. Soc.*

Amer., vol. 28, pp. 1068-1071; November, 1956.)

534.84 **2014**
The Development of Equipment for Measuring Intelligibility Ratio—W. Erler. (*Hochfreq. und Elektroak.*, vol. 65, pp. 53-59; September, 1956.) The apparatus described is used for the experimental determination of the ratio defined by Thiele (311 of 1954); it is suitable for direct tests or for tests on models to a scale of 1:20.

534.843 **2015**
Methods for Evaluating and Measuring the Diffusion of the Acoustic Field in Closed Rooms—W. W. Furdujev (Furduev). (*Nachr. Tech.*, vol. 6, pp. 448-454; October, 1956.) Critical survey and discussion of definitions and methods proposed by various authors. A measurement based on the correlation coefficient and taking account of the composition of the sound appears to be the most suitable and convenient method [see also 2973 of 1952 (Gershman)]. Twenty-one references.

534.845 **2016**
The Dynamic Flow Parameter (Flow Resistance) of Circular Short Ducts—W. Kraak. (*Hochfreq. und Elektroak.*, vol. 65, pp. 46-49; September, 1956.) The flow conditions in the short ducts of perforated sound-absorbing panels are calculated and a correction factor allowing for the length of the ducts is determined experimentally. Text results confirm the validity of the formulas given.

534.846 **2017**
Acoustics of Large Orchestral Studios and Concert Halls—T. Somerville and C. L. S. Gilford. (*Proc. IEE*, Part B, vol. 104, pp. 85-97; March, 1957.) A comparison between the acoustic properties of old-style concert halls and studios with more modern designs having fan-shaped plans and reflecting surfaces. The modern practice of directing sound to the back of the hall by reflection may improve speech audibility, but reduces musical quality.

621.395.61/.62 **2018**
Speech Communications in Noise: some Equipment Problems—M. E. Hawley. (*J. Acoust. Soc. Amer.*, vol. 28, pp. 1256-1260; November, 1956.) The paper includes discussions on the merits of pressure gradient microphones which discriminate against sound from distant sources, avc, and peak clipping and the use of headsets and earplugs.

621.395.623.7 **2019**
Investigation of the Reproduction of Audio Frequencies by a Cone-Type Loudspeaker—F. Valentin. (*C.R. Acad. Sci., Paris*, vol. 244, pp. 735-737; February 4, 1957.) Theory and experiment indicate that for true response above the resonance frequency a loudspeaker should be operated with constant-current rather than constant-voltage excitation.

621.395.625.3 **2020**
A Survey of Factors Limiting the Performance of Magnetic Recording Systems—E. D. Daniel, P. E. Axon, and W. T. Frost. (*Proc. IEE*, Part B, vol. 104, pp. 158-168; March, 1957.) The nature and magnitude of departures from ideal performance of the various system elements are examined together with the element properties required for improved performance.

ANTENNAS AND TRANSMISSION LINES

621.372.2 **2021**
A Theoretical Study of Propagation along Tape Ladder Lines—P. N. Butcher. (*Proc. IEE*, Part B, vol. 104, pp. 169-176; March, 1957.) Dispersion curves are calculated for single-ridge, double-ridge, single T-section and double-T-section ladder lines in which the

rungs of the ladder are thin tapes. Qualitative predictions are confirmed.

621.372.2 **2022**
The Coupling Impedance of Tape Structures—P. N. Butcher. (*Proc. IEE*, Part B, vol. 104, pp. 177-187; March, 1957.) The exact solution to the problem of TEM wave propagation along a periodic array of parallel straight tapes is applicable to the determination of coupling impedances and dispersion curves of a variety of tape structures.

621.372.2:621.318.134 **2023**
Design Considerations for Broad-Band Ferrite Coaxial-Line Isolators—J. Duncan, L. Swern, K. Tomiyasu, and J. Hannwacker. (*Proc. IRE*, vol. 45, pp. 483-490; April, 1957.) Circular polarization of the H vector is produced by partially filling the coaxial line with a low-loss dielectric. Results are given for isolators of this type having an octave bandwidth.

621.372.2:621.318.134 **2024**
Analysis of Nonreciprocal Effects in an N-Wire Ferrite-Loaded Transmission Line—H. Boyet and H. Seidel. (*Proc. IRE*, vol. 45, pp. 491-495; April, 1957.) An analysis for a structure of N wires surrounding a thin ferrite pencil magnetized longitudinally.

621.372.43:621.317.3.029.64 **2025**
An S-Band Coaxial Load—L. W. Shawe. (*Proc. IEE*, Part B, vol. 104, pp. 191-192; March, 1957.)

621.372.8 **2026**
Propagation of Radio Waves in Slightly Curved Waveguides—A. G. Sveshnikov. (*Radiotekhnika i Elektronika*, vol. 1, pp. 1222-1229; September, 1956.) An approximate method of calculating em wave propagation in slightly irregular waveguides is presented and the general formulas obtained are applied to the calculation of propagation in circular cross section waveguides with a) circular and b) sinusoidal curvature.

621.372.8 **2027**
Gyrotropic Infinitely Long Cylindrical Waveguide—R. G. Mirimanov and L. G. Lomize. (*Radiotekhnika i Elektronika*, vol. 1, pp. 1195-1221; September, 1956.) Review of theory of em wave propagation in cylindrical waveguides, completely filled with ferrite, in the presence of longitudinal and transverse magnetizing fields. Nineteen references, including six to Russian literature.

621.372.8 **2028**
Calculation of Losses in Smooth Walls of Circular Waveguides on the basis of Maxwell's Equations—A. Turski. (*Arch. Elektrotech.*, vol. 5, pp. 567-587; 1956. English summary, pp. 588-589.) The basic approach used is similar to that made by Sommerfeld in calculating the propagation of guided waves along a single solid conductor. By this approach, the field can be determined without assuming that the walls are perfectly conducting. A transcendental equation, which arises from the boundary conditions, is solved approximately giving the propagation constant and the damping factor. The errors introduced by other approximate methods for calculating the damping of various modes in circular waveguides are estimated.

621.372.8 **2029**
H-Guide—a New Microwave Concept—F. J. Tischer. (*Electronic Ind. Tele-Tech.*, vol. 15, pp. 50-51, 136; November, 1956.) The waveguide described consists of a dielectric slab of H-shaped cross section with flat metalized outer vertical surfaces. Its attenuation is lower than that of rectangular guides and decreases continuously with increasing frequency. Junctions can be made without special connec-

tors and the construction of microwave systems is simplified.

621.372.8:621.316.727.029.6 **2030**
A Microwave Waveguide Trombone Phase Shifter—A. W. Adey and J. Britton. (*Canad. J. Phys.*, vol. 34, pp. 1112-1118; November, 1956.) "A microwave phase shifter is described which is based on the sliding principle of the trombone and which involves the telescoping together of two snugly-fitting sections of rectangular waveguide of different cross sectional dimensions. $\lambda/2$ transformers are used to reduce the reflection at the change of waveguide cross section. An attempt is made to increase the bandwidth of the instrument by making the transformers of different lengths. A phase change of several wavelengths is possible with an error of approximately \pm one degree."

621.372.8:621.318.134 **2031**
The Character of Waveguide Modes in Gyromagnetic Media—H. Seidel. (*Bell Sys. Tech. J.*, vol. 36, pp. 409-426; March, 1957.) "The effect of birefringence is studied in rectangular and circular waveguides with special attention paid to propagation characteristics in guides of arbitrarily small cross section. Propagating, small-size structures are found in certain ranges of magnetization for both types of guide." See also 19 of 1957.

621.396.677.029.64:621.372.8 **2032**
An Experimental Dual Polarization Antenna Feed for Three Radio Relay Bands—R. W. Dawson. (*Bell Sys. Tech. J.*, vol. 36, pp. 391-408; March, 1957.) "The fundamental problems associated with coupled-wave transducers which operate over a 3-to-1 frequency band have been explored and usable solutions found. The experimental models described are directed toward the broad objectives of feeding the horn-reflector antenna with two polarizations of waves in the 4-, 6- and 11-kmc radio relay bands."

AUTOMATIC COMPUTERS

681.142 **2033**
The Wisconsin Integrally Synchronized Computer—a University Research Project—J. L. Asmuth, C. H. Davidson, J. B. Miller, D. S. Noble, and A. K. Scidmore. (*Commun. & Electronics*, no. 25, pp. 330-338; July, 1956.)

681.142 **2034**
Approximate Solution of Differential Equations with Partial Derivatives using Electrical Analogues—E. S. Kozlov and N. S. Nikolaev. (*Avtomatika i Telemekhanika*, vol. 17, pp. 890-896; October, 1956.) Analogs for solving Laplace, Poisson, and Fourier-type equations are briefly discussed.

681.142 **2035**
A New Analogue Computer using Matrix Iteration for Determining the Roots of Algebraic Equations—J. Miroux. (*Ann. Télécommun.*, vol. 11, pp. 226-232; November, 1956.) The mathematical principles underlying an experimental computer are detailed. Its application and possible development are discussed.

681.142:621.314.7 **2036**
The Junction Transistor as a Computing Element—E. Wolfendale, L. P. Morgan, and W. L. Stephenson. (*Electronic Eng.*, vol. 29, pp. 2-7, 83-87, and 136-139; January-March, 1957.) The small-signal and transient characteristics of the transistor and their application to the design of basic circuits are described and examples of computer elements using transistors are given.

CIRCUITS AND CIRCUIT ELEMENTS

621.3.011.6 **2037**
Time Constants—(*Wireless World*, vol. 63, pp. 218-223; May, 1957.) A discussion of the

rise and fall of voltage in RC and RL circuits with particular reference to blocking oscillators.

621.3.011.6:621.374 2038

Choice of Optimum Time Constants for Sections of Complex Pulse Systems—S. N. Kriz̄. (*Radiotekhnika i Elektronika*, vol. 1, pp. 1255–1257; September, 1956.) A method of selecting the time constants so as to obtain a maximally steep pulse front of the output voltage is discussed.

621.3.012 2039

The Approximate Representation of Attenuation Curves by Straight Lines—M. Gosewinkel. (*Frequenz*, vol. 10, pp. 348–356; November, 1956.) The method described is simpler, but less accurate, than others previously known [e.g., 2869 of 1955 (Kaufmann)]. It is particularly useful for evaluating the equivalent circuits of electroacoustic systems.

621.316.726.078.3 2040

Phase-Lock A.F.C. Loop—R. Leek. (*Electronic Radio Eng.*, vol. 34, pp. 141–146 and 177–183; April and May, 1957.) A detailed analysis is made of a system for tracking the rate of change of frequency (approximately 10 kc per second) of an input signal. Sources of error are discussed.

621.316.86:537.312.6 2041

Industrial Types of Thermistors and their Field of Application—B. T. Kolomiets, I. T. Sheftel', E. V. Kurlina, and G. I. Pavlova. (*Radiotekhnika i Elektronika*, vol. 1, pp. 1177–1185; August, 1956.) The characteristics of Russian thermistors are tabulated and presented graphically and section drawings showing the construction of various types are given.

621.318.43:538.221 2042

Analysis of Instability and Response of Reactors with Rectangular-Hysteresis-Loop Core Material in Series with Capacitors—J. T. Salih. (*Commun. & Electronics*, no. 25, pp. 296–305; July, 1956. Discussion, pp. 305–307.)

621.318.57:621.314.7 2043

The Symmetrical Transistor as a Bilateral Switching Element—R. B. Trousdale. (*Commun. & Electronics*, no. 26, pp. 400–403; September, 1956.) The application of a Ge alloy-junction transistor in switching circuits is described. Signal attenuation greater than 100 db in the "off"-position and insertion loss less than 0.2 db in the "on"-position can be obtained. Possible improvements are discussed.

621.319.4:537.311.33 2044

A Metal-Semiconductor Capacitor—R. L. Taylor and H. E. Haring. (*J. Electrochem. Soc.*, vol. 103, pp. 611–613; November, 1956.) A porous $Ta/Ta_2O_5/MnO_2$ capacitor is described. The characteristics are similar to those of wet electrolytic capacitors.

621.319.43 2045

Decade Air Condenser—W. H. F. Griffiths. (*Engineer, London*, vol. 202, pp. 691–693 and 728–731; November 16 and 23, 1956.) A detailed illustrated description is given of the design of a variable capacitor in which setting and reading errors are minimized. The moving plates, each comprising ten "fingers," are located by a click mechanism to give the required capacitance increments. Fixed plates are suitably slotted to compensate for edge capacitances. An instrument consisting of two decade units with increments 1000 and 100 pf and a continuously variable element is illustrated.

621.319.45 2046

On the Residual Voltage with Electrolytic Capacitors—W. C. van Geel and C. A. Pistorius. (*Philips Res. Rep.*, vol. 11, pp. 471–478; December, 1956.) The residual voltage occur-

ring in the electrolytic system Al/Al_2O_3 electrolyte is examined experimentally and the effect is explained on the assumption of a displacement of Al^{3+} ions in the Al_2O_3 lattice.

621.372.4+621.372.5 2047

Contribution to the Synthesis of Two-Terminal and Four-Terminal Reactance Networks—W. Saraga. (*Nachrichtentech. Z.*, vol. 9, pp. 519–532; November, 1956.) The method of synthesis discussed uses as primary design parameters the points at which suitably chosen rational functions become unity. The application of this method, although very restricted, permits the realization of networks with a minimum of calculation; analysis based on these "unity points" is much more widely applicable. Twenty-two references.

621.372.412:537.228.1 2048

The Concept of Resonance of Piezoelectric Crystal Resonators—G. Becker. (*Arch. elekt. Übertragung*, vol. 10, pp. 467–477; November, 1956.) The relation between the equivalent series and parallel resonance and the physical resonances is discussed and the definition of the concepts is extended. Criteria are given for differentiating between the two types of crystal oscillators.

621.372.413 2049

On the Coupling between Two Cavities—R. N. Gould and A. Cunliffe. (*Phil. Mag.*, vol. 1, pp. 1126–1129; December, 1956.) A general method of calculating the electric and magnetic field configurations and associated eigenvalues is derived in terms of orthogonal functions for two electromagnetic cavity resonators which are coupled through an iris closed by a thin partition.

621.372.5 2050

General Theory of Circuits with Nonlinear Magnetic Elements—S. A. Ginzburg. (*Avtomatika i Telemekhanika*, vol. 17, pp. 799–810; September, 1956.)

621.372.54 2051

Catalogued Filters—E. Glowatzki. (*Nachrichtentech. Z.*, vol. 9, pp. 508–513; November, 1956.) Report on systematic filter calculations carried out with the aid of the electronic computer G1 at Göttingen. A survey of data already tabulated is illustrated by examples from the catalogue. See also 351 of 1956.

621.372.54 2052

Frequency Transformations and Dissipative Effects in Electric Wave Filters—D. J. H. Maclean. (*Electronic Eng.*, vol. 29, pp. 108–114; March, 1957.) The relevant frequency transformation, e.g., low pass to band-pass, is applied to the root positions of the low-pass equivalent network; the resulting pattern is used in a graphical estimation of the effects of dissipation.

621.372.54 2053

Synthesis of Tchebycheff Parameter Symmetrical Filters—A. J. Grossman. (Proc. IRE, vol. 45, pp. 454–473; April, 1957.) A discussion of the earlier work of Darlington (1361 of 1940) on reactive Tchebycheff-type filters, with details of their design.

621.372.543 2054

Synchronous Filter-Oscillator for Frequency [controlled] Equipment in Telemechanics—V. L. Inosov and A. M. Lucluk. (*Avtomatika i Telemekhanika*, vol. 17, pp. 936–940; October, 1956.) The operation of this relay filter circuit is based on synchronism of the local-oscillator frequency with the input signal. The capture of the local-oscillator frequency by signals within a narrow band about the natural frequency of the oscillator results in an effective narrow-band filter. A suitable circuit is described.

621.372.543.2:538.652 2055

Equivalent Circuit of a Resonant, Finite, Isotropic, Elastic Circular Disk—R. L. Sharma. (*J. Acoust. Soc. Amer.*, vol. 28, pp. 1153–1158; November, 1956.) The analysis applies to the first three symmetrical flexural modes. The results are in fair agreement with experimental data on mechanical filters.

621.372.543.2:621.372.413 2056

A Resonant-Cavity Filter for the S-Band—A. A. L. Browne. (*Proc. IEE*, Part B, vol. 104, pp. 193–195; March, 1957.) A tunable filter terminated with coaxial couplings has a second-harmonic rejection of more than 30 db.

621.372.55:534.861.3 2057

Correct Low- and High-[frequency] Compensation of Sound Distortion—H. Völz. (*Funk-Technik, Berlin*, vol. 11, pp. 628–630; November, 1956.) The development of a tone-compensated volume control in the form of a RC network is described.

621.372.56.029.6 2058

Methods of Vapour Deposition and Measurement for the Manufacture and Calibration of Strip Attenuators for the Microwave Region—M. Bouitz. (*Nachr.-Tech.*, vol. 6, pp. 443–448; October, 1956.) Brief outline of method ensuring uniform deposition by using a plane source of evaporation, and description of a method of reasonable accuracy based on vswr for use where standard attenuators are not available.

621.372.6 2059

The Admittance Matrix of Passive and Active Networks—H. Pecher. (*Arch. elekt. Übertragung*, vol. 10, pp. 494–498; November, 1956.) General rules for the formation of the matrix are derived and applied to known tube and transistor circuits.

621.373.4 2060

Nonlinear Coupled Systems—L. Sideriades. (*J. Phys. Radium*, vol. 17, supplement to no. 11, *Phys. Appl.*, pp. 159A–175A; November, 1956.) See also 2339 and 2666 of 1956.

621.373.4 2061

Fluctuations in a Valve Oscillator in the Presence of Grid Current—L. I. Gudzenko. (*Radiotekhnika i Elektronika*, vol. 1, pp. 1240–1254; September, 1956.) Phase and amplitude fluctuations in tuned-anode and tuned-grid oscillators due to the thermal noise of the resistance in the tuned circuit and the shot noise in the anode and grid currents are considered; the depression of the shot noise by the space charge is neglected. Fluctuations in a tuned-grid oscillator with automatic cathode bias are also discussed.

621.373.4.029.6 2062

Influence of the Transit Angle of Electrons in a [reflex-klystron] Valve on the Synchronizing Action of an External Signal—F. M. Klement'ev. (*Radiotekhnika i Elektronika*, vol. 1, pp. 1284–1287; September, 1956.) Theoretical discussion. Conditions for the stability of synchronization are derived.

621.373.421.11 2063

The Fluctuation-Type Nature of the Establishment of Oscillation Amplitude in an Oscillator—V. I. Tikhonov. (*Radiotekhnika i Elektronika*, vol. 1, pp. 1262–1267; September, 1956.) A quantitative estimate is made of the effect of initial conditions on the variance of the times required to reach a given amplitude of oscillations.

621.373.421.13:621.372.412 2064

The Performance of Crystal Oscillators—R. A. Spears. (*A.T.E. J.*, vol. 12, pp. 234–240; October, 1956.) The effects of variations in circuit constants and parameters are described with particular reference to temperature effects.

- 621.373.43 2065
Experiments with Pulse Generators with High Pulse Repetition Frequency—R. Gerharz. (*Z. angew. Phys.*, vol. 8, pp. 531-535; November, 1956.) The apparatus investigated consists, basically, of a single-stage electron multiplier and a coaxial delay line; it produces pulses of consistent shape, at a maximum frequency of 40 mc, 2- μ s rise time, and peak amplitude of about 5 v. Modifications to obtain frequency multiplication and division are also discussed.
- 621.373.43:621.383.27:535.376 2066
An Electron Multiplier as a Pulsed Light Source—Gerharz. (See 2309.)
- 621.373.431.1:621.318.57:621.373.52 2067
Power Transistor Switching Circuit—C. Huang and E. Slobodzinski. (*Commun. & Electronics*, no. 25, pp. 290-296; July, 1956.) Methods and results of measurements of the dc parameters of the Type-2N68 transistor are discussed. Bistable transistor circuits with temperature compensation are described.
- 621.373.442:621.372.543.2 2068
Application of Underexcited RC Oscillators as Band [-pass] Filters—L. N. Kaptsov. (*Radiotekhnika i Elektronika* vol. 1, pp. 1258-1261; September, 1956.)
- 621.373.52 2069
A Single-Transistor Magnetic-Coupled Oscillator—Kan Chen and A. J. Schiewe. (*Commun. & Electronics*, no. 26, pp. 396-399; September, 1956. Discussion p. 400.) The oscillator circuit developed by Van Allen (*Trans. AIEE*, vol. 74, pp. 356-361; July, 1955) is discussed. This consists of two magnetic cores with two junction transistors acting as switches and produces a square wave of frequency proportional to the dc input voltage. From this circuit a single-core, single-transistor oscillator has been derived which has good frequency stability with temperature when a Si-transistor is used.
- 621.373.52 2070
Field-Effect-Transistor Applications—C. Huang, M. Marshall, and B. H. White. (*Commun. & Electronics*, no. 25, pp. 323-329; July, 1956.) Parameters of a Ge transistor are measured with reference to an ac equivalent circuit. The design of some suitable switching and oscillator circuits is outlined.
- 621.374.4:621.385.029.6 2071
Frequency Multiplication with a Reflex Klystron—E. N. Bazarov and M. E. Zhabotinski. (*Radiotekhnika i Elektronika*, vol. 1, p. 1292; September, 1956.) Brief note on conversion efficiency obtained with a klystron the resonator of which was tuned to the second harmonic. The theory was discussed earlier (1375 of 1957).
- 621.375.2:621.3.08.015.3 2072
Periodic Sampling Logarithmic Amplifier—S. J. Nettel. (*Rev. Sci. Instr.*, vol. 28, pp. 37-40; January, 1957.) This amplifier gives a logarithmic output over four decades, derived from the time taken for the voltage across a parallel RC combination to decay to a fixed value.
- 621.375.2.029.3 2073
Inexpensive Pre-amplifier—P. J. Baxandall. (*Wireless World*, vol. 63, pp. 209-212; May, 1957.) Description of a unit with negative-feedback tone control suitable for use with a crystal pickup and the high-quality amplifier described earlier (1706 of 1957), or for af tuning in an fm receiver.
- 621.375.23 2074
The Interaction Concept in Feedback Design—N. H. Crowhurst. (*Audio*, vol. 40, pp. 38, 85 and 32, 81; October and November, 1956.) A method of analyzing feedback amplifiers is presented which enables the effect of closing the feedback loop to be considered in isolation.
- 621.375.3 2075
Bibliography of Magnetic Amplifiers for 1955—G. V. Subbotina. (*Avtomatika i Telemekhanika*, vol. 17, pp. 858-864; September, 1956. Over 130 references, including over 30 to Russian papers, dissertations and patents, are listed.
- 621.375.3 2076
The Pulse-Stretch Coupling Circuit—H. W. Patton. (*Commun. & Electronics*, no. 26, pp. 377-379; September, 1956.) The circuit described is for use on half-wave and full-wave magnetic amplifiers where fast response and high-power gain are required. A biasing pulse is used to block the power winding of the reactor thus facilitating reset.
- 621.375.4 2077
The Design of Wide-Band Transistor Amplifiers—G. Meyer-Brötter and K. Felle. (*Nachrichtentech. Z.*, vol. 9, pp. 498-503; November, 1956.) Formulas are derived for calculating the approximate frequency characteristics of multistage amplifiers.
- 621.375.4 2078
Temperature Stabilization of Transistor Amplifiers—L. M. Vallese. (*Commun. & Electronics*, no. 26, pp. 379-384; September, 1956.) Design formulas, particularly for thermistor compensation, are derived from an analysis of the thermal behavior of the amplifier.
- 621.375.5:546.42/431:824-31 2079
Hysteresis Loops in Dielectric Amplifiers—E. Wingrove, L. Depian, and W. L. Shevel. (*Commun. & Electronics*, no. 25, pp. 283-288; July, 1956. Discussion, pp. 288-289.) The behavior of nonlinear capacitors used in dielectric amplifiers was investigated experimentally. The ceramic material examined consisted of sintered (Ba, Sr)TiO₃ crystals formed into 0.007-inch thick sheets silvered on both sides. Amplifier analysis is simplified by representing the nonlinear capacitor by equivalent linear circuit elements.
- 621.376.222.029.63 2080
Minimizing Incidental Frequency Modulation in Amplitude-Modulated U.H.F. Oscillators—G. Schlaaffner. (*Proc. IRE*, vol. 45, pp. 524-530; April, 1957.) Compensation for changes in cathode-grid transit time is obtained by adjustment of the feedback and cathode lines.
- 621.376.23:621.375.4:621.314.7 2081
A Transistor Demodulator—H. Sutcliffe. (*Electronic Eng.*, vol. 29, pp. 140-141; March, 1957.) The junction-type transistors provide linear signal amplification besides rectification.
- 621.376.54 2082
Pulse-Width-Modulation Unit for Investigating Pulse Control Systems by means of an Electronic Analogue—M. A. Shnaidman. (*Avtomatika i Telemekhanika* vol. 17, pp. 910-920; October, 1956.)
- 535.215+537.37 2083
New Views on the Mechanism of Photoconductivity and Phosphorescence—N. A. Tolstoi. (*Radiotekhnika i Elektronika*, vol. 1, pp. 1135-1143; August, 1956.) Discussion of the "two-step" excitation mechanism. This theory is contrasted with the "binolecular" theory.
- 537.226.1 2084
Remark on the Calculation of the Static Dielectric Constant—H. Fröhlich. (*Physica*, vol. 22, pp. 898-904; October, 1956.) "Macroscopic relations are derived between the dielectric constant and the fluctuations of the dipole moment of a substance. They can be used as a basis for a microscopic calculation of the dielectric constant."
- 537.226.2:537.311.33 2085
Measurement of the Permittivity of High-Conductivity Materials (Semiconductors)—F. M. Popov. (*Radiotekhnika i Elektronika*, vol. 1, pp. 1268-1271; September, 1956.) Results are tabulated of an experimental investigation of the validity of four different formulas for calculating the permittivity of a semiconductor by measurement of the dielectric constant of a mixture of the semiconductor and a dielectric with known permittivity.
- 537.226.2:537.311.62 2086
The Introduction of an Effective Dielectric Constant at High Frequencies—E. A. Kaner and M. I. Kaganov. (*Zh. Eksp. Teor. Fiz.*, vol. 31, pp. 459-461; September, 1956.) An effective dielectric constant given by the relation $\epsilon_{eff} = (4\pi/cZ)^2$, where Z is the surface impedance of the metal, is shown to apply under anomalous as well as normal skin-effect conditions.
- 537.226.3:621.317.335.029.63 2087
The Association of Dipole Molecules [determined] from an Investigation of the Dispersion and Absorption of their Solutions in the dm-Wave Region—E. Fischer and N. Zengin. (*Z. Phys.*, vol. 147, pp. 113-124; November 27, 1956.)
- 537.3 2088
Proceedings of the International Conference on Electron Transport in Metals and Solids—(*Canad. J. Phys.*, vol. 34, pp. 1171-1423; December, 1956.) A special issue containing the papers presented at the conference held in Ottawa in September, 1956, including the following:
- Interaction between Electrons and Lattice Vibrations**—J. Bardeen (pp. 1171-1186).
- On the Electrical Resistivity of Stacking Faults in Monovalent Metals**—A. Seeger (pp. 1219-1234).
- The General Variational Principle of Transport Theory**—J. M. Ziman (pp. 1256-1273).
- Remarks on the Anomalous Behaviour of Alloys Containing Traces of Manganese or Similar Elements**—G. J. Gorter, G. J. van den Berg, and J. de Nobel (pp. 1281-1284).
- Magnetization and Magnetoresistance of some Dilute Alloys of Mn in Cu**—R. W. Schmitt and I. S. Jacobs (pp. 1285-1289).
- On the Resistivity Anomalies in some Dilute Alloys**—J. Korringa (pp. 1290-1291).
- Heat Transfer in Semiconductors**—A. F. Joffé (pp. 1342-1353).
- On the Transition to Metallic Conduction in Semiconductors**—N. F. Mott (pp. 1356-1367).
- The Chemical Bond in Semiconductors. The Group VB to VIIB Elements and Compounds Formed Between Them**—E. Mooser and W. B. Pearson (pp. 1369-1376).
- Our Knowledge of the Fermi Surface**—R. G. Chambers (pp. 1395-1420).
- Discussion on the papers is also included.
- 537.311.1 2089
Phenomenological Theory of Conductivity—G. Beck. (*Nuovo Cim.*, vol. 4, pp. 1190-1191; November 1, 1956. In English.)
- 537.323.08 2090
Methods of Precision Measurement of the Peltier Effect and Thermoelectromotive Forces—M. Shtenbek and P. I. Baranski. (*Zh. Tekh. Fiz.*, vol. 26, pp. 1373-1388; July, 1956.) The methods used in an experimental investigation into the fundamental thermoelectric relation in single crystals of germanium are described in detail, and the possible errors are analyzed.

- 537.5 2091
Radiation Temperature of a Plasma—F. Bitter and J. F. Waymouth. (*J. Opt. Soc. Amer.*, vol. 46, pp. 882-884; October, 1956.)
- 537.533 2092
Electron Emission from Solids after Mechanical Work or Irradiation: Exo-electrons and Photoelectrons—E. L. Huguenin and J. G. Valat. (*J. Phys. Radium*, vol. 17, pp. 965-975; November, 1956.) Survey of theoretical work and experimental investigations of this effect. Nassenstein's theory (see 87 of 1955) appears to be the most generally applicable of those noted. Forty-nine references.
- 537.533:537.58 2093
Investigation of Thermionic Emission During the Transition from the Solid into the Liquid State—V. G. Bol'shov. (*Zh. Tekh. Fiz.*, vol. 26, pp. 1150-1162; June, 1956.) Measurements on Cu, Ag, and Ge are reported. Results show that at the melting point a) the thermionic current does not change sharply and b) the slope of the $\log(I/T^2)/(I/T)$ curve changes.
- 537.533:539.211 2094
The Surface Migration of Tungsten Atoms in an Electric Field—I. L. Sokol'skaya. (*Zh. Tekh. Fiz.*, vol. 26, pp. 1177-1184; June, 1956.) The temperature dependence of the time for a change of shape of a fine tungsten point in a field-emission microscope was investigated experimentally. The activation energies for the build-up and smoothing processes were 2.36 and 3.2 eV, respectively.
- 537.533.8:546.561-31 2095
Investigation of the Angular Distribution of Secondary Electrons from Cuprous Oxide and their Energy Distribution—N. B. Gornyi. (*Zh. Eksp. Teor. Fiz.*, vol. 31, pp. 386-392; September, 1956.) Experimental results, corrected for the effect of tertiary electrons, confirm the cosine-law angular distribution of secondary electrons. The energy distribution at various angles was also investigated and the effect of tertiary electrons on the experimental results is discussed.
- 537.56 2096
The Dissipation of Magnetic Energy in an Ionized Gas—T. G. Cowling. (*Mon. Not. R. Astr. Soc.*, vol. 116, pp. 114-124; November, 1956.) Piddington's theory (3578 and 3579 of 1955) is discussed with reference to the general formula derived; the application of the results to magnetic fields in interstellar clouds is considered.
- 537.56 2097
Kinetic Theory of Weakly Ionized Homogeneous Plasmas: Part 3—M. Bayet, J. L. Delcroix, and J. F. Denisse. (*J. Phys. Radium*, vol. 17, pp. 923-930; November, 1956.) This continuation of previous work (see 1624 and 2915 of 1955) deals with the investigation of an imperfect Lorentz-type gas where account is taken of the energy exchange between electrons and molecules. A collision operator is defined and associated functions and tubes are calculated.
- 537.56 2098
Study of Plasmas under Transient Conditions—J. Salmon. (*J. Phys. Radium*, vol. 17, pp. 931-933; November, 1956.) A formula is derived to represent the conditions in an imperfect Lorentz-type gas after the removal of the electric field. A comparison shows that results agree with those obtained by the method of Bayet, *et al.* (see 2097 above).
- 537.56:538.566 2099
Microwave Conductivity of an Ionized Decaying Plasma at Low Pressures—A. L. Gilardini and S. C. Brown. (*Phys. Rev.*, vol. 105, pp. 25-30; January 1, 1957.) The microwave conductivity of a bounded plasma in a slightly nonuniform field is calculated. The analysis is applied to two particular cases in the theory of the late afterglow of a diffusion-controlled decaying plasma, inelastic collisions being neglected.
- 537.56:538.6 2100
Experimental Investigations of the Motion Plasma Projected from a Button Source across Magnetic Fields—E. G. Harris, R. B. Theus, and W. H. Bostick. (*Phys. Rev.*, vol. 105, pp. 46-50; January 1, 1957.) The velocity with which the front of a "blob" of plasma moves across a magnetic field has been measured under various conditions; it was found to vary slowly with the field strength above 1 kg and to increase monotonically with the source voltage. See also 1057 of 1957 (Bostick).
- 537.564:538.566 2101
Microwave Determination of the Probability of Collision of Electrons in Neon—A. L. Gilardini and S. C. Brown. (*Phys. Rev.*, vol. 105, pp. 31-34; January 1, 1957.) Theory (2099 above) is used to determine the collision probability for momentum transfer of slow electrons.
- 538.2 2102
Magnetic Hysteresis Losses—K. M. Koch and K. Strnat. (*Elektrotech. u. Maschinenbau*, vol. 73, pp. 493-497; November 1, 1956.) A preliminary report on an experimental investigation of the mechanism of remagnetization processes.
- 538.221 2103
Magnetic After-Effect: Part 2—T. Huzimura. (*Sci. Rep. Res. Inst. Tohoku Univ., Ser. A*, vol. 8, pp. 313-318; August, 1956.) Theory based on exhaustion phenomena yields results similar to those derived from previous theoretical investigations establishing a logarithmic time variation of the after-effect, (*ibid.*, vol. 8, pp. 87-94; April, 1956.)
- 538.23 2104
A Relation between the Hysteresis Coefficient and Coercivity—M. Kornetzki. (*Z. angew. Phys.*, vol. 8, pp. 536-538; November, 1956.) The quantitative relation found on the basis of theoretical assumptions agrees with the mean value derived from previous measurements (see; *e.g.*, 3123 of 1956).
- 538.249 2105
On the Determination of the Time Constants of the Magnetic Diffusion After-Effect—P. Brissonneau. (*C.R. Acad. Sci., Paris*, vol. 244, pp. 1174-1177; February 25, 1957.)
- 538.3:52 2106
Some Aspects of Magnetohydrodynamics—G. H. A. Cole. (*Advances Phys.*, vol. 5, pp. 452-497; October, 1956.) A survey. The effects of small and of shock disturbances are discussed.
- 538.56 2107
On the Presence and Conservation of Reactive Power in a Radiation Phenomenon—C. Budeanu. (*C.R. Acad. Sci., Paris*, vol. 244, pp. 1171-1174; February 25, 1957.) Application of the complex form of the Poynting vector to a medium containing "regions of excitation."
- 538.561.029.6:621.373 2108
Operation of a Solid-State Maser—H. E. D. Scovil, G. Feher, and H. Seidel. (*Phys. Rev.*, vol. 105, pp. 762-763; January 15, 1957.) Details of the operation at 9 kmc of a maser oscillator of the type proposed by Bloembergen (1062 of 1957).
- 538.566.029.6:548.73:001.57 2109
Microwave Model Crystallography—J. F. Ramsay and S. C. Snook. (*Electronic Radio Eng.*, vol. 34, pp. 165-169; May, 1957.) A general account is given of the problem of X-ray diffraction simulation at millimeter wavelengths, together with the experimental equipment used and the nature of the phenomena.
- 538.569.4:538.221 2110
Ferromagnetic Resonance Phenomena—S. A. Ahern. (*Research, London*, vol. 10, pp. 15-22; January, 1957.) Theoretical and experimental aspects of ferromagnetic resonance phenomena are described with particular reference to applications in ferrite microwave circuit elements.
- 538.569.4:538.221 2111
Magnetostatic Modes in Ferromagnetic Resonance—L. R. Walker. (*Phys. Rev.*, vol. 105, pp. 390-399; January 15, 1957.) A sample placed in an inhomogeneous rf field of fixed frequency may absorb power at a number of magnetic fields. Theoretical analysis is presented to account for the case where exchange and em propagation can be ignored simultaneously.
- 538.569.4.029.6:53.08 2112
Sensitivity Considerations in Microwave Paramagnetic Resonance Absorption Techniques—G. Feher. (*Bell Sys. Tech. J.*, vol. 36, pp. 449-484; March, 1957.) Problems of setting up a high-sensitivity spectrometer are discussed, including coupling to resonant cavities for maximum output, the minimum detectable signal under ideal conditions, the optimum amount of sample to be used, noise due to frequency instabilities and to cavity vibrations, klystron noise, and signal/noise ratio for specific systems. Experimental results, using a 3-cm wavelength, are compared with theory. A detailed description of a superheterodyne spectrometer is given.
- 538.569.4.029.6:547 2113
Paramagnetic Resonance of Free Radicals at Millimeter-Wave Frequencies—A. van Roggen, L. van Roggen, and W. Gordy. (*Phys. Rev.*, vol. 105, pp. 50-55; January 1, 1957.) Experimental results are given for three radicals measured as single crystals and in solution at 36 and 75 kmc. The magnetic resonance spectrometer used is described.
- 539.11 2114
Theory of Local Electron States in an Isotropic Homopolar Crystal—M. F. Deigen. (*Zh. Eksp. Teor. Fiz.*, vol. 31, pp. 504-511; September, 1956.)
- GEOPHYSICAL AND EXTRATERRESTRIAL PHENOMENA**
- 523.16 2115
Intensity of the Radio Line of Galactic Deuterium—R. L. Adgie and J. S. Hey. (*Nature, London*, vol. 179, pp. 370-371; February 16, 1957.)
- 523.16 2116
Radio Star Scintillations and Interstellar Hydrogen—G. A. Harrower. (*Nature, London*, vol. 179, pp. 608-610; March 23, 1956.) Continuous records of 50-mc radiation from Cassiopeia during 1954 have been analyzed. An interpretation of the scintillation effects is discussed, based on the capture of interstellar particles by the sun's gravitational field.
- 523.16:523.3 2117
Reflexion of Radio Waves from the Moon—F. J. Kerr and C. A. Shain; J. D. Kraus. (*Nature, London*, vol. 179, p. 433; February 23, 1957.) Comment on 3358 of 1956 and author's reply. See also 2118 below.
- 523.16:523.75 2118
Relation of 11-Metre Solar System Phenomena to Solar Disturbances—J. D. Kraus. (*Nature, London*, vol. 179, pp. 371-372; February 16, 1957.) The reception of radio signals

associated with Venus and the moon (3357 and 3358 of 1956) is discussed in relation to solar disturbances during that period and the presence of a large cloud of charged particles near the moon.

523.5:621.396.9 2119

A Radio Echo Survey of Sporadic Meteor Radiants—G. S. Hawkins. (*Mon. Not. R. Astr. Soc.*, vol. 116, pp. 92–104; November, 1956.) An analysis of observations made at Jodrell Bank with two narrow-beam antennas over the period October, 1949–September, 1951. For a description of the equipment, see 3003 of 1951 (Aspinall *et al.*).

523.5:621.396.9 2120

A Radio Echo Method of Meteor Orbit Determination—J. C. Gill and J. G. Davies. (*Mon. Not. R. Astr. Soc.*, vol. 116, pp. 105–113; November, 1956.) The equipment used consists of a pulse transmitter operating at 36.3 mc and three receivers spaced at 3.5 km. The accuracy attainable is limited to ± 2 km in velocity and $\pm 3^\circ$ in radiant position.

550.385:523.78 2121

Geomagnetic Variation due to the Solar Eclipse of June 20th 1955—M. Ota and S. Hashizume. (*J. Geomag. Geoelec.*, vol. 8, pp. 76–80; June, 1956.) Vector diagrams of the magnetic variation observed at four Japanese stations and the *S_q*-field chart for the day are briefly analyzed.

551.510.53:551.594.6 2122

A Method to Detect the Presence of Ionized Hydrogen in the Outer Atmosphere—L. R. O. Storey. (*Canad. J. Phys.*, vol. 34, pp. 1153–1163; November, 1956.) The proposed method is based on the observation of the relation between frequency and time in a whistler. The ionized hydrogen should cause a departure of the relation at low frequencies from the form observed at high frequencies. At magnetic latitude 45° the effect should be detectable at frequencies below about 2 kc.

551.510.535 2123

Night-Time Ionization in the Lower Ionosphere: Part I—Recombination Processes. Part 2—Distribution of Electrons and Negative Ions—A. P. Mitra. (*J. Atmos. Terr. Phys.*, vol. 10, pp. 140–162; March, 1957.) From various ionospheric data, the variation of recombination coefficient with height, near 80 km and time during the night is obtained. Interpretation of the results is based on the recent suggestion that positive atomic ions of low ionization potential are present. The distribution of electrons, negative ions (O^- , O_2^-), positive molecular (YZ^+), and positive atomic ions of low ionization potential (X^+) are deduced from the observational results.

551.510.535 2124

Lunar Effects on the Equatorial E_s —S. Matsushita. (*J. Atmos. Terr. Phys.*, vol. 10, pp. 163–165; March, 1957.) The time of disappearance of equatorial E_s at Huancayo is shown to be earlier at times of full and new moon. This gives support to the author's theory that equatorial E_s is formed by the agency of the eastward electric current jet.

551.510.535 2125

The Characteristics of the F_2 Regions as deduced from the Daily Variations in the Ionospheric Layer—T. Shimazaki. (*Rep. Ionosphere Res. Japan*, vol. 10, pp. 124–142; September, 1956.) Summary and discussion of previous work (3050 of 1956) amplified by results of subsequent study.

551.510.535:523.7:518.3 2126

The Calculation of the Sunrise at the Altitudes of the Ionospheric Layers—H. Kautzleben. (*Z. Met.*, vol. 10, pp. 337–341; November,

1956.) A nomogram is derived which gives the true local time of sunrise or sunset at altitudes up to 500 km for any locality or date. It can also be used to determine the true local time at which the sun reaches any given height above the horizon. The presence of an atmospheric layer absorbing ultra-violet radiation necessitates the use of correction data so that the time of the effective sunrise can be found.

551.510.535:523.75 2127

Sweep-Frequency ft and h't Records of the Ionosphere at the Time of Solar Flares on February 14 and 23, 1956—Y. Nakata. (*Rep. Ionosphere Res. Japan*, vol. 10, pp. 149–151; September, 1956.) The records obtained in Japan are reproduced and briefly discussed.

551.510.535:523.75:621.396.11 2128

Some Effects of Intense Solar Activity on Radio Propagation—R. E. Houston, Jr, W. J. Ross, and E. R. Schmerling. (*J. Atmos. Terr. Phys.*, vol. 10, pp. 136–139; March, 1957.) Records are given showing the effects of a solar flare (observed at Tokyo) on nighttime measurements in Pennsylvania, U.S.A., of 75-kc pulsed vertical-incidence transmissions. A drop in phase height and increase in absorption occurred 15 minutes after the flare, while the group height remained unaltered.

551.510.535:550.38 2129

Relation between Noon F_2 -Layer Ionization and Magnetic Dip—J. N. Bhar. (*J. Atmos. Terr. Phys.*, vol. 10, pp. 168–172; March, 1957.) The relations are studied for constant values of χ rather than constant LMT.

551.510.535:551.55:523.5:621.396.96 2130

The Height Variation of Upper Atmospheric Winds—J. S. Greenhow and E. L. Neufeld. (*Phil. Mag.*, vol. 1, pp. 1157–1171; December, 1956.) The results of an investigation by the meteor radio-echo technique of variations between 80 and 100 km for the year ending August, 1955 are given in graphical form and discussed. For earlier results, also obtained at Jodrell Bank, see 3259 of 1955.

551.594.6 2131

A Theoretical Investigation on the Propagation Path of the Whistling Atmospheric—K. Maeda and I. Kimura. (*Rep. Ionosphere Res. Japan*, vol. 10, pp. 105–123; September, 1956.) Formulas are derived for the exact calculation of whistler paths by applying Fermat's principle, and are used to determine the ray paths for various geomagnetic latitudes. The paths do not generally follow the lines of magnetic force and in lower latitudes the paths are not symmetrical relative to the magnetic equator. The theory explains a number of observational results.

551.594.6 2132

On the Direction of Arrival and the Polarization of Whistling Atmospheric—J. Delloue. (*C.R. Acad. Sci., Paris*, vol. 244, pp. 797–799; February 4, 1957.) Measurements at 5.5 kc show the direction of arrival to be always close to that of the local geomagnetic field and to vary, for the same whistler, at the same time as the polarization.

551.594.6 2133

Waveguide Interpretation of Atmospheric Waveforms—F. Hepburn. (*J. Atmos. Terr. Phys.*, vol. 10, pp. 121–135; March, 1957.) Discusses atmospheric waveforms received by low-frequency propagation. A graphical construction is given for deducing received waveforms, assuming a modified current/time relationship for lightning return-strokes, and using waveguide propagation theory. The types of waveform encountered are qualitatively explained by the theory, and a directional dependence is reported.

551.594.6:621.396.11.029.45 2134

Lightning and the Propagation of Audio-Frequency Electromagnetic Waves—Ya. L. Al'pert. (*Uspekhi Fiz. Nauk*, vol. 60, pp. 396–389; November, 1956.) See 919 and 920 of 1957 (Al'pert and Borodina).

LOCATION AND AIDS TO NAVIGATION

621.396.93 2135

Some Developments of the Decca Navigator System—(*J. Inst. Nav.*, vol. 9, pp. 385–405; October, 1956.)

Part 1—**Decca for Helicopter Operations**—J. G. Adam (pp. 385–389).

Part 2—**The Use of the Flight Log**—E. R. Wright (pp. 389–393).

Part 3—**Dectra [Decca track/range]**—G. Hawker (pp. 394–403).

Discussion, pp. 403–405.

621.396.93 2136

The Total Error in an Adcock Goniometer System—K. Baur. (*Arch. elekt. Übertragung*, vol. 10, pp. 491–493; November, 1956.) The calculation presented takes into consideration the interrelation between the goniometer and antenna errors and thus accounts for the discrepancy between theory and practice at the higher frequencies. See also 451 of 1957 and 781 of 1957.

621.396.933.1 2137

Airborne Doppler Navigation—G. E. Beck. (*Wireless World*, vol. 63, pp. 225–227; May, 1957.) A note on the principles and requirements of a Doppler system.

621.396.933.2:551.594.6:621.396.11.029.45 2138

Very-Low-Frequency Propagation and Direction-Finding—Horner. (See 2272.)

621.396.963.325 2139

Detection of Separations between Adjacent Signals on a Simulated P.P.I. Radar Scope—R. M. Herrick, H. E. Adler, J. E. Coulson, and G. L. Howett. (*J. Opt. Soc. Amer.*, vol. 46, pp. 861–866; October, 1956.) Experiments indicate that background luminance is the most important factor affecting the threshold at which signals can be detected as separate; the influence of phosphorescence decay rate and scan rate is relatively small.

MATERIALS AND SUBSIDIARY TECHNIQUES

533.583:621.385 2140

Barium Getters and Oxygen—R. N. Bloomer. (*Brit. J. Appl. Phys.*, vol. 8, pp. 40–43; January, 1957.) Speed of gettering and flin capacity are studied under various conditions. Films deposited under a very good vacuum are initially inert towards oxygen, even in the presence of an ionizing electron discharge or of incandescent filaments.

533.583:621.385 2141

Performance Characteristics of Barium Getters—P. della Porta. (*Vacuum*, vol. 4, pp. 284–302; July, 1954.) Report of performance tests carried out on pure Ba getter material by means of an improved capillary method in which the pressure in the getter chamber is kept constant. Curves of the instantaneous absorption capacity and of the gettering rate are given for various gases and conditions.

535.215 2142

Spectral Distribution of the Internal Photoeffect in some Systems of Sulphides, Selenides and Tellurides—N. A. Goryunova and B. T. Kolomiets. (*Radiotekhnika i Elektronika*, vol. 1, pp. 1155–1161; August, 1956.) Experimental results are presented graphically of an investigation of the internal photoeffect in complex semiconducting systems of binary compounds. In all graphs the photocurrent per unit of incident energy is plotted in arbitrary units

along the y axis, and the wavelength in μ along the x axis.

535.215:539.23:546.817.231 2143

Photoconductivity in Lead Selenide. Experimental—J. N. Humphrey and W. W. Scanlon. (*Phys. Rev.*, vol. 105, pp. 469-476; January 15, 1956.) The effects of oxygen, sulphur, selenium, and the halogens on the photoconductive and electrical properties of thin evaporated films have been investigated. Each of the above sensitizers acts as an acceptor impurity.

535.215:546.482.21 2144

Internal Photoelectric Effect in Polycrystalline Cadmium Sulphide—B. T. Kolomiets, A. O. Olesk, and S. G. Pratushevich. (*Radiotekhnika i Elektronika*, vol. 1, pp. 1162-1166; August, 1956.) Report on experimental investigation of the effect of Cu impurity on the photoelectric properties of CdS, and of the quenching effect of Fe on photoconductivity in CdS containing 0.01 per cent Cu activator. Results are presented graphically.

535.215:546.482.21 2145

The Kinetics of the Growth of Photocurrent and the Phenomenon of Quenching of Photoconductivity in Cadmium Sulphide—A. D. Shneider. (*Zh. Tekh. Fiz.*, vol. 26, pp. 1428-1432; July, 1956.) The kinetic characteristics of the photoresistors were investigated experimentally at low intensities of illumination. Measurements also showed the absence of a 'photorectifying effect.'

535.215:546.482.31 2146

Cadmium Selenide Photoresistors—B. T. Kolomiets and S. G. Pratushevich. (*Radiotekhnika i Elektronika*, vol. 1, pp. 1174-1176; August, 1956.) Preliminary results of an experimental investigation of the spectral and integral sensitivity, current/voltage and current/wavelength characteristics of polycrystalline-CdSe photoresistors are presented graphically and are briefly discussed.

535.215:546.492.221 2147

Quenching of Photoconductivity in Mercuric Sulphide—A. D. Shneider. (*Zh. Tekh. Fiz.*, vol. 26, pp. 1433-1436; July, 1956.) An experimental investigation of infrared quenching at and below room temperature is reported. A theoretical interpretation of the results obtained is given.

535.215:546.561-31 2148

Properties of the Long-Period Component of Photoconductivity of Cuprous Oxide—Yu. I. Gritsenko and V. E. Lashkarev. (*Radiotekhnika i Elektronika*, vol. 1, pp. 1167-1173; August, 1956.)

535.215:546.817.221:539.23 2149

Noise, Time-Constant, and Hall Studies on Lead Sulphide Photoconductive Films—F. L. Lummis and R. L. Petritz. (*Phys. Rev.*, vol. 105, pp. 502-508; January 15, 1957.) Measurements at frequencies from 20 to 16000 cps showed a $1/f$ component of noise below 100 cps, a generation-recombination component between 100 and 10000 cps, and a Nyquist component at higher frequencies. In conjunction with the time-constant and Hall measurements, the results confirm the theory of photoconductivity in semiconductor films [1774 of 1957 (Petritz)].

535.215:547 2150

Photoelectronics of Organic Compounds—A. N. Terenin. (*Radiotekhnika i Elektronika*, vol. 1, pp. 1127-1134; August, 1956.) Survey of data on photoionization of organic dyes. The nature of photoconductivity of the dyes is discussed. Thirty references.

535.37 2151

The Emission Spectrum of an Exciton—

E. F. Gross and M. A. Yakobson. (*Zh. Tekh. Fiz.*, vol. 26, pp. 1369-1371; June, 1956.) Experimental results indicate that the "blue" luminescence of CdS may be considered as the emission by excitons during their annihilation in the lattice.

535.37 2152

Exciton Absorption and Emission Spectra for Cadmium Selenide Crystal—E. F. Gross and V. V. Sobolev. (*Zh. Tekh. Fiz.*, vol. 26, pp. 1622-1624; July, 1956.)

535.37 2153

Photoluminescence of Thallous Chloride—A. S. Vysochanski. (*C.R. Acad. Sci. U.R.S.S.*, vol. 112, pp. 228-231; January 11, 1957. In Russian.) An experimental investigation of the absorption, excitation and luminescence spectra of TlCl is reported. Results indicate that TlCl is a typical crystal phosphor in which the excess Tl atoms perform the function of an activator and are both the absorption and luminescence centers; absorption leads to the internal photoeffect, and luminescence is preceded by recombination of a conduction-zone electron with an excess Tl ion.

535.37 2154

Influence of the Absorption of Gases on the Luminescence of Zinc Oxide—K. V. Tagantsev and A. N. Terenin. (*C.R. Acad. Sci. U.R.S.S.*, vol. 112, pp. 241-244; January 11, 1957. In Russian.) An experimental investigation is reported of the effect of water vapour, oxygen, and ozone on the luminescence of ZnO illuminated a) continuously, and b) for 10-sec periods at intervals of not less than 5 minutes.

535.37 2155

Photofluorescence Decay Times of Organic Phosphors—T. D. S. Hamilton. (*Proc. Phys. Soc., London*, vol. 70, pp. 144-145; January 1, 1957.) Decay times for thick crystals and microcrystals of seven phosphors are given.

535.376 2156

Influence of Charge-Carrier Injection on Alternating-Field Luminescence—D. Hahn and F. W. Seeman. (*Z. Phys.*, vol. 146, pp. 644-654; November 13, 1956.) Additional luminescence observed in alternating-field excitation of ZnS-based phosphors was investigated. The phosphor, in powder form embedded in a dielectric, was excited at frequencies between 50 cps and 10 kc and field strengths of 10^4 - 10^6 v/cm. The additional luminescence is probably due to a charge transfer at the phosphor/electrode interface.

535.37 2157

The Energy Dependence of the Fluorescence of Polycrystalline Phosphors Excited by Electron Beams and X-Rays—D. Messner. (*Z. Phys.*, vol. 147, pp. 24-42; November 27, 1956.) Analysis of results of investigations carried out for an electron-beam energy range of 5 to 45 kev and with X-rays of 5 to 45 kev and with X rays of λ from about 0.08 to 0.4 Å. Thirty-three references.

537.226/.228.1:536.7 2158

Thermodynamic Theory of Ferroelectric Ceramics—H. G. Baerwald. (*Phys. Rev.*, vol. 105, pp. 480-486; January 15, 1957.) A new small-signal theory is developed. An elastic and a piezoelectric relation are given which are in agreement with experimental data.

537.226/.227 2159

New Ferroelectric Crystal Containing No Oxygen—R. Pepinsky and F. Jona. (*Phys. Rev.*, vol. 105, pp. 344-345; January 1, 1957.) Measurements of ferroelectric behavior in crystals of $(\text{NH}_4)_2 \text{BeF}_4$ are reported at temperatures below -94.7°C .

537.226.33:546.431.82A-31 2160

Investigations Concerning Polarization in

Barium Titanate Ceramics—G. W. Marks, D. L. Waidelich, and L. A. Monson. (*Commun. & Electronics*, no. 26, pp. 469-477; September, 1956.) The results of Fourier analyses of symmetrical and unsymmetrical hysteresis loops are presented. For a BaTiO₃-disk the second-harmonic content and the electro-mechanical coupling coefficient reach a maximum at a polarizing voltage of 15 kv dc per cm.

537.227/.228.1:546.431.824-31 2161

Effect of Pressure on the Curie Temperature of Polycrystalline Ceramic Barium Titanate—H. Jaffe, D. Berlincourt, and J. M. McKee. (*Phys. Rev.*, vol. 105, pp. 57-58; January 1, 1957.) The Curie point is found to increase as the square of the applied stress.

537.227 2162

The Effect of a Unilateral Mechanical Pressure on the Permittivity of Ceramic Ferroelectrics—M. S. Lur'e and A. I. Medvovoi. (*Zh. Tekh. Fiz.*, vol. 26, pp. 1437-1442; July, 1956.) Under pressures of the order of 10 kg/cm², the dependence of permittivity on pressure is nonstationary for temperatures below the Curie point and stationary above the Curie point. The nonstationary variation of permittivity under pressure becomes stationary when the ac field exceeds a certain critical value. The orientation of the domains by polarization and an additional dc field results in the appearance of a stationary dependence together with the remnants of the nonstationary process. It is suggested that the nonstationary dependence of permittivity observed is a result of the orientation processes of the domain structure of polycrystalline ferroelectrics.

537.227:547.476.3 2163

On the Upper Curie Point of Rochelle Salt—M. S. Kosman and A. N. Shevardin. (*Zh. Tekh. Fiz.*, vol. 26, pp. 1443-1450; July, 1956.) Hysteresis loops of Rochelle salt specimens were studied over a temperature range from 18 to 40°C at a frequency of 50 cps. Results show that in strong fields the ferroelectric properties do not disappear at higher temperatures. Although this investigation was carried out for the upper Curie point, there are good grounds for supposing that similar phenomena also occur at the lower Curie point.

537.228.1:546.431.824-31 2164

Dependence of the Ratio of Piezoelectric Coefficients on Density and Composition of Barium Titanate Ceramics—D. Berlincourt and H. H. A. Krueger. (*Phys. Rev.*, vol. 105, pp. 56-57; January 1, 1957.)

537.3 2165

Proceedings of the International Conference on Electron Transport in Metals and Solids—(See 2088).

537.31:[546.56+546.883 2166

The Reflection of Slow Electrons from Tantalum and Copper—J. P. Hobson. (*Canad. J. Phys.*, vol. 34, pp. 1089-1096; November, 1956.)

537.311.3:539.23:621.396.822 2167

Measurement of the Derivations from Ohm's Law and of Flicker Effect Shown by Very Thin Films of Silver, Gold and Aluminium—C. Uny and N. Nifontoff. (*C.R. Acad. Sci., Paris*, vol. 244, pp. 729-732; February 4, 1957.) Simultaneous measurements of resistance variation and flicker effect, the latter at 1 and 5 kc, are reported. Additional irregular fluctuations distinct from the flicker effect were observed, particularly with Ag films on glass. See also 3291 of 1955 (Nifontoff).

537.311.33 2168

Contemporary Semiconductor Materials—D. A. Petrov. (*Bull. Acad. Sci. U.R.S.S., Tech. Sci.*, no. 11, pp. 82-95; November, 1956. In

Russian.) A survey, with particular reference to the metallurgy and preparation of semiconductor materials.

537.311.33 2169

Spontaneous Radiative Recombination in Semiconductors—W. P. Dumke. (*Phys. Rev.*, vol. 105, pp. 139-144; January 1, 1957.) Expressions are derived for the radiative recombination lifetimes due to direct and indirect transitions. For intrinsic Ge at room temperature the calculated lifetimes for both direct and indirect transitions are of the order of a second. For intrinsic Si the lifetimes are much higher.

537.311.33 2170

Carrier Lifetime in Semiconductors for Transient Conditions—D. J. Sandiford. (*Phys. Rev.*, vol. 105, p. 524; January 15, 1957.) The solution for recombination under transient conditions contains a time constant associated with the readjustment in concentration of the recombination centers, in addition to that of the main recombination term.

537.311.33 2171

Surface Recombination and its Influence on the Characteristics of Semiconductor Devices—A. V. Rzhlanov. (*Radiotekhnika i Elektronika*, vol. 1, pp. 1086-1092; August, 1956.) A discussion.

537.311.33 2172

Behaviour of Semiconductors in Strong Electric Fields—Yu. K. Pozhela. (*Radiotekhnika i Elektronika*, vol. 1, pp. 1106-1112; August, 1956.) Continuation of work reported in 471 of 1957.

537.311.33 2173

On Surface Recombination—V. L. Bonch-Bruевич. (*Zh. Tekh. Fiz.*, vol. 26, pp. 1137-1140; June, 1956.)

537.311.33 2174

The Diffusion of Current Carriers in a Semiconductor in the Presence of an External Electric Field—E. I. Rashba. (*Zh. Tekh. Fiz.*, vol. 26, pp. 1415-1418; July, 1956.) Exact expressions are derived for determining the distribution of photo-holes in a bar or plate in the presence of an external electric field and illumination by a filament or point light probe.

537.311.33:535.21:535.8 2175

Two Optical Instruments Used in Semiconductor Research—D. G. Avery. (*J. Sci. Instr.*, vol. 34, pp. 16-17; January, 1957.) A single-prism monochromator and a light-spot microscope with reflecting objective are described.

537.311.33:537.312.5 2176

Bulk Photo-e.m.f. in Semiconductors—V. E. Lashkarev and V. A. Romanov. (*Radiotekhnika i Elektronika*, vol. 1, pp. 1144-1146; August, 1956.) The theory and the experimental verification of the bulk photovoltaic effect observed in Ge specimens with inhomogeneous resistivity are presented. For another theory of the effect; see *Czech. J. Phys.*, vol. 5, pp. 178-192; April, 1955. (Tanc.)

537.311.33:546.26-1 2177

Some Physical Properties of Diamonds—F. C. Champion. (*Advances Phys.*, vol. 5, pp. 383-411; October, 1956.) A survey including: a) theory of the properties of a pure diamond, b) physical behavior of real diamonds, c) applications of defect theory, d) discussion of conducting diamonds, the infrared absorption spectrum and the growth of diamonds, and e) a comparison between the properties of diamonds and of other materials.

537.311.33:[546.28+546.289] 2178

Electron Self-Energy and Temperature-Dependent Effective Masses in Semiconductors: *n*-Type Ge and Si—H. D. Vasileff. (*Phys.*

Rev., vol. 105, pp. 441-446; January 15, 1957.) A theoretical study of electron self-energy in some homopolar semiconductors from which the temperature dependence of the principal effective masses is deduced. The results are found to substantiate the observations of Macfarlane and Roberts (2656 and 3646 of 1955), but not those of Lax and Mavroides (1759 of 1956).

537.311.33:[546.28+546.289] 2179

On the Permeation of Hydrogen and Helium in Single-Crystal Silicon and Germanium at Elevated Temperatures—A. v. Wieringen and N. Warmoltz. (*Physica*, vol. 22, pp. 849-865; October, 1956.) Analysis of mass spectrometer measurements in the temperature range 967°-1207°C for Si and 766°-930°C for Ge. No evidence of any permanent influence of dissolved H₂ on the electrical properties of Si and Ge was found.

537.311.33:[546.28+546.289]:537.312.9 2180

Temperature Dependence of the Piezoresistance of High-Purity Silicon and Germanium—F. J. Morin, T. H. Geballe, and C. Herring. (*Phys. Rev.*, vol. 105, pp. 525-539; January 15, 1957.) Measurements were made over the temperature (*T*) ranges 5°-350°K for Ge and 20°-350°K for Si. For *n*-type Ge in the [110] direction, and *n*-type Si in the [100] direction, the piezoresistance is substantially linear in *T*⁻¹. For *p*-type Ge, the results suggest a *T*⁻¹ dependence for pure material, in both [110] and [100] directions. For *p*-type Si, no simple temperature dependence is found. The results are discussed in relation to theory.

537.311.33:546.28 2181

Removal of Boron from Silicon by Hydrogen Water Vapour Treatment—H. C. Theuerer. (*J. Metals*, vol. 8, pp. 1316-1319; October, 1956.) The treatment of liquid silicon with H₂ containing water vapour at various concentrations is investigated with regard to its boron-removal efficiency. In combination with zone refining this method provides silicon of higher purity than otherwise obtainable.

537.311.33:546.28 2182

Diffusion and Electrical Behaviour of Zinc in Silicon—C. S. Fuller and F. J. Morin. (*Phys. Rev.*, vol. 105, pp. 379-384; January 15, 1957.) The diffusivity and solubility of Zn in Si single crystals were measured. One acceptor level only was found for Zn at 0.31 eV above the valence band.

537.311.33:546.28 2183

Microplasma in Silicon—D. J. Rose. (*Phys. Rev.*, vol. 105, pp. 413-418; January 15, 1957.) Discrete current pulses and minute luminous spots are often observed at breakdown of reverse-biased Si junctions. The phenomena are postulated to be similar to the gas discharge cathode fall. The mechanism is illustrated for the case of the *n-i-p* structure, and analyzed approximately by using a simple equivalent circuit.

537.311.33:546.28 2184

Hall and Drift Mobility in High-Resistivity Single-Crystal Silicon—D. C. Cronemeyer. (*Phys. Rev.*, vol. 105, pp. 522-523; January 15, 1957.) Room-temperature measurements on specimens with resistivity ranging from nearly intrinsic down to 10⁻²Ω cm indicate that the Hall mobilities for lattice scattering are 1560 and 345 cm²/vsec for electrons and holes respectively, and the drift mobilities are 1360 and 510 cm²/vsec for electrons and holes respectively.

537.311.33:546.289 2185

Field-Effect Measurements and Publication to Semiconductor Surface Studies—Shyh Wang. (*Sylvania Technologist*, vol. 9, pp. 111-114; October, 1956.)

537.311.33:546.289 2186

Depth of Surface Damage due to Abrasion on Germanium—T. M. Buck and F. S. McKim. (*J. Electrochem. Soc.*, vol. 103, pp. 593-597; November, 1956.) The approximate depth of surface damage on Ge as it influences surface recombination velocity has been measured for a variety of abrasive treatments by etching, weighing, and making two types of photomagnetolectric measurements. Values range from 1μ or less for fine polishes to 35μ for heavy sandblasting. Close correlation is found with changes in reverse characteristics of grown-junction *p-n* diodes treated in the same manner.

537.311.33:546.289 2187

A Shot Tower for Producing Germanium Doping Pellets of Uniform Composition—I. A. Lesk. (*J. Electrochem. Soc.*, vol. 103, pp. 601-603; November, 1956.)

537.311.33:546.289 2188

Hydrogen and Oxygen in Single-Crystal Germanium as Determined by Vacuum Fusion Gas Analysis—C. D. Thurmond, W. G. Guldner, and A. L. Beach. (*J. Electrochem. Soc.*, vol. 103, pp. 603-605; November, 1956.) Concentration of hydrogen of 3-4×10¹⁸ at oms/cm² and of oxygen of 1-2×10¹⁸ atoms/cm³ were found in three special preparations of Ge obtained by hydrogen reduction of GeO₂ in graphite. The possibility exists that these elements may have been present in these crystals as H₂O. Vacuum crystal growing lowered the hydrogen and oxygen concentrations 20-30 fold.

537.311.33:546.289 2189

The Crucible Problem in the Prolonged Heat Treatment of Germanium—W. Bösenberg. (*Z. angew. Phys.*, vol. 8, pp. 551-552; November, 1956.) Four different methods of heating Ge crystals are compared. The use of a graphite crucible supporting the induction-heated crystal in a vacuum enclosed by a cold quartz-glass container is the best method for maintaining the purity of the crystal.

537.311.33:546.289 2190

The Effect of Impurities on the Lifetime of Excess Carriers of Charges in Germanium—A. V. Rzhlanov. (*Zh. Tekh. Fiz.*, vol. 26, pp. 1389-1393; July, 1956.) Results of an experimental investigation of the effect of impurity concentration are reported.

537.311.33:546.289 2191

Effects of Thick Oxides on Germanium Surface Properties—M. Lasser, C. Wysocki, and B. Bernstein. (*Phys. Rev.*, vol. 105, pp. 491-494; January 15, 1957.) Oxides grown on germanium by heating in oxygen are shown to inhibit interaction between the germanium and the ambient atmosphere. The decay-time of the dc-field-effect increases with increasing oxide thickness.

537.311.33:546.289 2192

Triple Acceptors in Germanium—H. H. Woodbury and W. W. Tyler. (*Phys. Rev.*, vol. 105, pp. 84-92; January 1, 1957.) Both copper and gold introduce three acceptor levels in the forbidden band. For copper the energy levels are 0.04 and 0.32 eV from the edge of the valence band and 0.26 eV from the edge of the conduction band. For gold they are 0.15 eV from the valence band and 0.04 and 0.20 eV from the conduction band; additionally, gold introduces a donor level 0.05 eV from the valence band.

537.311.33:546.289 2193

Formation of Ion Pairs and Triplets between Lithium and Zinc in Germanium—F. J. Morin and H. Reiss. (*Phys. Rev.*, vol. 105, pp. 384-389; January 15, 1957.) Measurements have been made of carrier mobility, relaxation, and energy levels; the results agree with the

- idea that zinc provides two energy levels for electrons in the forbidden gap.
- 537.311.33:546.289:546.33 2194
Absorption of Sodium Ions by Germanium Surfaces—S. P. Wolsky, P. M. Rodriguez, and W. Waring. (*J. Electrochem. Soc.*, vol. 103, pp. 606–609; November, 1956.)
- 537.311.33:546.289:546.811 2195
Solid Solubilities and Electrical Properties of Tin in Germanium Single Crystals—F. A. Trumbore. (*J. Electrochem. Soc.*, vol. 103, pp. 597–600; November, 1956.) An experimental investigation in the temperature range from 400°C to the melting point of Ge is reported. Results of electrical measurements confirm the neutrality of Sn in Ge.
- 537.311.33:[546.873.231+546.873.241] 2196
The Electrical Properties of Bismuth Chalkogenides: Part 2—Electrical Properties of Bismuth Selenide (Bi₂Se₃); Part 3—Electrical Properties of Bismuth Telluride (Bi₂Te₃)—P. P. Konorov. (*Zh. Tekh. Fiz.*, vol. 26, pp. 1394–1399 and 1400–1405; July, 1956.) Continuation of experimental investigation reported in 1500 of 1957. Results are presented graphically showing the temperature dependence of electrical conductivity, the concentration and mobility of current carriers, and the coefficient of thermo-emf for both Bi₂Se₃ and Bi₂Te₃ and of the Hall constant in Bi₂Te₃; the dependence of the mobility of current carriers in Bi₂Se₃ on their concentration is also shown graphically.
- 537.311.33:546.873.241 2197
An Ionization-Method X-Ray Structural Investigation of Bismuth Telluride—F. I. Vasenin and P. F. Konovalov. (*Zh. Tekh. Fiz.*, vol. 26, pp. 1406–1414; July, 1956.) An investigation of the cause of the inversion of polarity of the thermo-emf when the composition of the alloy approaches the stoichiometric ratio is reported. Results indicate that the phenomenon is probably due to the existence of two modifications of the alloy.
- 537.311.33:546.3-1-28-289 2198
The Electrical Conductivity of Germanium-Silicon Alloys in the Liquid State—M. S. Ahlova, O. D. Elpat'evskaya, and A. R. Regel. (*Zh. Tekh. Fiz.*, vol. 26, pp. 1366–1368; June, 1956.) A number of experimental curves are plotted showing the width of the forbidden band, the abrupt change in electrical conductivity during melting, and the maximum electrical conductivity in the liquid state vs the composition of the alloy.
- 537.311.33:[546.682.19+546.682.86] 2199
Effective Masses of Electrons in Indium Arsenide and Indium Antimonide—R. J. Sladek. (*Phys. Rev.*, vol. 105, pp. 460–464; January 15, 1957.) Measurements of the electrical conductivity and Hall effect made between 1.5° and 300°K.
- 537.311.33:546.682.86 2200
The Dependence of the Hall Coefficient of a Mixed Semiconductor upon Magnetic Induction as Exemplified by Indium Antimonide—D. J. Howarth, R. H. Jones, and E. H. Putley. (*Proc. Phys. Soc., London*, vol. 70, pp. 124–135; January 1, 1957.) The Bloch-Wilson theory is discussed and applied to InSb. Good agreement was found between the theory and the observed behavior of two *p*-type single crystals. Values found for the intrinsic carrier concentration are in good agreement with those found elsewhere.
- 537.311.33:549.351.12 2201
New Semiconductors with the Chalcopyrite Structure—I. G. Austin, C. H. L. Goodman, and A. E. Pengelly. (*J. Electrochem. Soc.*, vol. 103, pp. 609–610; November, 1956.) "Com- pounds of the chalcopyrite group are related to well-known semiconductors such as Ge and the zinc blend compounds. This relationship is discussed briefly and some new data are presented regarding the preparation and properties of five chalcopyrite compounds AgInS₂, AgInSe₂, CuInSe₂, AgInTe₂, and CuInTe₂."
- 537.311.33:621.314.63 2202
Rectifying Semiconductor Contacts—H. K. Henisch. (*J. Electrochem. Soc.*, vol. 103, pp. 637–643; November, 1956.) A review of present theory.
- 537.311.33:621.314.632:546.561.221 2203
Point Contact of Pt and γ -Cu₂S—S. Miyatani. (*J. Phys. Soc., Japan*, vol. 11, pp. 1059–1063; October, 1956.) Investigations reveal dc characteristics similar to those of other metal/semiconductor rectifiers, but attributed to ionic conduction. Experimental results appear to confirm the theory developed.
- 537.312.6+538.632]:546.3-1-76-59 2204
Hall Effect and Resistance of Dilute Gold-Chromium Alloys at Low Temperatures—W. B. Teutsch and W. F. Love. (*Phys. Rev.*, vol. 105, pp. 487–490; January 15, 1957.)
- 537.323 2205
Thermoelectric Properties of Bismuth—G. A. Ivanov and L. I. Mokievski. (*Zh. Tekh. Fiz.*, vol. 26, pp. 1343–1344; June, 1956.) Contrary to the results obtained by Sato (*J. Phys. Soc. Japan*, vol. 6, pp. 125–127; March/April, 1951.) it was found that the coefficient of the thermo-emf of bismuth remains constant for temperature differences across the specimen greater than 0.01°C.
- 538.2 2206
Material of the Conference on Radio-spectroscopy (Kazan', 30th May–2nd June 1955)—(*Bull. Acad. Sci. U.R.S.S., sér. phys.*, vol. 20, pp. 1199–1356; November, 1956. In Russian.) Texts are given of twenty-five papers presented at the conference. Subjects discussed included paramagnetic and ferromagnetic resonance and the characteristics of ferrites.
- 538.22 2207
On the Magnetic Properties of the System MnSb-CrSb—T. Hirone, S. Maeda, I. Tsubokawa, and N. Tsuya. (*J. Phys. Soc., Japan*, vol. 11, pp. 1083–1087; October, 1956.)
- 538.221 2208
Surface Structures and Ferromagnetic Domain Sizes—D. H. Martin. (*Proc. Phys. Soc., London*, vol. 70, pp. 77–84, plate; January 1, 1957.) Optimum domain sizes in iron and silicon-iron crystals have been calculated.
- 538.221 2209
An Investigation of the Magnetization of a Structure representing a Model of Magneto-Dielectric Material—M. N. Grigor'ev and I. M. Kirko. (*Zh. Tekh. Fiz.*, vol. 26, pp. 1501–1508; July, 1956.) A report is presented on an experimental investigation into the magnetization of mixtures of spherical or cylindrical magnetic particles and quartz sand, in dc and ac fields (from 0.1 to 20 kc). A number of experimental curves are shown, and, using the formulas given, magnetic characteristics can be derived for other frequencies and packing factors.
- 538.221 2210
An Analysis of the Magnetization Processes in Iron Single Crystals by an Electrical Method—R. Parker. (*Phil. Mag.*, vol. 1, pp. 1133–1146; December, 1956.)
- 538.221 2211
Hysteresis-Relaxation and Permeability of Carbon-Containing Silicon-Iron—F. Schreiber. (*Z. angew. Phys.*, vol. 8, pp. 539–551; Novem- ber, 1956.) Results of tests carried out at low field strengths on two types of Si-Fe laminations are given in graphical form and are analyzed with reference to the existing theory of magnetic after-effects and previous investigations.
- 538.221 2212
Study of Ferrous Ternary Diagrams in relation to Magnetic Interactions: Fe-Ni-Al System—U. H. Roesler. (*J. Metals*, vol. 8, pp. 1285–1289; October, 1956.) From a thermodynamic analysis of the γ -loop in iron alloys it appears that Al raises the temperature range in which atomic spins in iron become uncoupled from one another; this disagrees with Curie temperature data for Fe-Al alloys. The anomaly is interpreted by assuming that for alloys short-range magnetic order above the Curie point is maintained to higher temperatures than for pure Fe.
- 538.221 2213
The Influence of Heat Treatment on the Magnetic Properties of Face-Centered Cubic Nickel-Cobalt Alloys—M. Yamamoto and S. Taniguchi. (*Sci. Rep. Res. Inst. Tohoku Univ., Ser. A.*, vol. 8, pp. 280–292; August, 1956.) The anomalous magnetic behavior is explained in terms of domain-wall stabilization by induced uniaxial anisotropy [1827 of 1957 (Taniguchi)]. This provides a satisfactory interpretation of the sensitivity to heat treatment of simple ferromagnetic solid solutions.
- 538.221 2214
Ferromagnetic Domain Patterns on Nickel Crystals: Part 2—Domain Patterns on General Surfaces of Unmagnetized Crystals—T. Iwata and M. Yamamoto. (*Sci. Rep. Res. Inst. Tohoku Univ., Ser. A.*, vol. 8, pp. 293–312; August, 1956.) A magnetic colloid technique is used to photograph domain patterns of various types. A detailed interpretation of the complicated patterns is based on previous investigations (*ibid.*, vol. 5, pp. 433–459; October, 1953).
- 538.221 2215
The Influence of Plastic Deformation on the Magnetic Properties of Nickel Single Crystals—H. Dietrich and E. Kneller. (*Z. Metallkde.*, vol. 47, pp. 672–684 and 716–728; October and November, 1956. English summaries, pp. 683–684 and 728.) The influence of plastic deformation on the law of approach to magnetic saturation and on coercivity is investigated.
- 538.221:537.311 2216
Properties of the Temperature Dependence of the Electrical Resistance of Ferromagnetic Metals at Low Temperatures—A. I. Sudovtsov and E. E. Semenenko. (*Zh. Eksp. Teor. Fiz.*, vol. 31, pp. 525–526; September, 1956.) Experimentally determined resistance/temperature characteristics are presented graphically for iron and nickel for the temperature range 1.23–4.2°K.
- 538.221:538.249 2217
Anomalies in Hysteresis Cycles due to Diffusion After-Effect—P. Brissonneau. (*C.R. Acad. Sci., Paris*, vol. 244, pp. 868–870; February 11, 1957.) Results of measurements made on armco iron at –21.3°C, which are similar to those of Feldtkeller (126 of 1953) for an Si-Fe alloy, are interpreted in terms of Néel's theory.
- 538.221:538.569.4.029.6 2218
A Note on the Ferromagnetic Resonance in α -Fe₂O₃—M. Shimizu. (*J. Phys. Soc., Japan*, vol. 11, pp. 1078–1083; October, 1956.) Microwave resonance formulas are derived for a ferromagnet with hexagonal and uniaxial anisotropy. Results are compared with published experimental data.
- 538.221:621.318.12 2219
Magnetic Properties of Magnet Alloys of

- Iron, Wolfram [tungsten] and Molybdenum**—H. Masumoto and Y. Shirakawa. (*Sci. Rep. Res. Inst. Tohoku Univ., Ser. A*, vol. 8, pp. 319–324; August, 1956.) Results are given of a series of measurements on alloys of different composition. The best characteristics were obtained with a heat-treated alloy containing 15 per cent w and 15 per cent Mo.
- 538.221:621.318.132:538.569.4** 2220
Ferromagnetic Resonance in Metal Single Crystals—J. O. Artman. (*Phys. Rev.*, vol. 105, pp. 74–84; January 1, 1957.) The microwave susceptibility tensor components are calculated for single crystals with uniaxial or cubic magnetic symmetry, and the resonance relations derived. For a simple multidomain structure, two resonance conditions are found, depending on whether the microwave and static fields are parallel or orthogonal. These conditions involve the static field, saturation magnetization, anisotropy parameter, and ratio of skin depth to domain width; thus domain spacings can be inferred from microwave measurements.
- 538.221:621.318.134** 2221
Observation of Magnetic Viscosity of Ferrites at Low Temperatures—R. V. Telesnin and I. A. Lednev. (*C.R. Acad. Sci. U.R.S.S.*, vol. 112, p. 48; January 1, 1957. In Russian.) Brief note. The experimental results show that the magnetic induction at 78°K is lower than at 293°K and the hysteresis loop is broader.
- 538.221:621.318.134** 2222
Magnetic Viscosity of Nickel-Zinc Ferrites—I. A. Lednev and R. V. Telesnin. (*Radio-tekhnika i Elektronika*, vol. 1, pp. 1186–1192; August, 1956.) A systematic experimental investigation of a series of Ni-Zn ferrites at temperatures between 78°K and the Curie point is reported. The special circuit used in conjunction with a pulse oscillograph is described.
- 538.221:621.375.3** 2223
Flux Reversal in Magnetic Amplifier Cores—F. J. Friedlaender. (*Commun. & Electronics*, pp. 268–276; July, 1956. Discussion, pp. 277–278.) A model describing magnetization processes in grain-oriented 50 per cent Ni-Fe alloy tapes is developed. Results of tests made on eleven toroidal cores are compared with theoretical predictions.
- 538.221:621.318.134:538.569.4** 2224
Microwave Resonance Relations in Anisotropic Single-Crystal Ferrites—J. O. Artman. (*Phys. Rev.*, vol. 105, pp. 62–73; January 1, 1957.) Detailed analyses are given for spherical specimens possessing only first-order anisotropy. The resonance frequency for single-domain crystals is related to the anisotropy parameter, which may be positive or negative, and the magnitude and direction of the static field H , which is taken to lie in a (110) crystal plane. The case of a simple multidomain structure, appropriate below saturation conditions, is also treated. It is assumed that the domains are lamellas of equal volume, their planes being normal to H and their magnetizations being oriented in two directions which alternate in sequence. Two resonant frequencies are found for a given H , depending on whether it is parallel or normal to the microwave field. The theory agrees with recent experimental data.
- 539.23:546.87** 2225
Preparation and Electrical Properties of Thin Films of Bismuth—A. Colombani and P. Huet. (*C. R. Acad. Sci., Paris*, vol. 244, pp. 755–758; February 4, 1957.)
- 539.23:546.87:537.312.6** 2226
Thermal Development of the Electrical Resistance of Thin Films of Bismuth—P. Huet and A. Colombani. (*C. R. Acad. Sci., Paris*, vol. 244, pp. 865–868; February 11, 1957.) Resistance/temperature characteristics between 0°C and 320°C are shown for three ranges of film thickness.
- 549.514.51** 2227
Crystal Defects in Y-Cut Quartz and Their Effect on the Equivalent Resistance—II. Iwasaki. (*J. Radio Res. Labs., Japan*, vol. 3, pp. 259–264; October, 1956.) The nature of etch patterns is investigated. Plates exhibiting a crevice pattern, which is due to crystal imperfections, have a high equivalent resistance.
- 549.514.51:534.133-8** 2228
The Role of Internal Friction in Piezoelectric Quartz Crystals—A. G. Smagin. (*C.R. Acad. Sci. U.R.S.S.*, vol. 112, pp. 425–426; January 21, 1957. In Russian.) Experimental results indicate that internal friction is negligible in comparison with the surface-layer friction.
- 621.315.612.6.017.143** 2229
Further Experimental Investigation of the Dielectric Losses of Various Glasses at Low Temperatures—J. Volger and J. M. Stevels. (*Philips Res. Rep.* vol. 11, pp. 452–470; December, 1956.) Results of measurements are discussed qualitatively in relation to the glass structure. No effect of irradiation on the dielectric losses at low temperatures, such as the formation of color centers in quartz crystals (see 2768 of 1956), is found. Various loss mechanisms are summarized.
- 621.315.616** 2230
Variation with Pressure of the Permittivity of Polythene—A. C. Lynch and P. L. Parsons. (*Nature, London*, vol. 179, p. 686; March 30, 1957.)
- 621.318.132:621.314.22:(43)** 2231
Magnetically Soft Alloys as Material for Use in Instrument Transformers—O. E. Nölke. (*Arch. tech. Messen*, no. 250, pp. 259–262; November, 1956.) Details of German alloys are given. Characteristics and costs are compared in graphical form.
- 621.318.134:538.65:534.232** 2232
Performance of Ceramic Ferrite Resonators as Transducers and Filter Elements—C. M. van der Burgt. (*J. Acoust. Soc. Amer.*, vol. 28, pp. 1020–1032; November, 1956.) A detailed review with numerical and graphical data of the properties of modern piezomagnetic materials. Sixty-nine references.
- 621.318.2:(43)** 2233
Commercial Types of Permanent Magnet, particularly for Measuring Instruments—H. Fahlenbrach. (*Arch. tech. Messen*, pp. 237–240 and 263–264; October and November, 1956.) Summary of modern manufacturing processes, characteristics and applications of German magnetic materials. Twenty-five references.
- 529.23** 2234
Vacuum Deposition of Thin Films. [Book Review]—L. Holland. Chapman and Hall, London, 1956, 542 pp., 70s. (*Nature, London*, vol. 179, pp. 501–502; March 9, 1957.)
- MATHEMATICS**
- 51** 2235
On the Integration of Nonlinear Parabolic Equations by Implicit Difference Methods—M. E. Rose. (*Quart. Appl. Math.*, vol. 14, pp. 237–248; October, 1956.)
- 512.831** 2236
A Method for treating the Stability Problem in Matrix Eigenvalue Problems—H. R. Schwarz. (*Z. angew. Math. Phys.*, vol. 7, pp. 473–500; November 25, 1956.) Given the eigenvalue problem $(A-\lambda E)x=0$ for real or complex matrices A , the number of eigenvalues λ with positive real parts is determined without evaluating the characteristic polynomial. A procedure is developed for transforming the given matrix into a reduced form by applying a finite series of elementary transformations; the problem can then be solved immediately.
- 517** 2237
A Method for the Construction of Green's Functions—B. A. Boley. (*Quart. Appl. Math.*, vol. 14, pp. 249–257; October, 1956.) The Green's function associated with any partial differential equation is obtained as the solution of an integral equation, as the limit of an infinite sequence of functions. Convergence of this sequence is proved for the case of Helmholtz's equation.
- 517:535.13:538.56** 2238
On the Solution of Maxwell's Equations in Cylindrical Coordinates by means of Laplace Transforms and Finite Fourier and Hankel Transforms—II. Delavault. (*C.R. Acad. Sci., Paris*, vol. 244, pp. 1146–1149; February 25, 1957.)
- 519.2:621.39** 2239
Entropy of Stochastic Processes—M. Rozenblat-Rot. (*C.R. Acad. Sci. U.R.S.S.*, vol. 112, pp. 16–19; January 1, 1957. In Russian.)
- MEASUREMENTS AND TEST GEAR**
- 53.087/.088** 2240
Taking Account of Systematic Errors in Measurements—II. Weyerer. (*Naturwiss.*, vol. 43, p. 492; November, 1956.) Systematic errors cannot be dealt with by averaging techniques applicable to random errors; a formula is presented which permits the systematic errors to be taken into account.
- 621.317.335+621.317.41].029.64:621.318.134** 2241
Measurement of Dielectric and Magnetic Properties of Ferromagnetic Materials at Microwave Frequencies—W. von Aulock and J. H. Rowen. (*Bell Sys. Tech. J.*, vol. 36, pp. 427–448; March, 1957.) Measurements are made by observing the perturbation in a cylindrical cavity, excited at 9.2 kmc, due to the insertion of a small ferrite sample. Thin disk samples yield more accurate results below ferromagnetic resonance, whereas small spheres are preferable near resonance. Experimental results are given for low-loss BTL ferrite. The loss below resonance is considerably lower for polycrystalline ferrites than that predicted by Polder's theory for single-crystal ferrites.
- 621.317.335.2** 2242
A Simple Apparatus for Measuring Circuit Capacitances—J. C. S. Richards. (*Electronic Eng.*, vol. 29, pp. 118–120; March, 1957.) An instrument is described for measuring capacitance to earth in the range 0–300 pf with accuracy within ± 2 per cent.
- 621.317.444** 2243
Continuously Indicating Precision Magnetometer—G. W. Green, R. C. Hanna, and S. Waring. (*Rev. Sci., Instr.*, vol. 28, pp. 4–8; January, 1957.) A magnetic field can be measured by finding the resonance frequency of a coil suspended in it. Simple auxiliary apparatus gives an accuracy within 1 per cent and 0.01 per cent can be achieved.
- 621.317.7:621.316.87:621.396.822.029.6** 2244
A New Standard for Very Low Noise Powers in the Microwave Region—H. Jung. (*Hochfreq. u. Elektroak.*, vol. 65, pp. 50–52; September, 1956.) The use of heated polar liquids as noise sources is proposed. A tube through which the heated liquid flows is fitted to the waveguide in place of a gas-discharge noise generator. Good broad-band matching and accuracy is obtained; noise temperatures

of gas discharges found in this way agree fairly well with available data.

621.317.7:621.396.324 2245

Laboratory Test Equipment for Synchronous Regenerative Radiotelegraph Systems—Hilton, Law, Lee, and Levett. (See 2288.)

621.317.7:621.397.6 2246

Electronic Video-Pattern Generator with Continuously Variable Patterns—W. Dillenburg and J. Wolf. (*Elektronische Rundschau*, vol. 10, pp. 293-296; November, 1956.) The application and the basic circuits of such an instrument are described.

621.317.7.087.6 2247

Servo-Operated Recording Instruments—R. L. Gordon, A. J. Maddock. (*Proc. IEE*, Part B, vol. 104, p. 187; March, 1956.) Comment on 3830 of 1956 and author's reply.

621.317.742.029.64 2248

A Coaxial Standing-Wave Detector for the S-Band—L. W. Shawe and G. W. Fynn. (*Proc. IEE*, Part B, vol. 104, pp. 188-190; March, 1957.)

621.317.75:537.226/.227 2249

Bridge for Accurate Measurement of Ferroelectric Hysteresis—H. Diamant, K. Drenck, and R. Pepinsky. (*Rev. Sci. Instr.*, vol. 28, pp. 30-33; January, 1957.) This instrument gives an undistorted display of hysteresis loops even with samples of relatively high conductivity. The bridge measurements are independent of the frequency and waveform of the applied voltage.

621.317.755:621.385.83 2250

Blue-Trace Oscillograph, a New Instrument for Recording Nonperiodic Phenomena—W. Dietrich. (*Nachrichtentech. Z.*, vol. 9, pp. 504-507; November, 1956.) The equipment described uses a skiatron-type tube. The dark trace produced persists for several days, under appropriate conditions, or it can be erased in a few seconds by means of a built-in heater. Frequency components up to 15 kc can be recorded at writing speeds not exceeding 400 ms.

621.317.763 2251

Resistive Fins Improve Wavemeter Tuning—K. Ishii. (*Electronic Ind. Tele-Tech.*, vol. 15, pp. 59, 128; November, 1956.) To increase the absorption of electric field energy in cylindrical cavity wavemeters, a conventional flat power absorber was fitted with radial fins projecting into the cavity. The improvement is evident from a comparison of the tuning characteristics before and after modification.

OTHER APPLICATIONS OF RADIO AND ELECTRONICS

539.16.08:621.385.15 2252

Electron Multipliers for the Registration of Corpuscular and Hard Electromagnetic Radiations—T. M. Lifshits. (*Radiotekhnika i Elektronika*, vol. 1, pp. 1272-1283; September, 1956.) The 13-stage electron multiplier, which is similar to that described by Allen (1106 of 1948), uses an activated Cu-Al-Mg alloy cathode and secondary-electron emitters; the amplification factor lies between 10^9 and 10^{11} at a voltage of 300 v per stage. Mg or Ta photocathodes are used in the ultraviolet counter, and a cathode comprising 20 layers of Pt foil in the X- and γ -ray counters.

551.508.1:621.398 2253

The Scatter Error of the "Modell Lang" Radiosonde—W. Klinkow and R. Weide. (*Z. Met.*, vol. 10, pp. 308-313; October, 1956.) A report is presented of tests on this radiosonde, which is the type used in the East German meteorological service. Masking by fortuitous errors made it impossible to determine the scatter between readings given by different specimens of the same model.

616-7:621.374.3:621.314.7 2254

A Transistor Cardiometer—L. Molyneux. (*Electronic Eng.*, vol. 29, pp. 125-127; March, 1957.) A small, portable, battery-operated instrument designed for use in the operating suite of a hospital.

621.317.39:531.71:621.319.43 2255

Design of Capacitance Displacement Transducers—R. K. Vinycomb and F. E. Martyr. (*Instrum. Practice*, vol. 10, pp. 985-987; November, 1956.) Practical details, including a nomogram, are given for simple piston-type coaxial-cylinder capacitors for measuring mechanical displacements over a wide range.

621.373.52:621.43.04 2256

A New Electronic Ignition System for Motor Cars—M. J. Guiot. (*Électronique*, Paris, no. 120, pp. 51-52; November, 1956.) The equipment described, which is now produced commercially, uses an 80-kc transistor oscillator and step-up transformer producing 12 to 20 kv. High efficiency and output independent of motor speed are its chief advantages.

621.383.2:621.385.832:778.5 2257

The Myriatron—G. H. Lunn and R. A. Chippendale. (*Electronic Radio Eng.*, vol. 34, pp. 156-160; May, 1957.) The principles of operation of an image dissector for high-speed cinematography are described.

621.384.6 2258

Electrostatic Lens—N. P. Carleton. (*Rev. Sci. Instr.*, vol. 28, pp. 9-10; January, 1957.) A lens having the potential function $V(r,z) = a(2z^2 - r^2)$ in cylindrical coordinates was found to focus a highly divergent ion beam more effectively than conventional lenses.

621.384.6 2259

Variable-Energy Particle Accelerators—J. W. Gallop. (*Nature*, London, vol. 179, p. 492; March 2, 1957.) Comment on recent developments in design of proton accelerators.

621.384.612 2260

Method of Investigating Radial-Phase Oscillations of Electrons in a Synchrotron—Yu. M. Ado. (*Zh. Eksp. Teor. Fiz.*, vol. 31, pp. 533-534; September, 1956.) The principles of a method based on the observation of light radiated by the electrons are described.

621.384.613 2261

Approximations for Linear Betatron Oscillations—F. T. Adler and D. Baroncini. (*Nuovo Cim.*, vol. 4, pp. 959-974; November 1, 1956. In English.) "Approximation methods for calculating the characteristic exponent of extended Hill equations are derived and applied to the computation of linear betatron oscillations."

621.385.833 2262

Aperture Aberration of Strong-Focusing [electron] Lenses—M. Y. Bernard and J. Hue. (*C.R. Acad. Sci., Paris*, vol. 244, pp. 732-735; February 4, 1957.) Continuation of analysis (1559 of 1957) with a note on the size and shape of the focal distortion caused.

621.385.833 2263

The Theory of the Reflection Electron Microscope—D. Wiskott. (*Optik*, Stuttgart, vol. 13, pp. 463-478 and 481-493; October and November, 1956.) The theory of an electron microscope for viewing the object by reflected electrons is developed on the basis of geometrical optics and wave mechanics; the approximate solutions derived agree with experimental results. In practice, the resolution obtainable should reach 120-150Å for a field strength of 100 kv/cm.

621.385.833 2264

The Resolving Power of an Emission-Type Electron Microscope in the Presence of a Diaphragm, and the Velocity Spectrum of

Transmitted Electrons—C. Fert and R. Simon. (*C.R. Acad. Sci., Paris*, vol. 244, pp. 1177-1179; February 25, 1957.) The analysis of the microscope described earlier (904 of 1957) shows that the resolution is independent of the velocities of the electrons emitted by the cathode.

PROPAGATION OF WAVES

621.396.11 2265

Radio Wave Propagation—(*Nature*, London, vol. 179, pp. 354-356; February 16, 1957.) Report on a colloquium held in Paris, September, 1956, covering tropospheric and ionospheric propagation and general theoretical problems. Papers are to be published in *Onde élect.*

621.396.11 2266

On the Multiple Diffraction of Electromagnetic Waves by Spherical Mountains—K. Furutsu. (*J. Radio Res. Labs., Japan*, vol. 3, pp. 331-390; October, 1956.) The treatment discussed in 3186 of 1956 is extended to the problem of multiple diffraction. The formulas obtained cover a wide range of angles and are applicable to diffraction by the earth's surface.

621.396.11 2267

The Calculation of Field Strength over Mixed Paths on a Spherical Earth—K. Furutsu and S. Koimai. (*J. Radio Res. Labs., Japan*, vol. 3, pp. 391-407; October, 1956.) Graphs and tables of factors required in field strength calculations based on the formula derived in 2191 of 1956 (Furutsu) are given.

621.396.11:511.510.535 2268

D-E Layer Electron Model Revised from Considerations of the Diurnal Variation of Experimental Results—T. Kobayashi. (*J. Radio Res. Labs., Japan*, vol. 3, pp. 279-305; October, 1956.) The electron model (2194 of 1956) is modified on the basis of an analysis of experimental results obtained by various authors and a revision of Chapman's theory. Absorption charts are compared and the use of transmission curves in calculations is illustrated.

621.396.11:551.510.535:523.75 2269

Some Effects of Intense Solar Activity on Radio Preparation—Houston, Ross, and Schmerling. (See 2128.)

621.396.11:551.510.535:621.317.75 2270

Measurement of Ionospheric Path-Phase for Oblique Incidence—R. Price and P. E. Green, Jr. (*Nature London*, vol. 179, pp. 372-373; February 16, 1957.) Three techniques for direct measurement of path/phase variations at oblique incidence are outlined. They are based on heterodyning the received wave train with an IF that is an integral multiple of the pulse repetition rate. Sample records are shown. Experiments to be made using Cs frequency standards include the examination of multipath transmissions associated with forward scatter.

621.396.11.029.45 2271

Lightning and the Propagation of Audio-Frequency Electromagnetic Waves—Ya. L. Al'pert. (*Uspekhi Fiz. Nauk*, vol. 60, pp. 369-389; November, 1956.) See 919 and 920 of 1957 (Al'pert and Borodina).

621.396.11.029.45:621.396.933.2:551.594.6 2272

Very-Low-Frequency Propagation and Direction-Finding—F. Horner. (*Proc. IEE*, Part B, vol. 104, pp. 73-80; March, 1957.) Direction finding observations on a cw transmitter at 16 kc have established the magnitude of polarization errors with crossed-loop antennas. Errors on atmospheric are similar, but may have less practical importance depending on how the results are used. The reflecting properties of

the ionosphere at 16 kc were found to depend on the azimuthal direction of propagation.

621.396.11.029.55:551.510.535 2273

Propagation on 27 Mc/s via E_n -Layer Reflections—Y. Uesugi, I. Kasuya, and J. Orimo. (*J. Radio Res. Labs., Japan*, vol. 3, pp. 265–278; October, 1956.) Report on propagation tests carried out over 540–1470 km paths to investigate the validity of an empirical formula relating fEs to field strength, derived, by Kono, *et al.* (1770 of 1955). Disagreement at higher field strengths could be explained by assuming partial reflections.

621.396.81.029.55 2274

Index of Short Radio Wave Intensity—Y. Hakura and M. Miyamoto. (*J. Radio Res. Labs., Japan*, vol. 3, pp. 307–329; October, 1956.) The field strength of the 10- and 15-mc WWV transmissions received at Hiraiso, Japan was analyzed by the statistical method outlined. The daily indices from 1950 to 1955 are tabulated.

621.396.812.3.029.64/.65 2275

Some Problems Posed by Wave Propagation at 8-mm and 3-cm Wavelength over the Sea and through Rain—D. G. Kiely. (*Ann. Télécommun.*, vol. 11, pp. 233–244 and 267–279; November and December, 1956.) Account of tests carried out in 1951 and 1952 and separately covered by previous reports (see *e.g.*, 1554 and 1774 of 1954).

RECEPTION

621.396.621:621.376.33 2276

Principles of Design of Battery-Operated Frequency-Modulation Receivers—R. A. Lampitt and J. P. Hannifan. (*J. Brit. IRE*, vol. 17, pp. 173–185; March, 1957.) A theoretical circuit diagram of a nine-tube transportable receiver is included. The main emphasis of the discussion is on the mixer, IF amplifier, and demodulator stages.

621.396.621:621.376.33 2277

Limiters and Discriminators for F.M. Receivers—G. G. Johnstone. (*Wireless World*, vol. 63, pp. 124–127 and 235–240; March and May, 1957.) An analysis and design procedure are detailed for the "idealized" ratio detector, together with a comparison with the Foster-Seeley arrangement. Parts 1 and 2: 1220 of 1957.

621.396.621:621.396.215 2278

Frequency Diversity in the Reception of Selectively Fading Binary Frequency-Modulated Signals—J. W. Allnatt, E. D. J. Jones, and H. B. Law. (*Proc. IEE*, Part B, vol. 104, pp. 98–110; March, 1957. Discussion, pp. 147–152.) The use of frequency diversity is advocated to obtain all available information from both the marks and spaces in radio-telegraphy. An experimental demodulation unit showed, in laboratory tests and in the field, the advantages of diversity over conventional methods.

621.396.621:621.396.215 2279

The Signal/Noise Performance Rating of Receivers for Long-Distance Synchronous Radiotelegraph Systems using Frequency Modulation—H. B. Law. (*Proc. IEE*, Part B, vol. 104, pp. 124–129; March, 1957. Discussion, pp. 147–152.) Experimental and theoretical results indicate that the steady-signal error-liability of fm radio-telegraph receivers of the limiter-discriminator type is characterized by a simple exponential function of the signal/noise ratio. Fading-signal performance with or without diversity is readily derived from the steady-signal performance.

621.396.812:621.396.215 2280

The Detectability of Fading Radiotelegraph Signals in Noise—H. B. Law. (*Proc. IEE*, Part B, vol. 104, pp. 130–140; March, 1957.

Discussion, pp. 147–152.) An ideal receiver for binary synchronous telegraphy is defined and the noisy-signal performance of a practical receiver measured in terms of its departure from the ideal. Analysis leads to a mathematical specification for the ideal diversity receiver which provides a basis for the design of practical receivers.

621.396.812.029.64 2281

An Experimental Study of some Fading Characteristics of 10-mc Waves in the Scatter Region—D. G. Kiely, S. J. Robinson, and F. C. Chesterman. (*J. Brit. IRE*, vol. 17, pp. 161–171; March, 1957.) Data presented include the short-term fading rate, amplitude, and fading pattern correlation using spaced antennas, for a 100-mile path over the Bristol Channel, and the amplitude of mean-level fades in the North Sea area.

621.396.812.3.001.57 2282

An Improved Fading Machine—H. B. Law, F. J. Lee, R. C. Looser, and F. A. W. Levett. (*Proc. IEE*, Part B, vol. 104, pp. 117–123; March, 1957. Discussion, pp. 147–152.) A fading signal with a Rayleigh amplitude distribution and random phase variations was obtained by mixing six components, with slightly different and suitably varying frequencies.

STATIONS AND COMMUNICATION SYSTEMS

621.376.3 2283

An Investigation of the Spectra of Binary Frequency-Modulated Signals with Various Build-Up Waveforms—J. W. Allnatt and E. D. J. Jones. (*Proc. IEE*, Part B, vol. 104, pp. 111–116; March, 1957. Discussion, pp. 147–152.) Spectra were determined experimentally. Results suggest that trapezoidal modulation gives the smallest bandwidth for a given total build-up time.

621.376.5:621.373.431.1 2284

A Method of Time-Pulse Transformation—I. A. Zakaharya and V. N. Mikhailovskii. (*Avtomatika i Telemekhanika*, vol. 17, pp. 836–846; September, 1956.) The properties are considered of a new system of transforming the voltage amplitude of rectangular pulses into time intervals between the leading edges of pulses of higher frequency. The system includes a cathode-coupled multivibrator circuit. Analysis suggests applications in telemetry systems.

621.39:534.78 2285

A Development of the Collard Principle of Articulation Calculation—J. Collard; D. L. Richards and R. B. Archbold. (*Proc. IEE*, Part B, vol. 104, p. 196; March, 1957.) Comment on 3873 of 1956 and authors' reply.

621.39.001.11 2286

Theory of Transmission of Information through Stochastic Communication Channels—M. Rozenblat-Rot. (*C.R. Acad. Sci. U.R.S.S.*, vol. 112, pp. 202–205; January 11, 1957. In Russian.) Mathematical paper.

621.39.001.11 2287

On the Capacity of a Discrete Channel: Part 2—S. Muroga. (*J. Phys. Soc., Japan*, vol. 11, pp. 1109–1120; October, 1956.) Extension of the theoretical treatment of noisy channels outlined in Part 1 (254 of 1954).

621.396.324:621.317.7 2288

Laboratory Test Equipment for Synchronous Regenerative Radiotelegraph Systems—C. G. Hilton, H. B. Law, F. J. Lee and F. A. W. Levett. (*Proc. IEE*, Part B, vol. 104, pp. 141–147; March, 1957. Discussion, pp. 147–152.) Element error rate is measured directly.

621.396.41 2289

Double-Sideband vs Single-Sideband Systems—J. P. Costas. (*Proc. IRE*, vol. 45, pp.

534–537; April, 1957.) The utility of ssb as opposed to dsb transmissions is questioned on particular aspects such as spectrum conservation, power gain, waveform preservation, propagation, and expense.

621.396.41 2290

Synchronous Communications—R. R. McPherson. (*Proc. IRE*, vol. 45, pp. 537–538; April, 1957.) Comment on 936 of 1957 (Costas).

621.396.41 2291

Single-Sideband Techniques—(*Proc. IRE*, vol. 45, pp. 538, 540; April, 1957.) Comments on two of the papers noted in 937 of 1957 and authors' replies.

621.396.41 2292

S.S.B. Performance as a Function of Carrier Strength—N. II. Shepherd; W. L. Firestone. (*Proc. IRE*, vol. 45, pp. 541–543; April, 1957.) Comment on 938 of 1957 and author's reply.

621.396.41:621.396.11 2293

Single-Sideband Techniques in U.H.F. Long-Range Communications—J. E. Bartow; W. E. Morrow, Jr, C. L. Mack, Jr, B. E. Nichols, and J. Leonhard. (*Proc. IRE*, vol. 45, p. 539; April, 1957.) Note of correction to 939 of 1957.

621.396.5:621.396.65 2294

The Application of Rural Radio to Telephone Networks—C. B. Wooster. (*A.T.E. J.*, vol. 12, pp. 300–312; October, 1956.) A description of commercially available vhf fm equipment for both subscriber and junction working. Signal/noise ratios >51 db are attainable. See also 3040 of 1954 (Felix and Wooster).

621.396.65.029.6 2295

Propagation Test on Microwave Communications Systems—H. R. Mathwich, E. D. Nuttall, J. E. Pitman and A. M. Randolph. (*Elec. Eng.*, vol. 75, pp. 1020–1025; November, 1956. *Commun. & Electronics*, no. 28, pp. 685–691; January, 1957.) Reports of tests at 955.5, 1965 and 6730 mc over a land-path 20 miles long carried out over a period of 16 months.

SUBSIDIARY APPARATUS

621.311.6:541.133 2296

A Constant-Current Device for Use in the Measurement of Transference Numbers by the Moving-Boundary Method—D. T. Hopkins and A. K. Covington. (*J. Sci. Instr.*, vol. 34, pp. 20–21; January, 1957.) "A circuit is described which will supply a current of between 0.5 and 2.5 ma, constant to 0.1 per cent with a ten-fold load impedance change, in the range 5–500 k Ω ."

621.316.722.078.3 2297

A Low-Voltage D.C. Stabilizer using a Saturated-Diode Controller—F. A. Benson and M. S. Seaman. (*Electronic Eng.*, vol. 29, pp. 121–125; March, 1957.) Supplies current up to 30 a.

TELEVISION AND PHOTOTELEGRAPHY

621.397.2 2298

Increasing the Efficiency of the Transmission of Television Signals—D. A. Novik. (*Radiotekhnika i Elektronika*, vol. 1, pp. 1230–1239; September, 1956.) The bandwidth-compression system discussed is based on a transformation of the time-scale of the television signal. Block diagrams of the system are given.

621.397.24:621.315.212.1 2299

The "G-Line" Community TV System—R. B. Gary. (*Radio & Telev. News*, vol. 56, pp. 40–41; November, 1956.) Description of a 15-mile transmission system using the Goubau line to bring television signals to a U.S. community outside the normal reception area. The channel 13 signals are converted to channel

4 before launching by a 58-inch diameter, 45°-taper conical horn on to the polyethylene-coated line. The line is suspended from telephone poles. Nine line amplifiers are used along the line.

621.397.5:621.396.4 2300

Television with Multiple Sound Channels—A. Dubec. (*Électronique, Paris*, no. 120, pp. 31–36; November, 1956.) From a comparison of various methods of combining several different sound transmissions with a single picture signal a carrier-current multiplex system and a pam system appear the most suitable. Basic characteristics and circuits are discussed with reference to French standards.

621.397.621.2:535.623 2301

Some Considerations concerning the Gamma of a Tricolor Picture Tube—W. F. Niklas. (*J. Soc. Mot. Pict. Telev. Eng.*, vol. 65, pp. 546–551; October, 1956.) The expression for gamma is derived and its correlations with gun design parameters found. Methods of compensation for different red, blue, and green phosphor efficiencies and the influence of manufacturing tolerances on gamma are discussed. Among gun designs which permit the use of equal drives on all three guns the triplet with different spacings in the triode gives the best results if close tolerances can be maintained.

621.397.7:621.396.712.3 2302

The Du Mont Telecentre—R. D. Chipp. (*J. Soc. Mot. Pict. Telev. Eng.*, vol. 65, pp. 535–542; October, 1956.) Description of architectural features and of some of the equipment installed.

621.397.8 2303

The Black-White Step in Vestigial-Sideband Television Transmissions—D. Büne-mann and W. Händler. (*Arch. elekt. Übertragung*, vol. 10, pp. 457–466; November, 1956.) Analysis of investigations made to establish

tolerances for the various elements of television transmitters in conformity with CCIR standards. The reproduction of a black-white step as characterized by rise time, overshoot, and smearing was examined; some methods of improving picture quality are discussed.

621.397.5:535.623 2304

Principles of Color Television [Book Review]—K. McIlwain and C. E. Dean (eds), John Wiley & Sons, Inc., New York, N.Y. and Chapman & Hall, Ltd., London, 1956. (*Nature, London*, vol. 179, pp. 645–646; March 30, 1957.) A work by the Hazeltine Laboratories Staff. "This book should be of great value to professional television engineers engaged in research and development, in equipment design, or in broadcasting."

TRANSMISSION

621.396.61:621.376.3 2305

Out-of-Channel Radiation from Mobile F.M. V.H.F. Transmitters—A. L. Rowles. (*Electronic Eng.*, vol. 29, pp. 102–107; March, 1957.) A low-pass filter following the clipper-type limiter reduces the power radiated in unwanted sidebands produced by harmonic distortion in the limiter.

TUBES AND THERMIONICS

621.314.7:621.318.57 2306

The Symmetrical Transistor as a Bilateral Switching Element—Trousdale. (See 2043.)

621.314.7:621.375.4 2307

Transistor Bias Stabilization—J. S. Murray. (*Electronic Radio Eng.*, vol. 34, pp. 161–165; May, 1957.) "A method of using two transistors in cascade is described which enables the operating conditions of the first to be stabilized to a high degree. As a result, it becomes practicable to operate with a very low collector-base voltage and so to minimize semiconductor noise."

621.314:681.142 2308

The Junction Transistor as a Computing Element—Wolfendale, Morgan, and Stephenson. (See 2036.)

621.383.27:621.373.43:535.376 2309

An Electron Multiplier as a Pulsed Light Source—R. Gerharz. (*Z. angew. Math. Phys.*, vol. 7, pp. 529–536; November 25, 1956.) Experiments on multistage photomultipliers with grid control and high over-all conductance are discussed. For operation as a pulse generator, the tube has a coaxial-line feedback from either the collector or the last dynode to the control grid. The pulse amplitude was about 7v; the duration was about 8×10^{-9} s, or 3×10^{-8} s, when coaxial-line stubs were used. Pulse frequency was about 10 mc with a feedback line of length 25 m. Blueish luminescence was observed particularly at the dynodes carrying the higher currents; the total light energy is estimated at about 0.2 w and the luminescence pulses are coincident with the electrical ones; an electroluminescence process in the MgO secondary-emission layers is believed to be responsible.

621.385.83:621.317.755 2310

Blue-Trace Oscillograph, a New Instrument for recording Nonperiodic Phenomena—Dietrich. (See 2250.)

MISCELLANEOUS

621.3–71 2311

Heat Control in Electronic Equipment—E. N. Shaw. (*Electronic Eng.*, vol. 29, pp. 13–23, 65–70, and 115–118; January–March, 1957.) An experimental study of natural methods of cooling compact equipment by determining the mechanism of heat loss from basic units of simple design. An appreciation is obtained of the effectiveness of loss by conduction, convection, and radiation and the optimum use of each in the construction of single instruments and rack-mounted units is illustrated.

